Gene editing and specific MicroRNA inhibition

Lataniotis, Lazaros

Awarding institution:
King's College London

Gene Editing and Specific MicroRNA Inhibition

Lazaros Lataniotis, MSc

School of Cardiovascular Medicine & Sciences

British Heart Foundation Centre of Research Excellence

August 19

Submitted for the degree of Doctor of Philosophy

Supervisors: Dr Anna Zampetaki
Prof Manuel Mayr

King's College London, London, UK

Abstract

Background: MicroRNAs (miRNAs) are short, non-coding RNAs that are involved in the post-transcriptional regulation of gene expression. They are important regulators of diverse physiological and pathophysiological processes. MiRNA families and clusters are two key features in miRNA biology. Previous work on miRNAs in abdominal aortic aneurysm has focused on miR-195, a member of the miR-15 family. MiR-195 exhibits high homology with the other members of the family and therefore, its manipulation, overexpression or inhibition, inevitably affects the expression of other miRNAs of the family.

Objective: The current project explores the use of CRISPR/Cas9 as a gene editing tool to delineate the expression of miRNA families.

Methods and Results: We employed CRISPR/Cas9, an RNA-guided system able to provide highly specific alterations of targeted sequences in the genome of eukaryotic cells. We designed RNA guides and validated their efficiency in editing the mir-195 locus in various cell types while no off-target mutagenesis was observed. Quantification of the levels of miR-195 and other members of the miR-15 family, revealed a significant decrease of miR-195 and in the expression of the other miRNA in the cluster, miR-497. Three more miRNA clusters composed of miRNA members of the same or different family were analysed. Although no gene editing was detected in the miR-497 genomic locus, computational simulation revealed alteration in the three-dimensional structure of the pri-miR-497~195 that may affect its processing. RNA pull-down experiments, using wild type and an edited pri-miRNA of shorter length, were performed and the eluted proteins were analysed by Mass Spectrometry.

Conclusions: Our findings suggest that CRISPR/Cas9 is a powerful gene editing tool able to provide highly specific editing of the genomic locus of miRNAs, resulting in decrease of the levels of their mature transcripts. They also highlight different regulatory mechanisms in miRNA cluster regulation and function.

Table of Contents

Table of Figures

Table of Tables

Acknowledgments

First and foremost, I would like to thank my first supervisor, Dr Anna Zampetaki, for her help during my technical training and for explaining the protocols employed in this project. Also, I would like to thank her for her great support and guidance throughout the project. Her technical expertise, knowledge and continuous patience was of high importance for the completion of the project.

I would also like to thank my second supervisor Prof. Manuel Mayr for his support, technical advice and significant input in my project.

My thanks also to all the members of the Cardiovascular Proteomics Lab, past and present; Dr Ruifang Lu, Dr Ursula Mayr, Dr Xiaoke Yin, Dr Javier Barallobre-Barreiro, Dr Marika Fava, Dr Gonca Suna, Ms Ferheen Baig, Dr Temo Barwari, Mr Eloi Haudebourg, Mr Marc Lynch, Mr Joshua Goulding, Dr Adam Fellows, Dr Konstantinos Theofilatos, Dr Marieke Rienks, Mr Lukas Schmidt, Mrs Timnit Tekie, Mr Sean Burnap, Dr Abishek Joshi, Dr Christian Schulte, Dr Elisa Duregotti, Mr Christian Cassel, Mr James Campbell and Miss Ella Louise Reed for their help in my lab work and support throughout my PhD.

Finally, I would like to thank my family for their encouragement to pursue a PhD and their support to its completion.

Declaration of independent work

I, the author of this thesis, declare that the work presented here was conducted solely by me.

…….

Lazaros Lataniotis

Abbreviations

2D	two-dimensional
3D	three-dimensional
AAA	Abdominal Aortic Aneurysm
AAV	Adenoassociated Virus
ACN	Acetonitrile
ADAR1	Adenosine deaminases acting on RNA 1
AGO2	Argonaute 2
Apex1	apurinic/apyrimidinic (AP) endodeoxyribonuclease 1
a-SMA	alpha smooth muscle actin (Acta2)
ATP	Adenosine Triphospahate
BIM	Bcl-2-like protein 11
BMP	bone morphogenetic protein
BMPR2	Bone morphogenetic protein receptor type II
bp	base pair
BSA	Bovine Serum Albumin
CAD	Coronary Artery Disease
Carmn	cardiac mesoderm enhancer-associated non-coding RNA
Cas	CRIPSR Associated
Cas9	CRIPSR Associated 9
CRISPR	Clustered Regular Interspaced Short Palindormic Repeat
crRNA	CRISPR RNA
dCas9	Nuclease dead Cas9
DGCR8	Di George syndrome Critical Region 8
DMEM	Dulbecco's Modified Eagle Medium
DNA	Deoxyribonucleic Acid
dNTP	deoxynucleotide triphosphate
ds	double stranded
DSB	Double Stranded Break
DSRM	dsRNA binding motif
DTT	Dithiothreitol
dTTP	deoxyThymidine Triphosphate
E. Coli	Escherichia Coli
E2F1	E2F Transcription Factor 1
E2F2	E2F Transcription Factor 2
E2F3	E2F Transcription Factor 3
ECM	Extracellular Matrix
EDTA	ethylenediaminetetraacetic acid
EFS	EF-1 Alpha Short
ELISA	enzyme-linked immunosorbent assay
ER	Endoplasmatic Reticulum
FASTA	FAST-ALL
FBS	Foetal Bovine Serum
FDR	False Discovery Rate
GTP	Guanosine Triphosphate
HCD	Higher energy collision dissociation

HDR	Homology Directed Repair
HEK	Human Embryonic Kidney
Hnrnp	Heterogeneous nuclear Ribonucleoproteins
Hnrnp1	Heterogeneous nuclear Ribonucleoprotein 1
HnrnpA1	Heterogeneous nuclear Ribonucleoprotein A1
Hnrnpa2b1	Heterogeneous nuclear Ribonucleoproteins A2/B1
Hnrnph2	Heterogeneous nuclear Ribonucleoprotein h2
Hnrnpk	Heterogeneous nuclear Ribonucleoprotein K
HPLC	High-performance liquid chromatography
HRP	Horseradish Peroxidase
hSMCs	human Smooth Muscle Cells
HuR	Human antigen R
HUVECs	Human Umbilical Vein Endothelial Cells
IP	Immunoprecipitation
IPTG	Isopropyl β-D-1-thiogalactopyranoside
IRES	Internal ribosome entry site
IVT	*In vitro* Transcription
KH	K-homology
KLF4	Kupper-Like Factor 4
KO	Knock-out
KSRP	KH-type splicing regulatory protein
LB	Lysogeny broth
Loqs	Loquacious
M	Mitosis
MAPK	Mitogen-activated protein kinase
min	minute
miR	microRNA
miRNA	microRNA
miRNA*	microribonucleic acid passenger strand
MMP	Matrix Metalloproteinase
MREs	MicroRNA Response Elements
mRNA	messenger RNA
MS	Mass spectrometry
mt	mutant
Mut	mutant
ncRNA	non-coding RNA
NF-κB	Nuclear Factor kappa-light-chain-enhancer of activated B-cells
NHEJ	Non-Homology End Joining
NO	Nitric Oxide
nt	nucleotide
OFT	off-target
PAGE	Polyacrylamide Gel Electrophoresis
PAM	Protospacer Adjacent Motif
PASMCs	Pulmonary Arterial Smooth Muscle Cells
PAZ	Piwi/Argonaute/Zwille
PBS	phosphate-buffered saline
PCNA	proliferating cell nuclear antigen
PCR	Polymerase Chain Reaction

PEG	Polyethylene Glycol
PEI	Polyethyleneimine
PH	Pulmonary Hypertension
PI3K	phosphoinositide 3-kinase
PIWI	P-element Induced WImpy
pre-crRNA	premature CRISPR RNA
pre-miRNA	precursor microRNA
pri-miRNA	primary microRNA
PTEN	Phosphatase and tensin homolog
qPCR	quantitative real-time polymerase chain reaction
Ran	RAs-related Nuclear protein
RB	Retinoblastoma
RBM6	RNA Binding Motif Protein 6
RBPs	RNA Binding Proteins
RISC	RNA Induced Silencing Complex
RnaseIII	Ribonuclease III
RNP	Ribonucleoprotein
ROS	Reactive Oxygen Species
rpm	revolutions per minute
RRM	RNA Recognition Motif
R-SMAD	Receptor SMAD
RT	Reverse Transcription
S	Synthetic
SD	Standard Deviation
SDS	Sodium Dodecyl Sulphate
sgRNA	single guide RNA
shRNA	short hairpin RNA
SM22	Smooth Muscle 22
SMAD	Sma genes and the Drosophila Mad, Mothers against decapentaplegic
SMCs	Smooth Muscle Cells
SNP	Single Nucleotide Polymorphism
SpCas9	*Streptococcus pyogenes* Cas9
ss	single stranded
STRING	Search Tool for the Retrieval of Interacting Genes/Proteins
T7EI	T7 Endonuclease I
TAL	transcription activator-like
TALENs	Transcription Activator-Like Effector Nucleases
TBE	Tris/Borate/EDTA
TbRI	transforming growth factor beta receptor I
TbRII	transforming growth factor beta receptor II
TbRIII	transforming growth factor beta receptor III
TBS	Tris-buffered saline
TBS-T	Tris-buffered saline-Tween
TDP43	TAR DNA-binding protein 43
TEAB	triethylammonium bicarbonate
TFA	Trifluoroacetic acid
TGF	Transform Growth Factor
TGF-β	Transform Growth Factor-β

TGF-β1	Transforming Growth Factor beta-1
TGFBRII	Transform Growth Factor-β
TIMP	Tissue Inhibitors of Metalloproteinases
TLR2	Toll-like receptor 2
Tra2a	Transformer 2 Alpha Homolog
tracrRNA	Trans-activating crRNA
TRBP	TAR RNA binding protein
UTR	Untranslated Region
UV	Ultra Violet
VSMCs	Vascular Smooth Muscle Cells
WGS	Whole Genome Sequencing
WT	Wild Type
Zc3h10	Zinc finger ccch-type containing 10
ZFN	Zinc Finger Nucleases
α	alpha
β	beta
Δ	difference

Chapter 1 INTRODUCTION

1.1 MicroRNAs (miRNAs)

1.1.1 MiRNA biogenesis

MicroRNAs (miRNAs) are short, 19-24 nucleotide long, non-coding RNA molecules that regulate gene expression post-transcriptionally by binding target transcripts in animals through partial complementarity[1]. They represent the major subgroup of small ncRNAs, with more than 2000 miRNAs identified in the human genome[2]. In addition, they are evolutionary conserved and display distinct tissue expression profile[3].

1.1.1.1 MiRNA transcription and processing

MiRNA genes are transcribed by RNA Polymerase II as long precursor molecules, called primary miRNAs (pri-miRNAs), which can encode single or multiple miRNAs, forming miRNA clusters[4], (Figure 1.1). The pri-miRNAs consist of one or more hairpin-like structures, ~100nt long, which consist of a long stem with bulges and a terminal loop, (Figure 1.2). In a first step, they are processed by RNase III Drosha and its co-factor, DGCR8, which form the microprocessor complex[5], to release a ~65nt long hairpin-shaped precursor (pre-miRNA)[6]. It has been previously shown that a very specific and precise recognition of the primary transcript is needed in order for the Drosha-DGCR8 complex to recognise and cleave the pri-miRNAs. More specifically, basal elements are used as rulers by Drosha while DGCR8 ensures fidelity of the processing by interacting with apical elements[7, 8]. Thus it becomes apparent that sequence changes, like the abolition of specific sequence motifs, such as a UG motif at the base of the hairpin, a UGU/GUG motif in the apical loop and a CNNC motif downstream of the hairpin, as well as structural alterations in the secondary structure of the hairpin of the pri-miRNA, such as a shorter terminal loop, the size and the position of the bulge, the apical loop size, and especially the single stranded state of the basal segments, influence the Drosha processing efficiency[7-11].

The pre-miRNA is, then, exported to the cytoplasm with the help of the Exportin5[12] and is further processed by another RNase III protein, Dicer[13], (Figure 1.1). Drosha cleavage generates a two-nucleotide-long overhang on the 3'-end of the pre-miRNA that is bound by Dicer[14]. More specifically, the two cleavage sites of Dicer bind to the 3'-end of dsRNAs at a fixed distance, of 21–25 nucleotides in length (3'-counting rule), that is dependable on the type of Dicer[15,16,17]. In mammals, an additional mechanism is employed by Dicer to determine the cleavage site of pre-miRNA; it binds to the non-stable 5′-phosphorylated end of the pre-miRNA and cleaves it, at a distance of 22nt away from the 5′-end (5′-counting rule)[18] while a strongly paired 5′-end, through G-C base pairing, impairs its binding and further processing. Human Dicer shows two basic pockets in its PAZ domain that bind to the 5′-end and 3′-end of the pre-miRNA and are spatially arranged to occupy simultaneously the 5′-end and 3′-end of the pre-miRNA only in the case that there is a two-nucleotide 3′-overhang[18,19], (Figure 1.3).

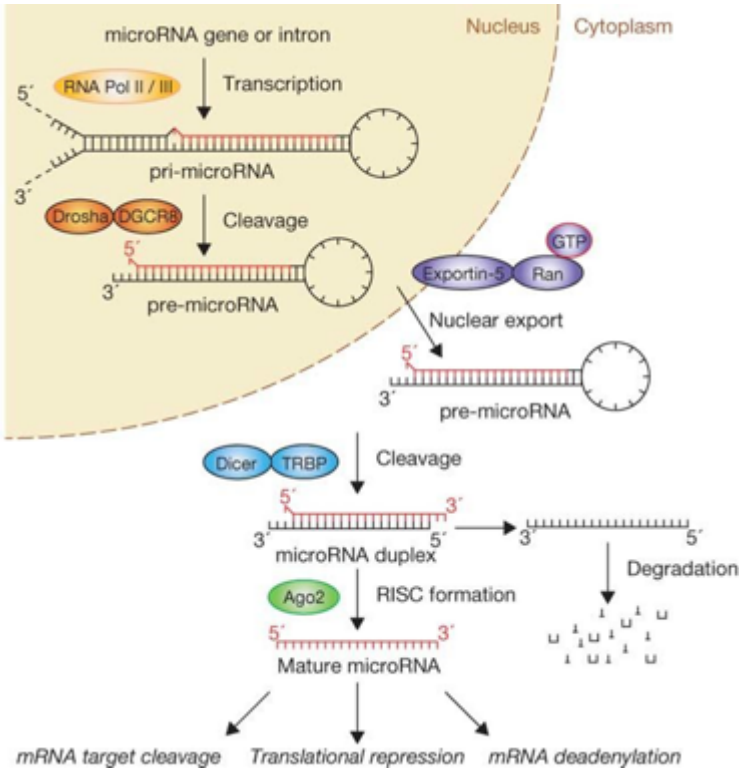

Figure 1.1 MiRNA biogenesis. MiRNAs mature through a multistep process. They are transcribed into pri-miRNAs and processed to pre-miRNAs by Drosha. The pre-miRNA is exported to the cytoplasm, where it is further cleaved to the miRNA:miRNA* duplex by Dicer. Both strands can be loaded to the RISC complex for silencing the mRNA. From Winter et al., 2009.

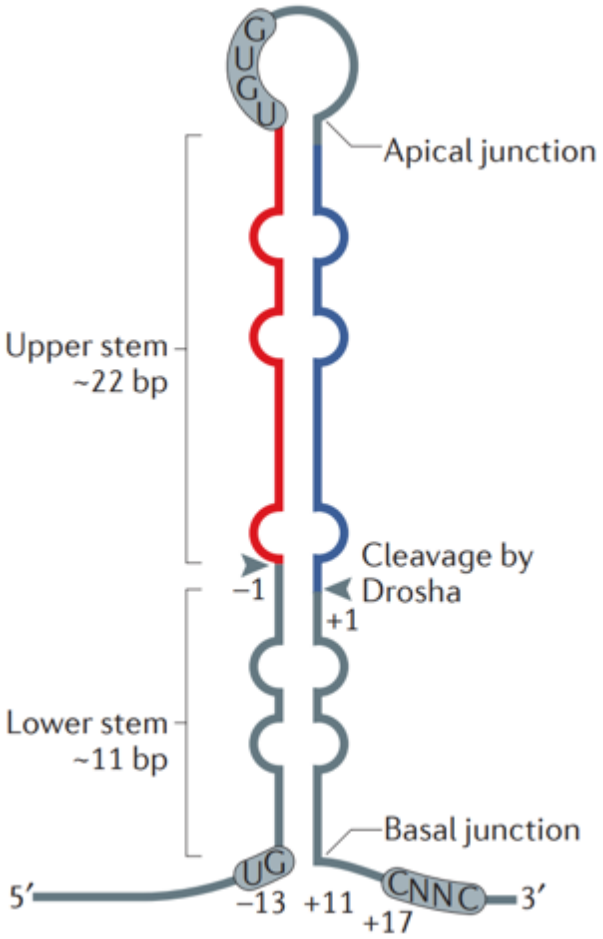

Figure 1.2. Primary miRNA transcript processing. Drosha and DGCR8, the microprocessor complex, recognises the single-stranded parts of the transcript, the length of the stem (~35 bp) and the terminal loop of the primary microRNA. Microprocessor measures the distances from the basal junction and the apical loop, ~11 bp and ~22 bp respectively, and Drosha cleaves the primary transcript. From Ha M. et al., 2014.

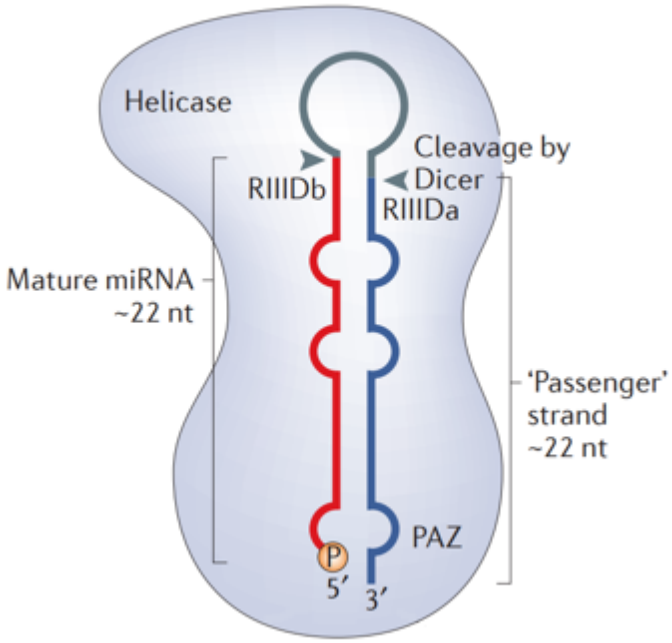

Figure 1.3. Pre-miRNA processing by Dicer. The PAZ (PIWI –Argonaute (AGO)–ZWILLE) domain of the Dicer recognises the ends of pre-miRNA. The two pockets of PAZ interact with the 5′-phosphorylated and the 3'-end of the pre-miRNA. Dicer measures a set distance from both termini, since both RNase III domains are placed ~22nt away from the termini. From Ha M. et al., 2014.

Dicer's processing results in a short (19-24 nucleotide) miRNA:miRNA* duplex[13]. In most cases, the miRNA strand is selected as the mature miRNA, that then binds the Argonaute 2 (Ago2) protein of the RNA induced Silencing Complex (RISC)[22], (Figure 1.1), while the miRNA* strand is degraded. Loaded into the RISC, miRNAs function as sequence-specific guides that direct the complex to mRNA transcripts, targeting mostly the 3' untranslated region (UTR) but, in some cases, also the 5'-UTR and the coding region. Although the mechanism of miRNA:mRNA interaction is not well understood, in mammalian cells this it occurs through incomplete complementarity[23]. Nucleotides 2-8 at the 5'-end of the miRNA constitute its 'seed region' that plays a critical role in the interaction of miRNA:mRNA. Binding of the miRNA to the miRNA Response Elements (MRE) on its targets negatively regulates their expression by preventing their translation and triggering transcript degradation mainly through de-adenylation. Consequently, miRNAs induce post transcriptional gene silencing by either the translational repression of the mRNA, its de-adenylation or its degradation, process that is influenced by the percentage of complementarity between the miRNA and its target[24] (Figure 1.1).

Because of the short length of the miRNA seed sequence and the partial complementarity that is needed for a miRNA to recognise and bind its corresponding targets, single miRNAs can regulate more than one gene. This partial complementarity enables miRNAs to target multiple transcripts that, in many cases, are effectors of the same signalling pathway thus creating a complex regulatory network and eliciting system wide biological responses[25]. Thus, miRNAs with similar seed regions may exert control on set of genes with similar, but not identical sequence to differing degrees.

Moreover, miRNAs with similar sequences form families that are comprised of multiple members that share a common seed region and often display high homology in the rest of their sequence (Figure 1.4). This means that a set of miRNAs can suppress the same gene or set of genes. Additionally, the fact that miRNAs are organised in families imply important roles for them in regulating the expression levels of their mRNA targets with their specific expression further supplementing a flexibility in regulating. Furthermore, control on the expression of genes is partial and a single mRNA can have multiple binding sites for miRNAs.

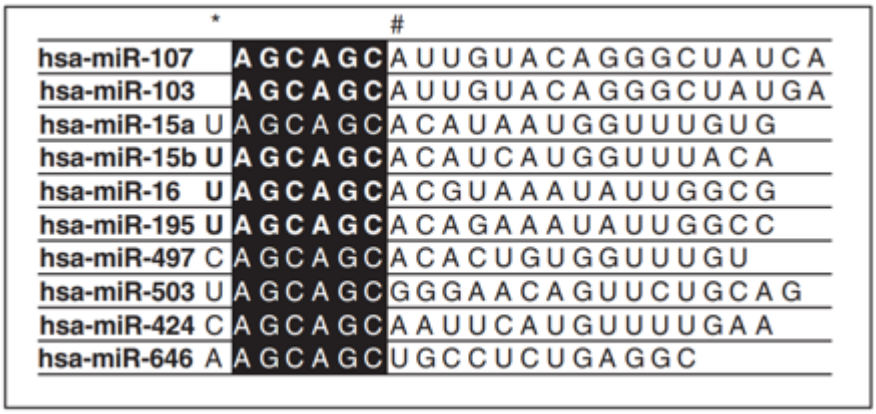

Figure 1.4. MiR-15 family. The extended miR-15 family is depicted with the aligned sequence of all the members and their seed sequence highlighted. From Finnerty et al., 2010.

Overall, miRNAs seem to be an evolutionary tool developed to absorb perturbations, reinforce the robustness of biological systems and ensure that gene expression occurs both at desirable levels and with appropriate timing. MiRNAs are largely considered to be the fine tuners of gene expression that exert mild effects under basal conditions and have more pronounced responses after stress. Intriguingly, several

miRNAs may target the same transcript forming a co-targeting network and implying redundancy in miRNA function[26].

Through regulating the expression of various effectors that function at different steps in complex biological pathways, miRNAs can coordinate important cellular processes such as cell differentiation, metabolism, and apoptosis[23]. Thus, miRNAs are able, by combining mild effects on multiple individual mRNA targets, to act synergistically within a common pathway in order to exert a more pronounced outcome[26]. Because miRNAs contribute to the gene expression in various burdensome diseases like cancer and cardiovascular diseases[1], they have emerged as an important field of study. Nonetheless, taking into consideration the complexity they present, studying the functions or manipulating their effects presents great challenges[27].

1.1.1.2 RNA Binding Proteins (RBPs) for the processing of miRNAs

RBPs are proteins that are capable of binding double or single stranded RNA in cells and participate in forming ribonucleoprotein complexes that are involved in gene expression[28]. They participate in the process of the post transcriptional gene regulation of coding and non-coding RNAs involving the transport, maturation and stability of the transcripts. RBPs bind RNAs using sequence and/or structural motifs in RNA molecules via using RNA-binding domains (RBDs) such as the RNA recognition motif (RRM)[29], K homology (KH) domain[30], DEAD box helicase domain[31], double-stranded RNA-binding motif (DSRM) or a zinc-finger domain[32]. Different mRNA-binding domain classes of RBPs are found in high frequency either in multiple repeats or in combination with other RBDs[33]. The most prominent example is that of ssRBD such as RPMs, KH domains and zinc-finger domains, that recognise motifs of 4-6 nucleotides and work in combinations[34]. Nonetheless, recent findings in respect of the structure and the function of the RBPs through the study of RNP machines like the spliceosome[35,36,37] and the ribosome[38,39,40], reveal the complexity of unconventional protein-RNA interactions that do not necessitate canonical RBDs.

RBPs exert effects on the miRNA biogenesis by interacting with Drosha, Dicer and specific miRNAs. RNase III proteins often interact with dsRBD proteins, such as Dcr-1 in *Drosophila spp.* that binds one of the two isoforms of Loquacious (Loqs), Loqs-

PA and Loqs-PB, necessary for the production of most miRNAs, each of which contains three dsRBDs[41,42]. Furthermore, a set of proteins, such as p68 and p72 are essential for the processing of a subset of miRNAs by Drosha[43] while proteins R-SMAd, SMAD1–3, SMAD5 and p53 modulate the activity of the Microprocessor complex through interaction with p68[44,45,46]. TDP43 RBP was reported to increase Drosha's stability[47] and to promote Drosha and Dicer processing[48]. It has also been demonstrated that human Dicer interacts with TAR RNA-binding protein (TRBP), a homologue of Loqs-PB, in a similar way[13,49] while cofactor PACT, that harbours a dsRBD, has also been shown to associate with mammalian Dicer[50]. Similarly, TRBP regulates the efficiency of processing of certain pre-miRNAs and regulates mature miRNA length[51]. Nonetheless, contrary to Loqs, mammalian TRBP or PACT are not essential for the Dicer-mediated processing of the pre-miRNA processing[49].

Moreover, various proteins have been reported to selectively bind the terminal loop of pri-miRNA. RBPs heterogeneous nuclear ribonucleoprotein A1 (HNRNPA1) and KH-type splicing regulatory protein (KSRP) facilitate the processing by Drosha via binding to the terminal loop of pri-miR-18a and pri-let-7[52,53]. Moreover, pri-let-7 is also regulated by LIN28A and its paralogue LIN28B, that bind its terminal loop and arrests both Drosha and Dicer-mediated processing.

Additionally, negative feedback loops between miRNAs and RBPs that regulate their expression levels have been reported. Human DICER1 mRNA is targeted by let-7 miRNA[54]. RBPs partake in the regulation of the processing of pre-miRNA. KSRP, interacts with the terminal loop of various pre-miRNAs and modulates their maturation process through affecting the Dicer-mediated processing[55] while LIN28 proteins, through binding to the terminal loop of pre-let-7, regulates the processing by Dicer by inducing oligouridylation of the pre-miRNA[56]. Additionally, modifications in the sequence of the stem loop of miRNA, through RNA editing with ADAR1, have demonstrated diminished maturation either at the processing by Drosha, as in the example of pri-miR-142[57], or by Dicer, as in the example of pre-miR-151[58].

1.2 Abdominal Aortic Aneurysm (AAA)

AAA is defined as a focal dilation of the wall of the abdominal aorta due to the loss of its elasticity, exceeding 50% of its normal size[59]. It corresponds to a region of the abdominal aorta that has weakened wall and is dilated usually affecting the infra-renal segment[60], (Figure 1.5). Aneurysmal disease is more common in the elderly population (>65 years old) with its prevalence in western populations being 0.4–0.67%[61]. Although mortality rate of AAA is improving because of the better intervention techniques[62], it still is a significant cause of death[63,64].

Figure 1.5. Angiogram of AAA. 3D MR angiogram with horizontal line demonstrating the location of the infrarenal area that present AAA. The distance from the left renal artery is showcased with a double-headed arrow. From Kramer et al., 2007.

Risk factors for development of AAA include advanced age (>65 years old), gender, with males presenting higher prevalence, genetic predilection via family history, obesity and smoking[66,67].

AAA is an asymptomatic disease[68], a characteristic that renders it more dangerous since patients are unaware of their condition. A major implication of the disease is the

acute rupture of the aneurysm, which leads to heavy bleeding into the abdomen that can be fatal and is associated with up to 80% mortality[61]. Given the burden of AAA and the lack of symptoms, that makes the diagnosis more difficult, there is a high interest for the discovery of new biomarkers that could indicate AAA development and rupture.

1.2.1 AAA pathogenesis

Although aneurysm formation is a complex process multiple histological features, important for the development of the disease, have been described such as vascular inflammatory processes, extracellular matrix (ECM) degradation and vascular smooth muscle cells (VSMCs) apoptosis[69]. In more detail, chronic infiltration of inflammatory cells in the adventitial and medial layers of the aorta, elastin degeneration and medial attenuation have been reported to participate in the formation of the disease[69]. These inflammatory stimuli together with mechanical injury that lead to phenotypic changes affect the proliferation, migration and apoptosis of the cells[70]. The infiltration of macrophages, leukocytes and lymphocytes[71], that lead to a higher production of cytokines under the effects of which the inflammatory response progresses further, results in neovascularisation, loss of SMCs and matrix degradation[72,73,74]. Further to this, ECM degradation seems to advance due to locally increased levels of matrix metalloproteinases (MMPs), cysteine and serine proteases which result in different degradation among collagen isoforms (type I and III) and the degradation of elastin which affects the elasticity of the aorta[75].

Moreover, both T-cells and B lymphocytes have been shown to be abundant in aneurysmal tissues and therefore they have been implicated in the progression of AAA process while depletion of B-cell has protective effects against the disease[71]. Additionally, regulatory T-cells have a protective effect against the formation of AAA with the secretion of IL-10 and TGF-β being implicated by stabilising the aneurysm[73] while CD4+ T-cells have been linked to the pathogenesis of AAA[71].

1.2.2 SMCs in health and in AAA disease

1.2.2.1 SMCs function and biology

VSMCs have been shown to play a major role in the pathogenesis of many disorders such as the aortic aneurysm formation, as they are key components of blood vessels[76]. They regulate the diameter of small arteries, controlling blood pressure and they are the main cells that constitute the aortic wall able to synthesise ECM proteins, participate in the regulation of proteases and protease inhibitors and recruit inflammatory cells upon cell injury. VSMCs do not proliferate at high rate, under physiological conditions, unless they undergo a phenotypic switch, from contractile to proliferating phenotype, as a response to stimuli like vascular injury and hypertension[77]. Additionally, the ability of VSMCs to contract and proliferate is affected by mechanical forces, ROS, ECM components and the TGF-β and SMAD3 signalling among others, changes that occur during aneurysmal formation[78, 79, 80]. In light of this, the pathophysiology of aortic aneurysms is associated with VSMC apoptosis and ECM proteins and elastin degradation, features that distinguish it from atherosclerosis albeit the common risk factors[81]. However, it is not clear how VSMCs participate in the formation of AAA. They can contribute to the development of the disease through inflammation and production of MMPs[82], while a third pathway of differential production of ECM has been suggested. It has been reported in mouse models that aneurysm formation can be reversed through prevention of VSMC apoptosis with caspase inhibitor treatment[83], data that support the important role of VSMCs in aneurysm pathogenesis. It, therefore, becomes clear that VSMCs can exert important control on the homeostasis of the aortic ECM.

Although VSMCs partake in the onset and development of aortic aneurysms through loss of synthetic capability, due to cell apoptosis or other mechanisms[84], there is growing evidence that aortic VSMCs are also capable of participating in the degenerative process[85]. Degradation of the ECM of the aortic wall by elastases has been considered to be predominantly due to the infiltration of inflammatory cells[86], namely macrophages[84] as well as neutrophils[87] and mast cells[88], as it has been shown by studies in murine models[89]. However, it has also been reported that apoptosis of aortic VSMCs may contribute to the pathogenesis of AAA via reducing the repair rate of the damaged aortic wall[90] while AAA-derived cells demonstrated increased levels of proteases and cysteine classes that participate in the elastolysis[82].

More specifically, a lack of upregulation of Tissue Inhibitor of Metalloproteinase (TIMP) -1 and -2 was reported while there was considerable upregulation of TIMP-3 whilst there is an increased MMP activity data that support an imbalanced proteolytic state[91].

These findings suggest that VSMCs can also participate in the formation of AAA through degradation of ECM via elastolytic activity[82]. In addition, evaluation of interactions of VSMC with macrophages demonstrated a significant increase in the elastolytic activity of the AAA-derived cells[82]. Further studies showed that in the case of AAA, the protein levels of MMP-9 and MMP-2 protein levels are substantially increased compared to non-AAA cells. Elevated levels of MMP-2 and MMP-9 activity have been reported in the aneurysmal part of the mouse aorta after AngII infusion[92]. MMP-9 is the most abundant gelatinolytic MMP and is secreted in high levels in AAA tissue with MMP-9-deficient mice demonstrating normal levels of the elastic lamellae in the aortic wall and, interestingly, resistance to the development of aneurysm[85]. These data suggest a posttranscriptional regulation in normal cells that is abrogated in the context of AAA[82]. A meta-analysis on serum and plasma levels has implicated higher levels of circulating MMP-9 to AAA[93] while the macrophage origin of the MMP-9 was shown when mice were infused with non-MMP9-deficient macrophages, reversing the protection effects on AAA[94]. Taken together, these data demonstrate that VSMCs, in the case of AAA, present a pro-elastolytic phenotype that is further pronounced in the presence of activated macrophages. This appears to be the effect of differentiated post-transcriptional control of MMP-9 synthesis resulting in activation of elastolytic MMPs[82].

1.2.2.2 MiRNAs and AAA

The maintenance of the physiological function of the cardiovascular system is of high importance for mammals while miRNA networks orchestrate cellular homeostasis, vascular inflammation, angiogenesis and metabolism and have been implicated in the control of important biological processes in the cardiovascular system and in many aspects of the development and pathophysiology of cardiovascular diseases[95]. A plethora of miRNAs, from the same or different families, have been implicated in various cardiovascular diseases, a feature that demonstrates the significant role the miRNA networks play in the physiology of the heart and blood vessels as well as the sensitivity they both demonstrate to disease[26, 96,97]. Studies have reported

perturbations in the levels of a vast number of miRNAs in both humans and mice models for many cardiovascular diseases such as heart failure, myocardial infarction, atherosclerosis and AAA[26, 98].

MiRNAs have also been strongly implicated in the formation and development of the AAA. Gain- and loss-of-function assays have demonstrated a direct link of specific miRNAs with AAA and highlighted the potential they have as novel targets for therapeutic applications[99,100,101,102]. Accumulating data, demonstrate that they are important regulators of the function of vascular cell homeostasis in atherosclerotic and inflammatory processes. As an example of the role of miRNAs in the function of SMCs, postnatal Dicer deletion led to loss of contractile differentiation for VSMCs and to lower blood pressure[103]. A variety of miRNAs have been connected with remodelling of vascular cells including miR-126, miR-10a, miR-143~145 and the miR-15/16 families[26, 104].

In more detail, in the vasculature, inhibition of miR-29 has been correlated with the reduction of the aortic aneurysm formation[105]. Additionally, members of the miR-15 family have been implicated in collagen remodelling and the postnatal silencing of elastin in aortas[101, 106]. Intriguingly, miR-195, a member of the miR-15 family, is known to share many of the same targets as miR-29b[101] with the seed sequence of miR-15 miRNAs (5'-AGCAGC-3') differing only by one nucleotide from that of the miR-29 family miRNAs (5'-AGCACC-3'). Proteomic analysis of the secretome of murine aortic SMCs revealed that miR-195 targets a group of ECM proteins, including elastin, collagens and proteoglycans. In mice treated with antagomiR-195, higher aortic elastin expression was associated with an increase of MMP-2 and MMP-9 while in human plasma the presence of AAA and aortic diameter was inversely correlated to the levels of miR-195[98].

1.2.2.3 MiR-195 and AAA

MiR-195 is a member of the miR-15 family and is located on chromosome 17 in humans and chromosome 11 in mice (Supplementary Table 1). It is transcribed together with miR-497 in one primary transcript, forming a homo-cluster since both miRNAs are members of the same miRNA family and they share the same seed sequence and high homology throughout their sequence (Figure 1.4). Although miR-

15 family and specifically miR-195 is not studied as intensely as other miRNAs, it is known to participate in various disorders like cardiovascular diseases and tumorigenesis[98, 107].

The ECM is an important component of the structure of aortic wall that determines the formation of aneurysm by the dilatation of the aortic wall[108]. AAAs are characterised by decreased levels of elastin and high turnover of collagen. Various miRNAs have been implicated in collagen turnover and as a result also in the development of the disease, with the members of the miR-15 family participating in postnatal silencing of elastin[101]. The murine miR-15 family consists of 6 highly conserved microRNAs (miR-15a, miR-15b, miR-16-1, miR-16-2, miR-195, and miR-497), which are clustered in 3 separate chromosomes. They have a common seed region (AGCAGCA) and varying degrees of sequence homology in the 3′ region of the mature microRNA[109,98]. Expression of miR-195 and miR-497, miRNAs that are transcribed in the same primary transcript, is altered in human aortic specimens[110] while various ECM transcripts have been shown to be directly targeted by miR-195 in H4 cancer[111] results that were confirmed *in vivo* in murine models where antagomiRs to miR-195 upregulated elastin levels[98].

Although miR-195 is not extensively studied in the context of AAA[98], data from preliminary studies suggest that downregulation of the miRNA lead to de-repression of MMP-2 while it is implicated in the downregulation of Smad3 levels by directly targeting it, thus leading to decreased proliferation of VSMCs, and increased expression of Collagen III[112]. From the above, it becomes clear that miR-195 is strongly correlated with the onset and the development of the disease although further studies are needed to conclusively demonstrate the connection.

1.2.2.4 MiR-143~145 in AAA

MiR-143 and miR-145 are two highly conserved miRNAs that form a hetero-cluster with their genes located on chromosome 5 in humans and chromosome 18 in mice (Supplementary Table 1). They are transcribed as one primary transcript although the two miRNAs do not share any sequence homology and belong to different miRNA families.

MiR-145 is highly expressed in VSMCs of healthy rat carotid arteries[113] while expression of both miRNAs of the cluster are observed during the differentiation of stem cells to VSMCs[114]. The miR-143~145 cluster has been implicated both in the differentiation and proliferation of the VSMCs since it has been reported that downregulation of their expression leads to higher proliferation of the cells with upregulation of their levels having the opposite effect[114]. ELK1 and KLF4 are among the validated targets of miR-143 and miR-145, respectively, and both factors control the differentiation of the VSMCs. In more detail, ELK1 promotes the proliferation of the cells while KLF4 regulates the contractile phenotype of the cells. Targeting by the miR-143~145 cluster modulates the phenotypic switch[114, 115].

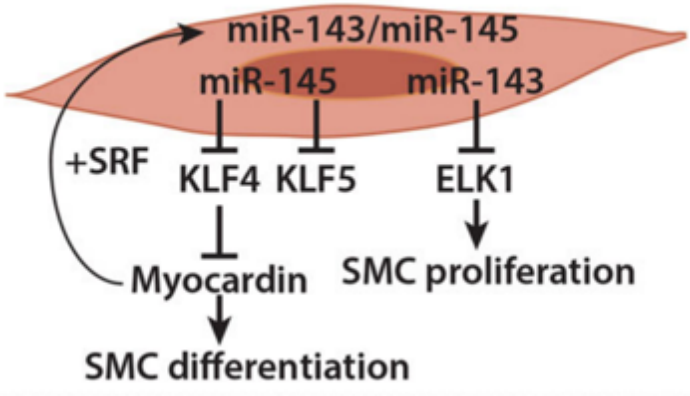

Figure 1.6. Hetero-cluster miR-143~145 controls VSMC differentiation. VSMC differentiation is regulated by Myocardin and myocardin-related transcription factors which also regulate the expression of miR-143 and miR-145 through a feedback loop. Inhibition of KLF4 miR-145 leads to SMC differentiation while targeting of ELK1 by miR-143 inhibits proliferation of SMCs. From Welten et al., 2016.

Studies in murine models where an IRES-lacZ promoter was fused to the pre-miR-143 sequence demonstrated that the expression of mmu-miR-143 and mmu-mR-145 in heterozygous mice was active in the heart in early developmental stages but at later stages was exclusively expressed in SMCs in the cardiovascular system, bladder and lungs, among other organs, while their expression levels were stable across adulthood[78]. These data unveiled miR-143~145 as a cell-type specific cluster for the regulation of the SMCs.

Although data from AAA tissues showed that there was no differences in the levels of neither miR-143 nor miR-145 when compared to healthy tissue, studies on intracranial aneurysm and thoracic aorta aneurysm demonstrated a decrease in the levels of both miRNAs[116,117,118]. Additionally, data from double knock-out mice revealed differences both in the structure and the phenotype of the VSMCs of the aorta as well as an increase in the migration and proliferation rate of the cells[78, 119]. More specifically, a significant decrease in the numbers of contractile VSMCs were observed by electron microscopy and a phenotypic switch to a synthetic phenotype was demonstrated together with the decrease in the size of the cells, alterations that contributed to a thinner size of the aorta. These data, together with the fact that neither the number nor the size of VSMCs were differentiated in other arteries of adult knock-out mice, suggest that the differences observed in the aorta were due to the phenotypic switch of the cells and to their lack of ability to adjust to the environment[78].

In fact, accumulation of synthetic VSMCs in knock-out vessels has been implicated in the loss of the vessels' ability to develop the same contractile forces. Synthetic VSMCs, contrary to the proliferative ones, demonstrate contractility defects that influence the response of the mutant vessels while various mechanisms have been implicated in the development of this phenotype. These suggest that miR-143 and miR-145 exert control the phenotypic switch to synthetic cells of smaller size that display reduced response to receptor-mediated signals[78].

1.2.2.5 MiR-17~92 cluster in cardiovascular diseases

MiR-17~92 is a well-studied cluster that has been implicated in many diseases including tumorigenesis, aging, neurodegenerative as well as cardiovascular diseases[120, 121]. It is located on chromosome 13 in humans and chromosome 14 in mice (Supplementary Table 1) and is transcribed in one primary transcript, pri-miR-17~92, harbouring 6 miRNA hairpins, miR-17, miR-18a, miR-19a, miR-19b-1, miR-20a and miR-92a-1 that comprise four different miRNA families[122].

Two paralogues of the main cluster have also been described (Figure 1.7), the miR-106b~25, located on chromosome 7 in humans, (7q22.1), in the 13th intron of the MCM7 gene, and chromosome 5 in mice, and the miR-106a/363 cluster, located on chromosome X in both organisms (Supplementary Table 1). In more detail, miR-106b~25 consists of six miRNAs miR-106a, miR-18b, miR-20b, miR-19b-2, miR-92a-

2 and miR-363 (Figure 1.7, middle panel) with miR-106b~25 cluster comprising three miRNAs, miR-106b, miR-93 and miR-25 (Figure 1.7, lower panel). Both miR-17~92 and miR-106b~25 are expressed abundantly in multiple tissues although miR-106a~363 is expressed at lower levels[120, 123]. MiR-17~92 cluster, together with the paralogue ones, presents a combined total of 15 miRNAs that form four miRNA families grouped according to their seed sequences, the miR-17 family, the miR-18 family, the miR-19 family and the miR-92 family.

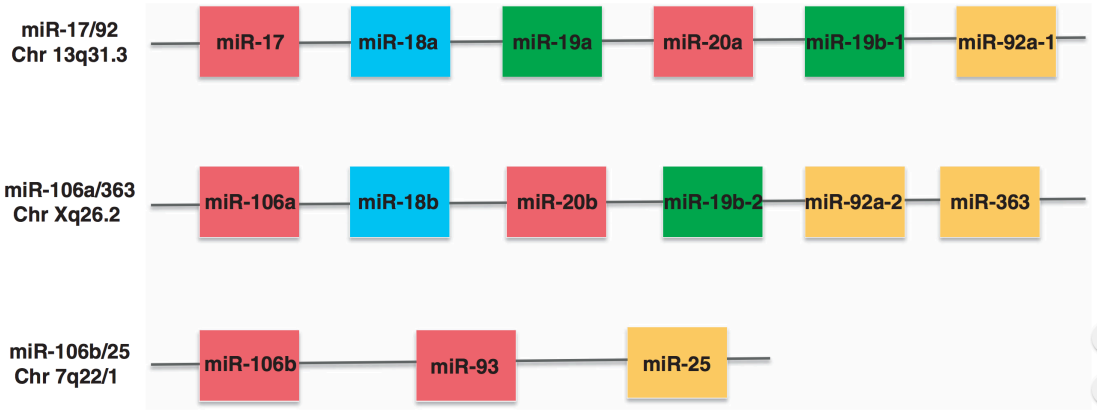

Figure 1.7. Schematic representation of miR-17~92 genomic locus cluster along with the genomic loci of its paralogue clusters. MiR-17~92 cluster consists of 6 members that form families with miRNAs that belong to paralogue clusters, miR-106a~363 and miR-106b~25. MiRNAs depicted in red rectangular belong to the miR-17 family, in blue rectangular to the miR-18 family, green to miR-19 family and orange to miR-92a family. From Mogilyansky et al., 2013.

Upregulation of miR-19a, miR-19b and miR-92a is implicated in the development of AAA, implying a differential expression for these miRNAs due to post-transcriptional regulation[124]. Additionally, different miRNAs of the cluster show implication in the control of different pathways of the pathophysiology of AAA and the development of the disease[125-127]. More specifically, phosphatase and tensin homolog (PTEN) is one of the validated targets of the cluster as shown in *in vitro* experiments[128]. MREs for miR-19a and miR-19b-1 have been reported in the 3'-UTR of PTEN while introduction of the two miRNAs in miR-17~92-deficient cells repressed PTEN expression levels[120].

However, studies on the vascular expression of miRNAs miR-19a and miR-19b-1 are limited and provide controversial results. Although studies in murine endothelial differentiation of stem cells have reported increased miR-19 levels, antagomir administration did not affect endothelial markers expression[129]. Additionally, miR-92a

is highly expressed in endothelial cells with this overexpression inhibiting angiogenesis in ischemic conditions[130]. Studies in endothelial cells isolated from patients with coronary artery disease (CAD) demonstrated elevated levels of both miR-17 and miR-92a[131] while studies in patients with acute coronary syndrome demonstrated increased levels of miR-19a contrary to the results from patients with CAD where a decrease in miR-19a levels was observed compared to healthy controls[132].

TGF-β has been shown by numerous studies to be implicated in every step of the development of AAA and TGF-β signaling has been shown to be down-regulated in human AAA[133] while in murine models it inhibits AAA[134]. TGF-β has been implicated in the inhibition of infiltration of inflammatory cells[135] while it promotes elastin and collagen formation[136]. By doing so, TGF-β hinders the degradation of the ECM of the aortic wall by inhibiting the TNF-α-induced MMP-9 expression[137].

Interestingly, the miRNAs of the cluster show antagonistic effects with regards to the regulation of various targets and pathways. MiR-18a, miR-19a, miR-17 and miR-20 have been reported to target the TGF-β tumour suppressor pathway, thus facilitating tumour angiogenesis, while miR-17 and miR-20 target the E2F transcription factor family[138-142]. In contrast to the effects mentioned above, miR-92a, which resides in the same cluster and is transcribed in the same primary transcript, has been shown to have antiangiogenic activity[130], features that highlight the regulation that the miRNA clusters exert in the same pathways and how they can control the equilibrium in these pathways by targeting different proteins that have contrasting effects.

With regards to SMCs, studies in mouse models of Pulmonary Hypertension (PH) showed that knock out of miR-17~92 cluster in SMCs attenuated hypoxia-induced PH whilst reconstitution of the expression of the cluster restored the condition. Additionally, it was demonstrated that miR-17~92 regulates SMC phenotype via the PDLIM5/transforming growth factor TGF-β 3/Smad3 pathway[143]. Furthermore, miR-17~92 is able to act on TGF-β and multiple TGF-β receptors, by inducing TGF-β 3 signaling to restore the differentiated SMC phenotype.

Discrepancies in the proliferation of VSMCs result in vascular remodeling and serve a key role in several vascular disorders, including atherosclerosis[144], pulmonary artery hypertension[145] and AAA[146]. However, the molecular mechanism underlying VSMC proliferation remains unclear. Studies have indicated that miRNA may also have roles in AAA through controlling the physiology and proliferation of VSMCs[121]. Studies have revealed that the miR-17~92 cluster promotes VSMC proliferation in a murine model[147] and mediates inhibition of VSMC proliferation via bone morphogenetic protein receptor type II (BMPR2)[148] while overexpression of miR-17 with mimics demonstrated that miR-17 stimulates VSMC proliferation. MiR-17 also targets the 3'-UTR of retinoblastoma (RB) protein, which regulates the proliferation rate of the VSMCs[149]. These results suggested that overexpression of miR-17 stimulated VSMC proliferation and enhanced cell cycle progression through promoting G1/S transition by increasing the levels of PCNA and E2F1.

Excess proliferation of VSMCs and inflammation have a key role in several vascular disorders while proliferation of VSMCs under inflammation is regulated by NF-κB p65/microRNA-17/RB pathway activation[150]. It has been previously shown that NF-κB regulates miR-143 expression, enhancing the metastasis of hepatocellular carcinoma[151]. The transcription factor NF-κB is activated in and is a master regulator of the vascular inflammatory response in many vascular diseases, including AAA formation[69]. NF-κB p65 signalling directly regulates the miR-17 promoter activity, through potential p65 binding sites in the upstream regulatory region of the miR-17 gene, while suppression of RB levels, by activation of p65, was de-repressed when miR-17 was downregulated with inhibitors[150]. NF-κB p65 regulates the expression of miR-17, while miR-17 directly targets RB which modulates the proliferation of VSMCs through interacting with E2Fs. Taken together, these data support that VSMC proliferation is regulated by the NF-κB p65/miR-17/RB pathway[150].

1.2.2.6 Limitations in miRNA research

Although, modulating miRNAs expression enables us to elucidate their role in disease, the specific inhibition of certain miRNAs can be cumbersome. So far, there are two common approaches employed in the research of miRNA inhibition: the antimiRs and the antagomiRs.

AntimiRs are chemically modified, single stranded DNA oligonucleotides that are used to inhibit miRNAs. They can be partially or fully complementary to their corresponding miRNA and they work by hybridising to their target miRNAs, thus inhibiting their function[152]. Nonetheless, due to their small size, the employment of antimiRs as a tool in miRNA studies carries the risk of affecting RNA molecules of even partial complementarity and miRNAs other than the targeted one, thus inducing unwanted inhibition of miRNAs of the same family (Figure 1.8).

Moreover, antagomiRs are synthetic, single-stranded RNA analogues that are used in animal models which are fully complementary to miRNAs. They are 3' cholesterol-conjugated, to facilitate the uptake by the cells, and they can inhibit miRNAs by hybridisation[153]. Systemic administration of the antagomiRs can effectively reduce the levels of the targeted miRNAs for a sufficient amount of time[152]. However, given that miRNAs of the same family share the same seed sequence, it becomes apparent that antagomiRs may have adverse effects. They are unable of providing specific targeting, and thus inhibition, of only one miRNA but instead they result in inhibition of multiple miRNAs of one family.

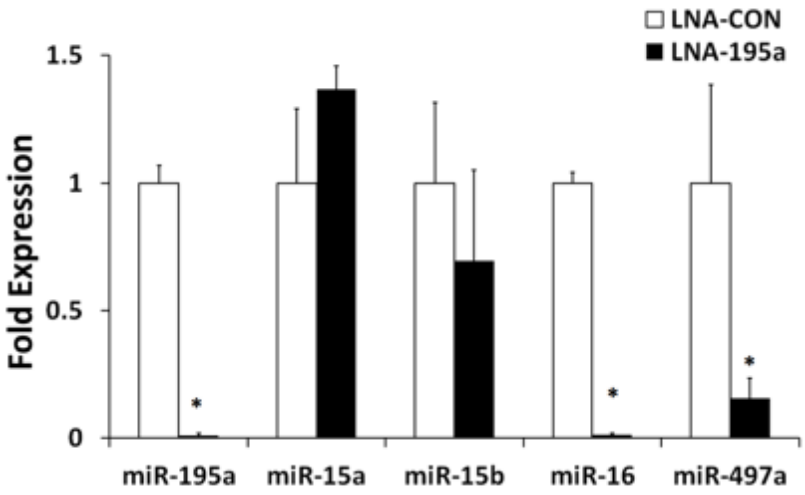

Figure 1.8. Expression levels of 5 members of the miR-15 family upon inhibition mmu-miR-195a. The levels of 5 members of the miR-15 family were quantified with qPCR following transfection of mouse VSMCs with LNA-195a. Except for mmu-miR-15a, the other miRNAs show a downregulation with mmu-miR-195a, mmu-miR-16 and mmu-miR-497a showing statistical significance. Lataniotis et al., 2017.

Taking into consideration the short length of the mature miRNAs (19-24 nucleotides) and that miRNAs of the same family share the highly homologous 7 nucleotide seed

sequence, it becomes evident that in order to sufficiently inhibit specific miRNAs, without affecting miRNAs of the same family, a different approach is needed. Given the higher diversity of the genomic loci among different miRNAs, targeting the genomic locus of a miRNA gene rather than the mature product seems to be a promising alternative. Editing the miRNA genes will subsequently affect the maturation process and will result in sufficient inhibition of specific miRNAs. Various gene editing platforms have been developed over the past years. Zinc-Finger Nucleases (ZFN), Transcription Activator-like Effector Nucleases (TALENs) and Clustered Regular Interspaced Short Palindromic Repeats (CRISPR) as well as studies *in vitro* and in multiple organism models have employed the above mentioned techniques to specifically inhibit miRNAs[154, 155, 156, 157, 158].

1.3 Gene editing

Gene editing is defined as DNA engineering that results in the deletion, insertion or insertion of specific sequences. Many platforms have been developed and used over the last few decades.

ZFNs was historically the first platform of gene editing of eukaryotic genome to be developed. It contains zinc-binding sequences in their DNA-binding domains and can provide specific recognition of sequences[159, 160]. Zinc domains can be modified to recognise any triplet of DNA thus being able to target any DNA sequence in eukaryotic cells[161]. Fused to bacterial endonuclease FokI and used in pairs, ZFNs can be employed to induce double stranded breaks (DSBs) effectively in any DNA sequence.

Alongside, TALENs employ TAL effector DNA-binding domains that is able to specifically recognise single nucleotides thus rendering their employment easier and faster than ZFNs leading to DSBs in living cells[162,]. In more detail, TALENs are able of being engineered in order to target any DNA sequence in the genome. For a DSB to be induced a pair of TALENs is engineered to recognise a 20nt DNA sequence. Each TALEN of the pair, fused to FokI, recognises and binds the sequence flanking the targeted position and induces a DSB [163, 164].

In addition to these techniques, a new and highly versatile RNA guided gene-editing technique, CRISPR/Cas, which is able to target DNA or RNA sequences with high specificity, has emerged as an attractive platform for specific gene editing. CRISPR was first described over 3 decades ago as a locus harbouring high numbers of short direct DNA repeats interspaced by short sequences[165]. A series of publications demonstrated that CRISPR is an adaptive immune system that, in nature, is used by bacteria as a defence mechanism against phages, upon re-infection[166, 167, 168, 169, 170, 171].

In the current study, the CRISPR/Cas9 platform was assessed as an alternative to the traditional miRNA inhibition techniques in order to inhibit specifically miRNAs by targeting the miRNA genomic locus rather than the mature RNA sequence.

1.3.1 Clustered Regularly Interspaced Short Palindromic Repeat (CRISPR)/ CRISPR associated (Cas)

CRISPR/Cas is an adaptive immune system, naturally found in ~50% of bacteria and 90% of archaea[172] and was firstly described in 1987[165]. The CRISPR locus consists of DNA sequences that encode for proteins and for a series of DNA repeats that are interspaced by non-repetitive DNA sequences originating from phages[173]. According to the organisation of their locus and the Cas proteins that are used, CRISPR/Cas systems are classified in six types (I-VI), (Figure 1.9)[174].

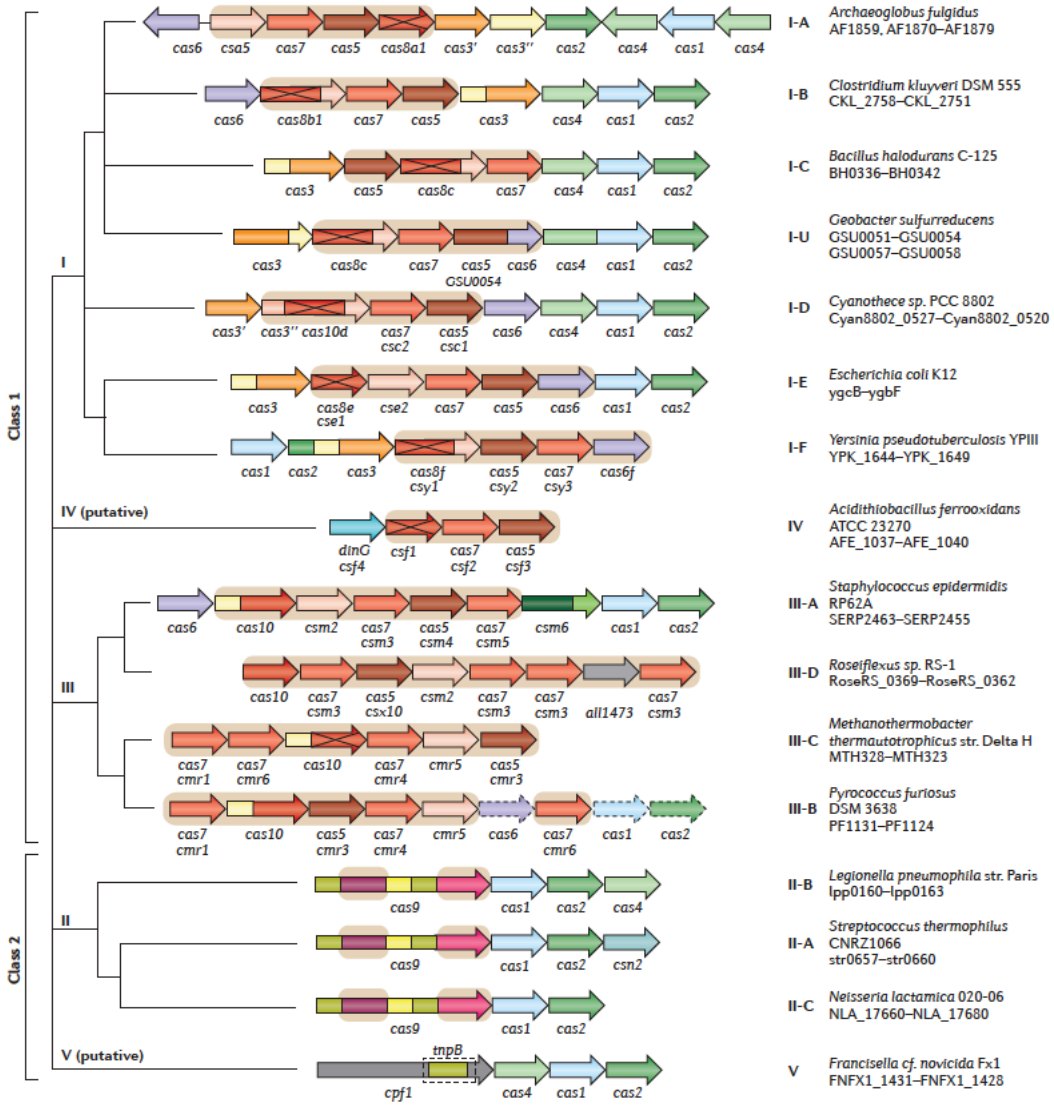

Figure 1.9 Classification scheme for Cas proteins. Two classes, and five types (the best described ones) of Cas proteins are presented along with *a s*chematic representation of the *operon and its* organisation together with the domain architecture. For each type of Cas system the name of the gene is indicated for each subunit. Genes that are homologous are colour-coded and identified by a family name. Genes and gene regions encoding components of the interference module (crRNA or Cas9 proteins) are highlighted with a light brown background. The adaptation nucleases (*cas1* and *cas2*) and *cas6* are dispensable in subtypes III-A and III-B. Also the regions of *cas9* that correspond to the RuvC-like nuclease (green), HNH nuclease (yellow), recognition lobe (purple) and PAM recognizing domain (pink) are depicted. The regions of cpf1 (also known as Cas12a) aside from the RuvC-like domain are shown in grey. Makarova et al., 2015.

Although there is a plethora of Cas proteins that are used in CRISPR systems in nature, the type II endonuclease Cas9 form *Streptococcus pyogenes* (SpCas9) is of particular interest since it is the Cas protein that is employed in the vast majority of studies. The reason for this is that although its relative big size (1,368 amino acids, 4.10 kbp)[175] in type II CRISPR systems only one Cas protein is used, contrary to

the other types that utilise multiple proteins to induce the DSB[176], (Figure 1.10). Regarding the organisation of the locus, viral sequences, that derive from viral genome after unsuccessful infection, are incorporated in the CRISPR repeat-spacer array with the help of the adaptation proteins of the cas operon (Figure 1.10).

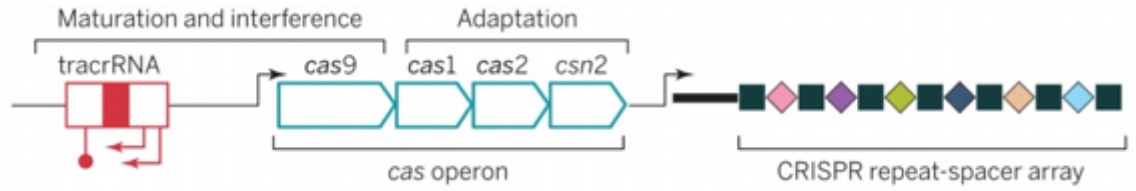

Figure 1.10. CRISPR genomic locus. The type II CRISPR locus from *Streptococcus pyogenes* is shown as an example. The CRISPR genomic locus is comprised of the Cas genes, the tracrRNA and of regularly interspaced repetitive sequences (spacers) that are processed to crRNA. The spacer sequences are complementary to viral DNA and are used for targeting viruses upon re-infection. From Doudna and Charpentier, 2014.

These sequences are transcribed into the precursor CRISPR RNA (pre-crRNA) that shares partially complementarity with the trans-activating crRNA (tracrRNA). This complementarity is used for the tracrRNA to bind the pre-crRNA in a duplex (pre-crRNA:tracrRNA) that is then recognised by RNase III and cleaves the pre-crRNA to mature crRNA[178] (Figure 1.11). The tracrRNA is then bound on the Cas9 protein and is used as a tether for the crRNA which guides the endonuclease to target specific DNA sequences according to the its sequence[179].

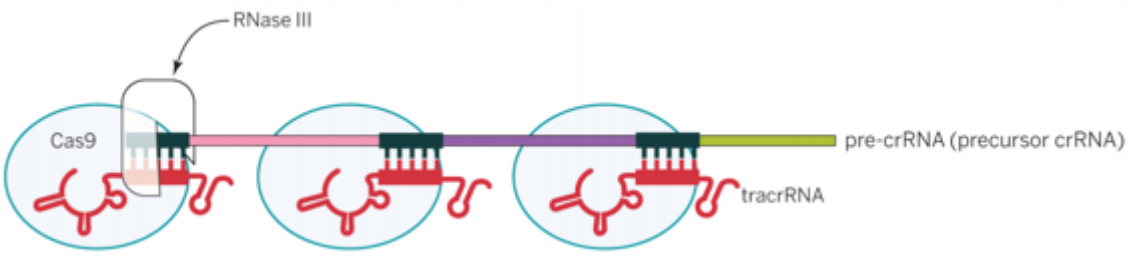

Figure 1.11. Precursor crRNA maturation. In nature, CRISPR locus is transcribed on a regular base and subsequently the spacer sequences are transcribed into pre-crRNA. The pre-crRNA shares a partial complementarity with the tracRNA and is bound by it. With the help of tracrRNA, the pre-crRNA is recognised by RNase III which then cleaves it into a mature crRNA. The functional crRNA:tracrRNA and Cas9 complex is then able to target the complementary viral sequence and degrade it by cleaving it. From Doudna and Charpentier, 2014.

As immune system, CRISPR/Cas9 in *Streptococcus pyogenes* functions by recognising and binding a tri-nucleotide sequence of the form 5'-NGG-3', called

Protospacer Adjacent Motif (PAM). DNA of the invading virus. Following the PAM binding, Cas9, using the crRNA as a guide, interrogates the adjacent sequence, through Watson and Crick base pairing, and if there is enough complementarity, it induces a blunt-end double stranded break (DSB), using its activated endonuclease domains, 3-4 nucleotides upstream of the PAM[179]. In order for the DSB to happen, the first 17-20 nucleotides of the 5'-end of the crRNA need to be complementary to the targeted sequence. Two separate endonuclease domains, HNH and RuvC, induces the DSB at 3 nucleotide upstream of the PAM (Figure 1.12)[179].

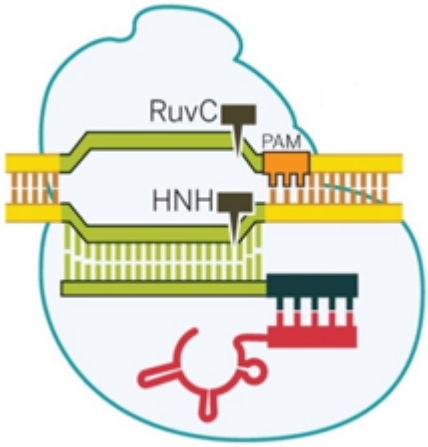

Figure 1.12. CRISPR/Cas9 in nature. The crRNA:tracrRNA duplex is of paramount importance for the function of the CRISPR/Cas9 system. By binding to the crRNA through its complementarity, the tracrRNA keeps it bound to the Cas9 protein which uses it as a guide to recognise the targeted sequence. This targeted sequence needs to be followed by a 5'-NGG-3'sequence for the SpCas9 to induce the DSB 3-4nt upstream of the PAM site with the RuvC and HNH domains. Adapted from Doudna and Charpentier, 2014.

Furthermore, it has been demonstrated that humanised SpCas9 is still functional in eukaryotic cells when the crRNA:tracrRNA is substituted by a chimeric single guide RNA (sgRNA) produced by fusing the 3'-end of the crRNA with the 5'-end of the tracrRNA (Figure 1.13) [179, 180], paving the way for fast, easy and cheap gene editing. SgRNA is an easy to design and fast to produce 20nt long RNA molecule that can be designed to target any sequence and is able of guiding SpCas9 to target and cleave any DNA sequence located upstream of the PAM sequence.

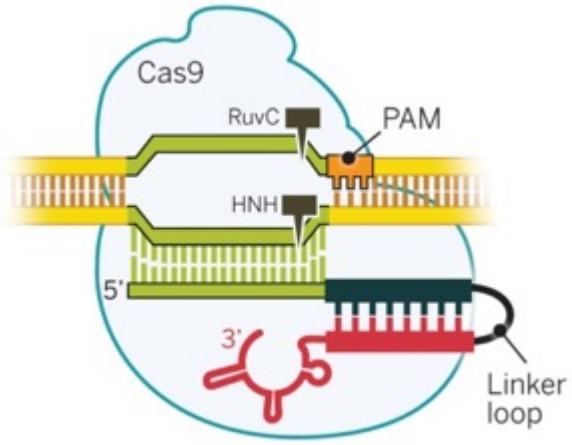

Figure 1.13. CRISPR/Cas9 with sgRNA. A chimeric sgRNA can be used in the place of crRNA:tracrRNA to guide the Cas9 protein to the targeted sequence. Upon recognition, Cas9 unravels the dsDNA using the PAM sequence, the first 20nt of the 5'-end of the sgRNA are bound to the targeted sequence and the Cas9 cleaves both strands of the DNA with two distinct domains with endonuclease activity, RuvC and HNH. From Doudna and Charpentier, 2014.

After the DSB, two different pathways can be employed to repair it: (A) the error prone Non Homologous End Joining (NHEJ), which alters the DNA sequence and can lead to premature stop codons, and (B) the Homology Directed Repair (HDR), which requires a highly homologous DNA template and can be employed for the insertion of specific sequences in the edited site (Figure 1.14).

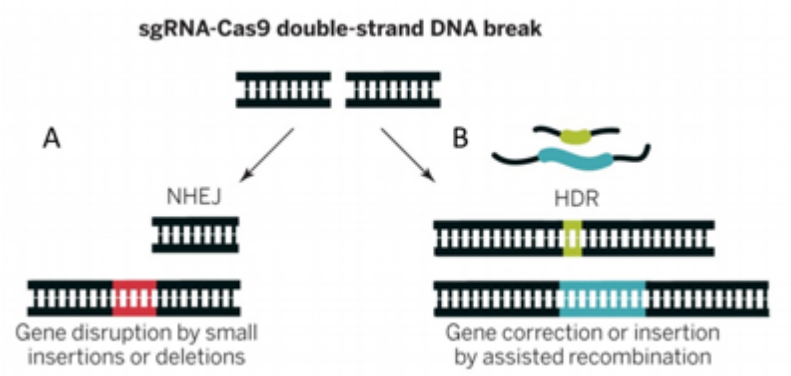

Figure 1.14. DSB repair in eukaryotic cells. Upon cleavage from the CRISPR/Cas9, the cell is trying to repair the DSB by following two distinct pathways. (**A**) The first, NHEJ, is an error prone repair which can potentially lead to a premature stop codon thus prematurely terminating the mRNA transcription, subsequently resulting to a non-functioning protein. (**B**) The second, less frequent pathway, HDR, can be employed for the introduction of specific sequences, such as genes or stop codons. Adapted from Doudna and Charpentier, 2014.

CRISPR/Cas9, due to its versatility, has emerged as an alternative to Zinc Finger Nucleases (ZFNs) and the Transcription Activator-Like Effector Nucleases (TALENs) gene editing techniques[181]. As an RNA-guided system, CRISPR/Cas9 is easier to use, faster to design and cheaper to produce compared to ZFNs and TALENs which rely on protein-DNA interaction. Moreover, since the 5'-NGG-3' motif is found in every 8 nucleotides, on average, in the human genome[182], CRISPR/Cas9, employing SpCas9, can be used to edit almost every genomic site. Adding to this, the discovery of new Cas proteins with different PAM requirements and different ways of inducing the DSB, expand the gene editing toolbox with new CRISPR/Cas systems that can be used to edit different genetic loci according to individual needs[183].

CRISPR's versatility and ease of use has sparked a series of publications that expand on the arsenal of gene editing providing myriad alternative options to SpCas9 depending on the chemical nature of the molecule (DNA or RNA), the sequence of the locus targeted, the nature of the intended induced DSB (staggered or blunt end) and the intended editing (gene disruption, DNA base editing, RNA base editing or RNA degradation) [183, 184, 185].

1.3.2 Limitations of CRISPR editing

CRISPR/Cas9 technology has revolutionised gene editing providing a highly advantageous platform for editing almost any sequence in the genome of multiple organisms, including humans and mice. Therefore, it is considered as being a highly promising approach to develop therapies against multiple diseases[186, 187] as well as an alternative to gene therapy, in order to battle a number of genetic diseases[188, 189, 190, 191, 192] . However, there are major innate limitations of the technique that hinder its universal application for therapeutic purposes. Namely, two of the most important limitations are the possibility of the off-target editing in unwanted loci and the delivery of the system, either in *in vitro* or *in vivo* models.

1.3.2.1 Off-target editing

Regardless of the advances CRISPR/Cas9 has introduced in the field of gene editing, important concerns remain about the possibility of inducing unwanted editing in non-

targeted sites. Although various, preliminary studies in murine models did not show any off-target editing[193, 194] the concerns about the precise editing of only the targeted sites have not yet convincingly addressed with further studying needed to decipher the full impact of CRISPR/Cas9 editing.

As described above, CRISPR/Cas9 employs a 20nt long sgRNA to target and edit DNA sequences[179]. The complementarity between the guide and the targeted sequence activates the endonuclease domains of Cas9. Regardless of the high specificity of the sgRNA to recognise and bind the targeted sequence, it can tolerate a small number (varying from 3 to 5) of mismatches in its sequence[195]. More specifically, the greater the distance of the mismatches from the 3'-end of the sgRNA the more tolerable the binding is, with nucleotides 2-8 (from the 3'-end) being the least tolerable[196]. Taken the short length of the sgRNA together with the relative tolerance to mismatches Cas9 can withstand into consideration, it becomes apparent that is likely that Cas9 is guided to target and induce DSBs in multiple unintended sites.

Software employed to design sgRNAs, addressing the problem of off-target mutagenesis, provide a list of putative off-target sites according to the tolerance of sgRNAs to mismatches. With regards to research and, more importantly, therapeutic and clinical applications of the system, off-target editing is a major concern. Although initial studies have provided data about the mechanism behind the recognition of off-target sites[196], data that are used for the prediction of sites of unintended editing, additional reports *in vitro* using mouse stem cells and differentiated human stem cells support that editing with CRISPR/Cas9 can lead to large deletions and sequence rearrangements[197]. These changes can potentially lead to editing oncogenes and/or protein coding genes resulting in severe implications.

Various strategies have been used to address the issue of unwanted editing. These include using shorter, 17nt long sgRNA, shortening the guide at its 5'-end which leads to a guide less tolerable to mismatches[195], the addition of two Guanine nucleotides at the 5'-end of the sgRNA[198], titrating the concentration of the Cas9 protein used[199], replacing the WT Cas9 with D10 nickases, where only one of the endonuclease domain is active, and using two sgRNAs flanking a specific point thus leading to immediate repair of any unintended edited sites[200], fusing inactive Cas9 (dCas9) with

FokI nuclease[201] and using phage-derived anti-Cas9 inhibitors that prevent Cas9 from editing the targeted DNA, thus needing higher complementarity to induce editing[202]. However, regardless of the numerous techniques that have been developed, the issue of the off-target editing still remains to be resolved.

1.3.2.2 Delivery of the CRISPR/Cas9 system

A second major limitation for the CRISPR/Cas9 platform is the delivery of the system to cells or organisms either at the embryo or adult stage. This limitation becomes even more prominent in therapeutic applications depending on the gene editing approach that is used to change the sequence of the disease-causing gene. As explained above, two pathways can be employed to repair the DSB that is induced upon editing with Cas9, the NHEJ or the HDR. The former pathway, which leads to the disruption of the sequence of the targeted gene, is used when silencing of a mutant gene is needed while the latter one is used for correcting a mutant gene back to its wild-type sequence. HDR based therapies demonstrate added advantages since they can address the off-target problems with the use of nickases as well as provide highly specific editing. However, the need to deliver Cas9 proteins, sgRNAs and the donor DNA simultaneously and in high efficiency in order for the HDR to occur, together with the low editing efficiency the pathway exhibits[189], renders this approach challenging.

Multiple *in vitro* techniques have been used with varying efficiencies. These include the use of liposomes[196], nucleofection[203], electroporation[204] lentiviral based delivery[158] and microinjections in embryos[205]. Additionally, *ex vivo* approaches have been studied for the delivery of the system to cells isolated from mice or patients under *in vitro* conditions and the re-introduction of the edited cells to the individuals[206]. Nonetheless, the *in vivo* delivery still remains the most promising approach for therapeutic applications.

One of the first techniques used for gene therapy was the employment of adeno-associated viruses (AAVs) which is to this day one of the most advanced technologies for *in vivo* editing[207]. However, this technique presents various limitations since AAV vectors are big in size, thus hindering the delivery efficiency, they can induce off-target editing[208] and can trigger immune response due to the bacterial origin of the

Cas proteins. A second approach is that of the direct delivery of Cas9/RNP, either *in vivo* or *in vitro,* with the use of lipoproteins[209, 210]. The advantages this approach presents are the ease at producing high levels of recombinant Cas proteins and the track record in protein therapeutics. Moreover, other *in vivo* deliveries have been developed. Hydrodynamic delivery of plasmid DNA, that harbours the sequence for Cas9, sgRNAs and donor DNA[211], is an alternative to lipoprotein or polyethylenimine (PEI) delivery of macromolecules, approaches that have not worked in the past. Lastly, two new, highly promising techniques have been described. The first one employs gold nanoparticles, conjugated with DNA, complexed with Cas9 RNP and donor DNA, entering the cells under *in vivo* conditions via endocytosis (gold nanoparticles) while the second one uses a sialoglycoprotein receptor ligands that facilitate the receptor-mediated endocytosis of the system[114, 212].

1.3.3 CRISPR/Cas9 and miRNAs

The use of gene editing for inhibition of miRNAs has already been demonstrated in various studies[213-215]. More specifically, with regards to CRISPR/Cas9, it has been reported that it can target the expression of miRNAs, although with contradicting results about its efficiency[202, 216]. Moreover, *in vivo* studies showed that the platform can be used for the excision of a 53-kb fragment leading to knock-out mice to study the effects of the deletion of the largest miRNA cluster[217], the targeting of entire families[218] while double knock out mice have also been reported[219]. Further to this, CRISPR/Cas9 has also been used to elucidate both the pathway of the miRNA induced silencing[220] as well as the miRNA biogenesis[221].

Chapter 2 AIMS OF THE STUDY

MiRNAs are important and powerful regulators of many cellular processes by targeting and modulating the expression levels of multiple mRNA targets that participate in various pathways. The study of the miRNAs, though, is hindered by the fact that they form families that are comprised of members that share identical seed sequences and high homology throughout their sequence. A new approach for the study of miRNAs using gene editing has emerged as a promising alternative to overcome these limitations.

In the current study CRISPR/Cas9 is employed as a powerful platform to induce editing in the miRNA genes in order to elucidate its application in the miRNA study and the role of miRNAs. More specifically, the aims of the study are:

1. To study whether gene editing with CRISPR/Cas9 is capable of replacing the traditional methods of inhibiting miRNAs, overcoming the non-specific inhibition of the miRNAs of the same family. Following this approach, instead of targeting the mature miRNAs, editing of their genomic locus was thought to provide specific knock out only of the targeted miRNA.

2. To establish a reliable workflow for inhibiting miRNAs. CRISPR/Cas9 is a highly versatile and easy to use platform for editing almost any locus in the genome. Valuable conclusions reached, through studying its application in the inhibition of miRNAs, were postulated to simplify miRNA inhibition with CRISPR/Cas9 and potentially add another tool in the arsenal of miRNA study if not replace the existing methods.

3. To study the regulatory mechanisms and function of miRNAs and more specifically of miR-195a. Various miRNAs have been implicated in cardiovascular diseases with miR-195a being among them. However, it is not as well studied as other miRNAs e.g. from the miR-17~92 cluster. The current study aimed to provide a better understanding of the maturation process of the primary transcript and more specifically of the proteins that recognise, bind and participate in the maturation process.

Chapter 3 MATERIALS AND METHODS

3.1 Cell Culture

Human Embryonic Kidney 293T cells

Human Embryonic Kidney (HEK) 293T cells (HEK293T) were at fetal age, obtained from ATCC (CRL-3216) and cultured according to the recommended protocol. The cells were cultured in Dulbecco's Modified Eagle's Medium (DMEM, ThermoFisher Scientific #12491-015), supplemented with 10% heat-inactivated Foetal Bovine Serum (FBS) and 1% penicillin/streptomycin (100 U/ml penicillin and 100 µg/ml streptomycin) at 37°C in a humidified atmosphere of 95% air/5% CO_2. HEK293T cells were subcultured with a ratio of 1:3 or 1:4 every 2-3 days up to passage 20.

Human Umbilical Vein Endothelial Cells

Human Umbilical Vein Endothelial Cells (HUVECs) were obtained from Lonza and cultured as described previously[222]. HUVECs were plated on gelatin coated flasks (Sigma-Aldrich #9000-70-8, 0.04% in DMEM) and cultured in Medium 199 (ThermoFisher Scientific #11150059) supplemented with 10% FBS, 1% penicillin/streptomycin (100 U/ml penicillin and 100 µg/ml streptomycin) and 3 ng/ml endothelial cell growth factor (Sigma, St Louis, Mo # E9640), 1µg/ml endothelial growth supplement from bovine neural tissue (Sigma # E2759-5X15MG), 10 U/ml heparin (Sigma # E4643), 1.25µg/ml thymidine at 37°C in a humidified atmosphere of 95% air / 5% CO_2. HUVECs were subcultured at a ratio of 1:3 every other day to passage 12.

Human Smooth Muscle Cells

Human Aortic SMCs were obtained from ATCC (PCS-100-012), were of male gender, adult age and plated in gelatin coated flasks (0.04% gelatin in DMEM) and cultured

in DMEM, supplemented with 15% FBS and 1% penicillin/streptomycin (100 U/ml penicillin and 100 µg/ml streptomycin) at 37°C in a humidified atmosphere of 95% air/5% CO_2. Cells were passaged at a ratio of 1:3 every three days to passage 10.

Mouse Smooth Muscle Cells

VSMCs were isolated by enzymatic digestion of mouse aortas derived from C57BL mice (8-10 week old) as described previously[222]. They were of male gender and cultured in Dulbecco's modifed Eagle's Medium (DMEM, ThermoFisher Scientific, Runcorn, UK, #11965-084) supplemented with 10% heat-inactivated Foetal Bovine Serum (FBS, # 16000044), 2mM L-glutamine and 1% penicillin/streptomycin (100U/ml penicillin and 100 µg/ml streptomycin, #15240062), at 37°C in a humidified atmosphere of 95% air/5% CO_2. VSMCs were plated on gelatin coated flasks (0.04% in DMEM, ThermoFisher Scientific, Runcorn, UK). Cells were passaged at a ratio of 1:3 every other day up to passage 30.

3.2 Single Guide RNA Design and Cloning

The CRISPR DESIGN tool (http://crispr.mit.edu, no longer available), provided by the Zhang Lab, MIT 2015, was used to design the single guide RNAs. Briefly, the DNA sequence of the locus of the miRNA was submitted in FASTA format. After analysing the sequence, the tool's algorithm returned a list of possible guides, ranked according to a quality score of inverse likelihood of off-target sites. It also provided information about the specific position of the sequence they target in the miR-195 locus, putative off-target sites, with their corresponding score, and the number and positions of the mismatches between the guides and their off-target sites. Moreover, CRISPR Finder on-line tool, provided by Wellcome Trust Sanger Institute, was used to identify additional off-target sites for the selected guides in order to eliminate the possibility of not detection due to algorithm bias. The highest scoring guides, which targeted sequences either in or close to the miRNA stem-loop, were selected.

After choosing the guides to be used, they were synthesized with overhangs which would facilitate the cloning into the backbone pX330 plasmid vector (Addgene

#42230), (Figure 3.1A) or LentiCRISPRv2 lentiviral vector (Addgene #52961), (Figure 3.1B).

A

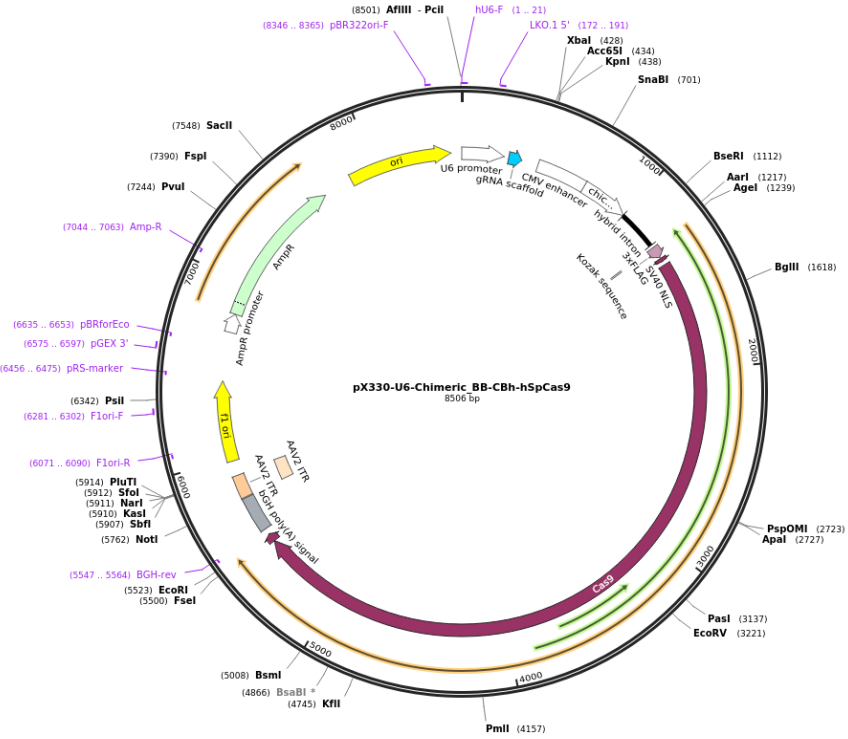

B

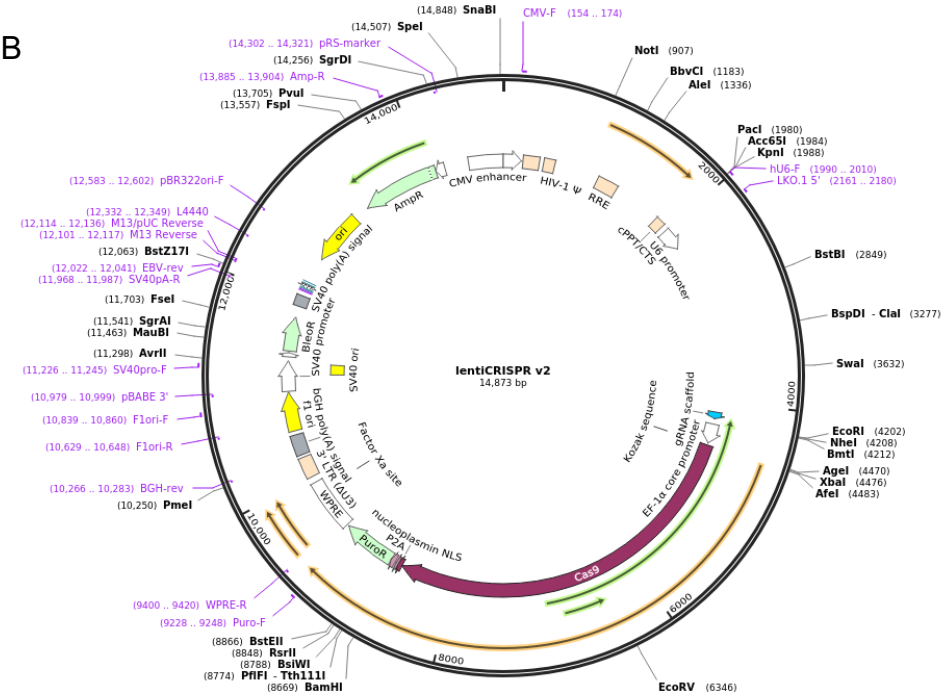

Figure 3.1 Vectors pX330 and LentiCRISPRv2. (**A**) Map of vector pX330 with its corresponding elements. (**B**) Map of vector LentiCRISPRv2 with its corresponding elements.

In detail, to clone the guide sequence into the vectors the two oligos were synthesized in the form:

Oligo1: 5'-CACCGNNNNNNNNNNNNNNNNNN -3'

Oligo2: 3'-CNNNNNNNNNNNNNNNNNNNCAAA-5'

For cloning the oligos into the backbone vector a single step digestion-ligation protocol[208] was used.

Firstly, the oligos were phosphorylated and annealed. For the reaction, 1µl Oligo1 (100µM), 1µl Oligo2 (100µM), 1µl 10x T4 Ligation Buffer (NEB #M0308S), 0.5µl T4 PNK (NEB) and 6.5µl nuclease free H_2O were added to a final volume of 10µl. The oligos were annealed in a thermocycler at 37°C for 30min, 95°C for 5min and then the temperature was ramped down to 25°C at 5°C/min. After the annealing, the oligos were diluted 250-fold (1:250) for the pX330 vector or 10-fold (1:10) for the LentiCRISPRv2 vector, respectively.

For the single digestion-ligation reaction, 1µl of vector (100ng), 2µl Phosphorylated and annealed diluted oligo duplex from the previous step, 2µl 10x Tango Buffer (NEB), 1µl FastDigest enzyme, 1µl DTT (10mM) (Sigma #D9779), 1µl ATP (10mM), 0.5µl T7 DNA ligase (NEB #M0318S) and 11.5µl nuclease free H_2O were added to a final volume of 20µl. The BbsI enzyme (ThermoFisher Scientific #FD1014) and Esp31 (ThermoFisher Scientific # ER0451) were used for the pX330 and LentiCRISPRv2 vectors, respectively. The digestion-ligation reaction was incubated in a thermocycler at 37°C for 5 min, 23°C for 5 min, repeated for 6 cycles and 15 cycles for the pX330 and LentiCRISPRv2 vectors, respectively.

The ligated product was treated with PlasmidSafe exonuclease to remove the un-ligated linear plasmids. For the PlasmidSafe reaction 11µl Ligation reaction (from the previous step), 1.5µl 10x PlasmidSafe Buffer, 1.5µl ATP (10mM) and 1µl PlasmidSafe

exonuclease (PlasmidSafe™ ATP-Dependent DNase kit #E3101K) were added to a final volume of 15µl. The reaction was incubated at 37°C for 30min.

Next, the ligated vectors were transformed into Stbl3 E. Coli competent cells (ThermoFisher Scientific #C7373-03). Briefly, 2µl of the PlasmidSafe treated product were added into a shot (20µl) of ice-cold chemically competent Stbl3 cells and incubated on ice for 30 min. They were then heat shocked at 42°C for 45sec and placed back on ice for 2 min. Next, 240µl of SOC medium was added to the transformed bacteria and incubated at 37°C for 40 min. Subsequently, 100µl of bacteria were plated on an LB agar petri dish containing ampicillin (50µg/ml) and incubated at 37°C overnight.

3.3 In Vitro Transcription (IVT) of sgRNA

For the IVT, the GeneArt™ Precision gRNA Synthesis Kit (Invitrogen #A29377) was used to generate single guide RNAs (sgRNAs), according to manufacturer's recommendations. The DNA template of the sgRNA was PCR assembled as shown in Figure 3.2. This DNA template was then used to generate the sgRNAs by IVT. All IVT Target primer sets are provided in Supplementary Table 2.

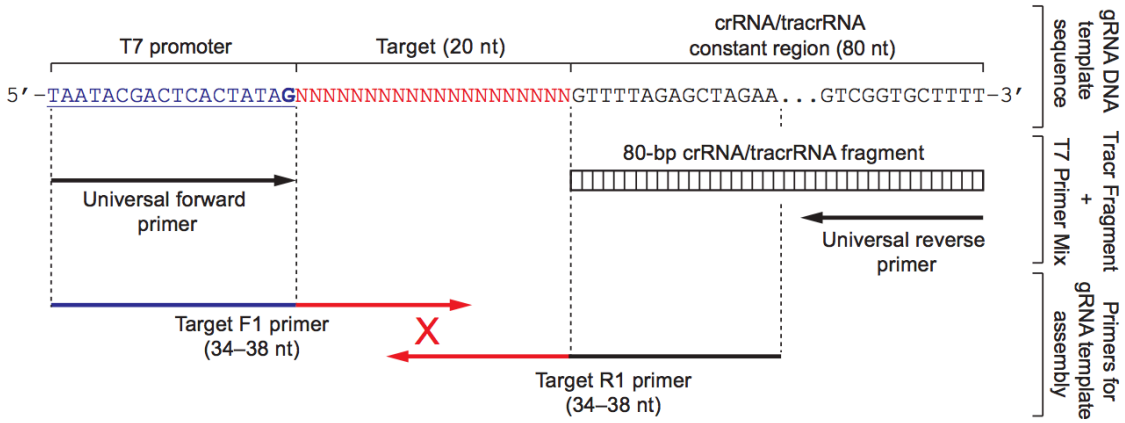

Figure 3.2. PCR assembly of the gRNA DNA template using the Target F1 and Target R1 oligonucleotides. The oligonucleotides were used both as primers and templates together with the T7 primer mix and the tracr fragment for the IVT of the sgRNA. Figure from http://www.thermofischer.com. Date accessed 15/08/2019.

PCR Assembly

The following PCR was used for the assembly of the gRNA DNA template: 12.5µl of 2x PfusionTM High-Fidelity PCR Master Mix, 1µl of Tracr Fragment + T7 Primer Mix, 1µl of Target F1/R1 oligonucleotide mix (0.3µM) and 10.5µl of nuclease free H_2O were added to a final volume of 25µl. The following PCR programme was run on a Veriti® 60-well Thermal Cycler: initial denaturation at 98°C for 10sec and then underwent 32 cycles of 98°C for 5sec, 55°C for 15sec and then a final extension step at 72°C for 1min.

IVT Reaction

After the DNA template assembly, IVT was used for the generation of the gRNA. The reaction mix for each sample contained 8µl of NTP mix (100mM), 6µl of gRNA DNA template from the previous step, 4µl of 5x TranscriptAid™ Reaction Buffer and 2µl of TranscriptAid™ Enzyme Mix to a final volume of 20µl. The samples were incubated on a Veriti® 60-well Thermal Cycler form Thermo Fisher Scientific at 37°C for 3h. As a final step, to remove the DNA template, 1µl of DNase I (1U/µl) was added to the reaction and was incubated at 37°C for a further 30min. After the DNA template digestion, the gRNA was purified using the gRNA Clean Up Kit following the manufacturer's recommendations.

Transfection

For transfection experiments, 293T cells were trypsinised and re-suspended into complete medium with no antibiotics. Subsequently, cells were counted using a haemocytometer and plated in 24 well plates at a cell density of 240,000 cells/ml. A total of 500µl of cell suspension was plated per well.

On the following day, cells were transfected with plasmid vectors using ViaFect™ Transfection Reagent by Promega (Catalog No E4981). Two mastermixes (A and B) were prepared. For mastermix A, 500ng of the plasmid were mixed with 25µl of DMEM per 24 well and for mastermix B, 2µl of ViaFect™ were added to 25µl of DMEM

per transfection. After incubating at RT for 5 min the two mastermixes were combined and incubated for further 20 min. Afterwards the transfection mastermix was added to the corresponding well. All transfection reactions were performed in duplicates.

After 24 hours of the transfection, the conditioned medium was supplemented with 500µl of complete medium. Two days later, HEK293T cells were detached by pipetting and 500µl of the cell suspension was re-plated to a 6 well plate, supplemented with 1.5ml of complete media. Cells were returned to the incubator and maintained for an additional 3 days. Additional DNA samples were harvested on Day5.

3.4 DNA Extraction

For the DNA extraction cells were pelleted and lysed in 300µl of QuickExtract™ DNA Extraction Solution 1.0 (Epicentre #QE09050). The samples were heated at 65°C for 20 min and then at 96°C for 10 min. The DNA concentration was measured using the NanoDrop 1000 (ThermoFisher Scientific) device.

3.5 Genomic PCR

For the amplification of the genomic locus of miR-195, primers were designed using the online tool OligoPerfect™ Designer by Thermo Fisher Scientific and Kapa HiFi PCR Kit Hot Start from Kapa Biosystems (Kapa Biosystems #KK2502) was used. The possible editing of the off-target sites, as provided by http://crispr.mit.edu, was also tested. The sequences of the genomic locus of the off-target sites were retrieved from www.ensebml.org, using the coordinates of the possible off-target sites as provided by the CRISPR DESIGN online tool. Details for the primer sequences are provided in Supplementary Table 3.

The reaction mix for each sample contained 9µl of 5x Kapa GC Buffer, 1.35µl of Forward Primer (10µM), 1.35µl of Reverse Primer (10µM), 1.35µl of dNTPs (10mM), 6µl of DNA template (50ng/µl), 0.45µl of Kapa Polymerase and 25.5µl of nuclease free H_2O to a final volume of 45µl.

The following PCR programme was run on a Veriti® 60-well Thermal Cycler for the miR-195 genomic locus (both human and mouse): initial denaturation and enzyme activation at 95°C for 5 min and then 30 cycles of 98°C for 20sec, 62°C for 15sec, 72°C for 20sec, then were heated at 72°C for 1min. Amplicons were visualized on a 2% agarose gel in 1xTBE buffer supplemented with Safe-view (10µl/150ml) run at 200V for 30 min.

3.6 PCR Clean Up

The PCR product was purified using the Thermo Scientific GeneJET Gel Extraction and DNA Cleanup Micro Kit (Catalog Number #K0702), following the manufacturer's recommendations. Briefly, the volume of the PCR product was adjusted to 200µl with nuclease free H_2O. Then, 100µl of binding buffer were added followed by 300µl of 100% ethanol. The solution was mixed thoroughly by pipetting, transferred to a DNA purification Micro Column and centrifuged at 14,000 x g for 1 min. The flow-through was discarded and 200µl of Pre-wash Buffer was added to the column before being centrifuged at 14,000 x g for 1 min. The flow-through was discarded and 700µl of Wash Buffer was added to the column before being centrifuged at 14,000 x g for 1min, a step that was repeated for a second time. The column was then transferred to a clean 1.5ml micro-centrifuge tube and centrifuge at 14,000 x g for 1 min for the removal of any residual buffer. The column was then transferred to a clean 1.5ml micro-centrifuge tube and 10µl of nuclease free water were added to the column for three min incubation. For the elution of the purified DNA product, the column was centrifuged at 14,000 x g for 1 min. The DNA concentration of the purified PCR product was measured using a NanoDrop 1000.

3.7 T7 Endonuclease I Assay

To assess the gene editing efficiency, the T7 Endonuclease I assay (T7EI) was employed as described recently[223]. Briefly, 90ng of the purified PCR product were diluted to a volume of 14µl, in nuclease free H_2O, and supplemented with 3.5µl 5x KAPA HiFi GC Buffer. PCR products were denatured by heating to 95°C for 10min

(Figure 3.3A) and then re-annealed by slowly ramping down the temperature to 25°C by a rate of 4.5% per minute (Figure 3.3B).

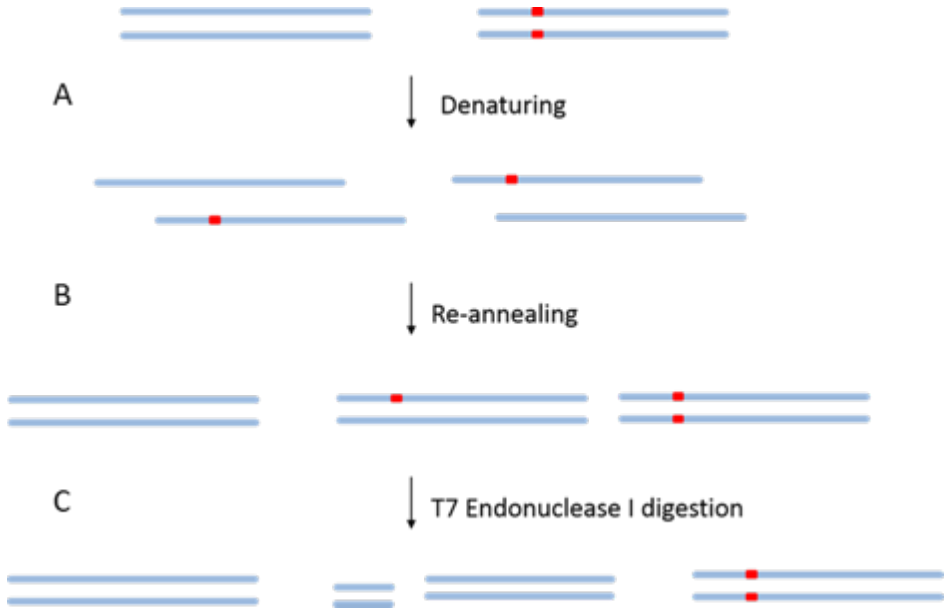

Figure 3.3. T7 Endonuclease I digestion. T7EI recognises and cleaves mismatched DNA. (**A**) The PCR amplicons were denatured and (**B**) re-annealed randomly. (**C**) Upon T7 endonuclease I digestion, the mismatched strands were cleaved at the edited site (red squares). The fragments were then analysed to assess the genome editing efficiency.

After the re-annealing, 2µl of 10x NEB Buffer 2 (NEB #B7002S) and 0.5µl of the T7EI (NEB #M0302S) were added to each sample, to a final volume of 20µl for a further 1h incubation at 37°C. As a final step, 4µl of 6x Purple Loading Buffer (NEB #B7024S) were added and the samples were heated to 70°C for 10min (Figure 3.3C).

To visualize the T7EI digestion products, a 2% agarose gel in 1xTBE buffer was prepared. The samples were loaded and run at 170V for 50 min alongside a 1kb Plus DNA ladder (ThermoFisher Scientific #10787018). After the run, the gel was, rinsed twice with 1x TBE Buffer. The gel was subsequently stained with SYBR® Gold Nucleic Acid Gel Stain (ThermoFisher Scientific #S-11494) in 1xTBE buffer for 30min, protected from light. The gel was visualized using the Ettan DIGE Imager by GE HealthCare.

For the quantification of the T7EI results, the ImageJ software was used (freely available at http://imagej.net). The band intensity of the uncut DNA substrate, the cleaved products and background was measured. The values of the band intensities were subtracted against the value of the background and the editing efficiency was calculated using the following formula:

Indel (%) = (1 - $\sqrt{1 - \frac{B+C}{A+B+C}}$) x 100,

where, A=uncut DNA substrate, B, C= digestion products

3.8 Restriction Enzyme Digestions

The SspI and MwoI digestions were set up in order to detect mutations in the genomic loci of mouse miR-195. More specifically, the SspI restriction enzyme identifies the sequence 5'-AATATT-3' and the MwoI identifies the sequences 5'-GCNNNNNNNGC-3' (Figure 3.4). Successful gene editing will interrupt these two sites, thus preventing the cleavage by the restriction enzymes. For the digestion, 8µl of the PCR reaction was used as a template in a digestion that contained 2µl 10x CutSmart (NEB #B7204S), 0.5µl of restriction enzyme and 9.5µl of nuclease free H_2O to a final volume of 20µl. The reaction was incubated in a thermocycler at 37°C for the SspI and at 60°C for the MwoI for 1h.

Restriction enzymes (all from NEB) were also used to assess gene editing with their corresponding sites outlined in Supplementary Table 4. Digestion reactions for all other restriction enzymes were incubated at 37 °C for 1 h in CutSmart Buffer with the exception of SspI that was incubated in NEB Buffer 2.1. Digestion products were visualised in 2% agarose gel in 1xTBE buffer.

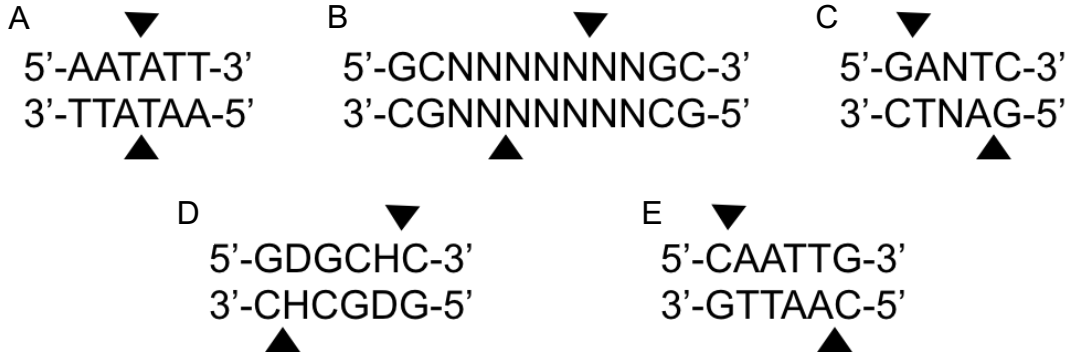

Figure 3.4. SspI, MwoI, HinfI, Bsp1286I and MefI restriction sites. (**A**) SspI restriction site. (**B**) MwoI restriction site. (**C**) HinfI restriction site. (**D**) Bsp1286I restriction site. (**E**) MfeI restriction site. The black arrows indicate the position of the cleavage. The black arrows indicate the position of the cleavage.

3.9 Lentiviral particle transduction

To confer Cas9 expression in VSMCs, we used the LentiCRISPRv2 vector (Addgene, #52961) that encodes a *Streptococcus pyogenes* Cas9 (SpCas9) under the control of an elongation 1a short promoter (EFS)[224]. Lentiviral particles were produced using the lentiviral vector LentiCRISPRv2 and packaging plasmids pMD2.G and psPAX2 (Addgene, #12259, #12260) as described previously[225]. HEK293T cells were seeded in T75 flasks. When they reached a confluency of 70-80%, they were transduced with lentiviral vectors for the production of the lentiviral particles. Briefly, two mastermixes were prepared. Mastermix A consisted of 590µl of Opti-MEM® I Reduced Serum Media (ThermoFisher Scientific #31985070) and 10µg of the lentiCRISPRv2 vector harbouring the guide sequence of interest, 5µg of the pMD2.G envelope plasmid (Addgene #12259) and 7.5µg of the psPAX2 plasmid (Addgene #12260) and Mastermix B consisted of 600µl of Opti-MEM® I Reduced Serum Media and 50µl of ViaFect™. The mastermixes were incubated for 5 min at RT and then combined and incubated for further 20 min at RT. In the meantime, the medium of the HEK293T cells was replaced with 6ml of Opti-MEM® I Reduced Serum Media per flask. The transfection complexes were subsequently added to the cells and incubated at 37°C. Following a 6h incubation, the medium was replaced with 8ml of DMEM with 10% FBS and antibiotics supplemented with 1% Bovine Serum Albumin (Sigma-Aldrich #9048-46-8). After 60h, the lentiviral supernatant was collected, centrifuged at 1000 rpm for 5min and filtered through 0.45µm VWR Syringe Filters #28145481. A p24

antigen ELISA (Cell Biolabs) was used to determine the viral titer[222]. The resulting solution was either used immediately or stored at -80°C.

3.10 Lentiviral Infection

VSMCs were seeded at T25 flasks at a density of 200,000 cells per flask. The next day cells were lentiviral infected using 1.6-2.4 x 10^7 TU/ml (Table 1). The media were supplemented with 8μg/μl of Polybrene (Sigma-Aldrich #28728-55-4) and cells were incubated for 24h with the viral suspension. The next day, the lentiviral supernatant was removed, discarded and replaced with 5ml of complete medium.

Table 1. List of Lentiviruses used.

Lentiviruses	**Titer**
LentiCrisprv2 (Addgene #52961)	1.7-2.3 x 10^7 TU/ml
pLKO.1 (Addgene #8453)	1.6-2.4 x 10^7 TU/m

3.11 TA Cloning

PCR amplicons from the edited samples was sequenced to determine mutation patterns. Purified, PCR amplified DNA from each sample was ligated to the pGEM®-T Vector (Promega #A3600). For the ligation reaction 5μl of 2x Rapid Ligation Reaction Buffer, 2μl of PCR purified product, 2μl of pGEM®-T vector (Figure 3.5) and 1μl of T4 DNA ligase (Promega, Catalog No M1801) were used. The reaction was incubated at RT for 1 hour.

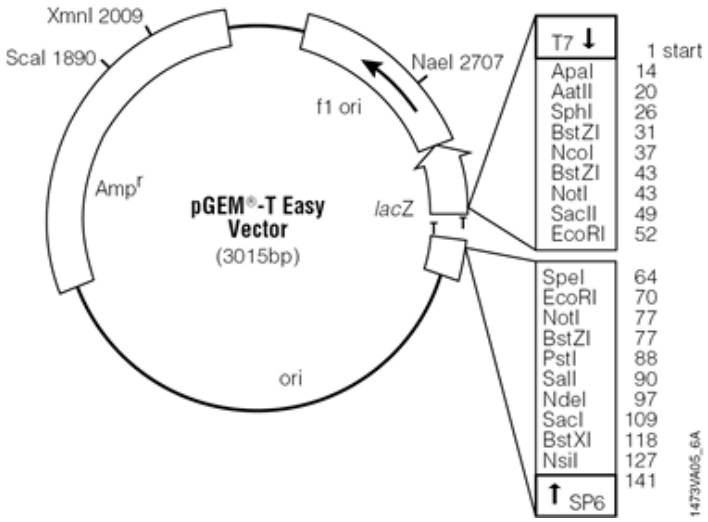

Figure 3.5. pGEM®-T vector. The map of pGEM®-T with the corresponding restriction sites.

Subsequently, 2.5μl of the ligation product were added to 50μl of JM109™ Chemically Competent E. Coli (Promega #L1001) and incubated on ice for 30 min. They were then heat shocked at 42°C for 45 sec and placed on ice for 2 min. A total of 240μl of SOC medium was added to the transformed bacteria that were incubated at 37°C for further 20 min. An ampicillin LB agar petri dish was precoated with 40μl of Xgal (50mg/ml) (Promega #V3941) and 40μl of IPTG (100mM) (Promega #V3955) and 70μl of bacteria culture were subsequently plated. The dish was incubated at 37°C, overnight.

Blue and white bacterial colonies were formed overnight, with blue colonies corresponding to the bacteria that were transformed with re-ligated, empty vectors. White bacterial colonies correspond to bacteria that were transformed with the vector conferring the PCR product. Individual bacterial colonies were picked and PCR screened as described above. Mutation patterns were identified by Sanger sequencing.

3.12 RNA Extraction

RNA was extracted using the miRNAeasy mini kit (Qiagen #74104). Briefly, cells were lysed using 700μl of QIAzol® Lysis Reagent. Following a brief incubation at ambient temperature, 140μl of chloroform was added to each sample and the solution was mixed vigorously for 15 sec. The samples were incubated for 5 min at RT and were

then centrifuged for 15 min at 12,000 x rpm at 4°C. Only 280µl of the upper aqueous phase were transferred to a new collection tube and 420µl of 100% ethanol were added and mixed thoroughly and transferred to an RNeasy® Mini column in a 2ml collection tube, washed according to the company's recommendations. Total RNA was eluted using 25µl of nuclease free H_2O and the RNA concentration was measured using a NanoDrop 1000.

3.13 MiRNA quantification

To assess miRNA expression RNA was reverse transcribed using the Megaplex Primer Pools from ThermoFisher (Cat. #4401009) as described previously[98]. A total of 100ng of RNA were reverse transcribed using the Megaplex Rodent Primer Pools A. The reaction was performed according to the company's recommendations (0.8µl of Pooled Primers were combined with 0.2µl of 100mM dNTPs with dTTP, 0.8µl of 10x Reverse-Transcription Buffer, 0.9µl of $MgCl_2$ (25mM), 1.5µl of Multiscribe Reverse-Transcriptase and 0.1µl of RNAsin (20U/µl) to a final volume of 7.5µl). The RT-PCR reaction was set as follows: 16°C for 2min, 42°C for 1min and 50°C for 1 sec for 40 cycles and then incubation at 85°C for 5min using a Veriti® thermocycler (Life Technologies). The RT reaction products were diluted to 1ng/µl corresponding RNA and stored at -20°C. Taqman miRNA assays were used to assess the expression of individual miRNAs. For the quantitative Polymerase Chain Reaction (qPCR), 2.25ng of Megaplex reverse transcription product were combined with 0.25µl of 20x Taqman miRNA Assay (Life Technologies) and 2.5µl of the 2x Taqman Universal PCR Master Mix No Amp Erase UNG (ThermoFisher Scientific #4324018) to a final volume of 5µl. QPCR was performed on a Viia7 thermocycler at 95°C for 10 min, followed by 40 cycles of 95°C for 15sec and 60°C for 1min. U6 was used as a normalization control.

3.14 MiRNA Overexpression

Cells were plated at 60–70% confluency on the day before transfection. Mouse miRNA mimics and a non-targeting control were obtained by ThermoFisher Scientific

and transfected at a final concentration of 20nM using Lipofectamine RMAiMAX (ThermoFisher Scientific, Runcorn, UK) as described previously[98].

3.15 Gene expression

QPCR was used to assess the gene expression levels. In these studies, 1µg of RNA was reversed transcribed into cDNA using the High Capacity Reverse Transcriptase kit (ThermoFisher Scientific, Runcorn, UK). Prior to pri-miRNA assessment RNA samples were treated with DNAse for 30min at 37°C, to remove any genomic DNA contamination in the preparations. For all genes, Taqman Assays were used with the exception of Carmn that was assessed using specific primers[226] (Supplementary Table 3) and SyBr Select Mastermix (TermoFisher Scientifc, Runcorn, UK). Beta Actin was used as a normalisation control.

3.16 Computational analysis

Secondary structures without pseudoknots were generated by RNAfold (Vienna RNA tools, http://rna.tbi.univie.ac.at/cgi-bin/RNAWebSuite/RNAfold.cgi) using the Turner model (Standard settings), while secondary structures with pseudoknots were generated by vsfold5[227] (Chiba Institute of Technology, Japan, http://www.rna.it-chiba.ac.jp/~vsfold/vsfold5/) and Settings: 37°C temperature; Kuhn length 6; Jacobson-Stockmayer gamma=1.75 and contiguous stems=6. Visualisation of the secondary structures with pseudoknots was performed using the Pseudoviewer software (Inha University, S Korea http://wilab.inha.ac.kr/ pseudoviewer/). The RNAComposer[228] (Poland, http://rnacomposer.cs.put.poznan.pl/) was used to generate the pbd-files through molecular RNA simulation from vsfold5 output. The RNAComposer output pdb-fles were then input to pyMOL to generate high quality 3D images. MiR-497a stem loop is depicted in green and its terminal loop in magenta. MiR-195a stem loop is depicted in red and its terminal loop in yellow.

3.17 pLKO.1 cloning

The pLKO.1[229] vector was used for pri-miRNA overexpression experiments, since it is the recommended vector for expression of shRNAs under a T7 promoter (Figure 3.6).

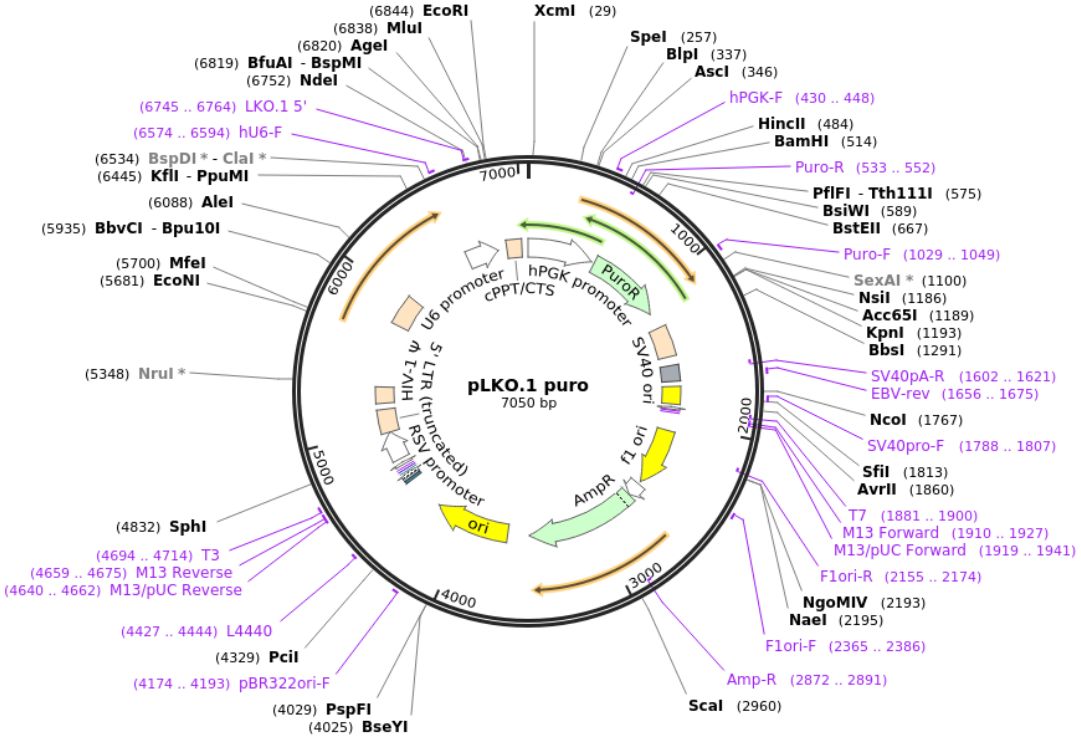

Figure 3.6. Vector pLKO.1-puro cloning vector. Map of vector pLKO.1 with its corresponding elements.

For the cloning of the DNA sequence of mmu-miR-497~195, pGEM®-T vectors harbouring WT or mutant sequences were used as template. These sequences were resulted from editing of the genomic locus of the primary transcript. For cloning purposes, new guides harbouring sequences corresponding to the restriction sites of AgeI and EcorI were designed (Supplementary Table 3). For the PCR amplification of the DNA sequence of the primary transcript, a specific programme was used on a Veriti® 60-well Thermal Cycler.

More specifically, two PCR reactions were prepared for each transcript (WT and mutants) to final volume of 45μl. The reaction mix for each sample contained 9μl of 5x Kapa GC Buffer, 1.35μl of Forward Primer (10μM), 1.35μl of Reverse Primer

(10μM), 1.35μl of dNTPs (10mM), 2μl of DNA template (50ng/μl), 0.45μl of Kapa Polymerase and 29.5μl of nuclease free H_2O to a final volume of 45μl.

The following PCR programme was run on a Veriti® 60-well Thermal Cycler for the miR-195 genomic locus (both human and mouse): initial denaturation and enzyme activation at 95°C for 5 min and then 5 cycles of 98°C for 20sec, 57°C for 20sec, 72°C for 40sec, followed by 30 cycles of 98°C for 20sec, 62°C for 20sec, 72°C for 40sec then were heated at 72°C for 1min. Next, the two reactions were combined and cleaned-up, following the same protocol as explained above, with the final elution being in15μl of H_2O. Then, the eluted DNA was run on a 0.8% agarose gel in 1xTBE buffer supplemented with Safeview (10μl/150ml) at 170V for 50 min. Following this, gel purification of the amplicons was performed using the Thermo Scientific GeneJET Gel Extraction and DNA Cleanup Micro Kit (Catalog Number #K0702) following the company's recommendations. In brief, the part of the gel that engulfed the DNA band of the correct size was excised using a scalpel and was transferred to a 1.5mL Eppendorf tube. Next, 200μl of Extraction Buffer were added and the gel mixture was incubated at 58°C for 10min. Then, 200μl of ethanol were added to the tube and mixed by pipetting. The mixture was afterwards transferred to a DNA purification Micro Column and was centrifuged for 60sec at 14,000 x g. Next, the column was washed with 200μl of Prewash Buffer and centrifuged for 60sec at 14,000 x g. Then, 700μl of Wash Buffer was added and centrifuged twice. The empty column was then centrifuged and then transfer to an empty microcentrifuge tube. In a final step, 15μl were added to the empty column to elute the DNA.

Following the clean-up, two digestions were set up with AgeI restriction enzyme. In more detail, a reaction with 5μl of Buffer O, 2μl of AgeI, with 15μl of PCR product and 28μl of H_2O was set-up for the gel purified PCR product. A second reaction with 5μl of Buffer O, 2μl of AgeI, 9.09μl of pLKO.1 vector (a total amount of 5000ng) and 33.91μl of H_2O was set-up and they were both incubated at 37°C for 2 hours.

Following these digestions, the products were cleaned-up as per standard protocol eluting in 15μl of H_2O. A second step of digestions was set-up with 5μl of CutSmart, 2μl of EcoRI, 15μl of PCR clean-up product and 28μl of H_2O and were incubated at 37°C for both the PCR product and the vector.

As a last step, the digested products were cleaned-up as per standard protocol and the final concentration was measured using the NanoDrop 1000.

For the ligation reaction, 1µl of 10x T4 ligase buffer, 240ng of pLKO.1, 420ng of PCR clean-up and 1µl of T4 ligase were added to a final volume of 10µl and they were incubated at RT overnight.

3.18 RNA Pull-down assay

Cell lysate preparation

RNA Pull-down experiments were conducted to assess how changes in the tertiary structure of the pri-miR-497~195, due to CRISPR/Cas9 editing, might affect its recognition and binding from RNA binding proteins. For the RNA Pull-down experiment, VSMC were cultured in T175 flasks to a confluency of 90% before they were harvested. In more detail, the culture medium was removed from the flasks and the flasks were washed off with 4ml of phosphate-buffered saline (PBS; Sigma, cat. no. D8537). Next, the cells were scraped, and the cell suspension was placed in a 50ml falcon tube before it was centrifuged at 1,000 rpm for 5min. After spinning, the supernatant was removed and 800µl of Pierce IP Lysis buffer (ThermoFisher #87787) supplemented with protease inhibitor (Roche Complete Mini, EDTA-free, cat. no. 11836170), phosphatase and RNAse inhibitors (Life Technologies) were added and the solution was incubated on ice for 30min while mixing occasionally. After the 30min had elapsed, the lysate was centrifuged at 13,000 rpm for 20min at 4°C, the supernatant was removed and stored at -20°C.

IVT of primary transcript

For the RNA Pull-down experiments, primary transcripts corresponding to the wild type or the mutated sequences conferring a 16-nucleotide deletion, were PCR amplified with the use of forward primers containing the T7 promoter. Afterwards, the

PCR products were run on a 0.8% agarose gel in 1xTBE buffer (ThermoFisher #15581-028), stained with Safe-view 10µl/150ml (NBS Biologicals, NBS-SV5), at 170V for 50min. The products were then gel purified using the GeneJET Genomic DNA Purification Kit (#K0721). The DNA concentration of the gel purified products was measured using the NanoDrop 1000 (ThermoFisher Scientific) device and 400ng of DNA were used for the IVT reaction to a final volume of 20µl as described above in Chapter 3.3. The samples were incubated on a Veriti® 60-well Thermal Cycler form ThermoFisher Scientific at 37°C for 2h. Finally, 1µl of DNase I (1U/µl) was added to the reaction and was incubated at 37°C for a further 30min to remove the DNA template. Afterwards, the RNA was purified using the RNA Clean Up Kit following the manufacturer's recommendations (ThermoFisher Scientific). Briefly, after adjusting the volume to 200µl with nuclease-free water, 100µl of Binding Buffer were added and mixed thoroughly. Then 300µl of of ethanol were added before the mixture was transferred to a GeneJet™ RNA Purification Micro Column and centrifuged at 14,000 x g for 60 seconds. After discarding the flow through, 700µl of Wash Buffer 1 was added and the column was centrifuged at 14,000 x g for 60 seconds. Next, 700µl of Wash Buffer 2 was added and the column was centrifuged again at 14,000 x g for 60 seconds. The empty purification column was centrifuged to remove any residual Buffer and 10µl of nuclease-free water was used to elute the RAN. After the clean-up, the concentration was measured with the NanoDrop 1000 (ThermoFisher Scientific) and 50pmol of cleaned-up RNA was used for labeling in a final volume of 5µl.

RNA labeling

For the RNA labeling the Pierce RNA 3' End Desthiobiotinylation Kit (#20163) was used. In more detail, the RNA was supplemented to a final volume of 6.25µl, 0.5 µl of DMSO were added and it was incubated on a Veriti® 60-well Thermal Cycler form Thermo Fisher Scientific at 85°C for 10min and then reannealed by ramping down the temperature to 10°C.

For the labelling reaction 1.75µl of nuclease-free water, 3µl of 10x RNA Ligase Reaction Buffer, 1µl of RNAse inhibitor, 6.25µl of 50pmol of reannealed RNA, 1µl of Biotinylated Cytidine Bisphosphate, 2µl of T4 RNA ligase and 15µl of PEG 30% were mixed in the above order to a final volume of 30µl. The reaction was carefully mixed

and incubated on a Veriti® 60-well Thermal Cycler from ThermoFisher Scientific at 16°C overnight.

After the overnight incubation, 70µl of nuclease-free water were added to the ligation reaction. As a next step, 100µl of chloroform were added in order to extract the RNA. The mixture was vortexed briefly and then centrifuged for 5min at 12,000 rpm to separate the phases. The aqueous phase was carefully removed and transferred to a 1.5ml Eppendorf tube. Then, 10µl of 5M NaCl, 1µl of glycogen and 300µl of ice-cold 100% ethanol were added before RNA being precipitated at -20°C for 2h. In the meantime, the cell lysate was precleared. In detail, 200µl (4ng/µl) of cell lysate per sample was used and 20µl of Pierce™ Streptavidin Magnetic Beads (1:10 of the lysate volume). A magnetic rack was used to gather the magnetic beads against the wall of the tube and washed twice with Tris-buffered saline (TBS, Product No. 28379, containing 0.05% Tween-20 Detergent). The beads were then re-suspended in 20µl of Tris and applied to the lysate. They were put in the cold room (4°C) at rotation for 2h. After the 2h had elapsed for the RNA precipitation, it was centrifuged at 13,000 × g for 15 minutes at 4°C. The supernatant was carefully removed and the pellet was washed with 300µl of ice-cold 70% ethanol carefully not to detach the pellet. The ethanol was carefully removed and the tubes flipped upside down for 5min to air-dry the pellet. Afterwards, the pellet was re-suspended in 20µl of re-suspension buffer (490µl of 20mM Tris-buffered saline supplemented with 10µl of 5M NaCl). They were incubated on a Veriti® 60-well Thermal Cycler from Thermo Fisher Scientific at 65°C for 10min before the temperature was ramped down to 4°C by 1.5% rate.

In the meantime, the RNA binding mastermix was prepared. In more detail, 20µl of Protein-RNA Binding Buffer, 60µl of 50% Glycerol, 1µl of 5M NaCl, 100µl of pre-cleared lysate and 19µl of nuclease-free water were mixed per sample. In a 1.5ml Eppendorf tubes, 200µl of the mastermix and 10µl of the labelled RNA were added and incubated at 4°C with rotation for 2h. In the meantime, 20µl of beads per sample were pre-cleared. In detail, a magnetic rack was used to gather the beads against the wall of the tube and they were washed twice with Tris. They were then re-suspended in 20µl of Tris and added to the RNA-protein samples and incubated for 2h at 4°C with rotation. Afterwards, a magnetic rack was used to gather the beads against the wall of the tube, the depleted supernatant was removed and kept at -20°C and the beads were washed off with 250µl of wash buffer for three times. Then, 40µl of elution

buffer was added, mixed well by vortexing and incubated at 37°C with mild agitation. With the help of a magnetic rack the beads were gathered against the wall of the tube and the eluate was removed and stored at -20°C.

3.19 In-gel digestion and HPLC-MS/MS analysis

To analyse the RNA Pull-down eluate, 20µl of each sample were loaded on to pre-cast 10-well NuPAGE Novex 4-12% gradient Bis-Tris polyacrylamide gels (Life Technologies), with 7µl of Novex Sharp Pre-stained Protein Standard (Invitrogen, Life Technologies) loaded as marker. Separation was achieved by electrophoresis for approximately 90min at 180V. Protein profiles of the gels were visualised by silver staining. All steps were performed with gentle shaking. After the electrophoresis, the gel was rinsed with ddH_2O and was incubated in fixing solution of 5% acetic acid and 50% methanol solution for 30min, at room temperature, followed by three brief washes in ddH_2O, and rehydration in ultrapure H_2O overnight at 4°C. The next day, gels were incubated in sensitising solution (1.25 mM sodium thiosulphate 5-hydrate) for 1min, washed for 1min with H_2O for three times and stained in 6mM silver nitrate solution for 30min at 4°C. After three brief washes in H_2O, gels were incubated in developing solution (280mM sodium carbonate, 5% formaldehyde) for approximately 5min until the protein bands are clearly discernable. Gels were washed in 5% acetic acid for 10min to stop the developing, followed by three washes in H_2O and placed in clear plastic bags to be scanned using a calibrated scanner (GS-800, Bio-Rad). Each gel lane was divided in twelve sections of various sizes, according to the amount of protein as judged by Silver staining, using a scalpel, and transferred to a 96-well plate for automated de-staining and tryptic digestion, using an Investigator ProGest (Digilab) robotic digestion system according to the manufacturer's protocol. The obtained peptide solution was frozen at - 80°C for at least 2 h and lyophilised under vacuum at -55°C for approximately 5h in a Christ Alpha 1-2 LD Freeze Dryer. The lyophilised peptides were re-suspended in 40 µl of 2% acetonitrile, 0.05% trifluoroacetic acid (TFA) in HPLC-grade H_2O and frozen at -20°C until mass spectrometric analysis.

3.20 In-solution digestion and HPLC-MS/MS analysis

After the preliminary results of the in-gel digestion were assessed an in-solution digestion was used due to the low number of proteins that were pulled-down. The eluates were denatured by the addition of 9M urea, 2M thiourea in a 1:2 ratio (final concentration 6M urea, 2M thiourea) and were vortexed briefly. Samples were then reduced by adding 100mM dithiothreitol (DTT; final concentration 10mM) followed by incubation at 37°C for 1 hour shaking at 600rpm. The samples were then cooled down to room temperature before alkylation of proteins using 500mM iodoacetamide (IAA, final concentration 50mM) followed by incubation in the dark for 1h at room temperature. Proteins were then precipitated using pre-chilled (-20°C) acetone in a 6:1 volume ratio, overnight. The next day, samples were briefly vortexed and centrifuged at 0°C for 40min. the protein pellets were fully dried using a SpeedVac Concentrator (ThermoFisher Scientific, Savant SPD131DDA) for approximately 30min. For protein digestion, samples were re-suspended in 40µl trypsin solution, containing 0.01µg/µl trypsin in 0.1 M triethylammonium bicarbonate (TEAB), pH 8.5, assuming 20µl, before briefly vortexing and centrifuging them. Proteins were digested overnight at 37°C under agitation (240rpm). The digestion was stopped by acidification of the samples with 10% v/v trifluoroacetic acid (TFA; final concentration 1%). Peptide samples were purified using a 96-well C18 spin plate (MicroSpin, Harvard Apparatus, cat. no. 745617). The resin was activated using 200 µl methanol and centrifuged at 1000 x *g* for 1 minute. Wash steps included 200 µl of 80% acetonitrile (ACN), 0.1% TFA in H_2O, and three equilibration steps using 200µl of 1% ACN, 0.1% TFA in H_2O with centrifugation (1000 x *g* for 1 minute) after each step. Samples were loaded onto the resin and centrifuged at 2250 x g for 1 minute; the flow through was reloaded onto the resin a second time and centrifugation repeated. The resin was then washed three times with 200µl 1% acetonitrile (ACN), 0.1% TFA in H_2O (centrifugation at 2250 x *g* for 1 minute). Finally, the samples were eluted with 170 µl of 50% acetonitrile, 0.1% TFA in H_2O (centrifugation at 1000 x g for 1 minute); this step was repeated, combining the collected eluate. Samples were then dried down using the SpeedVac Concentrator for approximately 5 hours. Dried peptide samples were reconstituted with TFA (0.05%) in ACN (2%) (Thermo Scientific, 51101) and separated by a nanoflow LC system (Dionex UltiMate 3000 RSLC nano). Samples were injected onto a nano-trap column (EASY-Spray PepMap® RSLC C18, 2µm 100Å, 75µm x 50cm) (Thermo Scientific, ES803), at a flow rate of 25 µL/min for three minutes, using 2% ACN, 0.1% FA in H_2O.

The following nano-LC gradient was then used to separate the peptides at 0.25 µL/min: 0−5min, 4-10% B; 5−75min, 10-30% B; 78−80min, 30−40% B; 85-89min, 99%B, 90-120min 4%B, where A=0.1% formic acid (FA) in H_2O, B=80% ACN, 0.1%FA in H_2O. The nano column (Acclaim® PepMap100 C18, 50 cm x 75 µm, 3µm, 100 Å) was set at 45°C and coupled to a nanospray source (Picoview, New Objective, US). The temperature of the analytical column was set at 45°C and connected to an EASY-Spray ion source (Thermo Scientific, ES081). Spectra were collected from an Orbitrap mass analyser (Q Exactive HF, Thermo Scientific) using full Mass Spectrometry (MS) mode (resolution of 60,000 at 200 m/z) over the range 350–1600 m/z. Data-dependent MS2 scan was performed using Quadrupole isolation in Top15 mode using higher energy collision dissociation (HCD) fragmentation in each full MS scan (resolution of 15,000 at 200m/z) with dynamic exclusion enabled. Data-dependent MS2 scan was performed using the top fifteen ions in each full MS scan (resolution of 17,500 at 200 m/z) with dynamic exclusion enabled. Proteome Discoverer software (Thermo Scientific, version 2.2.0.388) was used to search the raw data files against the mouse database (mouseSP201701, 16,844 protein entries) using Mascot (version 2.6.0, Matrix Science).

The mass tolerance for precursor ions and fragment ions was set at 10 ppm and 20 mmu, respectively. Trypsin was used as the digestion enzyme with up to two missed cleavages allowed. Variable modifications included acetylation of N-terminus, oxidation of methionine residues and deamination of asparagine in the presence of O_{18} water. MS/MS-based peptide and protein identifications were validated after filtering for a peptide probability of greater than 95%, a protein probability of greater than 99% and at least two proteins per sample group. Data was normalised to the total peptide amount to take into account inter-sample variations in abundances and scaled on all average. The normalised total precursor intensity was used for quantification.

3.21 Software analysis of proteomic data

For the analysis of the interactions of the proteins that were identified with Mass Spectrometry a set of the of software were used.

STRING (Search Tool for the Retrieval of Interacting Genes/Proteins) software provides information on known and predicted protein-protein interactions based on experimental evidences and multiple other sources. An additional advantage is that the interactions are presented according their confidence following statistical advantage.

Cytoscape, an open source software, employs protein-protein interaction data from large databases and provides information on the functionality of the proteins, their interaction networks and link the networks to databases of functional annotations. Moreover, Cytoscape offers a comprehensive visualisation of the interactions.

Lastly, Reactome, an open-source and curated database of pathways, integrates user-supplied data as well as data from a set of databases to perform a pathway and reaction analysis combined with statistical analysis of the results.

3.22 Immunoblotting

Western Blot analysis was used for the validation of the Mass Spectrometry data. Eluate from RNA Pull-down was separated on a pre-cast 10-well NuPAGE Novex 4-12% gradient Bis-Tris polyacrylamide gels (Life Technologies) as described above in 3.18. For immunoblotting, proteins were transferred from the polyacrylamide gel to a nitrocellulose membrane in ice-cold transfer buffer (25mM Tris base and 200mM glycine dissolved in 20% methanol) for 2h at 350mA. Proteins were then stained with Ponceau S solution (SIGMA, cat. no. P7170) to confirm adequate transfer. After washing in TBS with 0.1% Tween-20 (TBS-T), membranes were blocked with 5% milk in TBS-T for 1h at room temperature. Membranes were washed briefly in TBS-T and incubated overnight in primary antibody solution (see list below, Table 2) at a 1:1000 dilution in 5% bovine serum albumin (BSA; Sigma, cat. no. A9418) in TBS-T at 4 °C while rotating. Membranes were then washed thrice for 10min in TBS-T, followed by incubation with a light chain specific horseradish peroxidase (HRP)-conjugated secondary antibody (Dako) to detect the primary antibody, in a 1:5000 dilution in 5% fat-free milk in TBS-T for 1h at room temperature. After three washes in TBS-T (10min each), membranes were developed using enhanced chemiluminescence (ECL, GE

Healthcare) on a Xograph processor with exposure time dependent on signal intensity.

Table 2. Primary antibodies used for immunoblotting.

Primary antibody (species)	**Company, catalogue no.**
Larp1 (Rabbit)	Proteintech 13708-1-AP
IGF2BP2 (Rabbit)	Proteintech 11601-1-AP
hnRNPE1 (Rabbit)	Proteintech 145231-AP
DHX9 (Rabbit)	Proteintech 177211-AP
EIF2AK2 (Rabbit)	Proteintech 182441-AP
ILF3 (Rabbit)	Proteintech 198871-AP
Tra2b (Rabbit)	Abcam ab31353

3.23 Statistical analysis

Statistical analyses of the levels of the miRNAs of different clusters upon editing were performed with the ANOVA test with Dunnett post hoc test. Results are given as mean±SD. A value of $P<0.05$ was considered significant. Microsoft® Excel® (version 14.0.7208.5000) and GraphPad Prism (version 7.00) were used for statistical calculations. MS data were quantified using normalised total intensities and analysed as described previously. All other statistical analyses were performed with Microsoft® Excel® (version 14.0.7208.5000) and GraphPad Prism (version 7.00). FDR correction was used to correct for multiple testing for the statistical analysis of the Mass Spectrometry data. P-values<0.05 were considered significant with * signifying a p-value<0.05 and ** a p-value<0.01.

Chapter 4 EVALUATION OF THE DELIVERY METHOD FOR CRISPR/Cas9 AND ITS EFFICIENCY IN EDITING THE TARGETED SITES

4.1 Introduction

The extended miR-15 family comprises of 10 members (miR-107, miR-103, miR-15a, miR-15b, miR-16, miR-195, miR-497, miR-503, miR-424 and miR-646) of miRNAs which share an identical seed sequence (Figure 1.4).

The members of the family are clustered in three separate chromosomes, with miR-195, the miRNA of interest of the current study, being clustered together with miR-497. The inhibition of miR-195, with the use of antimiRs/antagomiRs, is not precise, due to the high homology of sequence that the two miRNAs of the same family share and their identical seed sequence, a feature that leads to the non-specific downregulation of multiple members of the same family.

In this project, CRISPR/Cas9 system was employed to edit the genomic locus of miR-195 to assess whether genome editing can result in specific inhibition of the miRNA without affecting the levels of the other members of the family. CRISPR/Cas9 has emerged as a fast, easy-to-use and highly specific method for editing DNA in eukaryotic cells[179, 196] although there are limitations, concerning the delivery of the system to cells, that need to be overcome[230]. The objective of the study was to take advantage of the CRISPR/Cas9 system to target the miR-195 genomic locus in primary cells with high specificity. By using sgRNAs designed to target specific sites in the stem loop of miR-195, a part of the genomic locus of the miR-195 was edited, a change that was expected to impair Drosha's ability to process the stem loop. In more detail, the aims were to:

- Establish a reliable workflow for miRNA inhibition using genome editing by:
    - Designing *in silico* and testing sgRNAs that target and edit miRNA genes,
    - Identifying the optimal delivery method for CRISPR/Cas9 in primary cells and

- Determining the appropriate conditions for achieving high editing efficiency

- To genetically engineer, with the use of CRISPR/Cas9, stable cell lines of SMCs that harbour deletions of miR-195 and

- To assess putative off target mutagenesis of the guides tested.

The results presented in this chapter demonstrated that transfection of mouse VSMCs stably expressing Cas9 with IVT guides lead to efficient editing of the mmu-miR-195a genomic locus and downregulation of the levels of the miRNA.

4.2 Experimental Design

The present study aimed to explore the use of CRISPR/Cas9 in editing miRNA genes in primary cells in order to investigate their regulation and function. The focus of it was miR-195, a miRNA previously shown to participate in the onset and development of AAA[98]. As an initial step, different strategies were tested to generate genetically engineered SMCs that harboured a deletion for miR-195. To achieve sufficient editing efficiency and take advantage of the latest technological developments in the field, a total of four experimental strategies were employed:

(A) Plasmid delivery of the CRISPR/Cas9 system,

(B) Lentiviral delivery of the CRISPR/Cas9 system,

(C) Cas9 ribonucleoproteins (Cas9/RNPs) and

(D) Transfection of VSMCs stably expressing Cas9, with IVT sgRNAs.

Firstly, after designing guides targeting the desired sites *in silico*, the plasmid delivery was assessed in human cells. By using plasmids, which harboured the corresponding guide sequences and the Cas9 gene, we tested their ability to edit the targeted site and their efficiency. The efficiency of editing was also assessed at different time points. By doing so, potential effects on the viability of the cells, as a result of the transfection or the editing, were assessed. Genomic DNA was also sequenced to identify the mutation patterns. However, the obtained results suggested a rather low efficiency and led to undertaking a different delivery technique.

As a second strategy, lentiviral particles were used to infect primary cells. Since the lentiviral infection results in the integration of the sequence of interest into the genome, we expected to have more efficient gene editing of the miR-195 locus. The second strategy was assessed in two different human cell types, HUVECs and human SMCs, with the results suggesting a substantial editing efficiency, and mouse VSMCs

with the efficiency reaching significant levels. However, the strategy was deemed as non-optimal because of the potential high off-target mutagenesis, due to the continuous presence of Cas9/RNP complexes in the cells, as well as due to the limitations of the lentiviral delivery.

To address these issues, a third strategy was employed. Transient transfection of cells with Cas9/RNPs was performed. Commercially available recombinant Cas9 proteins were used along with IVT sgRNA designed to target the human miR-195 and assessed in *in vitro* experiments. Additionally, HEK293T cells were transfected with Cas9/RNP complexes with the editing efficiency not reaching sufficient levels.

Furthermore, mouse VSMCs were infected with lentiviral particles that harboured only the Cas9 gene, thus generating stable cell lines that were stably expressing the Cas9 protein. The cells were then transfected with IVT guides. The approach was thought as the most suitable to overcome the limitations of transfecting cells, an approach that led to low efficiency of editing. After concluding to our approach of choice, the levels of the mature miRNA were assessed in mouse VSMCs to determine the impact of gene editing in the mmu-miR-195 inhibition. The effect on the expression levels of other members of the miR-15 family was also evaluated.

Finally, possible off-target mutagenesis was studied, with the experiments showing that there were no off-target sites for the guides used at the *in silico* predicted sites.

4.3 Results

4.3.1 Gene Editing in Human Cells

4.3.1.1 In Silico sgRNA Design for hsa-miR-195 and cloning

The CRISPR DESIGN Tool (http://crispr.mit.edu, Zhang Lab, MIT) was used to design the guides for the genomic locus of miR-195 (Figure 4.1). The DNA sequence corresponding to the locus of the miRNA gene was used as input sequence to the software. The following oligos, which targeted sites in the miR-195 stem loop (Figure 4.2), had the highest score:

sg195g1(G1): 5'-GGAAGCGAGTCTGCCAATAT-3'

sg195g2(G2): 5'-TTGAGGCAGAACTTACTCCC-3'

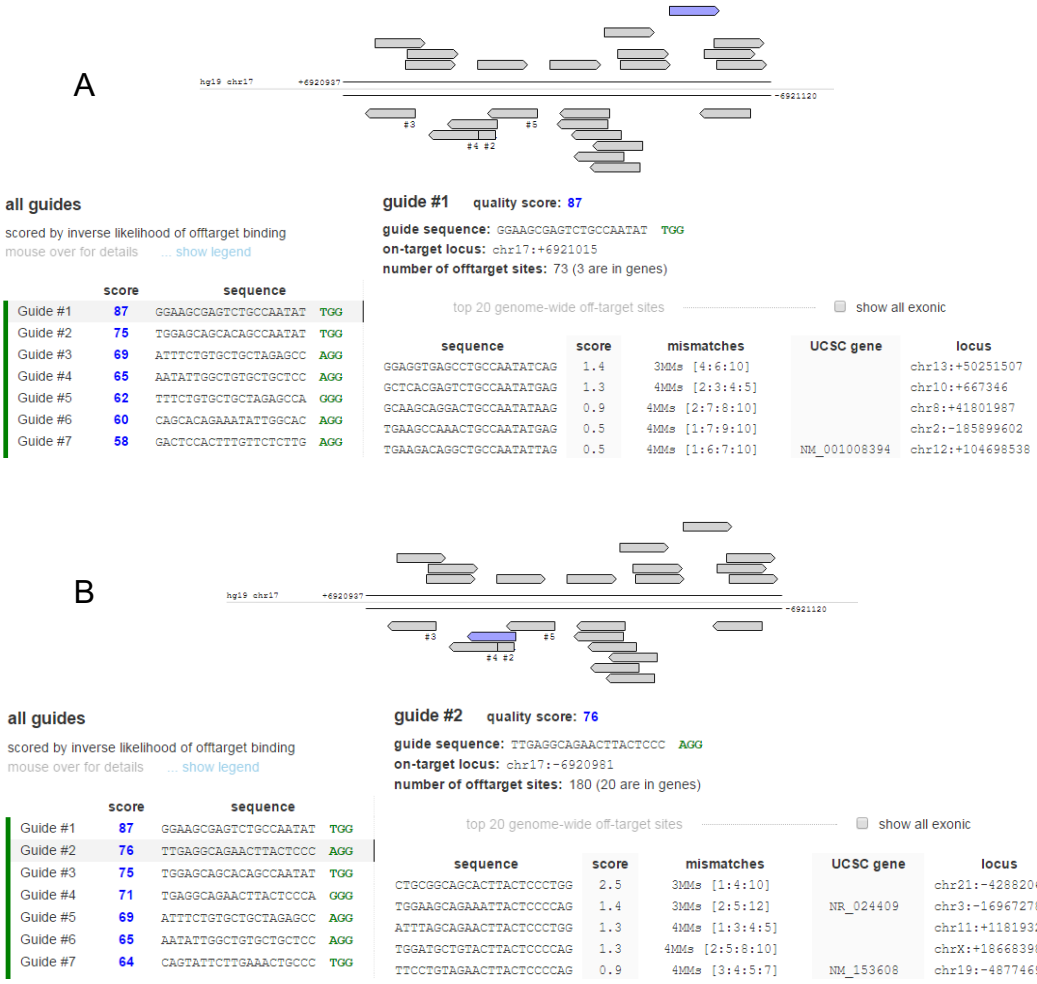

Figure 4.1 In silico design of the single-guide RNA for hsa-miR-195 locus. The guides used for the human miR-195 locus were designed with the help of the CRISPR DESIGN Tool (http://crispr.mit.edu, Zhang Lab, MIT). The guide sequence is depicted, with the corresponding score and the 5 most likely off target sites for guide (**A**) sg195G1 and (**B**) sg195G2.

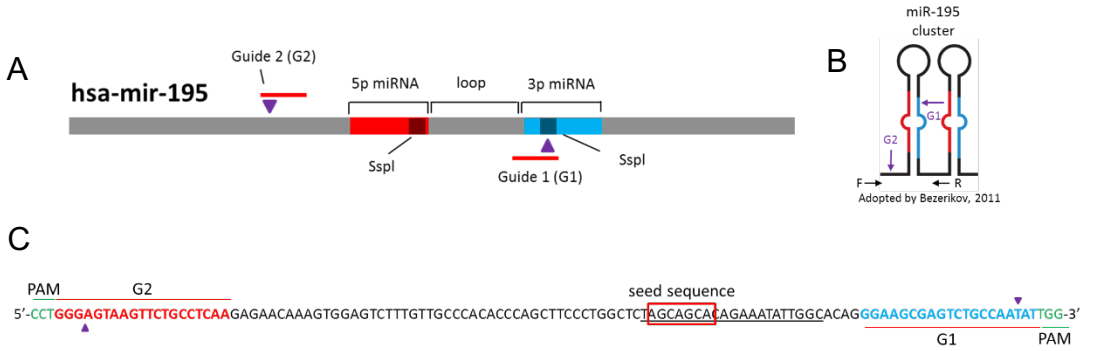

Figure 4.2 Schematic representation of the editing of the hsa-miR-195 genomic locus. (**A**) The hsa-miR-195 genomic locus with the corresponding elements. The location of the 5p arm of the miRNA is highlighted in red and the location of the 3p arm of the miRNA is highlighted in blue. The SspI restriction enzyme sites are depicted as squares. (**B**) Schematic of the miR-195~497 cluster and the location of the DSBs. (**C**) The genomic DNA sequence of the miR-195 locus. The mature miR-195 is underlined and the seed sequence is highlighted with a red rectangular. The target sites of the two guides are shown with their corresponding PAM sequences highlighted in green. The positions, where the DSB occurred, are depicted with a purple triangle. G1: sg195G1 and G2: sg195G2.

4.3.1.2 Strategy A: Plasmid Delivery

To determine the efficiency of the selected guides, HEK293T cells were transfected with pX330 plasmids harbouring the sgRNAs (pX330G1 and pX330G2). PCR amplification of the genomic locus revealed two bands in the samples that were transfected with both plasmids (Figure 4.3A), a long one corresponding to the full size and a shorter one corresponding to a truncated product. The latter was a result of the simultaneous editing of the locus by both guides and the perfect re-ligation of the strands which resulted in the deletion of a 105bp long fragment as confirmed by sequencing. The gene editing efficiency of each treatment was assessed with the T7EI assay (Figure 4.3B). Each of the single guides demonstrated an efficiency which varied from 24-27% while the combination of both guides showed an efficiency of 34%. Editing efficiency did not change between Day2 and Day5 post transfection. Sanger sequencing was used to identify the mutation patterns. In total, a variety of patterns were observed: (i) DNA that was not edited, (ii) DNA that had a deletion of a 105bp long sequence upon editing from both guides and perfect re-ligation of the DNA strands, (iii) DNA with short indels at the site where the DSB occurred and (iv) DNA with a 160bp long deletion and an insertion starting at the site of G1 (Figure 4.3E).

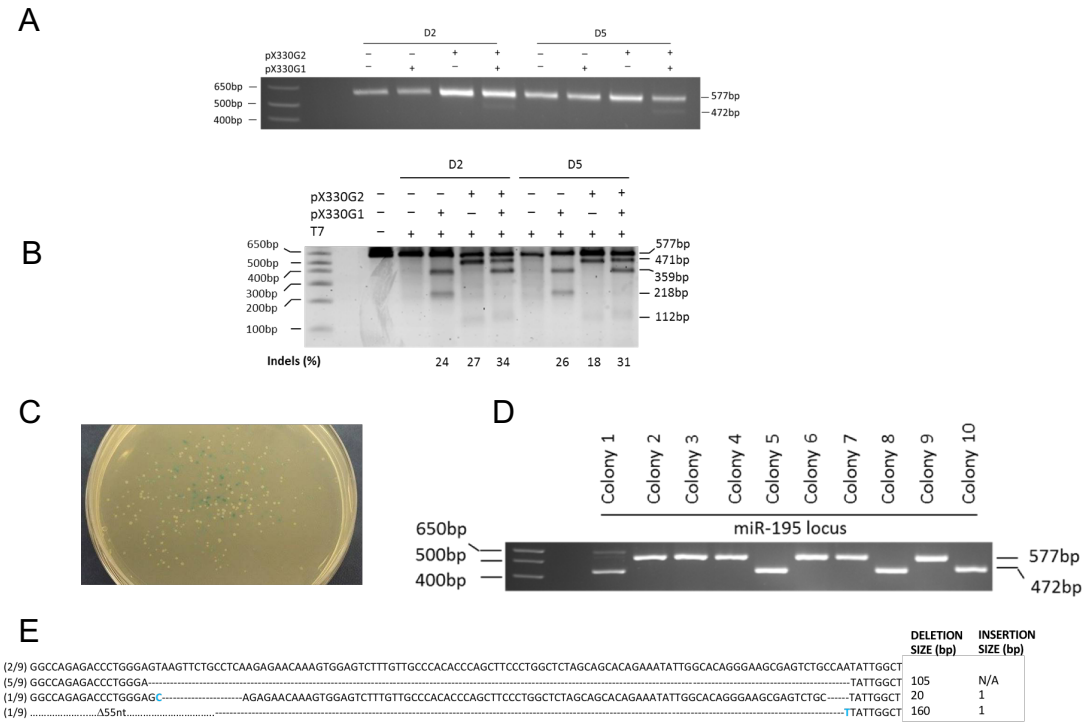

Figure 4.3 Gene editing of the miR-195 genomic locus using plasmid vectors. (**A**) HEK293T cells were transfected with the pX330 plasmid harbouring Cas9 and sgRNA1 or sgRNA2 (pX330G1 and pX330G2, respectively). On Day 2 (D2) and Day 5 (D5) post transfection, DNA was harvested and the genomic locus of miR-195 was PCR amplified. Agarose gel electrophoresis revealed two amplicons of different size in the cells that were transfected with both guides simultaneously, one corresponding to the full-size product (577bp) and one to the truncated product (471bp). (**B**) T7EI assay was used for assessing the gene editing efficiency that ranged from 18-34%. (**C**) Blue and white colony screening was used to pick the colonies that were successfully transformed with the PCR amplicons. (**D**) PCR amplification of the isolated plasmids indicated the differences in the size of the cloned sequences. (**E**) Nine colonies were selected according to the size of the PCR amplicon and were Sanger sequenced. Dashes represent deletions and insertions are highlighted in blue. G1: sg195G1 and G2: sg195G2, n=1.

4.3.1.3 Strategy B: Lentiviral Delivery in Human Primary Cells

4.3.1.3.1 Gene Editing in HUVECs

To facilitate the delivery of the CRISPR/Cas9 system to primary cells lentiviral particles were used. HUVECs were infected simultaneously with lentiviral particles harbouring both sgRNAs (LEG1 and LEG2).

Titration experiments with PLUS™ Reagent, a reagent that enhances cationic lipid-mediated transfection of DNA into cultured eukaryotic cells, were conducted. Indeed, high editing efficiency was observed based on the intensity of the bands that corresponded to the truncated product (Figure 4.4, lanes denoted with asterisks). The T7EI confirmed the high editing efficiency. Moreover, the fact that, after the T7EI only 4 distinct bands were observed indicates perfect re-ligation of the DNA bands while, the marginally higher editing efficiency in the case PLUS™ Reagent was not used, demonstrated the efficient delivery of the system (Figure 4.4).

Next, in three independent experiments PCR amplification of the locus revealed two bands for the edited cells with the shorter one corresponding to the truncated product in accordance with the results for the plasmid delivery (Figure 4.5A). The T7EI assay revealed editing efficiency varying from 81-96% (Figure 4.5B). Sanger sequencing revealed 3 different mutation patterns: (i) DNA that had a deletion of a 105bp long sequence upon editing from both guides and perfect re-ligation of the two strands and (ii) DNA with short indels at only one or (iii) both sites of the DSB (Figure 4.5C).

The pattern of the DNA bands, after the T7EI digestion, differs among the samples infected with only one of the two guides and those infected with both guides. In the latter occasion, only four bands are observed: (i) the band corresponding to the full sequence, (ii) the band of the truncated sequence, (iii) the band corresponding to a 359bp long sequence and (iv) the band of the 112bp long sequence while the 465bp and 218bp long bands, which are noticed in the treatments with either LEG1 or LEG2, are not detected. These differences are due to the simultaneous cleavage of the sequence by the two guides which result in the generation of a diverse cleaving pattern (Figure 4.6).

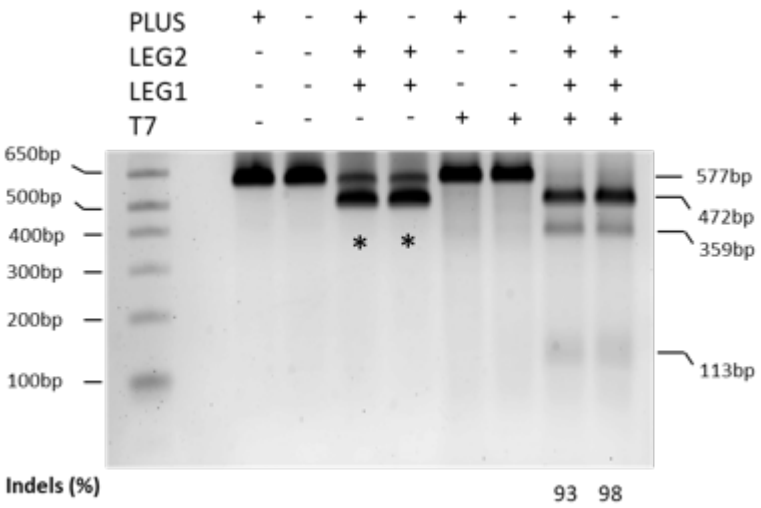

Figure 4.4 T7 Endonuclease I assay for HUVECs upon lentiviral infection. HUVECs were infected with lentiviral particles harbouring Cas9 and sg195g1 or sg195g2 (LEG1 and LEG2, respectively). On Day 3 post infection, DNA was harvested and the genomic locus of miR-195 was PCR amplified. In the cells that were infected with both guides simultaneously PCR revealed two bands, one corresponding to the full-size product (577bp) and one to the truncated product (471bp), derived from perfect re-ligation of the genomic DNA following the two DSBs, n=2.

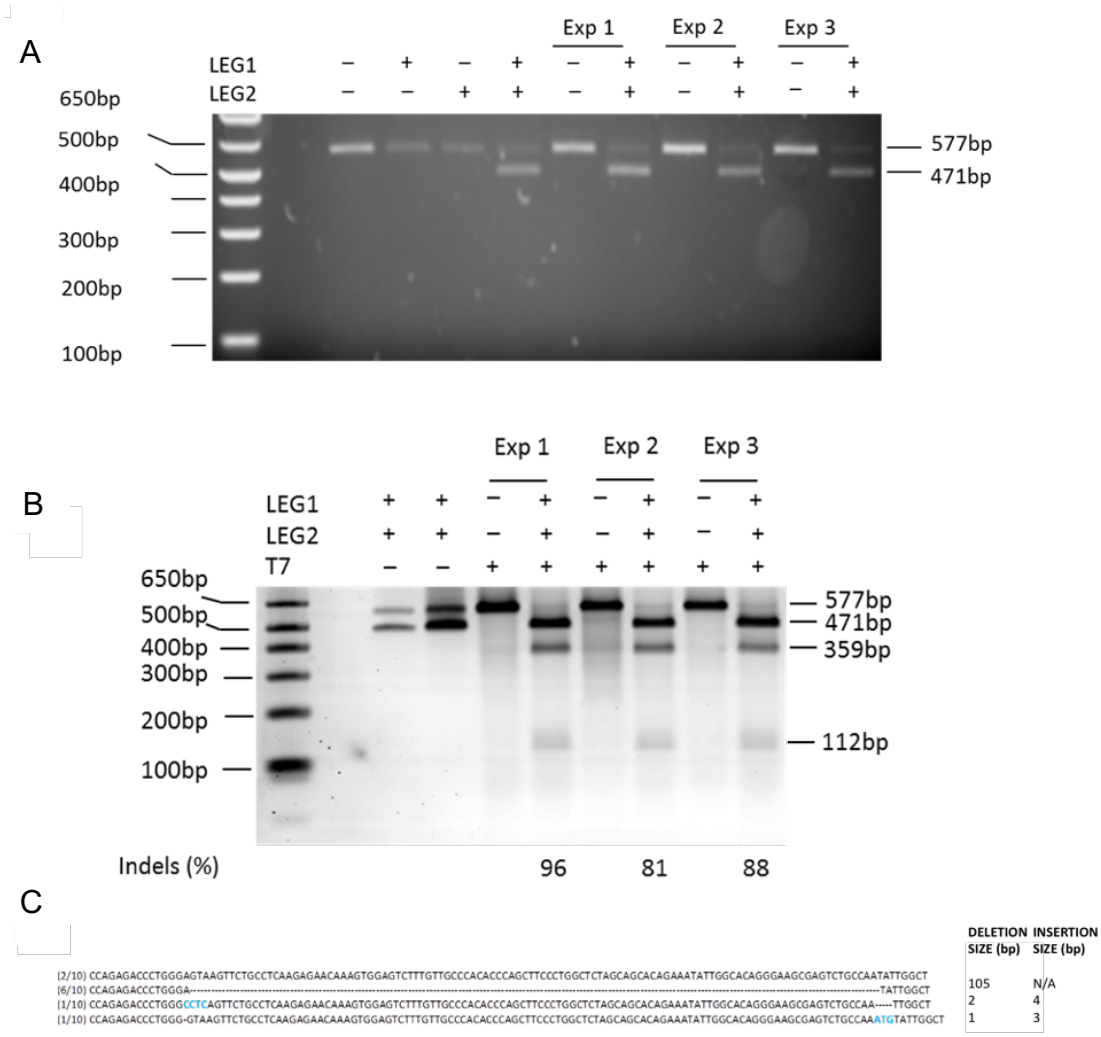

Figure 4.5 Lentiviral delivery of Cas9 and sgRNA. (**A**) HUVECs were infected with lentiviral particles harbouring Cas9 and sg195g1 or sg195g2 (LEG1 and LEG2, respectively). On Day 3 post infection, DNA was harvested and the genomic locus of miR-195 was PCR amplified. In the cells infected with both guides simultaneously PCR revealed two bands, one corresponding to the full-size product (577bp) and one to the truncated product (471bp). (**B**) The T7EI assay revealed an edited efficiency of 81-96%, in three independent experiments. (**C**) Mutation screening was assessed using Sanger sequencing. Dashes represent deletions, insertions are highlighted in blue. Exp=Experiment, (n=3).

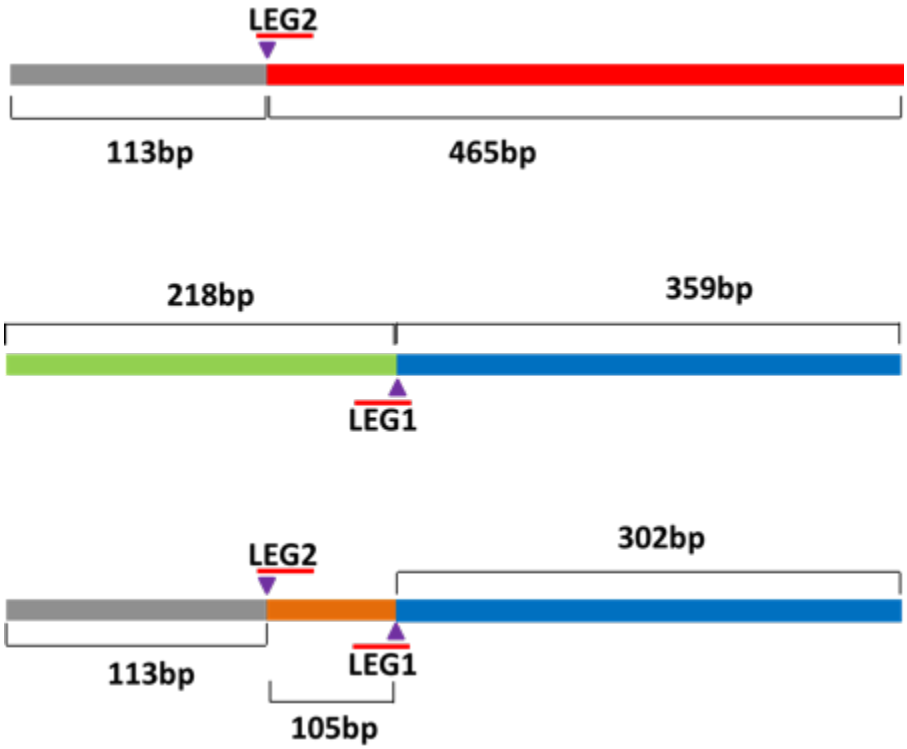

Figure 4.6 Schematic representation of the digestion products upon editing with guides sg195g1 and sg195g2. Upon T7EI digestion of the miR-195 amplicon (**A**) gene editing using the LEG2 is predicted to generate two fragments of 112bp and 465bp, (**B**) gene editing using the LEG1 is predicted to generate two fragments of 218bp and 395bp and (**C**) gene editing using the LEG12 and LEG2 followed by perfect re-ligation will generate a truncated product consisting of the two fragments of 1112bp and 359bp.

4.3.1.3.2 **Gene Editing in human SMCs**

Human SMCs were infected with lentiviral particles harbouring the designed sgRNAs (LEG1 and LEG2). PCR amplification of the locus revealed two bands. Based on T7EI assay gene editing efficiency that varied from 70-80% was identified (Figure 4.7).

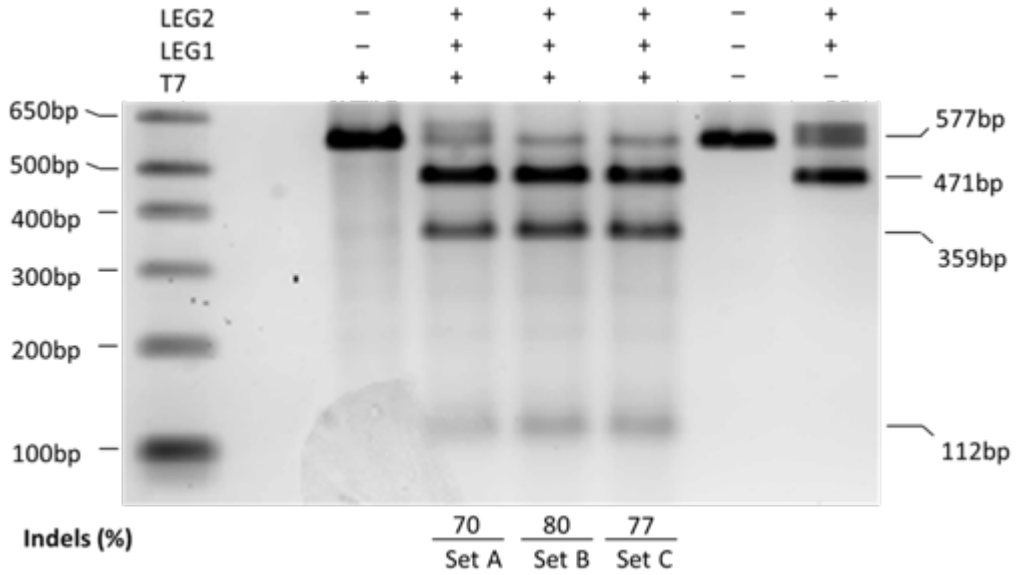

Figure 4.7 T7 Endonuclease I assay for hSMCs upon lentiviral infection. Human SMCs were infected with lentiviral particles harbouring Cas9 and sg195g1 or sg195g2 (LEG1 and LEG2, respectively). On Day 3 post infection, DNA was harvested and the genomic locus of miR-195 was PCR amplified. The cells infected with both guides simultaneously revealed, after PCR amplification, two bands, one corresponding to the full-size product (577bp) and one to the truncated product (471bp), (n=3).

4.3.1.4 Strategy C: Cas9/RNPs in HEK293T cells

As a third approach, Cas9/RNPs were used. *In vitro* transcribed guide G2 was used to form Cas9/RNP complexes. In order to test for the ability of the Cas9/RNP complex to cleave the targeted DNA sequence, an *in vitro* Cas9 digestion was performed which showed that Cas9 is able to cleave the PCR template when in complex with guide G2. The sizes of the two observed bands corresponded to the position of the cleavage by guide G2 and the digestion was complete (Figure 4.8A). Additionally, HEK293T cells were transfected with Cas9/RNPs to study the complexes' ability to recognise and cleave the targeted DNA in cells. T7E1 showed an editing efficiency of 25% (Figure 4.8B).

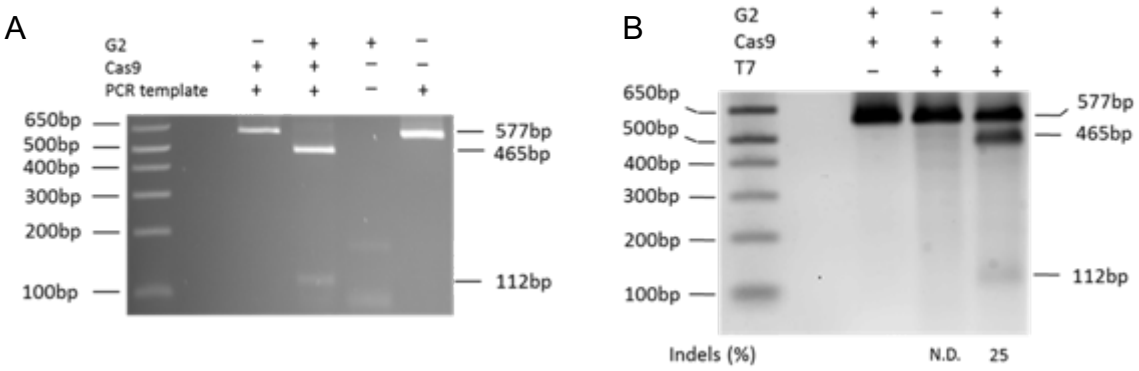

Figure 4.8 Assessment of Cas9/RNPs approach in HEK293T cells. (**A**) Cas9/RNPs complexes were generated by incubating Cas9 protein (0.5µg) with *in vitro* transcribed guide sg195g2 (G2), (125ng). The Cas9/RNPs were tested *in vitro* for their ability to recognise and cut the targeted DNA. (**B**) HEK293T cells were transfected with Cas9/G2 RNP complexes and the editing efficiency was assessed using T7EI assay. N.D: Not Detected, (n=3). Represantative results from only one experiment are shown.

4.3.1.5 Off-target Mutagenesis

Mutagenesis, in the most likely off-target sites (OFT), was assessed using the T7EI assay. DNA from lentiviral infected HUVECs that showed the highest editing efficiency was used. T7EI assay did not show any off-target editing. The non-specific bands, of shorter length, that were observed in some of the samples (Figure 4.9), did not result from gene editing, since they were observed in both the edited and unedited cells and their sizes did not correspond to the off-target cleavage of the LEGuides. OFT 2-5 for guide LEG1 and OFT 1, 2 and 4 for guide LEG2 were tested.

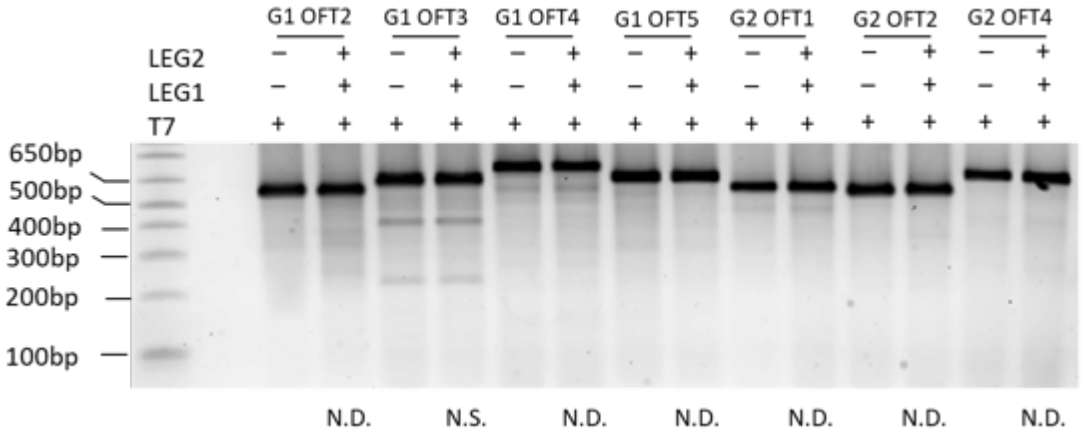

Figure 4.9 Assessment of possible off-target mutagenesis upon lentiviral infection of HUVECs. The most likely off-target sites for both guides (OFT 1-5), as suggested by the CRISPR DESIGN Tool (http://crispr.mit.edu, Zhang Lab, MIT), were assessed by T7EI assay. No off-target mutagenesis was detected for neither of the LEG1 and LEG2. OFT: Off-target, N.D.: Not Detected, n=1.

4.3.2 Gene Editing in Mouse Cells

4.3.2.1 In Silico sgRNA Design for mmu-miR-195 and cloning

The CRISPR DESIGN Tool (http://crispr.mit.edu, Zhang Lab, MIT) was used to design the guides targeting the mmu-miR-195 genomic locus (Figure 4.10). As an input, the DNA sequence of the locus of the miRNA was used. Three oligos, which targeted sites within the miRNA sequence (Figure 4.11 and Figure 4.12), with the highest scores, were selected:

sg195m2 (Gm2): 5'-TGGAGCAGCACAGCCAATAT-3'

sg195m4 (Gm4): 5'-CAGCACAGAAATATTGGCAT-3'

sg195mA (GmA): 5'-ATTTCTGTGCTGCTAGAGCC-3'

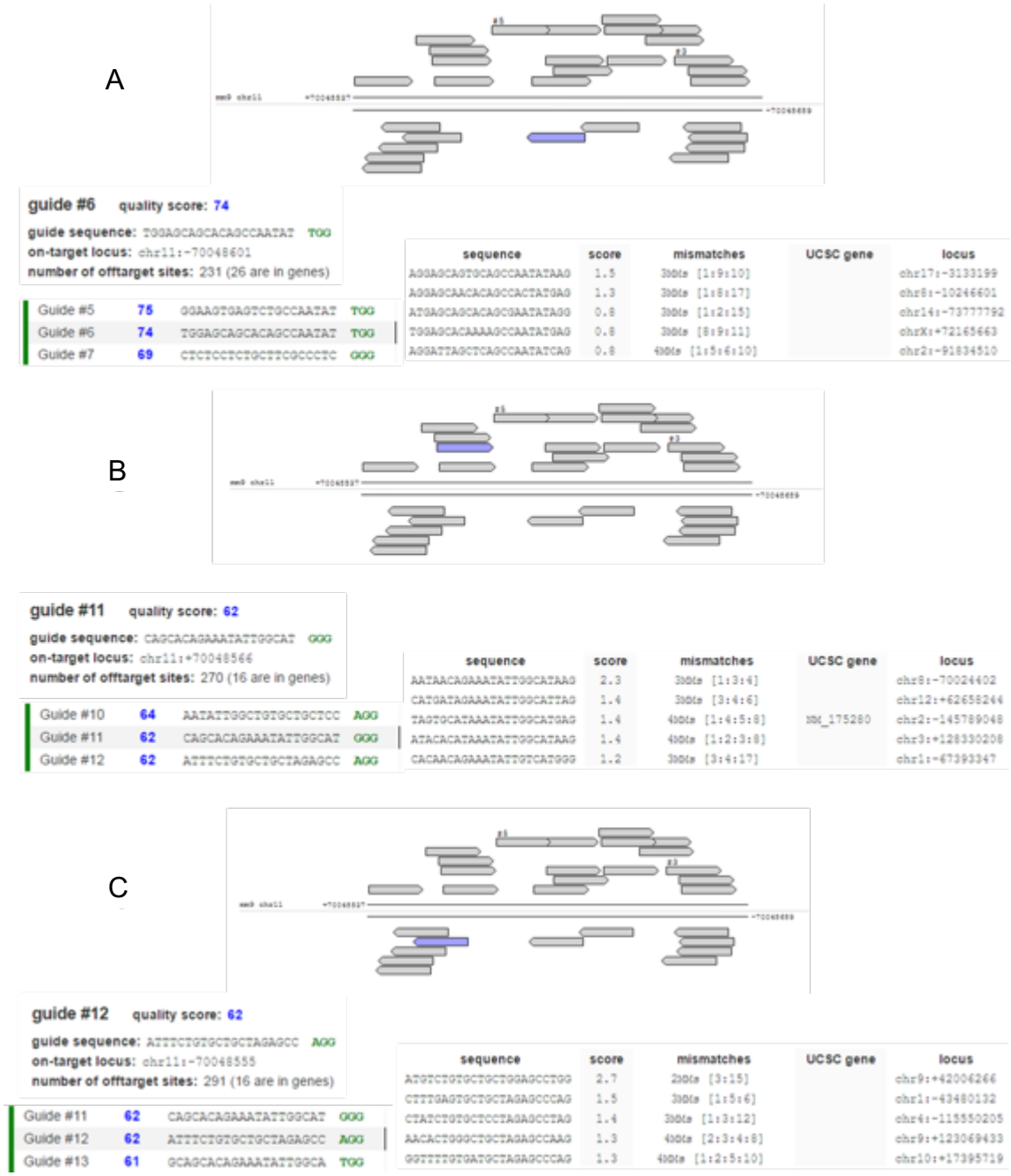

Figure 4.10 In silico design of the single-guide RNA for the mmu-miR-195a locus. The guides used for editing the mouse miR-195 locus were designed with the help of the CRISPR DESIGN Tool (http://crispr.mit.edu, Zhang Lab, MIT) on-line tool. The guide sequence is depicted, with the corresponding score and the 5 most likely off target sites for guide (**A**) sg195m2, (**B**) sg195Gm4 and (**C**) sg195GmA.

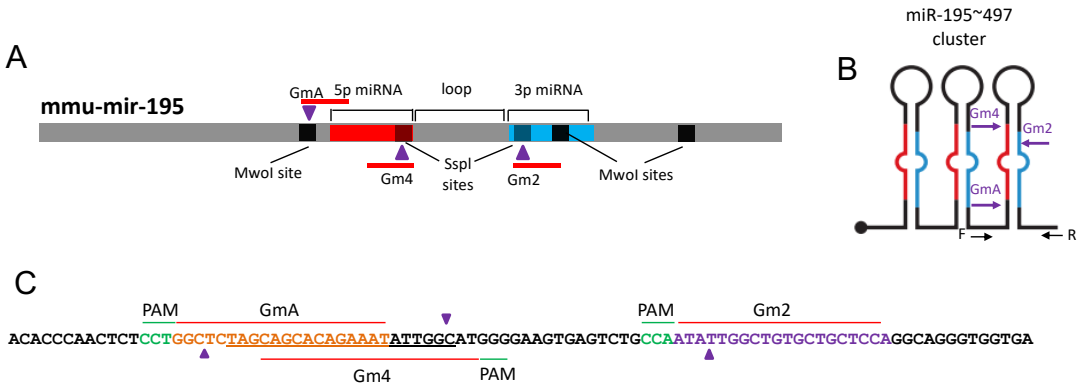

Figure 4.11 Schematic representation of the editing of the mmu-miR-195 genomic locus. (**A**) The mmu-miR-195 genomic locus. The location of the 5p arm of the miRNA is highlighted in red and the location of the 3p arm of the miRNA is highlighted in blue. DSBs are depicted as purple triangles and SspI and MwoI restriction sites are depicted as squares. (**B**) Schematic of the mmu-miR-195~497 cluster. (**C**) Part of the DNA sequence of the miR-195 locus. The DNA sequence of the mature mmu-miR-195 is underlined. The target sites of the guides are shown with their corresponding PAM sequences highlighted in green. The positions where the DSB occurs are depicted as purple triangles. Gm2: sg195m2, Gm4: sg195m4 and GmA: sg195GmA.

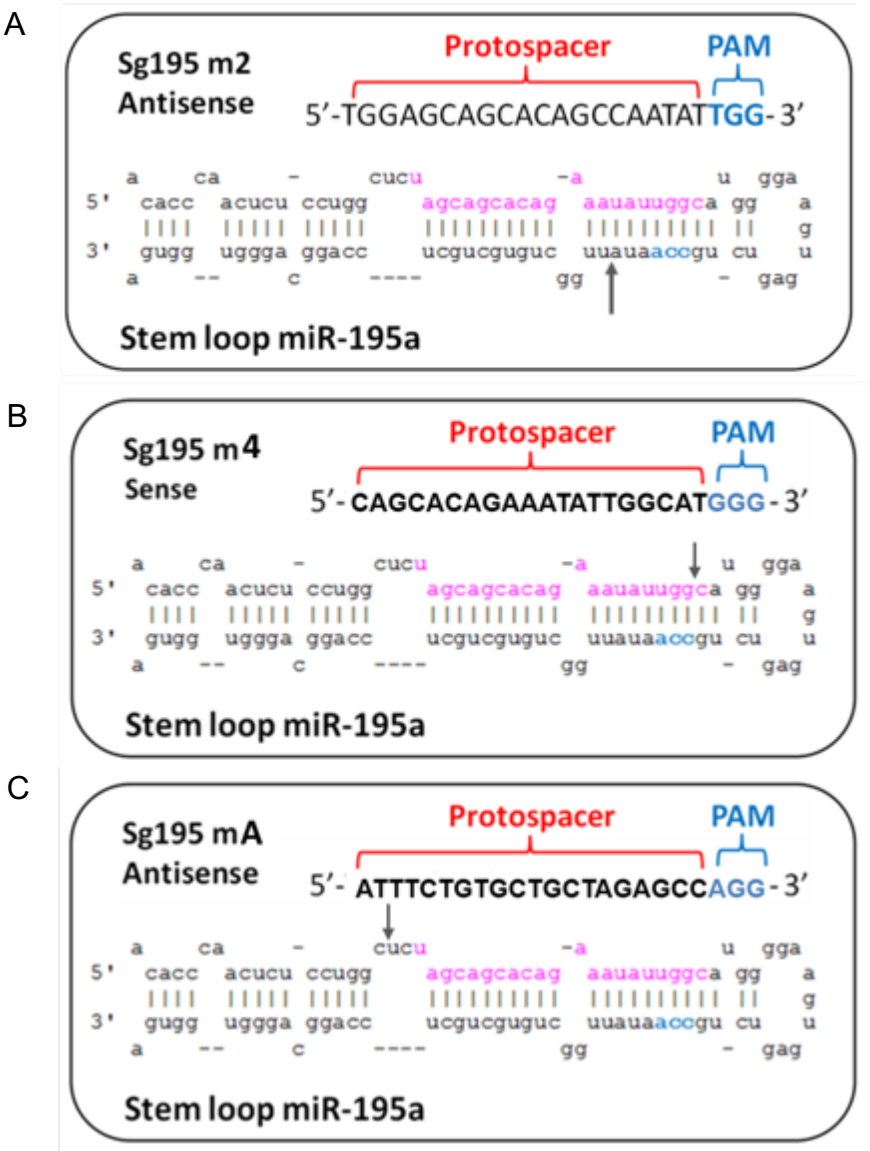

Figure 4.12 Schematic representation of the secondary structure of the mmu-miR-195a stem loop with guides. Representation of the mmu-miR-195a stem loop with the detailed sequence, bulges, mismatches and apical loop along with the targeted DNA sequence and the PAM sequence for (**A**) sg195m2, (**B**) sg195m4 and (**C**) sg195mA. PAM sequence is highlighted in blue. The mature miRNA sequence is highlighted in purple and grey arrows indicate the corresponding position of the DSB on the stem loop which is the site of mutations induced by random indels following editing of the genomic locus in mutant cells.

4.3.2.2 Strategy B: Lentiviral delivery in mouse VSMCs

4.3.2.2.1 Lentiviral particles Gm2 and Gm4

Mouse VSMCs were infected with lentiviral particles harbouring the designed guides Gm2 and Gm4 (LEGm2 and LEGm4). On Day 3 after the infection, gene editing efficiency was assessed by T7EI assay and it varied from 11-44%, (Figure 4.13).

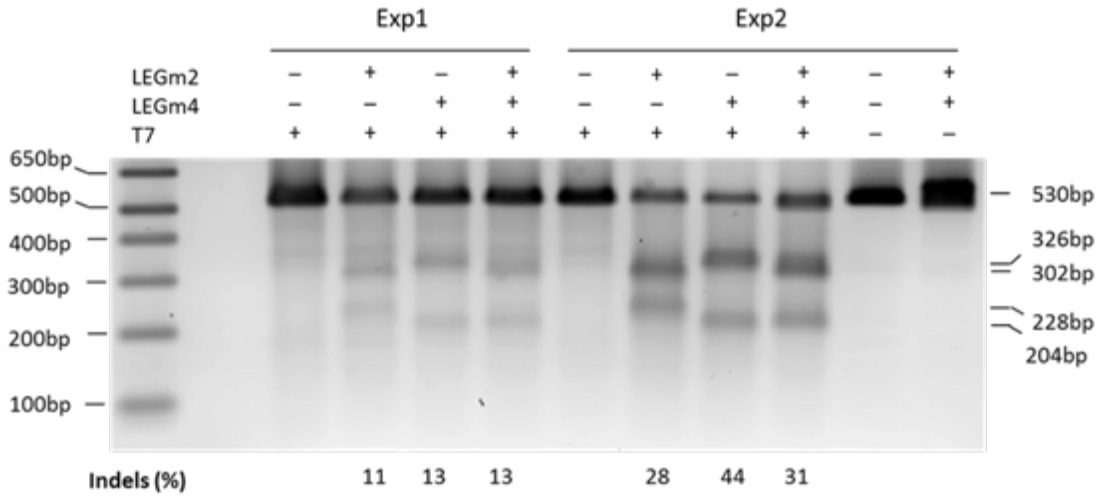

Figure 4.13 T7 Endonuclease I assay for mouse SMCs upon lentiviral infection with guides Gm2 and Gm4. Mouse SMCs were infected with lentiviral particles harbouring Cas9 and sg195m2 or sg195m4 (LEGm2 and LEGm4, respectively). On Day 3 post infection, DNA was harvested and the genomic locus of mmu-miR-195 was PCR amplified. T7EI assay was used to assess the efficiency of the editing in two independent experiments. Exp=Experiment, n=2.

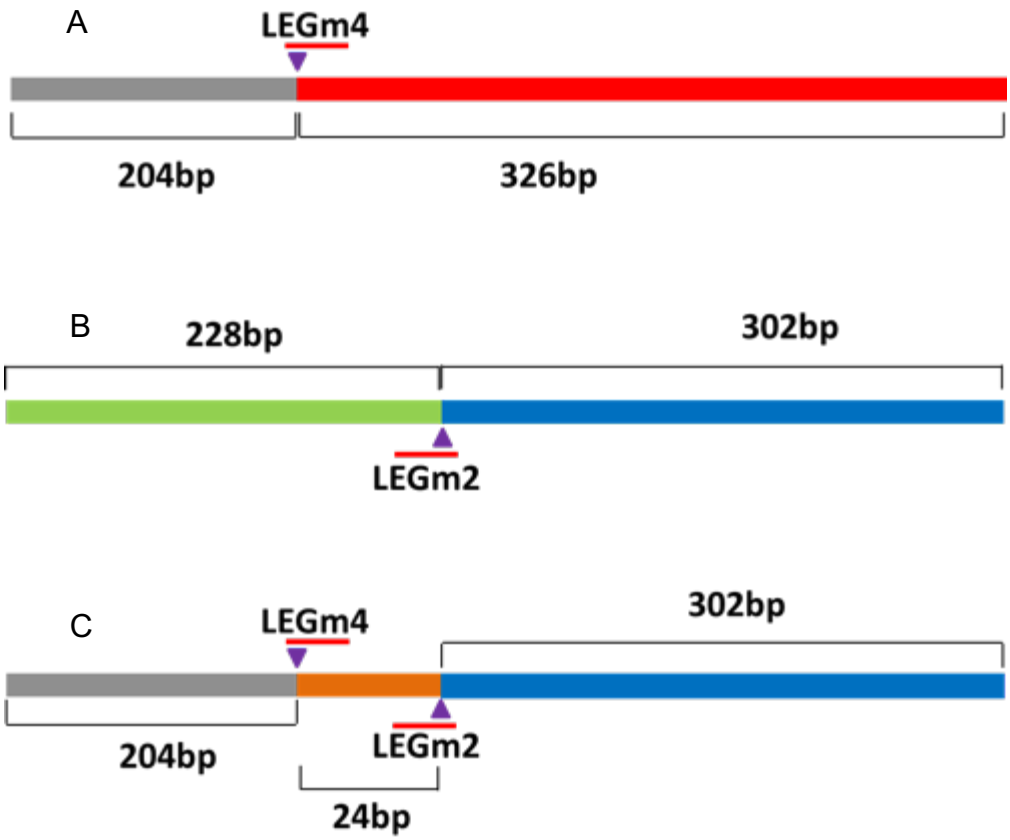

Figure 4.14 Schematic representation of the sizes of T7EI digestion products upon editing with guide Gm4 and Gm2. T7EI digestion of the mmu-miR-195 amplicon upon editing with (**A**) guide LEGm4 is predicted to generate two fragments of 204bp and 326bp, (**B**) guide LEGm2 is predicted to generate two fragments of 228bp and 302bp and (**C**) both guides simultaneously, followed by perfect re-ligation, will generate a truncated product consisting of two fragments of 204bp and 302bp.

4.3.2.2.2 **Lentiviral particles Gm2 and GmA**

Mouse VSMCs were infected with lentiviral particles harbouring the designed sgRNAs (LEGm2 and LEGmA). PCR amplification of the DNA harvested from the cells revealed two bands for the infected mouse VSMCs while T7EI assay showed a gene editing efficiency of 32% and 26% for LEGm2 and LEGmA respectively and 48-51% for cells infected with both guides simultaneously (Figure 4.15). The pattern of the DNA bands, after the T7EI digestion, differs according to the treatment. When mouse SMCs were infected with both guides at the same time, four bands can be observed: (i) a band of the full sequence (530bp), (ii) a band of the truncated sequence (484bp), (iii) a band corresponding to a 302bp long sequence and (iv) a band of the 182bp long sequence. These differences in the pattern between the single use of the guides and the infection with both together are the result of the simultaneous cleavage of the genomic locus by the two guides simultaneously (Figure 4.16).

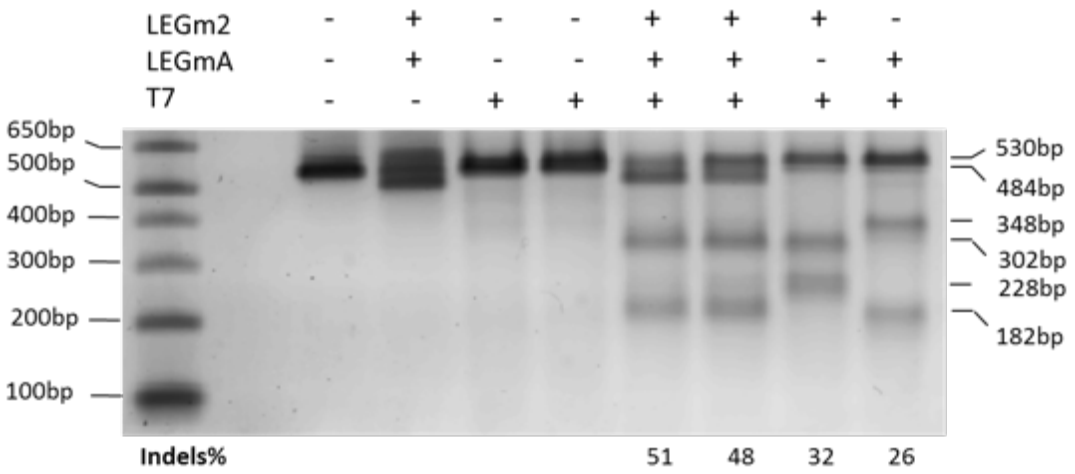

Figure 4.15 T7 Endonuclease I assay for mouse VSMCs upon lentiviral infection with guides Gm2 and GmA. Mouse VSMCs were infected with lentiviral particles harbouring Cas9 and guides sg195m2 or sg195mA expression (LEGm2 and LEGmA, respectively). On Day 3 post infection, DNA was harvested and the genomic locus of mmu-miR-195 was PCR amplified. The T7EI assay was used for assessing the efficiency of the editing, n=2.

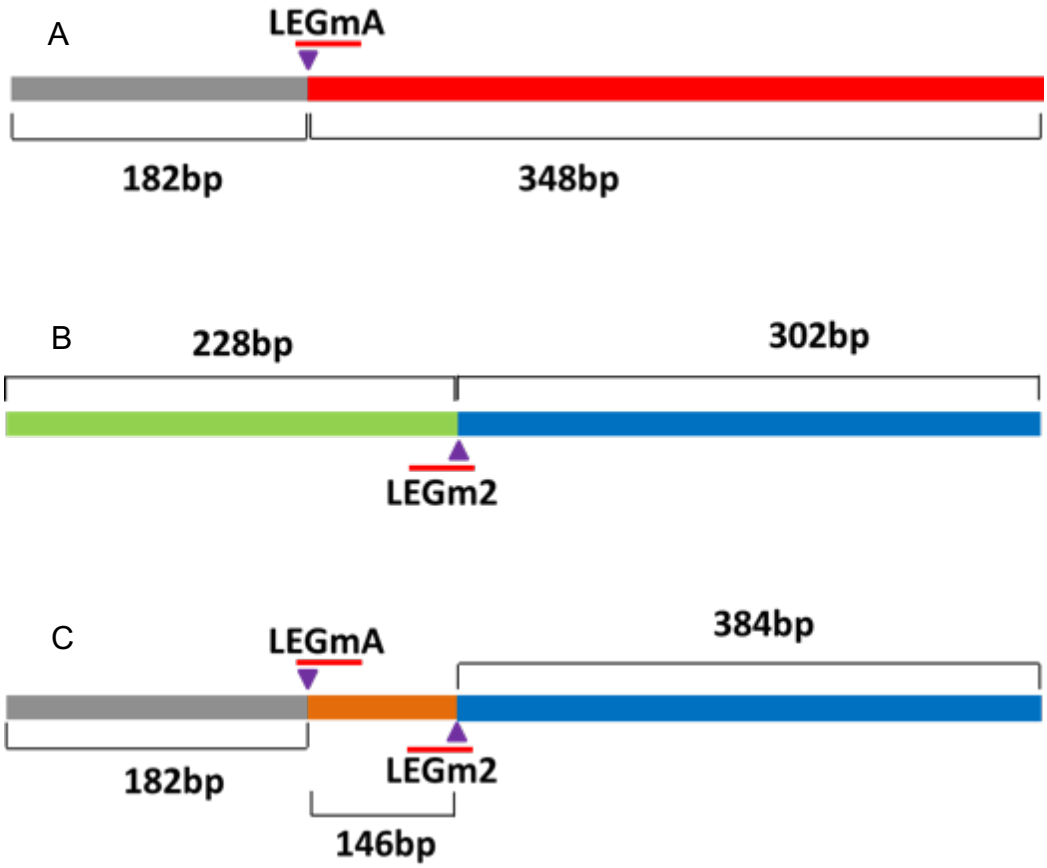

Figure 4.16 Schematic representation of the T7EI digestion products upon editing with guide GmA and Gm2. Upon T7EI digestion of the mmu-miR-195 amplicon (**A**) gene editing using the LEGmA is predicted to generate two fragments of 182bp and 348bp, (**B**) gene editing using the LEGm2 is predicted to generate two fragments of 228bp and 302bp and (**C**) gene editing using the LEGmA and LEGm2 followed by perfect re-ligation will generate a truncated product consisting of two fragments of 182bp and 302bp.

4.3.2.3 Strategy D: Transfection of mouse VSMCs stably expressing Cas9 with sgRNAs

Mouse VSMCs stably expressing Cas9 were generated by infecting cells with lentiviral particles harbouring Cas9. Following infection, cells were selected with Puromycin treatment (2µg/ml) for 48h, (Figure 4.17).

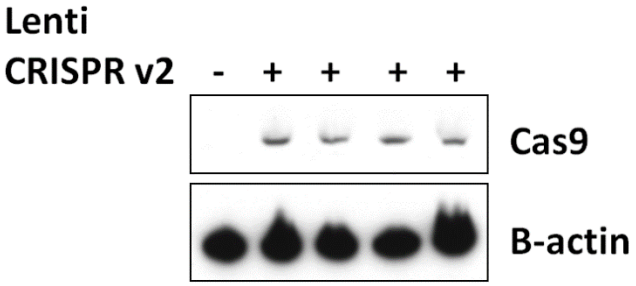

Figure 4.17 Cas9 expression in VSMCs infected with LentiCRISPRv2 lentiviral particles. Lysates from mouse VSMCs infected with lentiviral particels harbouring Cas9 were harvested and blotted with antibody against the protein (TherrmoFisher Scientific, #MA5-23519. Four different lines are presented. B-actin was used as a normalisation control. For comparison, a similar exposure time was applied.

Next, the ability of the Cas9/RNP complexes to form and cleave the targeted DNA sequence was tested by an *in vitro* Cas9 digestion. *In vitro* transcribed guides were used to form Cas9/RNP complexes with the digestion showing that Cas9 is able to cleave the PCR template when in complex with either Gm2 or GmA. The sizes of the observed bands corresponded to the position of the cleavage by the Gm2 or GmA and the digestion was nearly complete (Figure 4.18A). Additionally, mouse VSMCs infected with lentiviral particles harbouring Cas9, were transfected with IVT guides to assess the ability of the single guide RNAs to form complexes with the Cas9, recognise and cleave the targeted DNA in cells. Two conditions were tested, cells infected with lentiviral particles harbouring Cas9 but not treated with puromycin and selected cells. T7EI showed that only the selected cells had successful editing of the targeted locus with an efficiency of 22% (Figure 4.18B).

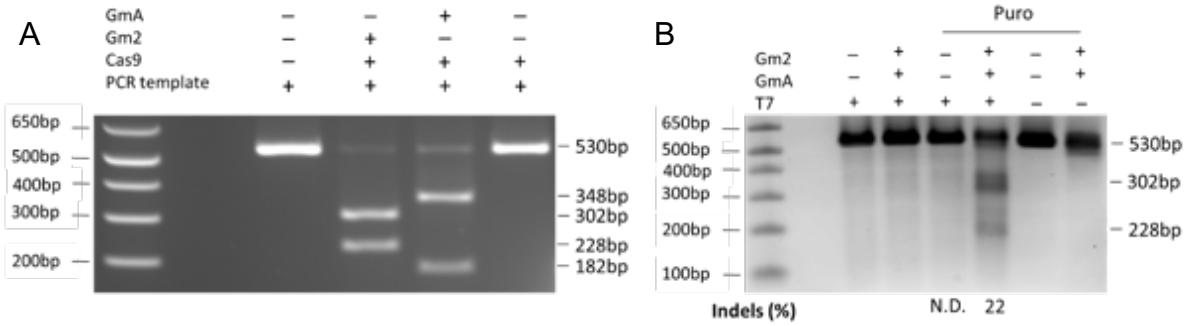

Figure 4.18 Assessment of gene editing in mouse VSMCs stably expressing Cas9. (**A**) Cas9/RNPs complexes were generated by incubating Cas9 protein (0.5µg) with *in vitro* transcribed guide (125ng). The Cas9/RNPs were tested *in vitro* for their ability to recognise and cut the targeted DNA. (**B**) Mouse VSMCs, stably expressing Cas9, were transfected with IVT guides GmA or Gm2. Two days post transfection, DNA was harvested and the genomic locus of mmu-miR-195 was PCR amplified. The T7EI assay was used for assessing the efficiency of the editing of 22%. The digested products corresponded to the expected sizes as described above. Gm2: sg195m2 and GmA: sg195mA, (n=3). Represantative results from only one experiment are shown.

Selected mouse VSMCs were then transfected simultaneously with IVT guides GmA and Gm2. DNA was extracted on two different days, Day2 (D2) and Day7 (D7) and the editing efficiency showing levels that were stable across the two timepoints (Figure 4.19).

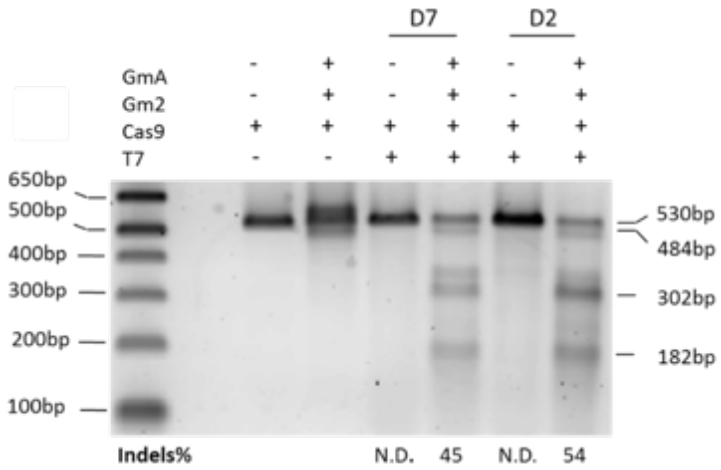

Figure 4.19. T7EI assay for mouse VSMCs stably expressing Cas9 after transfection with IVT guides. Mouse VSMCs that were infected with lentiviral particles harbouring Cas9 were selected with puromycin treatment and compared to non-selected cells. Gm2: sg195m2 and GmA: sg195mA. n=3, represantative results from only one experiment are shown.

The mmu-miR-195 locus has two SspI restriction sites (5'-AATATT-3') with single guide Gm2 disrupting one of them and 3 MwoI restriction sites (5'-GCNNNNNNNGC-3') with single guide GmA disrupting one (Figure 4.11A). Mouse VSMCs stably

expressing Cas9 were transfected with IVT guides and SspI and MwoI restriction digestions were performed for rapid assessment of gene editing. After the simultaneous or single transfection of mouse VSMCs stably expressing Cas9 with single guides Gm2 and GmA, digestion with SspI or MwoI restriction enzymes were used to rapidly assess the success of the editing. According to the disruption of the digestion sites that each guide conferred, different patterns were observed. Transfection solely with single guide Gm2 and digestion with SspI resulted in three bands corresponding to 331bp and 199bp after the successful editing of the targeted site and the disruption of the one of the two SspI sites (as depicted above in Figure 4.11), and bands of 303bp and 199bp after no editing of the two sites resulting in digestion of both of them. In the latter case, the digestion resulted in a third band of 28bp which diffused in the agarose gel and is non-discernible. Upon transfection with single guide GmA, no SspI site got disrupted. Simultaneous transfection with both guides and digestion with SspI showed the same pattern as previously described (Figure 4.20A). The 530bp corresponded to non-complete digestion of the full-length PCR product. Upon digestion with MwoI restriction enzyme, multiple bands for the non-edited PCR product were observed, corresponding to 184bp, 177bp, 102bp and a band of shorter length of 67bp. After, transfection with single guide GmA, only one MwoI got disrupted upon successful editing, resulting in the presence of a band 286bp long. Upon editing with both guides simultaneously, the pattern changed as a result of the perfect re-ligation of the DNA and the digestion of a shorter PCR product which resulted to a 244bp (Figure 4.20B). In both cases, editing with both guides but not digestion with either restriction enzyme, revealed a 484bp long band, which corresponded to the perfect re-ligation of the DNA after editing with the guides (right panel of the two figures A and B).

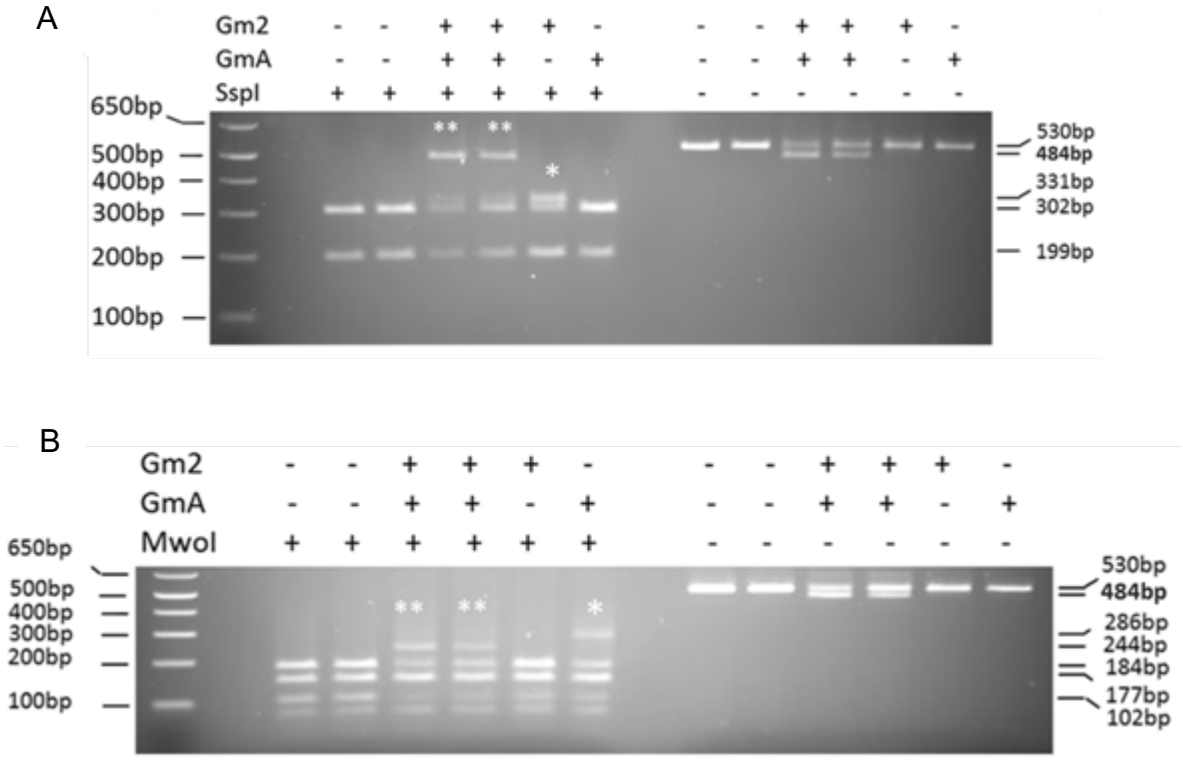

Figure 4.20 Restriction enzyme digestion with SspI and MwoI. Mouse VSMCs stably expressing Cas9 were transfected with IVT Gm2 or GmA. On Day3 post transfection, DNA was harvested and the genomic locus of miR-195 was PCR amplified. (**A**) Upon SspI digestion, only cells transfected with both guides (denoted with two asterisks) showed an undigested product of 484bp. Cells transfected only with Gm2 had a disruption of one of the SspI sites (one asterisk). (**B**) MwoI digestion showed a different pattern for transfection with Gm2 together with GmA and Gm2 only transfected cells (denoted with asterisks). Gm2: sg195m2 and GmA: sg195mA, n=2.

4.3.2.4 Off-target mutagenesis in mouse VSMCs

4.3.2.4.1 Off-target mutagenesis upon lentiviral infection

Mutagenesis, in the most likely off-target sites (OFT) as returned by the CRISPR online tool, was assessed using the T7EI assay. DNA from lentiviral infected mouse VSMCs did not show any off-target editing. The non-specific bands, of shorter length, that were observed in some of the samples (Figure 4.21), did not result from gene editing, since they were observed in both the edited and unedited cells and their sizes did not correspond to the predicted site of off-target cleavage of the LEGuides. The five most likely off-targets were tested for each guide (Figure 4.21).

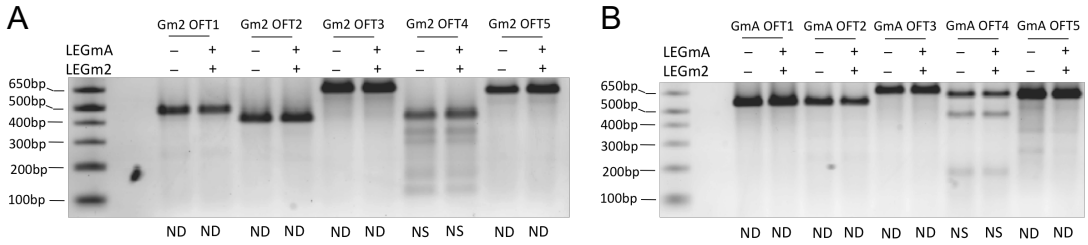

Figure 4.21 Assessment of possible off-target mutagenesis upon lentiviral infection of mouse SMCs. The five most likely off-target (OFT 1-5) for both guides (**A**) Gm2 and (**B**) GmA, as suggested by the CRISPR DESIGN Tool (http://crispr.mit.edu, Zhang Lab, MIT), were assessed by T7EI assay. No off-target mutagenesis was detected for neither of the LEGm2 and LEGmA. OFT.:Off-target, ND: Non Detectable, NS: Non Specific, n=1.

4.3.2.4.2 **Off-target mutagenesis upon transfection of mouse VSMCs stably expressing Cas9 with IVT guides**

For the assessment of putative off-target mutagenesis the 7 most likely off-target sites (OFT) as returned by the CRISPR DESIGN Tool (http://crispr.mit.edu, Zhang Lab, MIT) and CRISPR Finder (Wellcome Trust Sanger Institute), was assessed using the T7EI assay. DNA from mouse VSMCs stably expressing Cas9 were transfected with IVT single guide Gm2 and did not show any off-target editing. The digested observed bands, of shorter length (Figure 4.22), did not result from gene editing, since they were observed in both the edited and unedited cells and their sizes did not correspond to the predicted site of off-target cleavage of the guides.

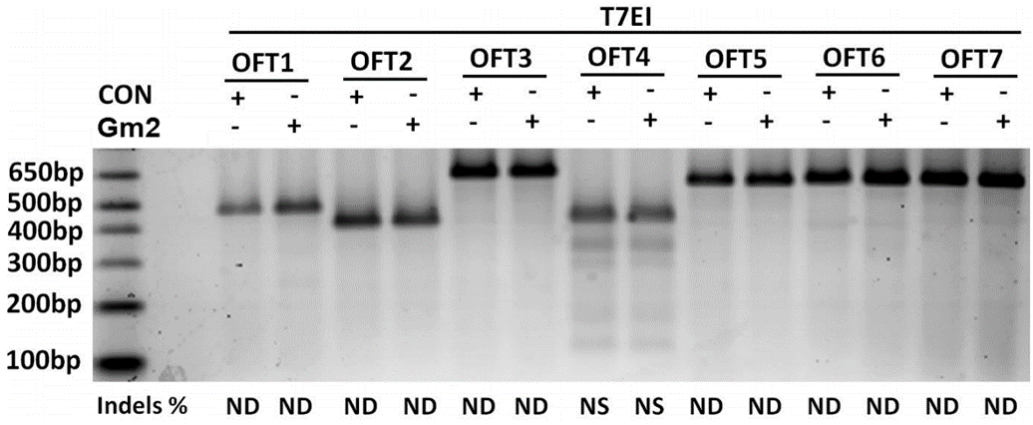

Figure 4.22 Assessment of possible off-target mutagenesis upon editing with IVT Gm2. T7EI assessment of gene editing in the loci of putative off-target sites for Gm2 as predicted by the CRISPR DESIGN Tool (http://cripsr.mit.edu, Zhang Lab, MIT) and CRISPR Finder (Wellcome Trust Sanger Institute). OFT; Off-Target, ND: Non-Detectable, NS: Non Specific. Gm2: sg195m2, n=1.

4.4 Discussion

CRISPR/Cas9 is a novel, versatile gene editing technique that appears to be able to overcome the problem of the unspecific miRNA inhibition, a limitation that hinders the study of miRNAs. In the present study, we investigated whether genome editing, with the use of CRISPR/Cas9, can be employed for specifically inhibiting miR-195 in primary cells by testing four different approaches. Although gene editing has been used in the past for the knock-out of miRNAs[157, 231, 232], to the best of my knowledge, this is the first time the CRISPR/Cas9 is used in primary cells to inhibit miR-195.

4.4.1 Gene Editing in Human Cells

For the current project, the first step undertaken was to design guides to edit the miR-195 genomic locus. The objective was to target two sites in the genomic locus of the hsa-miR-195 stem loop, one close to the seed sequence and one further upstream of the stem loop of the miRNA. It has already been shown that a combination of sgRNAs can be used for editing a locus more effectively[233]. However, the short length of the DNA sequence corresponding to the stem loop together with the PAM requirements of the CRISPR/Cas9 was an important limiting factor since the chances of finding 5'-NGG-3' sequences in such a short sequence were poor. Moreover, although it has been shown that Cas9 is able to induce DSBs in different sites in short distances within the same genomic locus and lead to the deletion of the flanked sequence,[233, 234] the short distance between putative targeted sites can interfere with the ability of Cas9 protein to physically approach the sequences. Considering results reported in previous studies along with the CRISPR requirements, the guides were designed accordingly. A sequence of a total length of 250nt, flanking the hsa-miR-195 gene, was used as an input to the CRISPR Design Tool and because of the need to target specific sites in the miRNA stem loop, the guides were chosen primarily based on the position of the site they targeted and not necessarily on their ranking score (Figure 4.1, Figure 4.2). Four different delivery strategies with different advantages and limitations were tested (Figure 4.23).

Figure 4.23. A comprehensive summary of the experimental approaches and their effects.

4.4.1.1 Strategy A: Plasmid Delivery

Plasmid delivery to HEK293T cells was used to induce gene editing to the hsa-miR-195 locus. Plasmid delivery would have only transient expression of the Cas9 protein thus minimising the effects of the protein accumulation that could possibly lead to off-target effects[235]. Nevertheless, according to our results, the efficiency of the gene editing, as the T7EI assay revealed, was rather modest. The highest percentage of indels was achieved after transfection with plasmids harbouring both guides, simultaneously, reaching a 34% on Day2. These results come in accordance with previous studies reporting higher efficiency upon editing with two guides[233, 236]. Although T7EI assay is a quantitative technique used for assessing successful editing that cannot provide qualitative information and is thought to marginally underestimate its efficiency due to innate limitations of the assay, it is regarded as the gold standard assay. The sizes of the bands after the T7EI indicated the sites where editing was induced. In more detail, T7EI is an *in vitro* assay that is used to assess the editing by employing the T7 endonuclease which is able to recognise and cleave mismatches in double stranded DNA. The digestion products have sizes that correspond to the site of the edit (Figure 3.3). Formation of homoduplexes between edited strands or incomplete digestion by T7 endonuclease underestimate the editing efficiency and limit the assay[208].

Next, the results from T7EI were confirmed by DNA sequencing, which showed that the editing occurred specifically in the sites targeted by the designed guides. In line with published results[237], editing of the hsa-miR-195 genomic locus resulted in the formation mainly of deletions, rather than insertions, while, in the case of transfection with both guides simultaneously, either the formation of indels in both targeted sites

or the excision of the sequence flanked by the designed guides and perfect re-ligation of the DNA strands (Figure 4.3E). Further to this, it has already been reported that two guides can be used for the excision of DNA sequences as was observed in the current project[200]. Of note is the fact that although the predicted length of the excised sequence was 106bp, Sanger sequencing revealed that in 50% of the blue and white colonies screened (data not shown) the length of the excised sequence was in fact 105bp. Although it could be the result of an insertion of an adenine following the editing, it seems more likely to be the result of Cas9 cutting 4nt upstream of the PAM sequence instead of 3nt, as was expected, in either of the two targeted sites. Although this discrepancy has been reported[179], due to sequencing limitations, there was not a way of deciphering at which site that discrepancy occurred. In more detail, both of the two trinucleotide sequences upstream of the PAM sequences of the two guides used are followed by an adenine. In both cases the expected outcome would have been the adenine to be excised although sequencing data did not confirm that. A single unexpected adenine was identified in all of the sequences where the 105nt excision occurred although, based on these results, we can conclude in which case DSB happened 4nt upstream of the PAM sequence. However, taking into consideration the high percentage of the transfection (data not shown), that was observed and the relatively modest percentage of the gene editing, the plasmid delivery did not appear as a favourable delivery system in primary cells. Nevertheless, plasmid delivery was confirmed as a suitable delivery approach to quickly test for the ability of the designed guides to edit the sequence of choice in human cells.

4.4.1.2 Strategy B: Lentiviral Delivery

In order to address the low efficiency of the plasmid delivery, lentiviral delivery of the CRISPR/Cas9 was chosen as an alternative approach and it was tested in primary human cells. Previous studies on HUVECs, using lentiviral particles, demonstrated that it is a powerful method[238] and taking advantage of the high proliferation rate of the cells, preliminary experiments were conducted. It has been reported that CRIPSR/Cas9 leads to higher editing efficiency in dividing cells[203]. Upon division and more specifically during the mitotic (M) phase of the cell cycle, the nuclear envelope breaks down due to the karyokinesis. During this, the CRISPR/Cas9 system can more easily access the DNA and edit it. Since initial experiments were conducted in human cells, there was no need to design new guides. Firstly, optimisation experiments were

used to identify the optimal conditions of infection (Figure 4.4) and results from three independent experiments suggested that infection with lentiviral particles resulted in almost complete gene editing as shown in Figure 4.5. PCR amplification showed two bands of different sizes with the intensity of the shorter one, corresponding to the size of the truncated DNA upon successful editing, indicating high efficiency (Figure 4.5A). Indeed, T7EI confirmed that lentiviral infection had high levels of editing with the efficiency reaching a 98% occurrence (Figure 4.5B). These results can be attributed to both the high proliferation rate of the cells as well as the efficacy of the delivery. DNA sequencing established that editing occurred in the targeted sites while the cells showed the same editing patterns as with plasmid delivery (Figure 4.5C). According to our results, we observed a high percentage of targeted genomic deletions, while in the instances when the flanked sequence was not excised, indels were observed in the cleaved sites, in agreement with previous findings[239]. Interesting are the changes of the pattern of the digested bands following T7EI digestion with the sizes of the bands showing as a mix following the editing with the two guides alone (Figure 4.5B). This can be explained by the fact that when editing with both guides occurred, a DNA sequence is excised and the DNA strands are perfectly re-ligated, not leading to any cleavage by T7EI, while editing at the corresponding sites with the two guides at different timepoints induce the formation of indels that upon cleavage resulted in fragments of different lengths, unique to this treatment (Figure 4.6).

Following the preliminary results on HUVECs and given that the study aimed at using human SMCs, since the apoptosis of SMCs is a key component in triggering the AAA, the system's efficiency was investigated in human SMCs. Although lentiviral infection confirmed the high editing efficiency, with a percentage of 80% (Figure 4.7), miRNA quantification (data not shown) showed that the levels of the miR-195 in prolonged cell culture conditions were extremely low, thus leading to the conclusion that the human SMCs would not be an appropriate model for the study. Therefore, mouse VSMCs were used.

4.4.1.3 Strategy C: Cas9/RNPs

In a third approach, the use of Cas9/RNPs appeared as a favourable alternative to the previous strategies deployed because of its transient effects and to its quick turnover[240]. Taking advantage of the latest developments in the CRISPR/Cas research and the reagents that became widely commercially available, such as recombinant Cas9 protein and IVT and synthetic sgRNAs, a new set of experiments was conducted. In order to test the ability of the Cas9 recombinant protein to bind the IVT guides and form RNP complexes and to recognise the targeted DNA, *in vitro* experiments were conducted. Guide G2 was used because of the high editing efficiency it showed in preliminary experiments (Figure 4.3). Following IVT and purification of the guide, it was added to recombinant Cas9 in vitro and was incubated with the corresponding DNA template leading to its cleavage at the targeted site, as the length of the digested bands indicated (Figure 4.8A). Next, HEK293T cells were transfected with Cas9/RNPs complexes with IVT guide G2, showed an efficiency of 25% (Figure 4.8B). The fact that the editing efficiency was similar to the one observed after plasmid transfection with the same guide, suggested that for the hsa-miR-195 locus and the specific guide it was not possible to obtain a higher efficiency for Cas9/RNPs compared to plasmid delivery as described in the literature[208].

4.4.1.4 Off-target mutagenesis

One of CRISPR's major limitation is the putative off-target mutagenesis as a result of the tolerance the guide shows in mismatches in their complementarity with the targeted DNA[235]. In more detail, the sgRNA can recognise and bind DNA sequences that show up to 3nt differences in their complementarity, leading Cas9 to edit the off-target sites. This activity occurs more easily in the 5'-end of the guide, which is its distal end from the endonuclease domains of Cas9. This off-target activity can result in unwanted editing of the DNA sequence, although with lower efficiency[203]. Given the importance of the gene editing to be specific together with the possibility of the off-target sites to be in onco-suppressor genes, the need to test for possible off-target mutagenesis becomes vital. An increasing number of studies suggest that CRISPR/Cas9 is likely to induce high off-target mutagenesis in multiple sites although with no conclusive data[241]. To address this issue, the CRISPR design software provide a list of possible off-target sites as predicted by an algorithm that penalises

the suggested guides according to the number of mismatches between the guide and the putatively recognised DNA sequence, ranking them in an inverse order of off-target likelihood (Figure 4.1). To assess the off-target mutagenesis, primers flanking the 7 most likely off-target sites for guides G1 and G2, as predicted by CRISPR Online tool, were designed (Supplementary Table 5), with T7EI showing no editing at said sites (Figure 4.9). Taking into consideration the high efficiency of the guides used together with the fact that no off-target editing was detected, we can securely conclude in that guides G1 and G2 did not induce any off-target editing in these sites, although the possibility that the guides can have other sites cannot be excluded. Whole genome sequencing is the technique of choice for assessing possible off-target mutagenesis by scanning the whole genome for discrepancies in the sequence[242] although, even in this case, no definitive results can be obtained due to the presence of SNPs[243].

4.4.2 Gene Editing in Mouse Cells

Mouse VSMCs appeared as a favourable alternative to human SMCs. As in human cells, the first step undertaken was the design of guides. Although human miR-195 genomic locus shares high sequence similarity with the corresponding mouse one, the prerequisite for the guides to be fully complementary to the targeted sequence meant that new guides needed to be designed. For the mouse VSMCs three guides were designed since PAM sequences were more common in the mouse genomic locus of miR-195a compared to the human one. However, due to the need of the guides to target sites in the stem loop of miR-195a, guides that did not have the highest score were selected (Figure 4.10, Figure 4.11 and Figure 4.12).

4.4.2.1 Strategy B: Lentiviral delivery

Lentiviral delivery of the system was tested and editing efficiency in two independent experiments with guides Gm2 and Gm4 reached 31% when both guides were used simultaneously (Figure 4.13). Of interest is the fact that the pattern of the edited bands changed according to the guides used (Figure 4.14). A second set of experiments with guides Gm2 and GmA showed that they were more efficient when used together (Figure 4.15). In more detail, although guide GmA showed lower efficiency compared

to Gm4 (26% and 48%, respectively), infection of mouse VSMCs together with lentiviral particles conferring Gm2 resulted in editing of 51% efficiency, higher than the one observed when Gm2 and Gm4 guides were used simultaneously. The difference between the efficiency when targeting with both guides and with each guide alone can possibly be explained by the fact that guides Gm2 and Gm4 target sites that are located closer together (24nt apart), thus hampering the accessibility of the sequence by the Cas9/RNP complexes. The observed differences in the editing efficiency between the two guides for mouse VSMCs and between the two species (human and mouse) SMCs can be explained by the fact that different guides were employed targeting the same or different genomic loci, respectively. Discrepancies among the efficiency of different guides, targeting the same locus, have been reported previously for experiments in the same cell type with some guides failing to induce any editing[190] while it has also been illustrated that the gene editing efficiency can vary greatly among different loci [180, 208]. These observations can be possibly explained by the different organisation and accessibility of the various loci or by possible instability or secondary structures of the sgRNAs[196]. Since lentiviral delivery was deemed to be the most effective, it was concluded that no significantly higher editing efficiency could be induced in mouse VSMCs.

4.4.2.2 Strategy D: Transfection of mouse VSMCs stably expressing Cas9 with IVT guides

Although lentiviral delivery of the system to mouse VSMCs was shown to be highly effective, the constant expression of Cas9 together with the guides was deemed to be a non-favourable feature. Moreover, lentiviral infection also presents substantial limitations and risks. Considering these, in order to circumvent the difficulties raised, a different approach was followed. Cells stably expressing Cas9 were generated by infecting mouse VSMCs with lentiviral particles harbouring only the gene for Cas9. Next, IVT sgRNAs GmA and Gm2 was used to test their ability to form Cas9/RNP complexes to form and cleave the targeted sequence *in vitro*, showing a successful and almost complete digestion with the sizes of the resulting bands corresponding to the sites of cleavage (Figure 4.18A). Following these results, optimisation of the infection showed that selection of the infected cells with the use of Puromycin resulted in successful editing compared to no selection (Figure 4.18B). Following these results, newly engineered and selected cells were transfected with IVT guides Gm2

and GmA, simultaneously, with T7EI showing a similar efficiency with that achieved with lentiviral infection (54% on Day 2, Figure 4.19), results indicative of the efficacy of this approach. In addition, the editing efficiency on two different timepoints (Day2 and Day7) indicated the viability of the edited cells.

In addition, the guides selected for editing mmu-miR-195a interrupted different restriction sites upon successful editing (Figure 4.11). That provided the opportunity to test, in a fast and easy way, with the use of restriction enzymes, the editing efficiency. In detail, since editing interrupted the restriction sites restriction enzymes recognised, formation of any indel would result in the corresponding site to stay intact upon digestion (Figure 4.20). Furthermore, the T7EI assay was employed to evaluate the level of efficiency.

All in all, by using this approach no off-target editing was expected to occur since the accumulation of the Cas9 was not expected to result in any off-target editing. The presence of sgRNAs, that could potentially form a complex with the stably expressed Cas9 and guide it to edit off-target sites, was transient[179]. Not only Cas9 is incapable to target any sequence without the help of the sgRNA but, further to this, it is the interrogation of the targeted sequence and its binding by the sgRNA, that activates the endonuclease domains of the protein[244]. In more detail, Cas9 endonuclease scans the genome for PAM sequences which it binds and releases rapidly if no complementarity is recognised between the sgRNAs and the adjacent to the PAM genomic DNA. Upon recognition of a highly complementary sequence, the conformation of the Cas9 changes, because of the DNA binding by the sgRNA, an alteration that brings the two nuclease domains of Cas9 (HNH and RuvC) closer together and activates them. Therefore, the transient presence of IVT guides in the cells would mean that the accumulated Cas9 would stay inactive. Thus, with this approach, gene editing occurs only upon transfection with the guides while their presence in the cells is transient. Taken together the above, transfecting VSMCs stably expressing Cas9 with IVT guides was concluded to be the most favourable delivery approach for the aim of the current study.

4.4.2.3 Off-target mutagenesis

To address the limitation of the unintended mutagenesis, the same approach, as previously described, was followed. Moreover, since a new delivery system was

tested, that of the transfection of mouse VSMCs stably expressing Cas9 with transiently present IVT sgRNA, the need to test for off-target editing was high. Firstly, the 5 most likely off-target sites for either guides, as returned by the CRISPR Design Tool (Figure 4.10), were tested in cells infected with lentiviral particles with no mutagenesis being detected (Figure 4.21). Furthermore, new guides were identified and tested for guide Gm2. Various software, freely available online, can be employed for the design of guides with different software using different algorithms to predict possible off-target sites. These algorithms penalise mismatches between the DNA sequence scanned and the suggested guides in a different way resulting in a list of possible off-target sites that vary among the different software. To address this, a set of 7 possible off-target sites was tested consisting of sites that were returned both by CRISPR Online Tool and CRISPR Finder, provided by Sanger Institute (Figure 4.22). By testing sites that appeared in both software the chances of false positive sites were eliminated. T7EI results in Cas9 expressing mouse VSMCs demonstrated that guide Gm2 did not induce any off-target mutagenesis.

Chapter 5 INVESTIGATION OF THE REGULATION AND FUNCTION OF CLUSTERED miRNAS WITH CRISPR/Cas9 EDITING

5.1 Introduction

MiRNAs provide rapid responses in physiological and non-physiological conditions to counteract rapid and variable fluctuations and safeguard the robustness of biological systems[245].

MiRNA biogenesis is a multistep process that starts with the miRNAs being transcribed by RNA polymerase II as pri-miRNAs which encode for either single or multiple miRNAs[4, 246]. A large portion of miRNAs organise in miRNA clusters while computational analysis suggests that the existence of miRNA clusters is much higher than expected by chance[247]. MiRNAs being transcribed in the same primary transcript are organised in homo-clusters, that consist of members of the same family, and hetero-clusters, that consist of miRNA from different families[248]. Pri-miRNAs present a very specific secondary structure by folding into hairpins, that contain imperfectly base-paired stems. They are then processed via a two-step, sequential maturation process during which they get cleaved by two RNA III nucleases. During the canonical pathway, they are cleaved, in a first step in the nucleus by Drosha and DGCR8, resulting in the release of a premature miRNA and its export to the cytoplasm. In a second step the pre-miRNA is cleaved by Dicer, leading to a miRNA duplex and subsequently to a mature miRNA[5]. A precise recognition of the pri-miRNA by the microprocessor have emerged as important for the fidelity of processing[5]. Several determinants, such as the secondary structure of the stem loop and sequence motifs, need to interact in a co-ordinated response for pri-miRNA recognition and cleavage[7, 8, 11, 249]. These findings imply that CRISPR/Cas9 gene editing of miRNA genes can affect processing of the hairpin in a dual manner either through the alteration of its sequence or of its secondary structure.

In this chapter, the use of gene editing as a tool to understand the clustered miRNA regulation was examined. Previous experiments, outlined in Chapter 4, demonstrated that CRISPR/Cas9 system is a very precise tool, inducing indel formation only in the

vicinity of DSB. Intriguingly, it was shown that in mmu-miR-497~195 cluster mutations in the mmu-miR-195a stem loop can affect the expression of mmu-miR-497a that resides in the other hairpin of the cluster. It was hypothesised that the editing of the mmu-miR-195a exerts an effect on the maturation of mmu-miR-497a by affecting its processing by Drosha.

Following the literature and the results outlined in Chapter 4, the study focused on four clusters, the homo-cluster mmu-miR-497~195, the hetero-clusters mmu-miR-143~145 and mmu-miR-17~92 and cluster mmu-miR-106b~25, a paralogue of cluster miR-17~92. The objective was to determine whether editing the sequence of one miRNA of the cluster is able to affect the expression levels of the other clustered miRNAs by influencing their maturation.

The results presented in this Chapter demonstrated diverse regulatory mechanisms of expression for clustered miRNAs. Firstly, they confirmed that mutations in the genomic locus of mmu-miR-497~195, induced by CRISPR/Cas9 editing affect the expression levels of the mature mmu-miR-497a that resides in the other hairpin of the same cluster. Secondly, experiments in different clusters showed that although editing of clustered miRNAs is capable of affecting the expression levels of the other miRNAs of the cluster, these results cannot be extrapolated to all of the clusters. In some cases, editing of a clustered miRNA did not affect the expression of the rest of the miRNAs.

5.2 Experimental Design

The aim of the experiments presented in the current chapter was to elaborate on the findings outlined in Chapter 4, on editing of mmu-miR-195a, and to elucidate whether editing of clustered miRNAs can affect the expression levels of the other miRNAs of the cluster. Four different clusters were chosen to be studied.

Firstly, cluster mmu-miR-497~195 was further studied in more detail and a new guide was designed and used to confirm that the observed results were not guide specific. Next, the effects of editing were evaluated in the hetero-cluster mmu-miR-143~145[114] which consists of two miRNAs, mmu-miR-143 and mmu-miR-145a, that are not members of the same miRNA family and do not share seed sequence similarities. The objective was to overcome the limitations in studying possible autoregulatory effects of miRNAs of homo-clusters and to assess whether editing of hetero-clusters shows different effects. Guides editing different sites in or close to the stem loop of mmu-miR-145a were designed while changes in its secondary structure upon editing was also evaluated. In addition, clusters mmu-miR-17~92 and mmu-miR-106b-25 were studied. Guides targeting mmu-miR-18 were designed and used and it was hypothesised that the abolition of its hairpin would affect the maturation only of the flanking miRNA hairpins as was the expected outcome of editing mmu-miR-25. However, results showed that the effect of genomic editing in miRNA clusters can differ.

5.3 Results

5.3.1 Regulation of mmu-miR-195~497 cluster in VSMCs

5.3.1.1 Editing of mmu-miR-195 locus with sg195m2

Mmu-miR-195a forms a homo-cluster together with mmu-miR-497 as they are member of the same miR-15 family and get transcribed in one primary transcript with the stem loops located within 500bp. For the editing of mmu-miR-195a locus, mouse VSMCs stably expressing Cas9 were transfected with guide sg195m2 targeting a site in the stem loop of the miRNA disrupting one of the two SspI sites located in the sequence of mmu-miR-195a (Figure 5.1A). Digestion with SspI restriction enzyme showed successful editing (Figure 5.1C) while T7EI confirmed the editing with the efficiency varying from 28-30% (Figure 5.1D). Sanger sequencing demonstrated the formation of a panel of indels, mainly deletions flanking the targeted area (Figure 5.1E). QPCR quantification showed a reduction in the expression levels of mmu-miR-195a by 55% and of mmu-miR-497a by 62%, with the levels of mmu-miR-15a, mmu-miR-15b and mmu-miR-16 not being affected (Figure 5.1F) confirming results shown above.

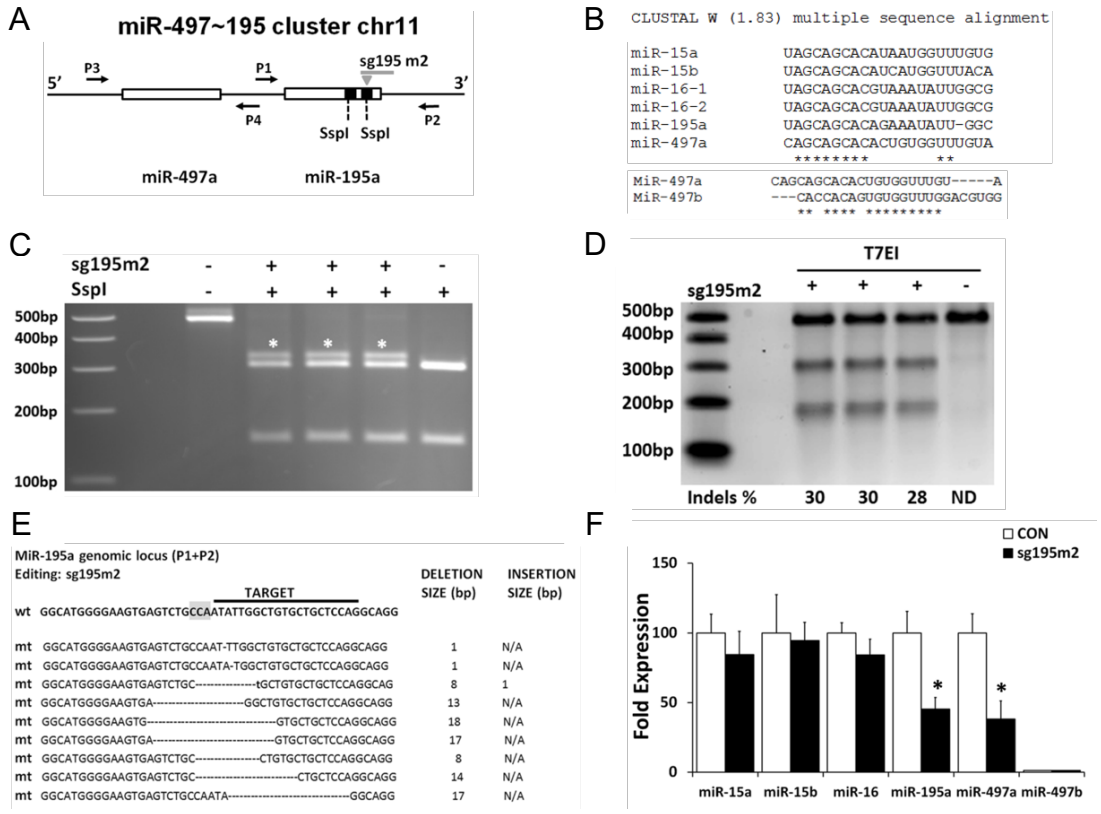

Figure 5.1 Gene editing of the miR-195a locus using IVT sgRNA195m2. (**A**) Schematic representation of the genomic locus of the mmu-miR-497~195 cluster with the two stem loops of mmu-miR-497a and mmu-miR-195a being depicted as empty rectangular. The corresponding site of editing is depicted as a grey triangle and the position of the guide upon editing as a grey line. (**B**) The T-Coffee multiple sequence alignment programme was used to compare the mouse miR-15 family members. Bottom Panel: mmu-miR-497a displays high homology with mmu-miR-497b. Mmu-miR-497b is encoded by the antisense strand of the mmu-miR-497a~195 cluster and does not harbour the same seed sequence. (**C**) SspI digestion results upon editing of mmu-miR-195a with sg195m2 (**D**) T7EI assay for the mmu-miR-195a locus following editing with sg195m2. ND: Non-detectable. P1 and P2: Genomic PCR primers. (**E**) Sanger sequencing showing the editing of the mmu-miR-195 locus. The presence of random indels, mainly deletions was detected and represented as dashes. The PAM sequence is highlighted in grey. Insertions are shown in bold small case fonts. N/A: Not Applicable. (**F**) Gene editing of the mmu-miR-195a locus resulted in the down-regulation of both mmu-miR-195a and mmu-miR-497a without affecting the expression of other members of the miR-15 family as assessed by qPCR. U6 was used as a normalization control. n=4, * $p<0.05$. Assessment of the levels of miR-497b showed that it is not expressed in mouse VSMCs.

5.3.1.2 Possible gene editing of miR-497a locus with sg195m2

Following the assessment of the levels of miR-497a miRNAs upon editing of the miR-195 with the sg195m2, T7EI and Sanger sequencing was used to investigate putative editing and formation of indels in the genomic locus of mmu-miR-497a with neither of the assays showing any editing (Figure 5.2).

A

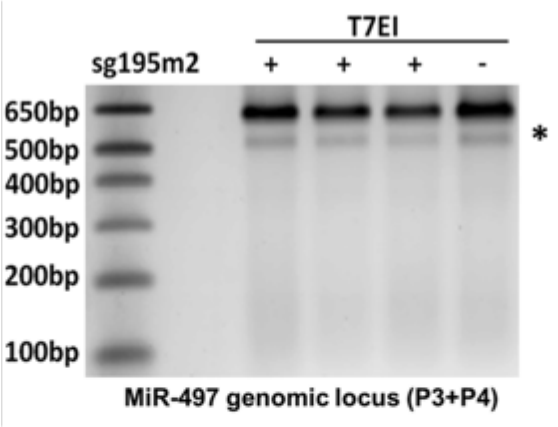

B

MiR-497a genomic locus (P3+P4)
Editing: sg195m2

```
wt  CCTGCCCCCGCCCCAGCAGCACACTGTGGTTTGTACGGCACTGTGGCCACGTCCAAACCACACTGTGGTGTTAGAGCGAGGGTA
1   CCTGCCCCCGCCCCAGCAGCACACTGTGGTTTGTACGGCACTGTGGCCACGTCCAAACCACACTGTGGTGTTAGAGCGAGGGTA
2   CCTGCCCCCGCCCCAGCAGCACACTGTGGTTTGTACGGCACTGTGGCCACGTCCAAACCACACTGTGGTGTTAGAGCGAGGGTA
3   CCTGCCCCCGCCCCAGCAGCACACTGTGGTTTGTACGGCACTGTGGCCACGTCCAAACCACACTGTGGTGTTAGAGCGAGGGTA
4   CCTGCCCCCGCCCCAGCAGCACACTGTGGTTTGTACGGCACTGTGGCCACGTCCAAACCACACTGTGGTGTTAGAGCGAGGGTA
5   CCTGCCCCCGCCCCAGCAGCACACTGTGGTTTGTACGGCACTGTGGCCACGTCCAAACCACACTGTGGTGTTAGAGCGAGGGTA
6   CCTGCCCCCGCCCCAGCAGCACACTGTGGTTTGTACGGCACTGTGGCCACGTCCAAACCACACTGTGGTGTTAGAGCGAGGGTA
7   CCTGCCCCCGCCCCAGCAGCACACTGTGGTTTGTACGGCACTGTGGCCACGTCCAAACCACACTGTGGTGTTAGAGCGAGGGTA
8   CCTGCCCCCGCCCCAGCAGCACACTGTGGTTTGTACGGCACTGTGGCCACGTCCAAACCACACTGTGGTGTTAGAGCGAGGGTA
9   CCTGCCCCCGCCCCAGCAGCACACTGTGGTTTGTACGGCACTGTGGCCACGTCCAAACCACACTGTGGTGTTAGAGCGAGGGTA
10  CCTGCCCCCGCCCCAGCAGCACACTGTGGTTTGTACGGCACTGTGGCCACGTCCAAACCACACTGTGGTGTTAGAGCGAGGGTA
    ********************************************************************************
```

Figure 5.2 Investigation of editing in the miR-497a locus with sg195m2. (**A**) T7EI assay showed no editing at the locus of mmu-miR-497a upon editing with sg195m2. (**B**) Clustal alignment of Sanger sequencing data of the genomic locus of the mmu-miR-497a stem loop following sg195m2 editing in VSMCs. Wt: unedited cells, 1-10 randomly picked individual colonies harbouring genomic PCR amplicons from sg195m2 edited VSMCs. P3, P4: Genomic PCR primers as depicted in Figure 5.1, (n=3).

5.3.1.3 Editing of mmu-miR-195a locus with sg195m3

Editing of mmu-miR-195a locus was induced with transfection with guide sg195m3 of mouse VSMCs stably expressing Cas9. The newly designed guide targeted a site in the stem loop of the miRNA disrupting an SspI site (Figure 5.3A and B). T7EI showed efficient editing with the efficiency varying from 24-33% (Figure 5.3C). Sanger sequencing demonstrated the formation of indels, mainly deletions (Figure 5.3D), while qPCR quantification showed a reduction in the expression levels of both mmu-miR-195a and of mmu-miR-497a, without affecting the levels of mmu-miR-15a, mmu-miR-15b and mmu-miR-16 (Figure 5.3E), as previously shown (Figure 5.1). Off-target mutagenesis assessment did not show any editing in the six most likely off-target sites (Figure 5.4) with Sanger sequencing data of the mmu-miR-497a locus not revealing any editing (Figure 5.5).

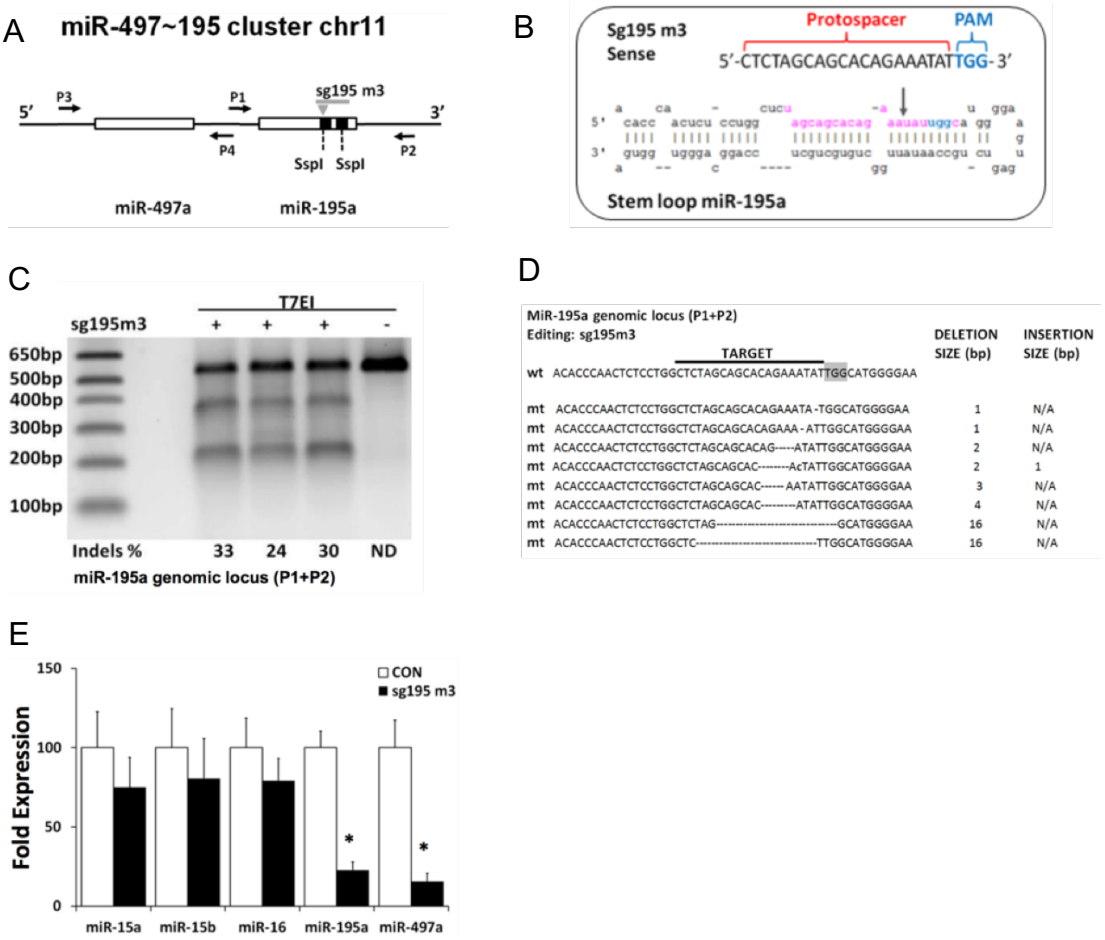

Figure 5.3 Gene editing of the mmu-miR-195a locus using sgRNA195m3. (**A**) Schematic representation of the genomic locus of the mmu-miR-497~195 cluster with the two stem loops of mmu-miR-497 and mmu-miR-195 being depicted as an empty rectangular. The corresponding site of editing with sg195m3 is depicted as a grey triangle. (**B**) Representation of the mmu-miR-195a stem loop with the detailed sequence along with the targeted DNA sequence and the PAM sequence for sg195m3. (**C**) T7EI assay for the miR-195a locus following editing with sg195m3. ND: Non-detectable. P1 and P2: Genomic PCR primers. (**D**) Sanger sequencing showing the editing of the mmu-miR-195a locus. The presence of random indels, mainly deletions was detected and represented as dashes. The PAM sequence is highlighted in grey. Insertions are shown in bold small case fonts. N/A: Not Applicable. (**E**) Gene editing of the mmu-miR-195a locus resulted in the down-regulation of both mmu-miR-195a and mmu-miR-497a without affecting the expression of other members of the miR-15 family as assessed by qPCR. U6 was used as a normalization control. n=4, * $p<0.05$.

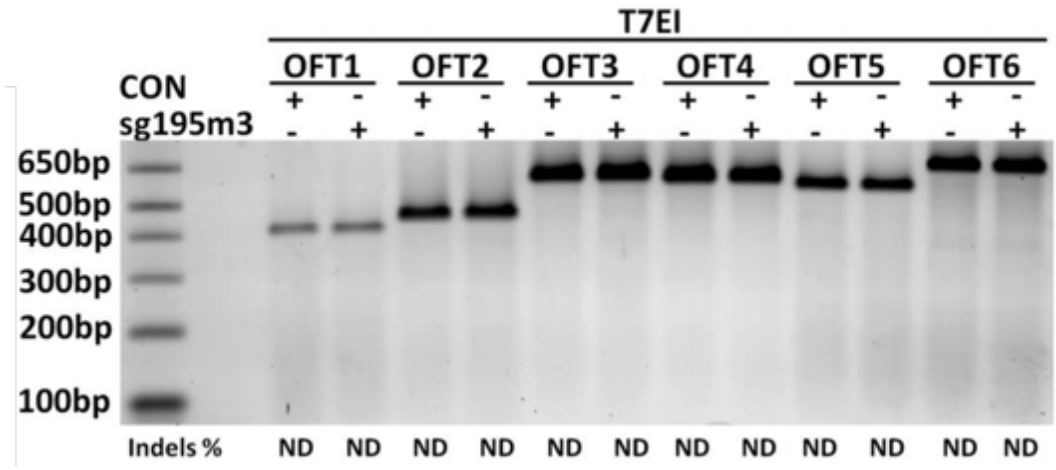

Figure 5.4 Assessment of off-target editing with sg195m3. T7EI did not show any gene editing in the loci of the 6 most likely putative off-target sites for sg195m3 as predicted by the CRISPR DESIGN Tool (http://cripsr.mit.edu, Zhang Lab, MIT) and the CRISPR Finder (Wellcome Trust Sanger Institute). OFT; Off-Target, ND: Non-detectable, n=1.

Figure 5.5 Investigation of editing in the miR-497a locus with sg195m3. Clustal alignment of Sanger sequencing data of the miR-497a stem loop locus following sg195m3 editing in VSMCs. Wt: unedited cells, 1-10 randomly picked individual colonies harbouring genomic PCR amplicons from sg195m3 edited VSMCs. P3, P4: Genomic PCR primers as depicted in Figure 5.1.

5.3.1.4 Regulation of the mmu-miR-497a expression

In order to determine whether the downregulation of mmu-miR-497a occurred as a secondary effect due to the downregulation of mmu-miR-195a, gain of function experiments were conducted. Overexpression of mmu-miR-195a in mouse VSMCs with the use of miRNA mimics demonstrated no increase in the levels of mmu-miR-497a (Figure 5.6).

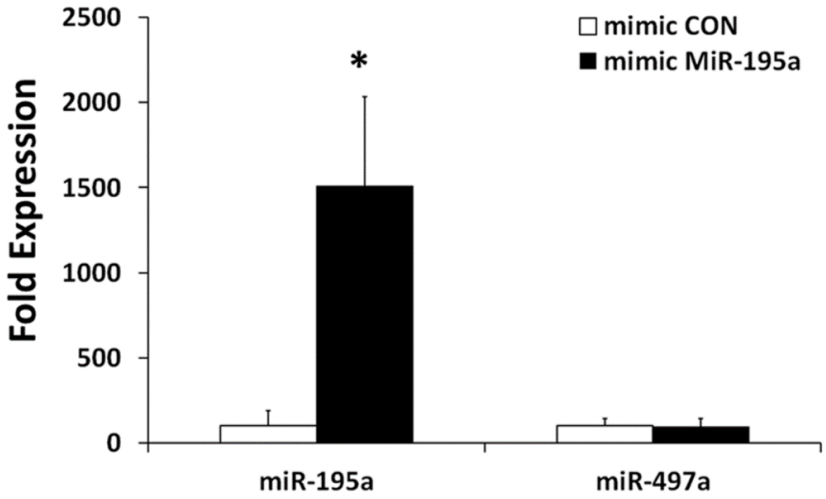

Figure 5.6. Overexpression of miR-195a. QPCR quantification of the levels of mature mmu-miR-195a and mmu-miR-497a, following overexpression of miR-195a using miRNA mimics. U6 was used as a normalisation. n=3, *p-value<0.05, (ANOVA with Dunnett post hoc test).

5.3.1.5 Secondary structure of mmu-miR-195a stem loop upon editing

Computational analysis was performed in collaboration with Dr Kathleen Steinhofel and Prof Andreas Albrecht. Analysis with RNAfold prediction programme was used to determine the secondary structure of the stem loop upon editing with guide sg195m2 (Figure 5.7A) and sg195m3 (Figure 5.7B). The structure of the wild-type mmu-miR-195a stem loop presented the expected bulges and apical loop while one nucleotide deletion with either guide resulted in a predicted formation with a more pronounced bulge. A 18nt deletion with guide sg195m2 (Figure 5.7A, Left Panel) resulted in a shorter stem and a bigger apical loop while a 16nt deletion with guide sg195m3 (Figure 5.7B, Right Panel) resulted in a predicted secondary structure with no evident stem and apical loop.

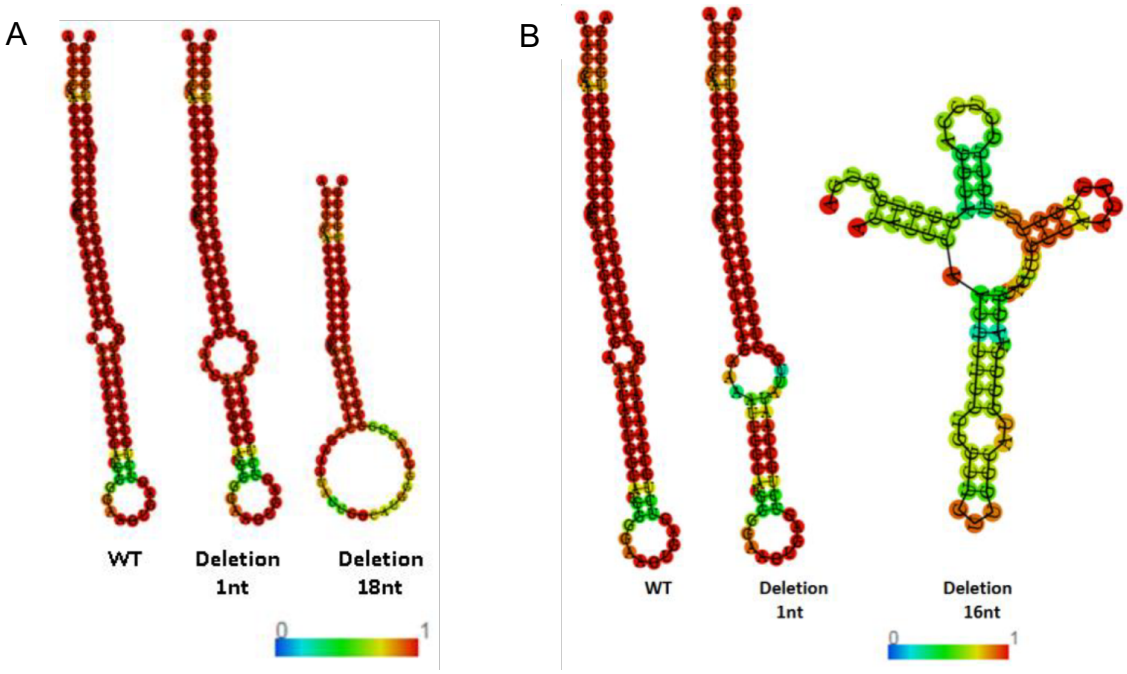

Figure 5.7 Predicted secondary structure of the mmu-miR-195a stem loop upon editing. Minimum free energy structure of the mmu-miR-195a stem loop following editing with (**A**) sg195m2 and (**B**) sg195m3, as assessed by the structure prediction software RNAfold. The base pairing probability, as indication of structural remodelling or dynamics, was used for colour-coding.

5.3.1.6 Tertiary structure of mmu-miR-497~195 primary transcript upon editing

For the investigation of the effects of editing with guide sg195m2 on the tertiary structure of mmu-miR-497-195 primary transcript, the RNAComposer fully automated

RNA structure modelling server was used. The secondary structure without pseudoknots, as returned by vsfold5 was used as an input for the unedited transcript (wt, Figure 5.8A), after a 1nt mutation (mut1, Figure 5.8B) and an 18nt deletion (mut5, Figure 5.8C). The three 3D simulations appear different with the wild type showing a prominent mmu-miR-195a stem loop and a compressed but still accessible miR-497a stem loop (Figure 5.8A) while the conformation of the 1nt deletion (mut1) had no effect on mmu-miR-195a stem loop but led to a mmu-miR-497a stem loop strongly attached to the main core of the primary transcript (Figure 5.8B). In the case of the 18nt deletion (mut5), profound differences were observed as no typical hairpin for pri-miR-195a could be detected and the whole structure was more strongly entangled with the main core. The miR-497a stem loop displayed a compact shape in closer proximity with the miR-195a stem loop and with no clear accessibility to the hairpin.

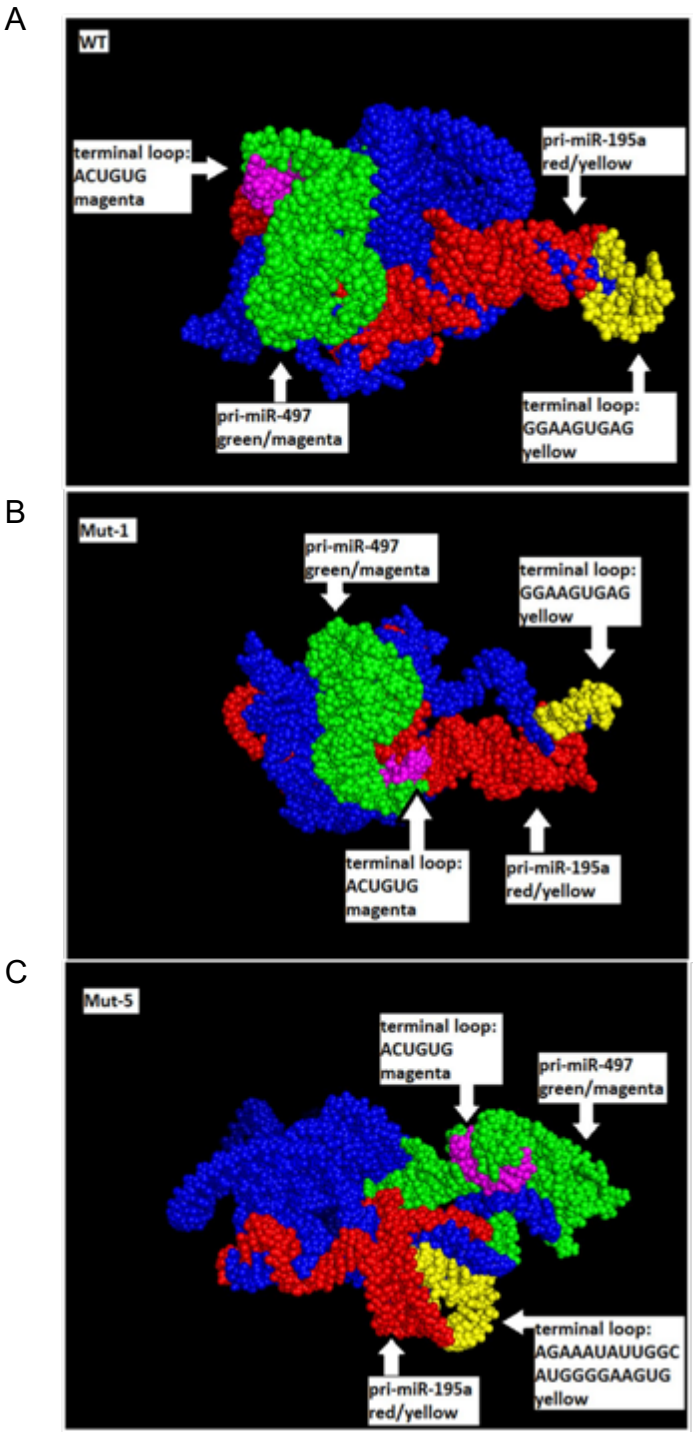

Figure 5.8 Effect of CRISPR/Cas9 editing in the tertiary structure of mmu-miR-497~195 cluster. Computational simulation of the 3D structure (generated by vsfold5 - with pseudoknots – as input to RNAComposer, pdb-fle visualised by PyMOL) of the pri-miR-497~195 in (**A**) unedited WT, (**B**) mutant harbouring a deletion of 1nt (mut1) and (**C**) a mutant harbouring a deletion of 18nt (mut5). Mmu-miR-497a stem loop is depicted in green and its terminal loop in magenta. Mmu-miR-195a stem loop is depicted in red and its terminal loop in yellow. A full movie of the 3D structure of the different transcripts can be accessed on https://nms.kcl.ac.uk/kks/projects/SREP-17-12031.php (Username: cluster Password: 195497).

5.3.2 Gene editing in different miRNA clusters

5.3.2.1 Gene editing in mmu-miR-143~145 cluster

5.3.2.1.1 In silico design of guides

To design the guides targeting the genomic locus of mmu-miR-145, the CRISPR DESIGN Tool (http://crispr.mit.edu, Zhang Lab, MIT) was employed (Figure 5.9). The DNA sequence, corresponding to the transcript annotated as miRNA stem loop in miRBasev21, was uploaded to the software. The two following oligos, which targeted sites upstream of the stem loop and in the mmu-miR-145 stem loop (Figure 5.10), were deemed as the most suitable ones:

sg145m1: 5'-AGGGGCGTGGCACGTGCTGA-3'

sg145m2: 5'-GATGCTAAGATGGGGATTCC-3'

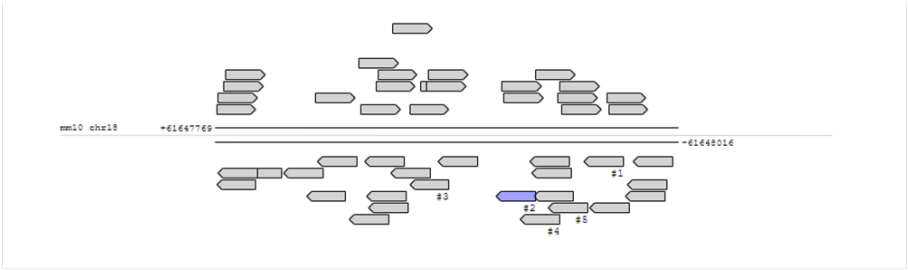

all guides

scored by inverse likelihood of offtarget binding
mouse over for details ... show legend

	score	sequence	
Guide #1	91	GTGTATACAGCGCCCCACGG	TGG
Guide #2	89	AGGGTGTATACAGCGCCCCA	CGG
Guide #3	83	AGGGGCGTGGCACGTGCTGA	AGG
Guide #4	83	CAGGACGCTGCATCCCGGGA	AGG
Guide #5	80	CCTGGGAAAACTGGACCGTG	AGG
Guide #6	79	CCTCACGGTCCAGTTTTCCC	AGG
Guide #7	76	ACTGCTGGTCCCTAGGGGCG	TGG

guide #3 quality score: 83

guide sequence: AGGGGCGTGGCACGTGCTGA AGG
on-target locus: chr18:-61647918
number of offtarget sites: 135 (0 are in genes)

top 20 genome-wide off-target sites — show all exonic

sequence	score	mismatches	UCSC gene	locus
AAGGGCATTGCACGTGCTGACAG	1.1	3MMs [2:7:9]		chr11:-70702272
GGGGGCGTGGCGCGTGCTGCCAG	0.8	3MMs [1:12:20]		chrY:+86121767
TGGGGCGGGGCACGTCCTGAAGG	0.6	3MMs [1:8:16]		chr6:+40320262
TGGGGCGGGCCATGTGCTGAAGG	0.5	4MMs [1:8:10:13]		chr3:-83287297
AGGAGCCTGGCACGAGCTGAGGG	0.5	3MMs [4:7:15]		chr8:+10809694

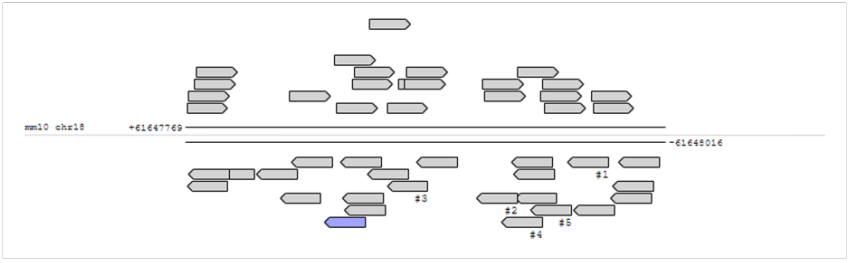

Guide #15	71	GATGCTAAGATGGGGATTCC	TGG	GATGCTTCATCCTGGGAAGGAAG	0.7	3MMs [3:7:13]	chr10:+10722313
Guide #16	70	AATCCCTTGGATGCTAAGAT	GGG	GTTGCTGCAGGCCGGGAAGGAGG	0.7	4MMs [2:3:10:11]	chr4:+98958825
Guide #17	70	GACGCTGCATCCCGGGAAGG	AGG	GGCGCGGCATCCTGGGAAGGTAG	0.7	3MMs [2:6:13]	chr7:-125032987
Guide #18	70	AGAGAACTGCTGGTCCCTAG	GGG	GCGGCTGCACCTCGGGAAGGGGG	0.6	4MMs [2:3:10:12]	chrY:+46679268
Guide #19	69	CGAGAGAACTGCTGGTCCCT	AGG	GACTCCGCATCCAGGGAAGGAGG	0.6	3MMs [4:6:13]	chr6:-125838821

Figure 5.9 In silico design of the sgRNAs for mmu-miR-145a locus. The CRISPR DESIGN Tool (http://crispr.mit.edu, Zhang Lab, MIT) was used to design the guides for editing the mmu-miR-145 locus. In the above figures, the sequences of the two guides, their corresponding score and the 5 most likely off-target sites are depicted for (**A**) guide sg145m1 (**B**) and sg145m2.

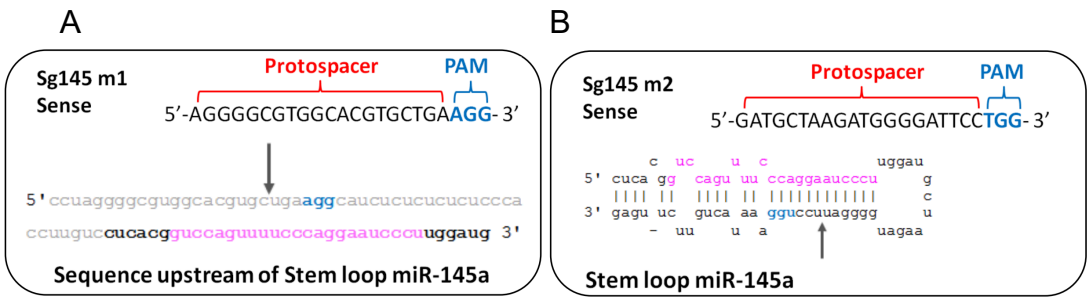

Figure 5.10 Schematic representation of the secondary structure of the mmu-miR-145a stem loop with guides. Representation of the mmu-miR-145a stem loop with the detailed sequence for (**A**) sg145m1 and (**B**) sg195m2. PAM sequence is highlighted in blue. The mature miRNA sequence is highlighted in purple and grey arrows indicate the corresponding position of the DSB on the stem loop which is the site of mutations induced by random indels following editing of the genomic locus in mutant cells.

5.3.2.1.2 **Editing of the mmu-miR-145a locus**

Mmu-miR-145a is transcribed in one primary transcript together with mmu-miR-143 forming a hetero-cluster, since the two miRNAs are not members of the same miRNA family. For the editing of mmu-miR-145a locus, two guides were designed, sg145m1 and sg145m2 with the former one targeting a site 30bp upstream of the mmu-miR-145a stem loop and the latter one disrupting a HinfI site in the mmu-miR-145a stem loop (Figure 5.11A). The two miRNAs do not share the same seed sequence neither any sequence homology (Figure 5.11B). T7EI results indicate successful editing with guide sg145m1 demonstrating editing efficiency varying from 47-57% while guide sg145m2 showed an efficiency of 24-29% (Figure 5.11C). HinfI restriction digestion enzyme confirmed the editing with guide sg145m2 (Figure 5.11D) and Sanger sequencing demonstrated the formation of small indels, mainly deletions with either guide (Figure 5.11E).

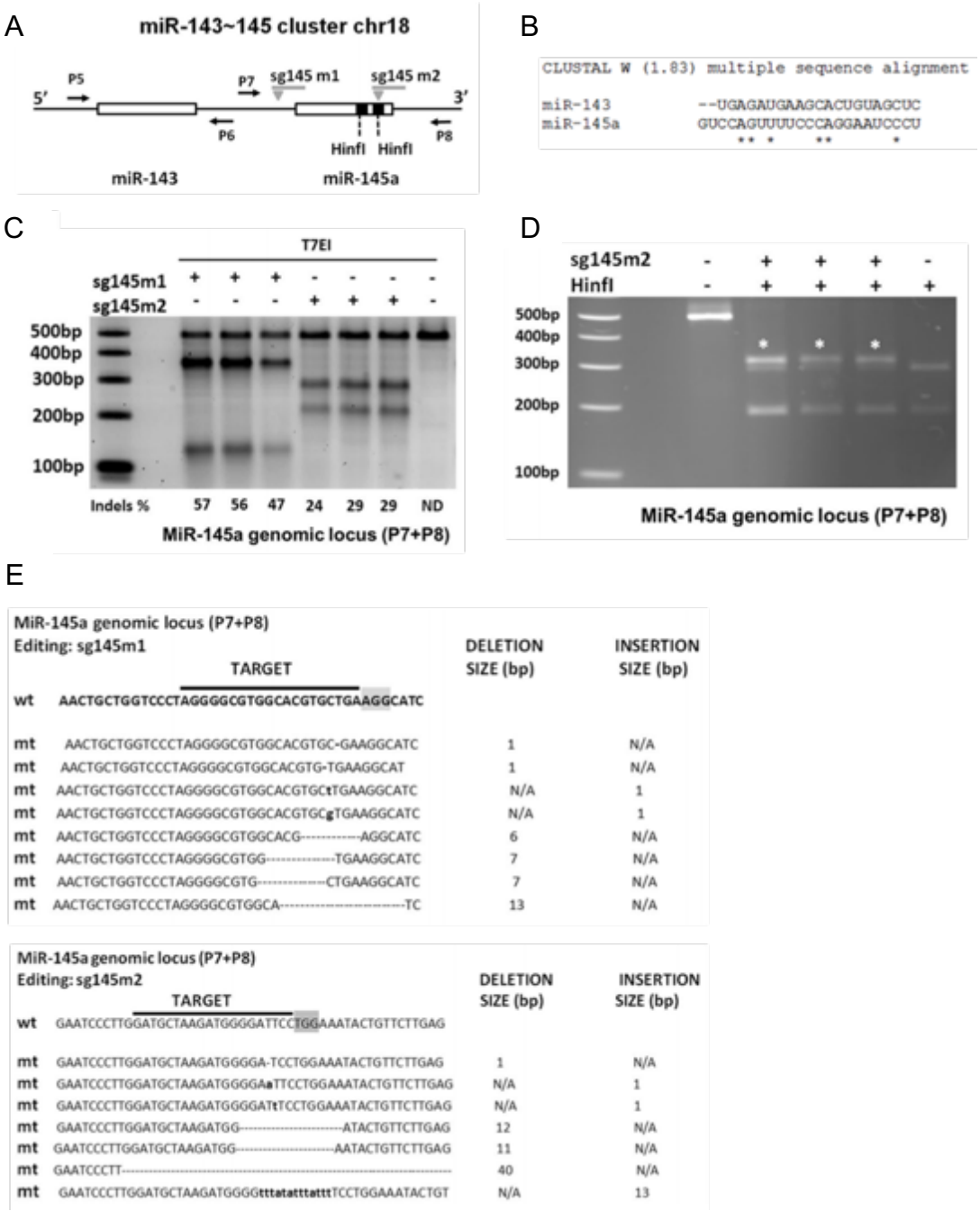

Figure 5.11 Gene editing of the mmu-miR-145a locus. (**A**) The genomic locus of the miR-143~145 cluster with the corresponding sites of the DSBs induced by sg145m1 and sg145m2. (**B**) MiRNAs miR-145a and miR-143 do not share a common seed region or any sequence homology, as the T-Coffee multiple sequence alignment programme indicates. (**C**) T7EI assay in three independent experiments for the miR-145a locus after editing with either guide. ND: non-detectable, (n=3). (**D**) The sg145m2 targets the miR-145 genomic locus and disrupts a HinfI restriction site. Asterisks (*) indicate differential digestion products. (**E**) Sanger sequencing data for the edited mmu-miR-145a genomic locus using guides sg145m1 and sg145m2, respectively. The PAM sequence is highlighted in grey. Deletions are represented as dashes, insertions are shown in bold small case fonts. N/A: Not Applicable. P7 and P8: Genomic PCR primers.

The assessment of the effect of editing on the levels of the miRNAs with qPCR revealed a downregulation of both mmu-miR143 and mmu-miR-145a upon editing with either guide although guide sg145m2 showed a sharper effect (Figure 5.12). In more detail, guide sg145m1 resulted in a 28% downregulation of miR-143 and 33% downregulation of miR-145 while guide sg145m2 showed a downregulation of 50% and 89% for miR-143 and miR-145a, respectively.

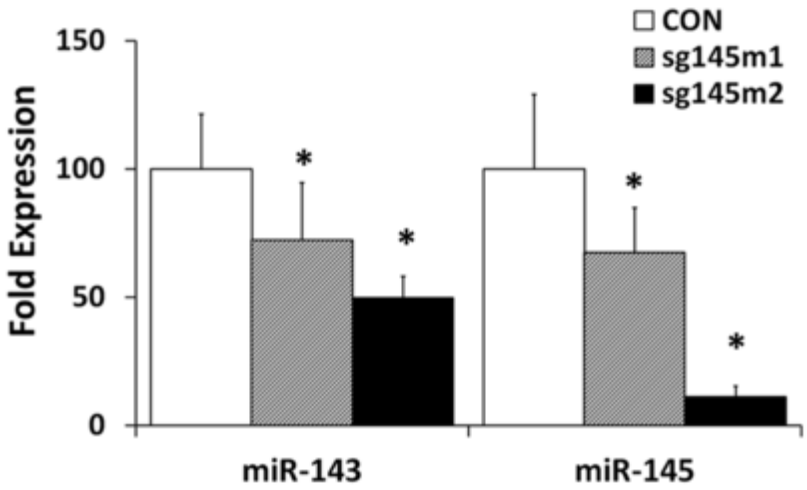

Figure 5.12 Assessment of the levels of mmu-miR-143 and mmu-miR-145a upon editing. QPCR quantifcation of the primiR-143~145 expression in sg145m2 edited cells. Pri-miRNA Taqman assays that are specifcally designed to amplify fanking sequences within 500 base pairs on either side of the stem loop were used. Beta actin was used as a normalization control. n=3, *p<0.05 (ANOVA with Dunnett post hoc test).

T7EI did not reveal any off-target effect in the mmu-miR-143 locus with either guide (Figure 5.13A), results that were confirmed by Sanger sequencing (Figure 5.13B).

A

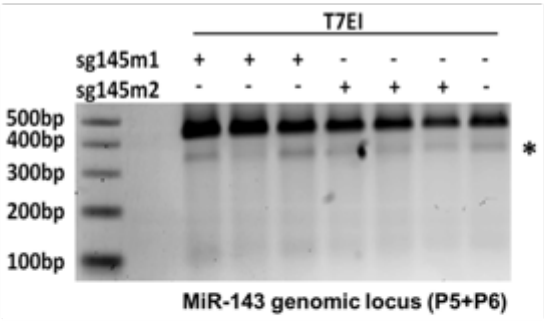

B

MiR-143 genomic locus (P5+P6)
Editing: sg145m1

```
wt  CCTGAGGTGCAGTGCTGCATCTCTGGTCAGTTGGGAGTCTGAGATGAAGCACTGTAGCTCAGG
1   CCTGAGGTGCAGTGCTGCATCTCTGGTCAGTTGGGAGTCTGAGATGAAGCACTGTAGCTCAGG
2   CCTGAGGTGCAGTGCTGCATCTCTGGTCAGTTGGGAGTCTGAGATGAAGCACTGTAGCTCAGG
3   CCTGAGGTGCAGTGCTGCATCTCTGGTCAGTTGGGAGTCTGAGATGAAGCACTGTAGCTCAGG
4   CCTGAGGTGCAGTGCTGCATCTCTGGTCAGTTGGGAGTCTGAGATGAAGCACTGTAGCTCAGG
5   CCTGAGGTGCAGTGCTGCATCTCTGGTCAGTTGGGAGTCTGAGATGAAGCACTGTAGCTCAGG
6   CCTGAGGTGCAGTGCTGCATCTCTGGTCAGTTGGGAGTCTGAGATGAAGCACTGTAGCTCAGG
7   CCTGAGGTGCAGTGCTGCATCTCTGGTCAGTTGGGAGTCTGAGATGAAGCACTGTAGCTCAGG
8   CCTGAGGTGCAGTGCTGCATCTCTGGTCAGTTGGGAGTCTGAGATGAAGCACTGTAGCTCAGG
9   CCTGAGGTGCAGTGCTGCATCTCTGGTCAGTTGGGAGTCTGAGATGAAGCACTGTAGCTCAGG
10  CCTGAGGTGCAGTGCTGCATCTCTGGTCAGTTGGGAGTCTGAGATGAAGCACTGTAGCTCAGG
    ************************************************************
```

MiR-143 genomic locus (P5+P6)
Editing: sg145m2

```
wt  CCTGAGGTGCAGTGCTGCATCTCTGGTCAGTTGGGAGTCTGAGATGAAGCACTGTAGCTCAGG
1   CCTGAGGTGCAGTGCTGCATCTCTGGTCAGTTGGGAGTCTGAGATGAAGCACTGTAGCTCAGG
2   CCTGAGGTGCAGTGCTGCATCTCTGGTCAGTTGGGAGTCTGAGATGAAGCACTGTAGCTCAGG
3   CCTGAGGTGCAGTGCTGCATCTCTGGTCAGTTGGGAGTCTGAGATGAAGCACTGTAGCTCAGG
4   CCTGAGGTGCAGTGCTGCATCTCTGGTCAGTTGGGAGTCTGAGATGAAGCACTGTAGCTCAGG
5   CCTGAGGTGCAGTGCTGCATCTCTGGTCAGTTGGGAGTCTGAGATGAAGCACTGTAGCTCAGG
6   CCTGAGGTGCAGTGCTGCATCTCTGGTCAGTTGGGAGTCTGAGATGAAGCACTGTAGCTCAGG
7   CCTGAGGTGCAGTGCTGCATCTCTGGTCAGTTGGGAGTCTGAGATGAAGCACTGTAGCTCAGG
8   CCTGAGGTGCAGTGCTGCATCTCTGGTCAGTTGGGAGTCTGAGATGAAGCACTGTAGCTCAGG
9   CCTGAGGTGCAGTGCTGCATCTCTGGTCAGTTGGGAGTCTGAGATGAAGCACTGTAGCTCAGG
10  CCTGAGGTGCAGTGCTGCATCTCTGGTCAGTTGGGAGTCTGAGATGAAGCACTGTAGCTCAGG
    ************************************************************
```

Figure 5.13 Off-target editing in miR-143 locus. (**A**) T7EI assay showed no editing at the locus of mmu-miR-143 upon editing with sg145m1 or sg145m2. The asterisk (*) depicts a non-specific band as a result of the T7EI digestion that is not due to editing, (n=3). (**B**) Clustal alignment of Sanger sequencing data for the mmu-miR-143 stem loop locus following sg145m1 and sg145m2 editing, respectively. Wt: unedited cells, 1-10 randomly picked individual colonies harbouring genomic PCR amplicons from edited VSMCs. P5, P6: Genomic PCR primers as depicted in Figure 5.11.

The expression levels of pri-miR-143 and pri-miR-145a were quantified with qPCR in sg145m2 edited cells. Targeting of mmu-miR-145a led to a robust decline of the levels

of both pri-miR-143 and pri-miR-145a (Figure 5.14A) while transfection of mouse VSMCs with miR-145a mimics resulted in a significant increase in the expression of mmu-miR-143 (250%) accompanied by an increase in pri-miR-143 and pri-miR-145a of 162% and 165%, respectively. The levels of KLF4, as a validated target of miR-145a, were subsequently downregulated by 40% (Figure 5.14B).

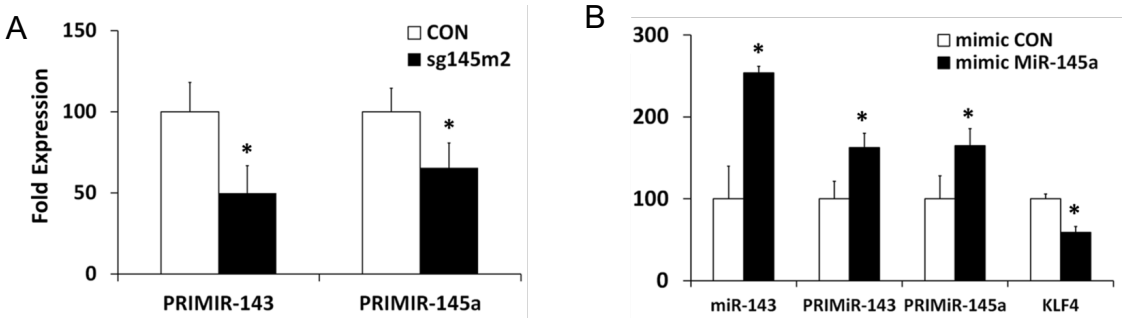

Figure 5.14 Assessment of the levels of pri-miR-143 and pri-miR-145a. (**A**) QPCR quantification of the pri-miR-143~145 expression in sg145m2 edited cells. Pri-miRNA Taqman assays that are specifically designed to amplify flanking sequences within 500 base pairs on either side of the stem loop were used. Beta actin was used as a normalisation control. n=3, *p <0.05 (ANOVA with Dunnett post hoc test). (**B**) The expression of the mature mmu-miR-143 and pri-miR-143~145, following mmu-miR-145a overexpression with mmu-miR-145a mimics, was quantified by qPCR. Kruppel Like Factor 4 (KLF4), a validated target of miR-145a was also assessed. Beta actin was used as a normalization control. n=3, *p<0.05 (ANOVA with Dunnett post hoc test).

RNAfold prediction programme demonstrated changes in the secondary structure of the stem loop upon editing with guide sg145m2 (Figure 5.15). The structure of the WT mmu-miR-145a stem loop presented the expected bulges and apical loop while 1nt deletion did not lead to any significant changes. On the other hand, a 12nt deletion with guide sg145m2 resulted in a stem with no bulges and the loss of the apical loop.

Figure 5.15 Predicted secondary structure of mmu-miR-145a stem loop. Minimum free energy structure of the mmu-miR145a stem loop as assessed by the structure prediction software RNAfold after editing with sg145m2. The base-pairing probability, as indication of structural remodelling or dynamics, was used for colour-coding.

The expression of the long non-coding RNA Carmn, that overlaps the miR-143~145a cluster and constitutes an independent transcription unit (Figure 5.16B), did not differ after editing with either of the guides (Figure 5.16A).

A

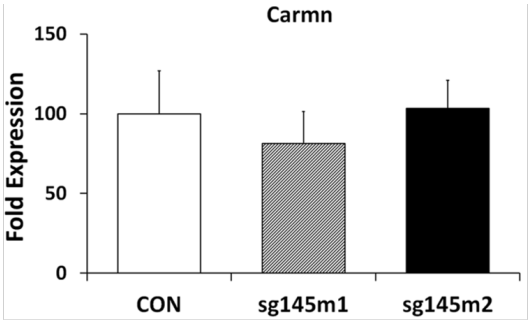

B

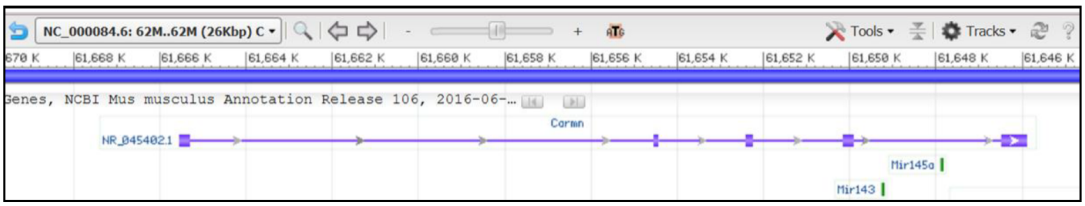

Figure 5.16 Expression of long non-coding RNA Carmn. (**A**) QPCR quantification of Carmn in sg145m2 edited cells. Beta actin was used as a normalisation control, (n=3), (ANOVA with Dunnett post hoc test). (**B**) Snapshot obtained from NCBI database (https://www.ncbi.nlm.nih.gov/gene/328968) depicting the genomic locus of Carmn (cardiac mesoderm enhancer-associated non-coding RNA) and mmu-miR-143~145 cluster.

5.3.3 Gene editing of mmu-miR-17~92 cluster

5.3.3.1 In silico design of the guide

CRISPR DESIGN Tool (http://crispr.mit.edu, Zhang Lab, MIT) was used to design the guides for the genomic locus of miR-18a, the (Figure 5.17). The DNA sequence corresponding to the transcript annotated in miRBasev21 was used as input sequence to the software. The following oligo, targeting a site in the stem loop of miR-18a (Figure 5.18), was concluded to be the most suitable one:

Sg18: 5'-TTATGCCAGAAGGAGCAGTT-3'

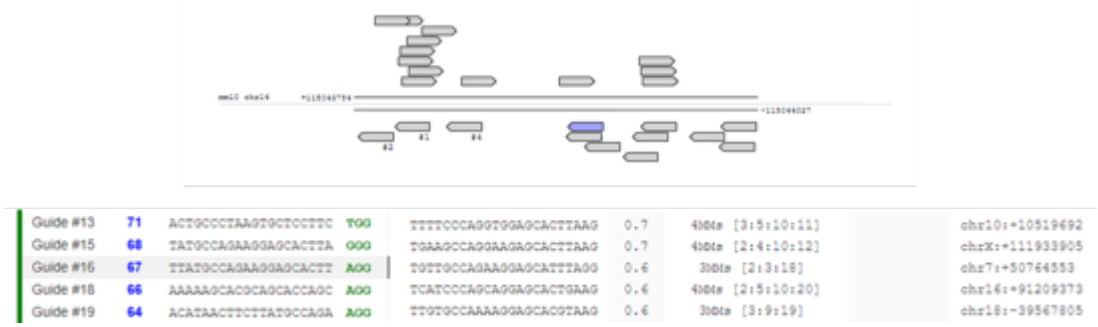

Figure 5.17 In silico design of the single-guide RNAs for mmu-miR-18 locus. The CRISPR DESIGN Tool (http://crispr.mit.edu, Zhang Lab, MIT) was used to design the guide for editing the mmu-miR-18 locus. In the figure, the sequence of the guide, the corresponding score and the 5 most likely off-target sites are depicted.

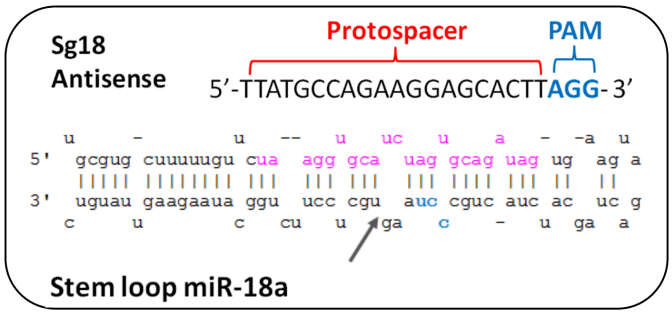

Figure 5.18 Schematic representation of the secondary structure of the miR-18a stem loop with guides. Representation of the miR-18a stem loop with the detailed sequence and the corresponding site of the DSB with sg18. PAM sequence is highlighted in blue, the mature miRNA sequence is highlighted in purple and grey arrow indicates the corresponding position of the DSB on the stem loop which is the site of mutations induced by random indels following editing of the genomic locus in mutant cells.

5.3.3.2 Editing of miR-18a

Cluster mmu-miR-17~92 consists of 6 miRNAs (Figure 5.19A) that do not share the same seed sequence and any sequence homology (Figure 5.19B). Gene editing of miR-18a with guide sg18 resulted in an efficiency varying from 32-37%, as shown by T7EI (Figure 5.19C), while digestion with restriction enzyme Bsp1286I confirmed the editing (Figure 5.19D). Sanger sequencing demonstrated the formation of small indels (Figure 5.19E) and qPCR revealed the robust downregulation only of miR-18a levels by 88% (Figure 5.19F).

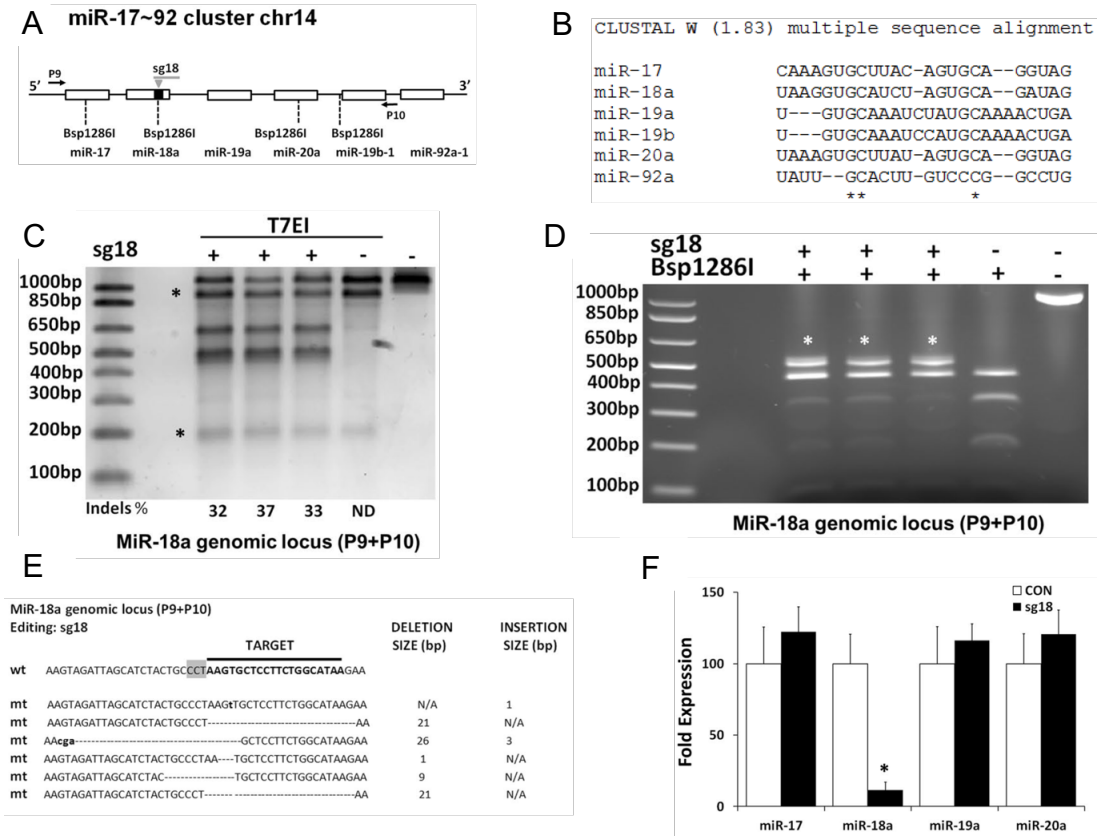

Figure 5.19 Gene editing of the miR-18a locus. (**A**) The genomic locus of the miR-17~92 cluster with the corresponding sites of the DSB induced by sg18. (**B**) T-Coffee multiple sequence alignment programme indicates that the miRNAs of the cluster do not share a common seed region or any sequence homology. (**C**) T7EI assay in three independent experiments for the miR-18a locus after editing. ND: non-detectable (**D**) The sg18 disrupts a Bsp1286I restriction site. Asterisks (*) indicate differential digestion products. (**E**) Sanger sequencing of the edited miR-18a genomic locus. The PAM sequence is highlighted in grey, deletions are represented as dashes, insertions are shown in bold small case fonts. N/A: Not Applicable. P9 and P10: Genomic PCR primers. (**F**) Gene editing of the miR-18a locus resulted in the down-regulation only of mmu-miR-18a without affecting the expression of other members of the cluster as assessed by qPCR. U6 was used as a normalization control. n=4, * $p<0.05$.

Sanger sequencing did not reveal any off-target formation of indels in the loci of either mmu-miR-17, miR-19a or miR-20a (Figure 5.20).

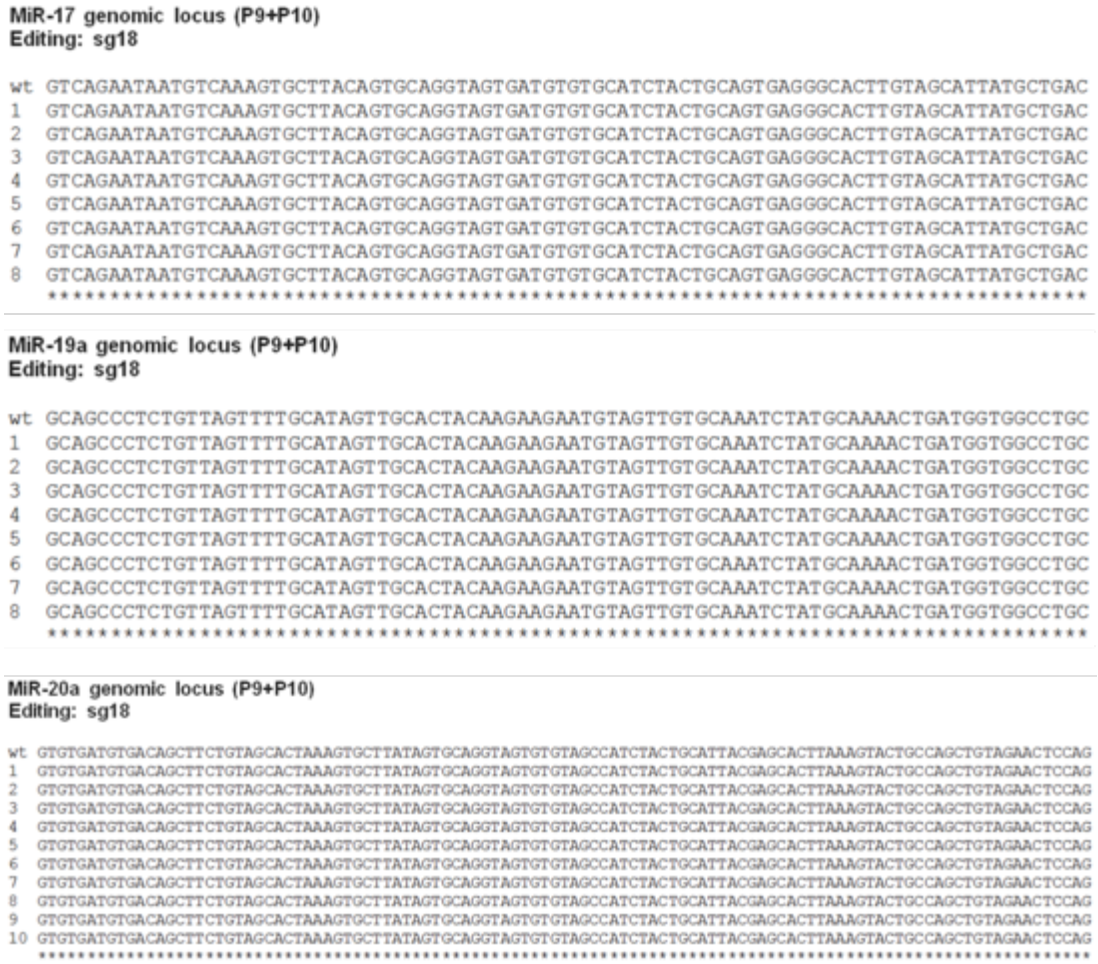

Figure 5.20 Off-target editing in mmu-miR-17~92 locus. Clustal alignment of Sanger sequencing data for the mmu-miR-17~92 cluster following editing. Top Panel: miR-17 locus, Middle Panel: miR-19a locus and Bottom Panel: miR-20a locus Wt: unedited cells, randomly picked individual colonies harbouring genomic PCR amplicons from edited VSMCs. P9 and P10: Genomic PCR primers as depicted in Figure 5.19.

Computational analysis with RNAfold prediction programme was used for assessing the secondary structure of the stem loop upon editing with guide sg18 (Figure 5.21). The structure of the wild-type miR-18a stem loop presented the expected bulges and apical loop while neither a 2nt nor a 14nt deletion led to significant changes with the latter resulting in an apical loop of smaller size.

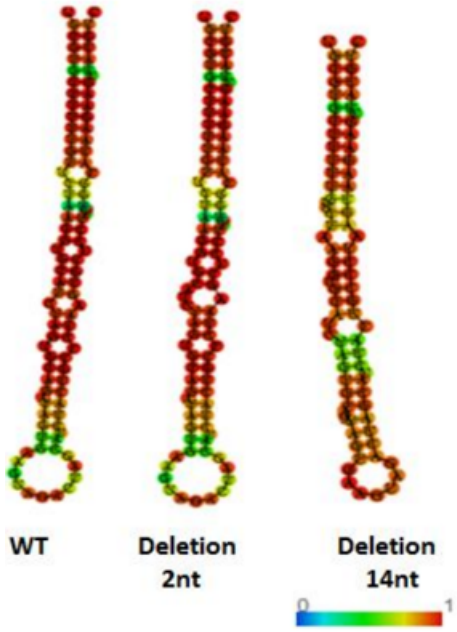

Figure 5.21 Predicted secondary structure of miR-18a stem loop. Minimum free energy structure of the miR-18a stem loop as assessed by the structure prediction software RNAfold upon editing. The base-pairing probability, as indication of structural remodelling or dynamics, was used for colour-coding.

5.3.4 Gene editing of mmu-miR-106b~25 cluster

5.3.4.1 In silico design of the guide

The guide targeting the genomic locus of mmu-miR-25 was designed in CRISPR DESIGN Tool (http://crispr.mit.edu, Zhang Lab, MIT), (Figure 5.22) by using the DNA sequence corresponding to the transcript annotated in miRBasev21 as the miRNA stem loop. The highest scoring oligo, targeting the stem of the mmu-miR-25 hairpin (Figure 5.23), was selected as the most suitable one:

Figure 5.22 In silico design of the single-guide RNAs for mmu-miR-25 locus. The guide for editing the mmu-miR-25 locus was designed with the help of the CRISPR DESIGN Tool (http://crispr.mit.edu, Zhang Lab, MIT). In the figure, the sequence of the guide, the corresponding score and the 5 most likely off-target sites are depicted.

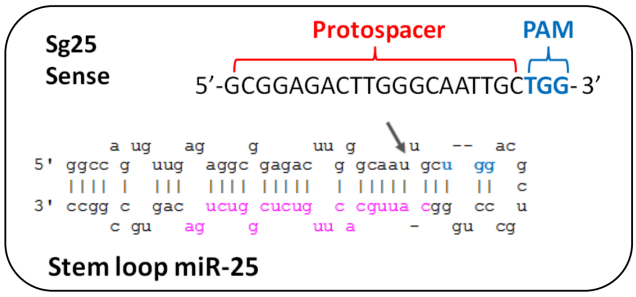

Figure 5.23 Schematic representation of the secondary structure of the mmu-miR-25 stem loop with the designed guide. Representation of the mmu-miR-25 stem loop with the detailed sequence and the corresponding site of the DSB with sg25. PAM sequence is highlighted in blue, the mature miRNA sequence is highlighted in purple and grey arrow indicate the corresponding position of the DSB on the stem loop which is the site of the formation of random indels following editing of the genomic locus.

MiR-25 is part of the miR-106b~25 cluster and is transcribed in one primary transcript together with mmu-miR-106b and mmu-miR-93. For the editing of mmu-miR-25, guide sg25 was designed, targeting a site in the mmu-miR-25 stem loop disrupting an MfeI site (Figure 5.24A). The two miRNAs do not share the same seed sequence neither any sequence homology (Figure 5.24B). T7EI results indicate successful editing with an indel formation efficiency varying from 20-27% (Figure 5.24C). MfeI restriction digestion enzyme confirmed the editing (Figure 5.24D) and Sanger sequencing demonstrated the formation of small indels, mainly deletions (Figure 5.24E). Assessment of the levels of expression of miR-25 showed a significant downregulation only of miR-25 levels by 49% (Figure 5.24F).

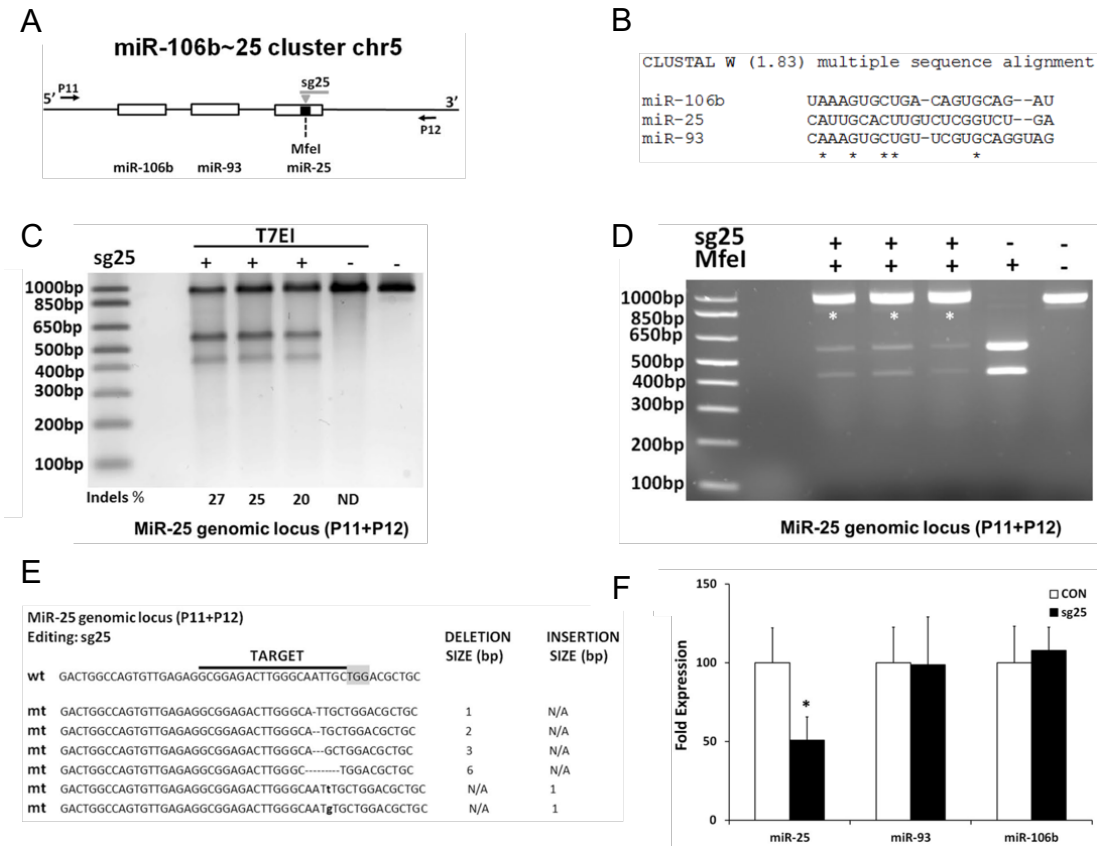

Figure 5.24 Gene editing of the miR-25 locus. (**A**) The genomic locus of the miR-106b~25 cluster with the corresponding sites of the DSB induced by sg25. (**B**) T-Coffee multiple sequence alignment program indicates that miRNAs miR-106b, miR-25 and miR-93 that form the cluster do not share a common seed region or any sequence homology. (**C**) T7EI assay in three independent experiments for the miR-25 locus after editing. ND: non-detectable (**D**) The sg25 disrupts an MfeI restriction site. Asterisks (*) indicate differential digestion products. (**E**) Sanger sequencing of the edited miR-25 genomic locus. The PAM sequence is highlighted in grey, deletions are represented as dashes, and insertions are shown in bold small case fonts. N/A: Not Applicable. P11 and P12: Genomic PCR primers. (**F**) Gene editing of the miR-25 locus resulted in the down-regulation only of miR-25 without affecting the expression of other members of the cluster as assessed by qPCR. U6 was used as a normalization control. n=4, * $p<0.05$. Assessment of the levels of miR-497b showed that it is not expressed in mouse VSMCs.

Sanger sequencing did not reveal any off-target formation of indels in the loci of either miR-93 or miR-106b (Figure 5.25).

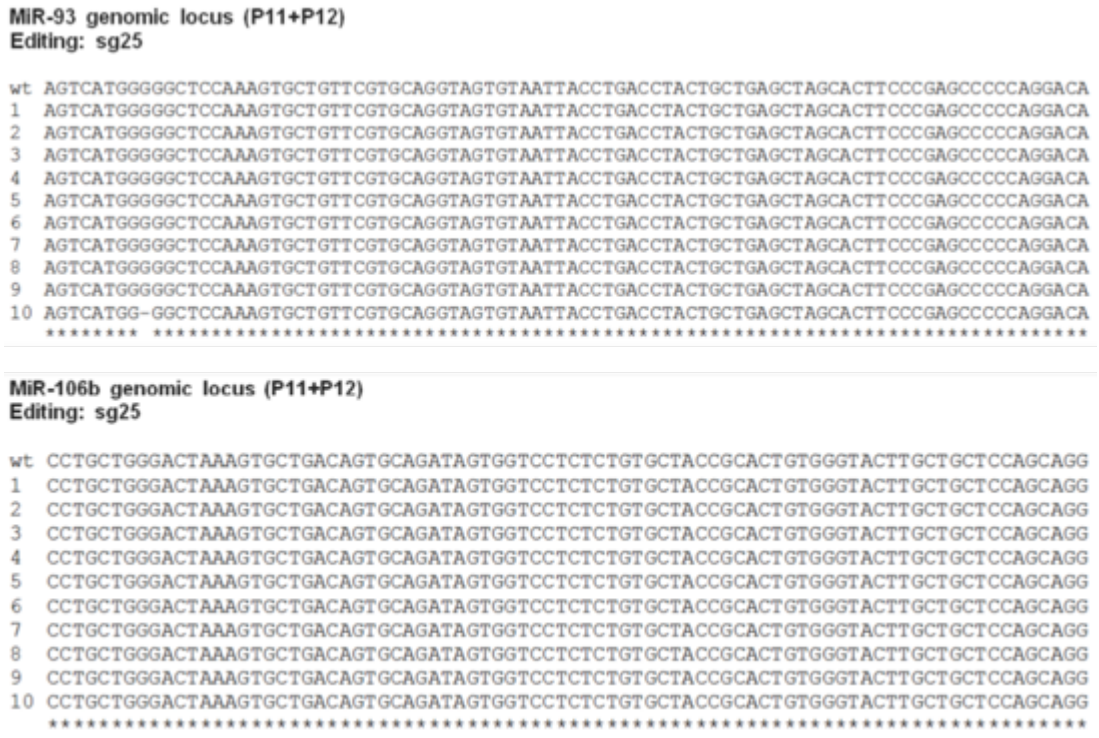

Figure 5.25 Off-target editing in mmu-miR-106b~25 locus. Clustal alignment of Sanger sequencing of the mmu-miR-106b~25 cluster following editing. Top Panel: miR-93 locus and Bottom Panel: miR-106b locus Wt: unedited cells, randomly picked individual colonies harbouring genomic PCR amplicons from edited VSMCs. P9 and P10: Genomic PCR primers as depicted above in Figure 5.24.

RNAfold prediction programme revealed a secondary structure of the stem loop upon editing with guide sg25 with the 1nt deletion not conferring any important changes in contrast to the 6nt deletion that resulted to a short stem loop and a significant change in the structure of the apical loop (Figure 5.26).

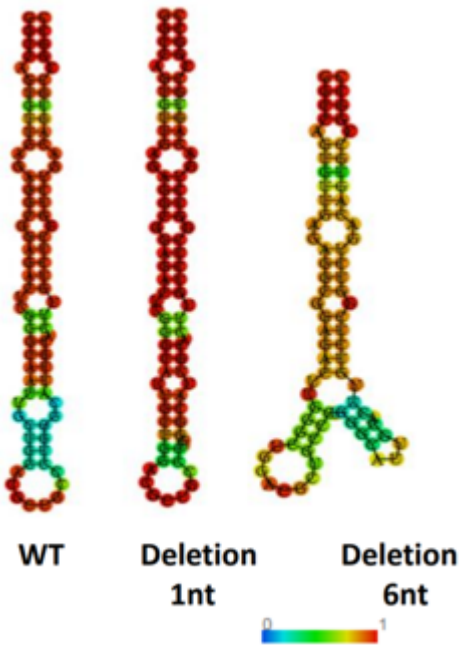

Figure 5.26 Predicted secondary structure of mmu-miR-25 stem loop. Minimum free energy structure of the miR-25 stem loop as assessed by the structure prediction software RNAfold upon editing. The base-pairing probability, as an indication of structural remodelling or dynamics, was used for colour-coding.

5.4 Discussion

MiRNA maturation is a complex process which asserts the fidelity of the biogenesis of miRNAs. In an initial step the miRNA genes are transcribed to a pri-miRNA before getting cleaved by Drosha. The fidelity of the processing is ensured by a very specific and precise recognition of the pri-miRNA by the microprocessor. During the microprocessor recognition of the primary transcript a trimeric complex is formed including one Drosha, that recognises basal elements of the transcript, thus serving as a ruler, and two DGCR8 adaptors that interact with the apical elements[5]. This modular model predicts varying contributions of several determinants that need to interact in a coordinated response for pri-miRNA recognition[7]. Elegant experimental approaches have identified additional recognition and processing features[8, 11]. Secondary structures such as stem length, hairpin pairing, bulge size and position and apical loop size has been shown to contribute to effective miRNA biogenesis. Moreover, sequence motifs, such as a UG motif at the base of the hairpin, a UGU/GUG motif in the apical loop and a CNNC motif downstream of the hairpin, can enhance processing[7, 8, 249]. Importantly, these primary sequence motifs exert their effects in some pri-miRNAs but not in others and are thought to have an additive effect in pri-miRNA processing. An intricate set of rules and modifications that are preferentially utilised in miRNAs over non-miRNA hairpins were also uncovered[11]. These findings led to the prediction and experimental validation for a significant role of single-nucleotide polymorphisms (SNPs) in altering pri-miRNA processing and miRNA biogenesis in several occasions[11]. Intriguingly they also imply that CRISPR/Cas9 gene editing of miRNA genes can affect processing of the hairpin in a dual manner either by altering the sequences or the tertiary structure.

Adding to the complexity of miRNA biogenesis, RBPs can also modify various steps of the processing post-transcriptionally thus affecting the miRNA maturation[21]. Additionally, an optimal length for the stem of the hairpin and two bulge-depleted regions in the stem, regions that may function as protein-interacting surfaces, were proposed as necessary for the RBP:miRNA interactions.

MiRNA clusters, based on their genomic locus organisation and regulation, can be divided into homo-clusters, that are composed of members of the same miRNA family and get transcribed together as one primary transcript, and hetero-clusters that are

comprised of miRNAs that belong to different families. In regarding how they exert their regulation, homo-clusters are capable of controlling their targets in a single step thus resulting in a rapid regulation, contrary to hetero-clusters that typically control their targets in multiple steps or targets and in a more delayed response[248]. Thus, miRNAs are able to control the expression of multiple proteins, by binding their corresponding mRNAs, that function at different steps in various complex biological pathways. Through this, miRNAs can exert powerful effects on important processes of cell growth, differentiation, and apoptosis[7, 23, 250] . Therefore, albeit the minor effects that an individual miRNA may have on a specific target, the combined effects of clustered miRNAs on multiple mRNA targets, of a common pathway, can be more pronounced and efficient.

Downregulation of the levels of mature mmu-miR-497a

In the current chapter, gene editing with CRISPR/Cas9 was assessed as a tool to understand the regulation of clustered miRNAs. Preliminary results demonstrated the effectiveness of CRISPR/Cas9 for the precise editing of the DNA sequence of miRNAs inducing indel formation in the vicinity of the DSB. As discussed previously, editing of mmu-miR-195a led to the downregulation of the expression levels of the edited miRNA as well as those of mmu-miR-497a, the miRNA that resides on the other hairpin of the same cluster.

After establishing the most effective delivery approach to edit the genomic loci of miRNAs, additional experiments were conducted in mouse VSMCs to edit mmu-miR-195a to decipher whether the downregulation was either the direct result of the editing or of the impaired processing of the pri-miRNA. The experiments focused on the genomic locus of the pri-miR-497~195 (Figure 5.1A). Guide sg195m2 was selected for the new set of experiments since it had previously shown the highest efficiency of the set of guides tested and Sanger sequencing had shown that the use of one guide resulted in the formation of various indels. Furthermore, compared to other guides tested, sg195m2 targeted a site in the stem loop of the miRNA but did not change the sequence of the mature miRNA and offered a better insight in the processing of the primary transcript of mmu-miR-195a. By not disrupting the sequence of the mature miRNA but, in contrast, by inducing indels in the stem loop, editing with sg195m2 can lead to an altered primary transcript with an intact mature sequence. Thus, the editing would lead to differential processing of the primary transcript and downregulation of the levels of mature mmu-miR-195a while in the case the maturation was not hindered the processing would result in a mature mmu-miR-195a with the WT sequence able to function physiologically.

Newly edited mouse VSMCs with guide sg195m2 were generated and restriction digestion showed successful editing (Figure 5.1C, D). Sanger sequencing confirmed the formation of indels (Figure 5.1D) and qPCR quantification, with more replicates than previously shown (n=4,) demonstrated the statistically significant downregulation of the levels of both the mature mmu-miR-195a and mmu-miR-497a (Figure 5.1E.), without affecting the levels of the other members of the miR-15 family, results that came in accordance with the results outlined in 4.4.2.2 in Chapter 4.

Nonetheless, the above results are not indicative of the mechanism that led to the downregulation of the levels of the mature mmu-miR-497a. Despite computational analysis not showing any complementarity between the DNA sequence of the genomic locus of mmu-miR-497a and sg195m2, the possibility of off-target mutagenesis could not be excluded, especially in light of the published studies reporting editing in off-target sites that were not predicted by online software[251]. Moreover, the off-target editing of mmu-miR-497a due to the proximal editing by Cas9 of the targeted sites in mmu-miR-195a, could not be excluded. Although sequencing data showed precise editing in the vicinity of the DSBs induced by the designed guides due to innate PCR limitations and its incapability of amplifying long stretches of DNA with high fidelity, the genomic locus of the pri-miR-497~195 was tested in two independent sequencing experiments. Following the sequencing of the genomic locus of mmu-miR-195a, -PCR primers designed to amplify the genomic locus of mmu-miR-497a (Figure 5.1A) were used and T7EI showed no specific editing (Figure 5.2A) with Sanger sequencing confirming its absence (Figure 5.2B).

Further to this, sg195m3, as a newly designed guide with no sequence homology with sg195m2, induced gene editing with an overall efficiency that approximated that of sg195m2 (Figure 5.3C) resulting in statistically significant downregulation only of the levels of both the mature mmu-miR-195a and mmu-miR-497a (Figure 5.3D) with Sanger sequencing revealing the formation of indels in the vicinity of the induced DSB in the genomic locus of mmu-miR-195a. Noteworthy, no editing in a panel of off-target sites, predicted by both the CRISPR Online Tool and the CRISPR Finder was detected (Figure 5.4). Following the same approach, as outlined above, T7EI was used to assess unexpected off-target mutagenesis in the genomic locus of the mmu-miR-497a, with the results showing no editing (Figure 5.5).

Mmu-miR-195a and mmu-miR-497a form a cluster on chromosome 11 (Figure 5.1A and Figure 5.3A) and are transcribed as one primary transcript, with both stem loops located within 500bp[114]. While no editing was detected in the genomic locus of mmu-miR-497a, the downregulation of the miRNAs needed to be further investigated. Gain and loss of function experiments could be employed in order to determine whether the mature downregulation of mmu-miR-497a may occur as a secondary effect due to reduced levels of mature mmu-miR-195a. In the case of the mmu-miR-497~195

cluster however, the sequence similarities between the two miRNAs indicate that the inhibitor can effectively silence both miRNAs and thus no conclusive data could be obtained. Overexpression of a miRNA can be achieved using short synthetic oligonucleotides that function as mature miRNA without requiring any processing by the Drosha or Dicer complexes. Following mmu-miR-195a overexpression using miRNA mimics, no differences on the expression of the mature miR-497a were observed (Figure 5.6), suggesting that the mmu-miR-497a expression is not controlled by miR-195a.

The tertiary structure of the primary miRNA transcripts can affect the accessibility of the stem loops by RNase III RBPs Drosha and Dicer and thus miRNA biogenesis may depend on this structure[252]. Therefore, a computational analysis was conducted to assess whether structural constraints could hinder the processing of the mutant pri-miRNAs. The analysis for mmu-miR-195a focused on mutant 1 that harboured a deletion of 1 nucleotide (mut1), mutant 5 that harboured a deletion of 18 nucleotides (mut5) and the unedited transcript (WT). Three software prediction programmes (RNAfold, Sfold, Co-fold) were used and all of them returned identical results (Figure 5.7). Despite 1nt deletion not demonstrating any prominent changes in the secondary structure of the mmu-miR-195a hairpin, the 18nt deletion resulted in a wider apical loop and the abolition of a bulge in the stem of the hairpin (Figure 5.7A). Similarly, in the case of editing with sg195m3, 1nt deletion resulted in subtle changes whereas a 16nt deletion in the DNA sequence of the mature mmu-miR-195a led to substantial changes in the structure of the hairpin, with the elimination of the apical loop and the severe shortening of the stem (Figure 5.7B).

Furthermore, the 3D simulation highlighted even more pronounced differences. In the wt, the mmu-miR-195a stem loop was prominent while the mmu-miR-497a stem loop more compressed but clearly accessible. In the mut1, the conformation of mmu-miR-195a stem loop was similar although the single nucleotide mutation had an effect leading to a mmu-miR-497a stem loop strongly attached to the main core and not as accessible as in WT. Nevertheless, profound differences were observed in the conformation of mut5. No typical hairpin for pri-miR-195a could be detected and the structure was more strongly entangled with the main core. The mmu-miR-497a stem loop displayed a compact shape in close proximity with the mmu-miR-195a stem loop but relatively distal from the main core and with no clear accessibility to the hairpin

(Figure 5.8). Overall, the 3D remodelling indicated a clear difference between the entire structure of wt and mut5 and to a lesser extent also between wt and mut1 with accessibility of the mmu-miR-497a stem loop being affected in both mutants. These results suggested that extensive deletions (in this case 18nt) in the genomics locus of mmu-miR-195 stem loop can alter the tertiary structure of the entire mmu-miR-497~195 transcript.

Although these results cannot safely lead to definitive conclusions about the mechanism through which the editing of the mmu-miR-195a gene can affect the levels of the mature mmu-miR-497a, the possibility of impairing the maturation in a dual manner directly through sequence and structural alterations and disruptions cannot be excluded. Computational analysis showed that disrupting the mmu-miR-195a stem loop can impose tertiary constraints that influence the processing of the entire pri-miR-497~195 resulting in downregulation of the expression levels of both miRNAs.

In the case of the mmu-miR-195a stem loop, the UGU/GUG motif in the apical loop is not present implying that the sequence is not important for the maturation of the hairpin. Nonetheless, editing with CRISPR/Cas9 led to the direct deletion of the terminal loop of the hairpin affecting its secondary and tertiary structure (Figure 5.7). These findings are in line with the literature that reports that mutations in the apical loop of miRNA hairpins lead to less effective processing and an autoregulatory role of the tertiary structure[252, 253].

5.4.1 Editing of mmu-miR-143~145 cluster

Next, to determine the effect of gene editing in a hetero-cluster the study focused on the mmu-miR-143~145 cluster[114]. This locus spans approximately 1400bp in mice and harbours mmu-miR-143 and mmu-miR-145a, two miRNAs that do not share sequence similarities (Figure 5.11A and B) but regulate essential functions for VSMCs growth, differentiation, and contractility[78, 254].

Following the same rationale presented previously, two sgRNAs targeting the mmu-miR-145a locus were designed using the CRISPR Online Tool (Figure 5.9). The

guides used were selected according to the site they targeted with guide sg145m1 generating a DSB 30bp upstream of the stem loop of mmu-miR-145a and guide sg145m2 targeting directly the stem loop, disrupting a HinfI restriction site, (Figure 5.10 and Figure 5.11A). T7EI results indicated that sgRNA145m1 was more efficient in inducing gene editing (Figure 5.11C) while digestion with HinfI confirmed the editing (Figure 5.11D). Sanger sequencing demonstrated small indel formation (1–40bp) with either sgRNA (Figure 5.11E), in accordance with previous results from mmu-miR-497~195 cluster.

QPCR quantification showed that the gene editing had a robust effect on miRNA expression. Editing with guide sg145m1 led to largely similar and significant downregulation of the levels of both the mmu-miR-143 (28%) and mmu-miR-145a (33%). A strong inhibition of mature mmu-miR-145a and mmu-miR-143 (89% and 50%, respectively) expression was observed following sg145m2 application (Figure 5.12). Interestingly, despite the high levels of gene editing induced by the sgRNAm1 guide the downregulation in mature mmu-miR-145a and mmu-miR-143 expression was significant but lower than when guide sgRNA145m2 was used, suggesting that targeting directly the stem loop is a more efficient strategy for inhibiting miRNA expression (Figure 5.12). Further support to this notion was provided by Sanger sequencing. The sg145m1 guide led to indels that did not disrupt the mmu-miR-145a stem loop sequence, while sg145m2 guide resulted in mutations within the hairpin. These results showed that the effects of targeting directly the stem loop of the miRNA is a more effective strategy of downregulating its expression since a DSB induced within the miRNA sequence can result in the formation of indels and the direct disruption of its secondary structure contrary to the effects of sg145m1 which induced a DSB in a substantial distance from the stem loop.

Despite the significant decrease in mmu-miR-143 expression, no editing of the mmu-miR-143 genomic locus was observed with either guide (Figure 5.13A), as was expected. Mutation screening revealed no indels in the mmu-miR-143 locus in edited cells with either guide (Figure 5.13B).

Two different approaches, previously reported, have shown that mutations in the pri-miRNA sequence of mmu-miR-143~145 can be tolerated provided that they do not disrupt critical structural elements. In more detail, introducing loxP sites for Cre-

mediated recombination in the genomic loci of mmu-miR-143 or mmu-miR-145a resulted in mutant mice that do not exhibit any effect on the expression of any of the two miRNAs in either case[254]. This approach deleted the stem–loop sequence of the pre-miRNA for each of the miRNAs, or the genomic sequence for both miRNAs, and replaced it an exogenous DNA. Interestingly though, replacing the genomic region of mmu-miR-143 with the exogenous sequence of the LacZ reporter not only disrupted the expression of mmu-miR-143 but also led to effective silencing of the mmu-miR-145a expression[118]. This construct permitted the cells that produced miR-143 and miR-145 to be visualised through staining with β-galactosidase. From these experiments, it becomes apparent that while both approaches disrupt the miRNA gene, the introduction of a reporter in the DNA sequence of the primary transcript renders it unsuitable for downstream processing and hinders the maturation of mmu-miR145a despite the presence of an intact mmu-miR-145a stem loop. Although not conclusive, these reports imply a critical role of the tertiary structure as a critical determinant in the maturation of clustered miRNAs. Furthermore, they indicate that the introduction of mutations in the pri-miR-143~145 sequence per se does not hamper miRNA maturation[254]. This is in line with findings presented in the current study that sg145m1, which induces sequence changes upstream of the mmu-miR-145a stem loop, had not but a minimal effect on the expression of the clustered miRNAs inducing effective editing of the locus, a conclusion that becomes even more evident when the indel efficiency of the two guides are compared to their final effects on the expression of the miRNAs.

To elaborate on the regulatory mechanisms involved, the expression of pri-miR-143 and pri-miR-145a in sg145m2 edited cells was quantified. To this end, commercially available assays, designed to target the flanking sequences on either side of the miRNA stem loop, were used. Effectively, the assays employed to quantify the pri-miR-143 and pri-miR-145a targeted the hairpin of mmu-miR-143 and mmu-miR-145a, respectively. A sharp decrease was observed indicating that targeting mmu-miR-145a affects the expression of the entire pri-miR-143~145 (Figure 5.14A), in line with the results for homo-cluster mmu-miR-497~195.

In order to determine whether mature miR-145a expression exerts transcriptional control on the miR-143~145 cluster, mmu-miR-145a was overexpressed in VSMCs using miRNA mimics. These are short synthetic oligonucleotides that function as mature miRNA without requiring any processing by the Drosha or Dicer complexes. High levels of mmu-miR-145a led to increased miR-143 expression (250%) that was

accompanied by a coordinated increase in pri-miR-143 and miR-145a expression (162% and 165% respectively), indicating transcriptional regulation. As expected the levels of KLF4, a validated target of miR-145a[114] were significantly downregulated (40%) following miR-145a overexpression (Figure 5.14B).

These findings provide a helpful insight in the co-ordination in the maturation of clustered miRNAs. In the case of the mmu-miR-143~145 cluster an interdependency in the mature miRNA expression was demonstrated. The results outlined above were indicative of a transcriptional regulation of mmu-miR-145a on mmu-miR-143 and a feed-forward loop that reinforces the expression of the entire cluster. Gene editing of the mmu-miR-145a stem loop led to decreased expression of both the miRNAs of the cluster while mmu-miR-145a mimics led to increased levels of pri-miR-143 and mature mmu-miR-143. Thus, a direct evidence for the role of mature mmu-miR-145a in triggering the expression of the cluster mmu-miR-143~145 is provided. Although it is difficult to dissect whether the differences in mmu-miR-143 expression are due to structural changes or due to transcriptional regulation triggered by the reduced mmu-miR-145a levels, the two possibilities are not mutually exclusive. It is important to point out that mmu-miR-143 and mmu-miR-145a show no sequence homology suggesting that they do not have common targets[114]. Nonetheless, the two miRNAs participate in a regulatory network that controls cytoskeletal remodelling and phenotypic switching of VSMCs under pathological conditions[254]. This underlines the added value of miRNA clusters that provide an effective mechanism of cellular response and may explain the evolutionary pressure for their sequence conservation.

Next, RNAfold revealed that induction of 1nt deletion in the hairpin of mmu-miR-145a with sg145m2 did not change the secondary structure while a 12nt deletion changed the structure significantly (Figure 5.15). Intriguingly, the expression of Carmn (cardiac mesoderm enhancer-associated non-coding RNA), a long non-coding RNA overlapping the mmu-miR-143~145 cluster that constitutes an independent transcription unit[226] did not differ in mmu-miR-145a edited cells (Figure 5.16), confirming that only the primary transcript (pri-miR-143~145) and not the wider locus is affected.

With regards to the tertiary structure of the cluster miR-143~145, as its length is about 1400bp, it cannot be analysed using the algorithms currently available for the

computational simulation. The development of more elegant tools to predict the tertiary structure of longer sequences will provide further insights.

Although not adequate results that support the notion were obtained, it is tempting to speculate that the downregulation of the clustered miRNA is due to both a disruption of a feed-forward loop as well as of the hindering of the processing of the primary transcript due to alterations in its tertiary structure.

5.4.2 Editing of mmu-miR-17~92 cluster

Next, the study focused on a highly studied miRNA clusters in the mouse genome, the miR-17~92, spanning 800 bp. The miR-17~92 cluster plays a pivotal role in the cardiovascular system and in cancer and mediates processes such as angiogenesis[120, 122]. This cluster consists of six miRNAs that can be grouped in four families based on their seed sequence (Figure 5.19A and B). Intriguingly, two paralogs, the miR-106a~363 and miR-106b~25 clusters are believed to be derived from a series of duplication and deletion events during vertebrate evolution have been identifed[255].

Gene editing using sg18 that targets the miR-18a stem loop (Figure 5.19A) was efficient (32–37%) as assessed by T7EI assay (Figure 5.19B) and disrupted the Bsp1286I restriction site (Figure 5.19D). Sanger sequencing revealed the presence of small deletions in the miR-18a stem loop (Figure 5.19E) that were predicted to induce a differential secondary conformation (Figure 5.21). As previously, these deletions were very specific and occurred only in the vicinity of the DSB. No mutations were identified in a 1 kb region that encodes the cluster (Figure 5.20). Interestingly, in contrast to the results presented for clusters mmu-miR-497~195 and mmu-miR-143~145, in the case of mmu-miR-17~92 cluster, although the expression of miR-18a diminished significantly (88%) there was no impact on miR-17, miR-19a and miR-20a levels, miRNAs that are all located on the same cluster (Figure 5.19F). Additionally, discrepancies between the editing efficiency as evaluated by T7EI and the levels of downregulation of mmu-miR-18 showcased the limitations of the assay for assessing the impact of editing. Although underestimation of the indel efficiency is expected these results demonstrate that T7EI is not as sensitive as a technique. The expression of miR-19b-1 and miR-92a-1 could not be assessed as they are also encoded by a second miRNA cluster on chromosome X (Supplementary Table 1).

Intriguingly, analysing Sanger sequencing data with RNAfold did not show any significant secondary structure alterations despite the deletion of a long sequence, although these results are not conclusive. Thus, in the case of mmu-miR-18 it is tempting to speculate that is neither the structural changes of the targeted hairpin nor the deletion of sequence motifs but, possibly, the deletion of miRNA specific sequences that led to the downregulation of the levels of the mature miRNA.

Nonetheless, there is also the possibility that the 6nt deletion that was chosen to be assessed with RNAfold had no effect neither on the structure nor on the expression levels of the miRNA.

In agreement with the results shown above, it has been reported that pri-miR-17~92 shows a highly specific globular, tertiary structure that affects the processing of the transcript by Drosha[252, 253]. More specifically, Chaulk et al have demonstrated that pri-miR-17~92 takes a folded structure of globular shape that results in the internalisation of the 3'-end of the transcript while the 5'-end of the cluster folds on top of it, leading to a less efficient processing of the internalised miRNAs[253, 256]. Moreover, a non-miRNA containing stem loop in the core of the primary transcript, showing a high sequence conservation, has been reported [256]. This stem loop interacts with other hairpins in the transcript, namely miR-19b, and affects the processing of the whole structure. Interestingly, physiological interactions of the two hairpins lead to low levels of miR-92a while disruption of the primary transcript's structure, due to mutations, leads to enhanced expression[252, 256]. In addition, this structure affects the maturation of other miRNAs of the 3' core suppressing the expression of miR-19b and miR-18a[256] while removal of miR-19b resulted in the upregulation of miR-92a and, to a lesser extent, of miR-18a. These data also indicate that miR-18a hairpin, although not part of the 3' core, is internalised upon folding of the primary transcript.

These data further support the notion that miRNA processing is complex and highly sensitive in tertiary structure changes and showcase how sequence alterations, with the subsequent disruption of the structure, can affect miRNA maturation. Taken together, with the data outlined above, they show how CRISPR/Cas9 editing can be employed for the downregulation of different miRNAs of the same cluster with the use of specific guides depending on the intended result. Nonetheless, editing of the cluster's DNA sequence although successful, was shown not to exert any effects on the maturation of the clustered miRNAs in contrast to previous results, highlighting that the processing differs among miRNA clusters.

5.4.3 Editing of mmu-miR-106~25

Similar results, as discussed in 5.4.2, were obtained when the stem loop of miR-25 was targeted in the miR-106b~25 cluster (Figure 5.22 and Figure 5.23). Effective editing was observed with sg25, as determined by both the T7EI assay (20–27%, Figure 5.24C) and the disruption of the MfeI restriction digestion site (Figure 5.24D). Sanger sequencing demonstrated a mutation pattern of small indels (Figure 5.24E), while qPCR quantification showed a significant downregulation of miR-25 expression (49%, Figure 5.24F) with the levels of miR-93 and miR-106b not being affected. Off-target mutagenesis assessment showed no editing for the miR-93 and miR-106b loci (Figure 5.25). The DNA sequence alterations led to a secondary structure of the miR-25 stem loop with a disrupted terminal loop (Figure 5.26).

Interestingly, interdependency in expression does not seem to be a common feature in all clustered miRNAs. Gene editing in mmu-miR-497~195 homo-cluster and mmu-miR-143~145 hetero-cluster revealed that targeting of one of the hairpins of the cluster led to downregulation of both of the clustered miRNAs. Although overexpression of mmu-miR-195a did not result in enhanced levels of mature mmu-miR-497a, suggesting no interdependency in the mmu-miR-497~195 cluster, in the case of mmu-miR-143~145 cluster the levels of mature mmu-miR-143 were affected by those of mmu-miR-145.

However, targeting of miR-18a and mmu-miR-25 revealed that the expression of other miRNAs in the corresponding clusters are not affected by changes in the structure of the targeted hairpins. No compensatory increase of these miRNAs was observed in edited cells either. Thus, it seems that while coordinated expression of miRNAs in clusters is a shared feature, feed-forward and feedback loops are in place only when a synergistic effect and combined regulation of multiple pathways is required.

Overall, it has been shown that despite the sequence diversity of pri-miRNAs, mutations can be well tolerated, provided that they do not disrupt critical elements such as stem length, bulge position and terminal loops. Furthermore, it was demonstrated that although miRNAs in a cluster form a co-transcriptional unit their expression is not always interdependent.

In conclusion, these data confirmed that the CRISPR/Cas9 editing technology is extremely precise, since indels occurred only in the vicinity of the DSB while no mutations were identified in the regions encoding the cluster. All in all, CRISPR/Cas9 emerged as a robust system for miRNA inhibition that is able of revealing novel regulatory mechanisms for clustered miRNA expression.

Chapter 6 ASSESSMENT OF THE LEVELS OF RBPS THAT BIND PRIMARY MMU-MIR-195A

6.1 Introduction

RBPs are important regulators of various steps in the expression of genes either co- or post-transcriptionally and they participate in multiple steps such as RNA splicing, capping, polyadenylation, export and translation[7, 257]. Following the same recognition patterns, RBPs participate in the maturation process of the miRNAs by controlling their post-transcriptional processing, tightly and in various steps such as the primary transcript cleavage, the export, the pre-miRNA cleavage, the stability control and the loading to RISC complex.

The regulation of the maturation of miRNAs is a multistep process that is controlled both by the rate and the efficiency of the recognition and the binding of the RNase III nucleases Drosha and Dicer. This efficiency is influenced by both structural and sequence characteristics of the miRNA precursors[7]. Further to this, RBPs are able of recognising specific sequence motifs in precursor miRNAs and regulate the maturation according to the cell type or exogenous signals[258-260]. In addition, RBPs have been shown to be capable of binding short single-stranded or double-stranded RNA[1, 260-262].

Only a small portion of the putative RBPs have been studied in eukaryotic cells with regards to their function with the reported results not being conclusive due to the diverse experimental approaches followed and the cell line specific RNA interactions that the RBPs showed[221, 263]. Some of the discrepancies among the data reported cannot be conclusively explained but could be due to discrepancies between *in vitro* and *in vivo* conditions, different binding conditions, and/or the proteins *per se* analysed[221].

The cell type specific interactions between RBPs and miRNAs are an aspect of the proteins that restricts their study and the universal application of the conclusions drawn from the studies while some RBPs recognise multiple hairpin-forming RNAs,

indicating a wider range of interacting repertoire[263]. Nonetheless, in the latter case, the recognition was specific only to hairpin structures but not generic dsRNAs, implying that other co-factors, and not the secondary structure alone, are necessary for the recognition of the miRNAs. This duality that the RBPs present in their function suggests that they might have specific context or cofactor-dependent effects on their targets.

Multiple RBPs have been implicated in the biogenesis of the miRNAs such as KSRP and TRIM25 in the regulation of let-7[55, 264], MSI1/2 in miR-7 processing[265]. However, an exhaustive approach to identify and describe RBPs that bind and regulate miRNAs during all the stages of their biogenesis and turnover has yet to be conducted. This would provide the needed information for a comprehensive picture of the dynamic interactome of pri-/pre-miRNAs to be drawn. Taken together, these data highlight the importance of the *in vitro* studies for the identification of the interactions between RBPs and miRNAs, although the limitations of the approach need to be also taken into consideration[221].

Although studies have reported data regarding recognition of specific RNA sequence motifs and secondary structures for various miRNAs during their maturation, namely miRNAs that participate in tumorigenesis, miR-195 is one of the least studied ones. In light of this, in the current chapter the project focused in establishing a workflow to identify the RBPs that bind the pri-miR-195a and participate in its maturation. Additionally, a comprehensive panel of RBPs that bind the mutant pri-miRNA was assessed in order to elucidate the downregulation of the miRNA levels upon editing with CRISPR/Cas9.

6.2 Experimental Design

The scope of the current chapter was to establish the RBPs that recognise and bind either the WT or the mutant pri-miR-195a, and to compare the panels of the proteins that bound differentially on the two primary transcripts. The objective of this approach was to provide *in vitro* data for proteins that can participate in the maturation process of the primary transcript of the miRNA. Moreover, by using a mutant primary transcript, the goal of the study was to decipher the alterations in the processing of the transcript that can lead to differential expression. In order to do so, RNA molecules were *in vitro* transcribed.

In more detail, DNA sequences of pri-miR-195a that corresponded to either the WT or a mutant sequence, the latter one harbouring a 16nt deletion upon editing with sg195m3, were *in vitro* transcribed as described in Chapter 3.18 and were labelled with biotin. Next, they were bound to streptavidin magnetic beads and they were used as baits to bind and pull-down proteins from mouse VSMC lysates, proteins that are capable of recognising and binding the two distinct RNA molecules. The eluted proteins were then analysed with Mass Spectrometry (MS) with the aim to be validated by an independent approach, like Western Blotting. These experiments were performed in collaboration with Prof Manuel Mayr and the hypothesis to be tested was that, since no editing of the genomic locus of the mmu-miR-497 was identified, the downregulation observed was the result of the differential processing of the whole primary transcript due to a new panel of RBPs that recognise and bind the mutant pri-miR-497~195 that either restrained its processing or led to its cleavage.

It is the first time, to the best of my knowledge, that a pull-down experiment was conducted aiming to identify the network of RBPs that recognise the pri-miR-195a. According to the data received and analysed, a higher number of RBPs bound the mutant transcript, despite the shorter sequence and the decreased number of the putative sequence motifs that can potentially be recognised and bound. Lastly, analysis of the networks of the identified proteins, with the use of online tools, demonstrated that these proteins participate in the differential splicing of the mRNAs and the clearance of mRNAs.

6.3 Results

6.3.1 Differences in expression of RBPs

The levels of a panel of 14 RBPs that have been previously identified to participate in the maturation process of miRNAs[221], and share RNA binding motifs with the primary transcript of mmu-mir-195a, were tested. In more detail, three different edited sequences were expressed, with the use of pLKO.1 vector, that harboured 1nt, 4nt and 126nt deletions. VSMCs were infected with lentiviral particles with either an empty pLKO.1 vector, a vector with the unedited sequence of the primary transcript or with vectors harbouring each of the edited sequence resulting in their overexpression. Assessment of the expression levels of the 14 RBPs without showing any statistically significant difference in their expression. The proteins with their corresponding RNA binding motifs are depicted in Supplementary Table 6.

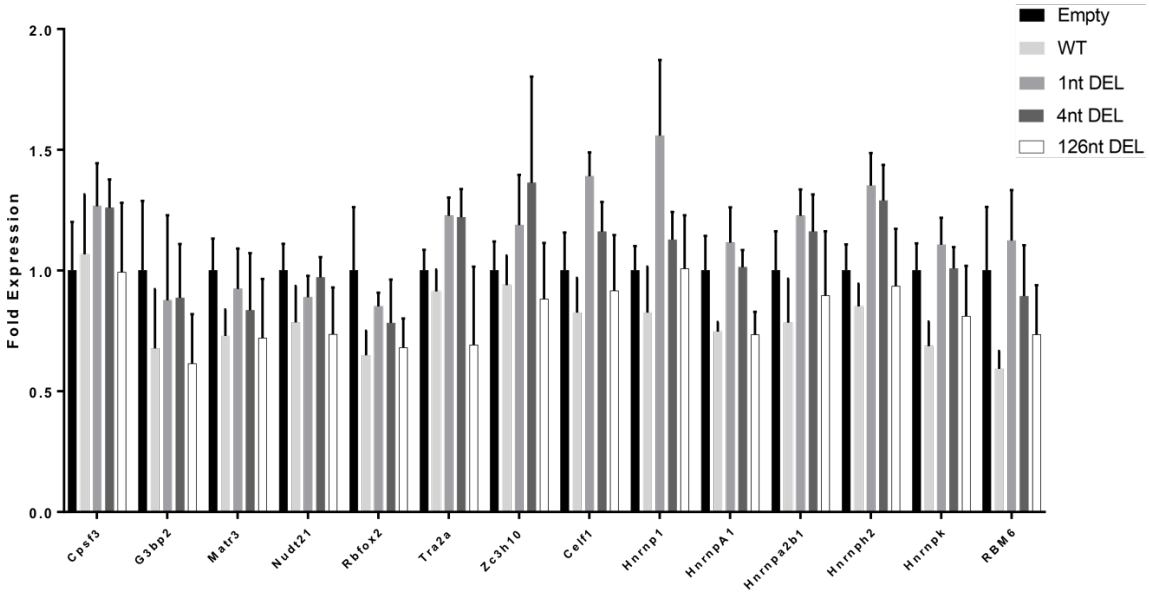

Figure 6.1 Assessment of the expression levels of a panel of RBPs. The level of 14 RBPs were quantified in VSMCs after transfection with pLKO.1 expressing mutants of mmu-miR-195a harbouring different stretches of deletion.

6.3.1.1 Validation of the Mass Spectrometry data using Western Blot

6.3.1.1.1 Titration of the Pull-down conditions

Titration experiments were conducted to identify the optimal conditions for the RNA Pull-down assays. IVT RNA transcripts corresponding to the WT or the mutant pri-miR-497~195 were tested in two individual Pull-down experiments. Blotting against human antigen R (HuR) showed that the two transcripts were able to bind to the protein and pull it down in the conditions tested.

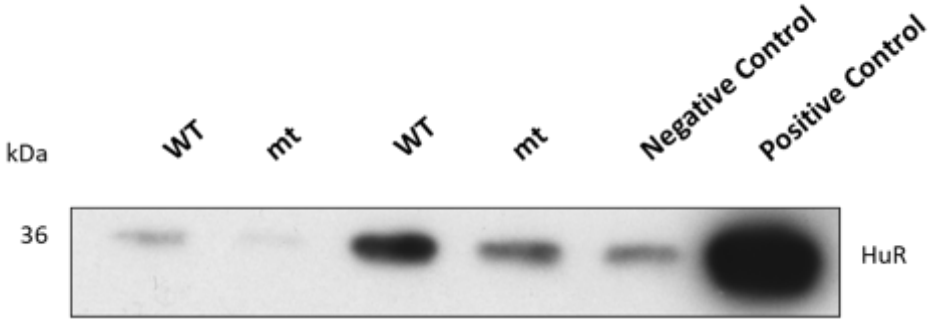

Figure 6.2. Western blot analysis for HuR. Two independent experiments were used to assess the ability of the IVT transcripts to recognise and pull-down HuR protein (lanes 1-2 and lanes 3-4, respectively). The negative and positive RNA controls that were provided with the kit were used as controls for the Pull-down. As negative control a poly(A)$_{25}$ RNA and as positive control the 3´ untranslated-region of androgen receptor (UC-rich region) was used. WT: wild type transcript, mt: mutant transcript.

In addition to the first set of titration experiments, further optimisation revealed that regardless of the amount of DNA used in the IVT, the efficiency of the Pull-down was not affected. This indicated that the IVT reaction was not affected by the amount of DNA. Furthermore, the streptavidin beads bound to the positive RNA control, following elution under the recommended conditions, were boiled with sample buffer containing SDS, and assessment of the eluted proteins, demonstrated that the initial elution, although efficient, is not complete (Figure 6.3).

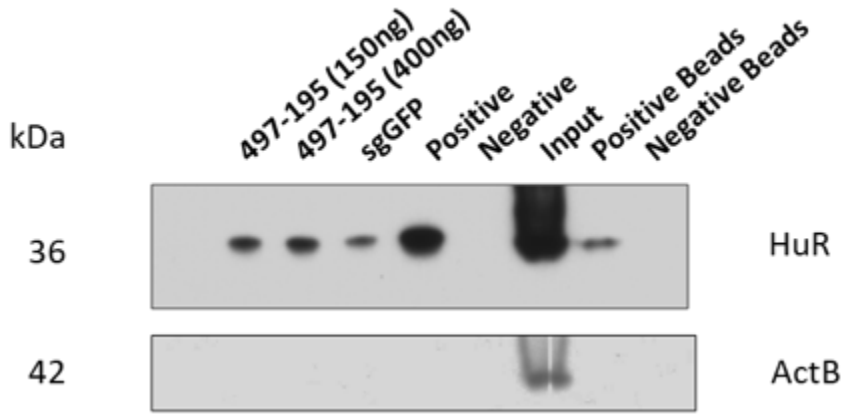

Figure 6.3. Titration experiment for the RNA template of the Pull-down. Different amount of DNA was used for the IVT reaction, preceding the labelling and the Pull-down. An IVT RNA that corresponded to GFP was used as a negative control alongside the negative and positive RNA controls that were provided with the kit. Input was used as a control for the antibody together with the eluate from the streptavidin beads bound to the labelled positive or negative RNA controls.

Further optimisation of the Pull-down assay reached the conclusion that there are no detectable differences in the efficiency of the Pull-down when either 25 or 50pmol were used while the absence of 30% PEG during the labelling reaction was detrimental for the assay (Figure 6.4). In addition, blotting with Dicer antibody showed the same efficiency pattern although the differences were less pronounced (Figure 6.5).

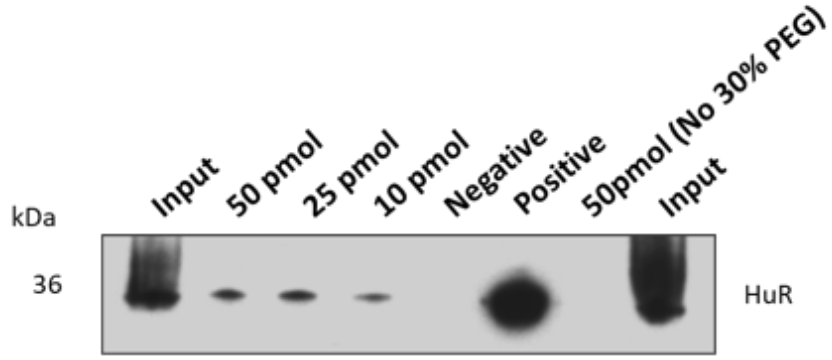

Figure 6.4. Titration experiment for the amount of labelled RNA to be used for the Pull-down. Different amounts of labelled RNA were tested to assess the optimal conditions for the assay.

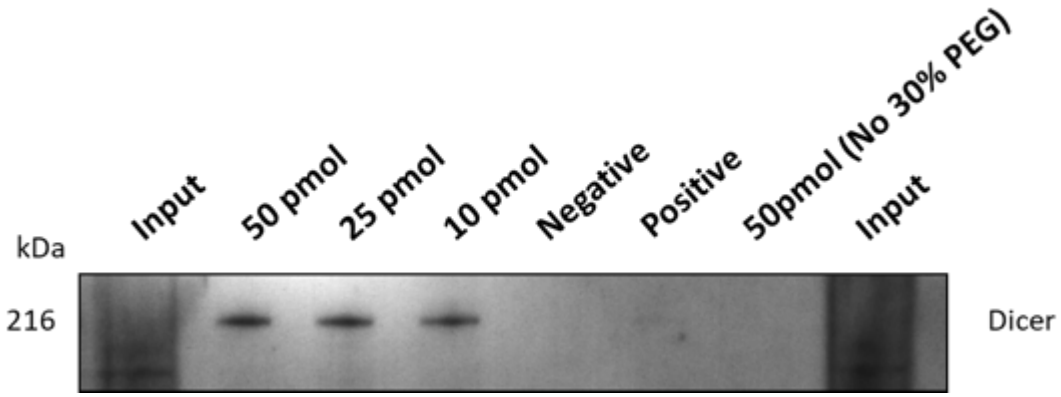

Figure 6.5. Western blot analysis for Dicer. Different amounts of labelled RNA were tested to assess the optimal conditions for the assay. They were then tested for their ability to identify and pull-down Dicer.

6.3.2 Proteomic Analysis of the RNA Pull-down proteins

6.3.2.1 Mass Spectrometry analysis of the RNA Pull-down proteins

The proteins that were pulled down using the IVT transcripts corresponding to the WT and mutant pri-miR-497~195 were analysed using MS. The eluted proteins were then injected onto the nano-LC-MS/MS system for data dependent analysis on a Q Exactive™ Plus Quadrupole-Orbitrap MS. Overall, 766 proteins were detected.

Protein abundance was measured using normalised TIC of MS/MS spectra in Scaffold (version 4.8.7). In the untargeted proteomics analysis, 139 proteins were considered quantifiable with the following criteria: the protein was present in a minimum of 2 samples in at least 1 group. Statistical analysis of the MS results revealed a number of proteins of which about 45% were RNA binding and 55% non-RNA binding as annotated in Uniprot (Figure 6.6). Moreover, their localization was reviewed, with the majority of them being found in the nucleus (42% (Figure 6.7) as well as the number of their RNA Binding Domains (RBDs).

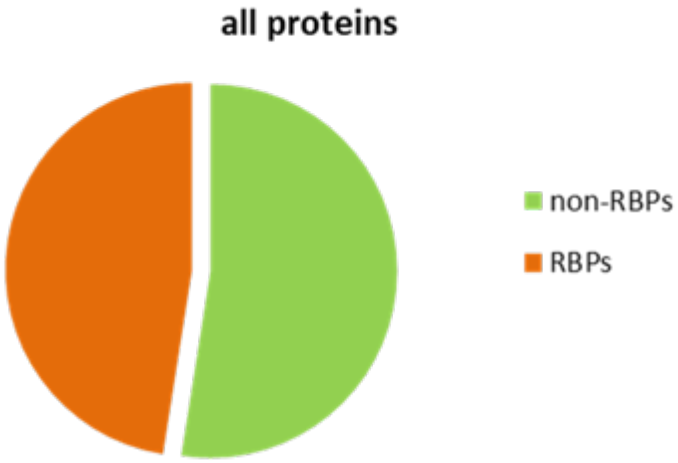

Figure 6.6. Distribution of RNA pulled down proteins. The proteins that were pulled down with either of the two transcripts (WT or mutant) were grouped with regards to their ability to bind RNA or not.

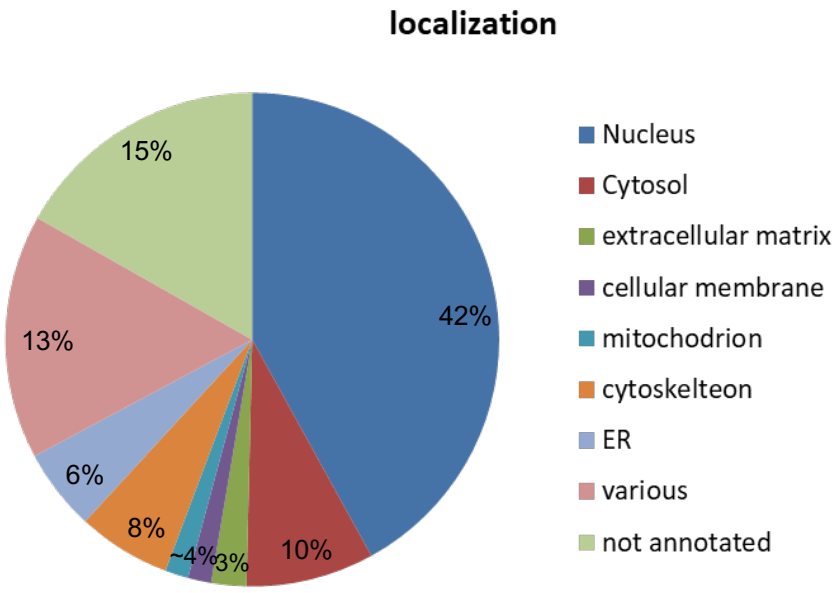

Figure 6.7. Chart for the localization of the RNA pulled down proteins. UNIPROT annotation was used to investigate the localization of the pulled down proteins.

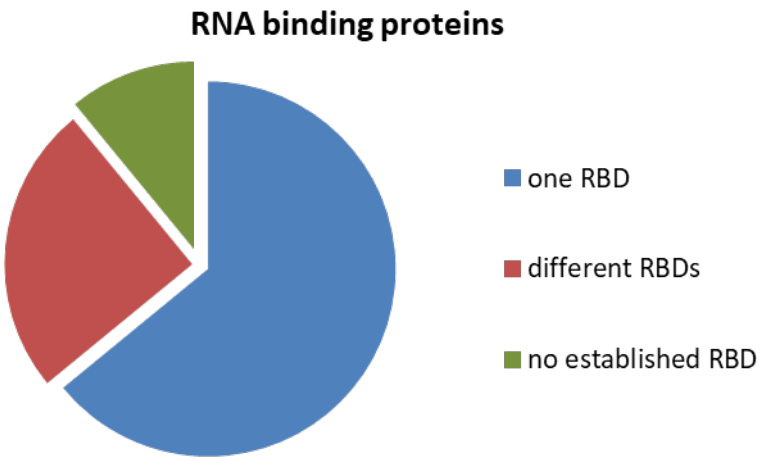

Figure 6.8 Number of RBDs in the pulled down proteins. Of the proteins that were pulled down, the RBDs were grouped according to the number of the RBDs that they harbour as per UNIPROT annotation.

Statistical analysis of the MS results revealed 5 proteins that are bound to the mutant transcript in higher abundancy than to the WT one.

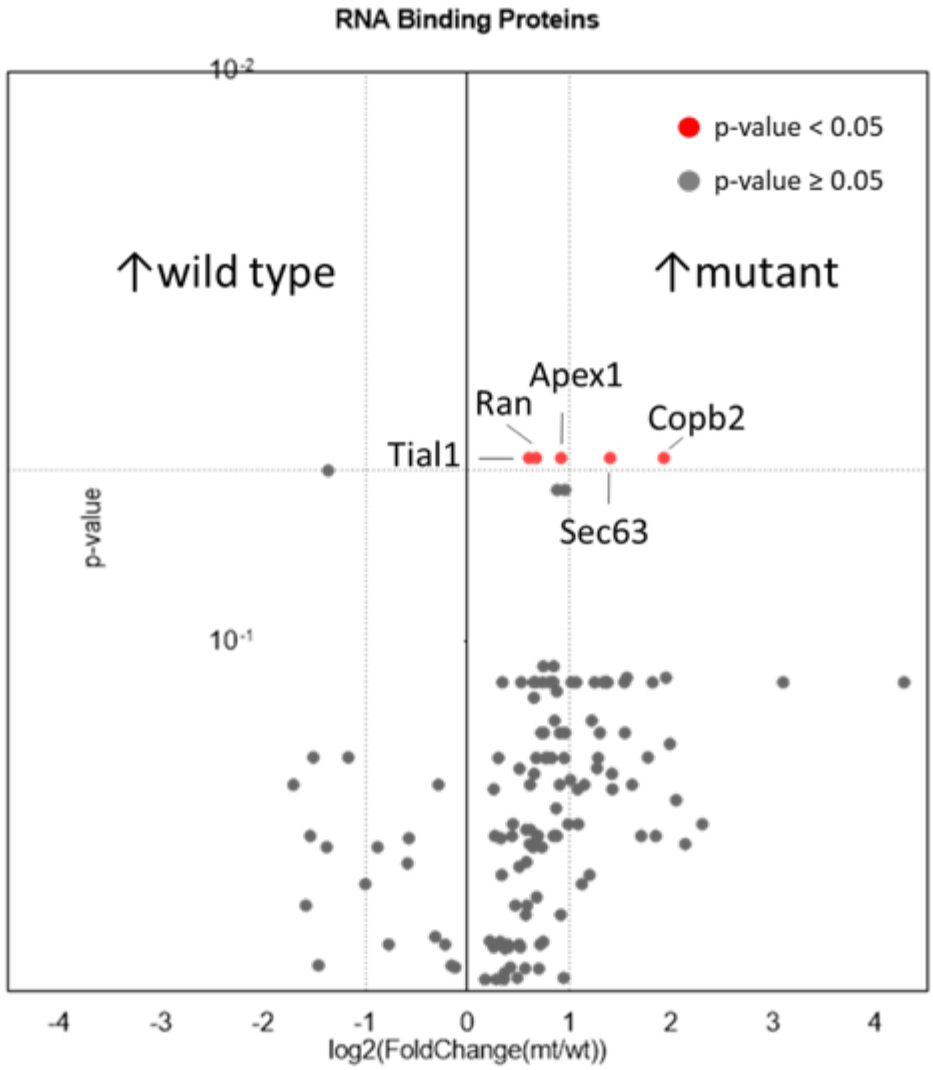

Figure 6.9. Volcano plot analysis for the RNA pulled down proteins that were differentially bound on the two transcripts. Statistical analysis of the Mass Spectrometry data revealed 5 proteins that bound the mutant transcript in significantly higher abundance. Red dots signify a p-value <0.05.

In addition, the proteins that bound exclusively to the mutant transcript were analysed and 12 proteins were identified to bind to RNA, 4 of which participate in the formation of complexes that are involved in the pre-mRNA splicing (Figure 6.10).

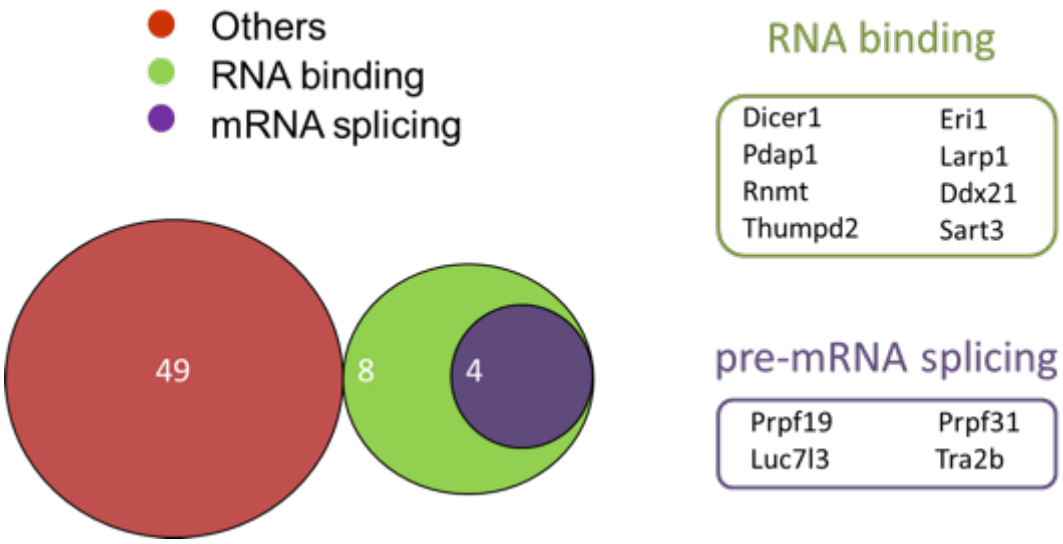

Figure 6.10. Clusters of proteins that bind exclusively on the mutant transcript. UNIPROT annotation was used to assess the function of the proteins that were identified to bind solely on the mutant transcript.

6.3.2.2 In silico analysis of the interactions of the pulled down RBPs

In silico analysis of the proteins that bound solely to the mutant IVT transcript of the pri-miR-497~195, with the use of STRING software, showed experimentally confirmed interactions between the identified proteins (Figure 6.11, Figure 6.12 and Figure 6.13).

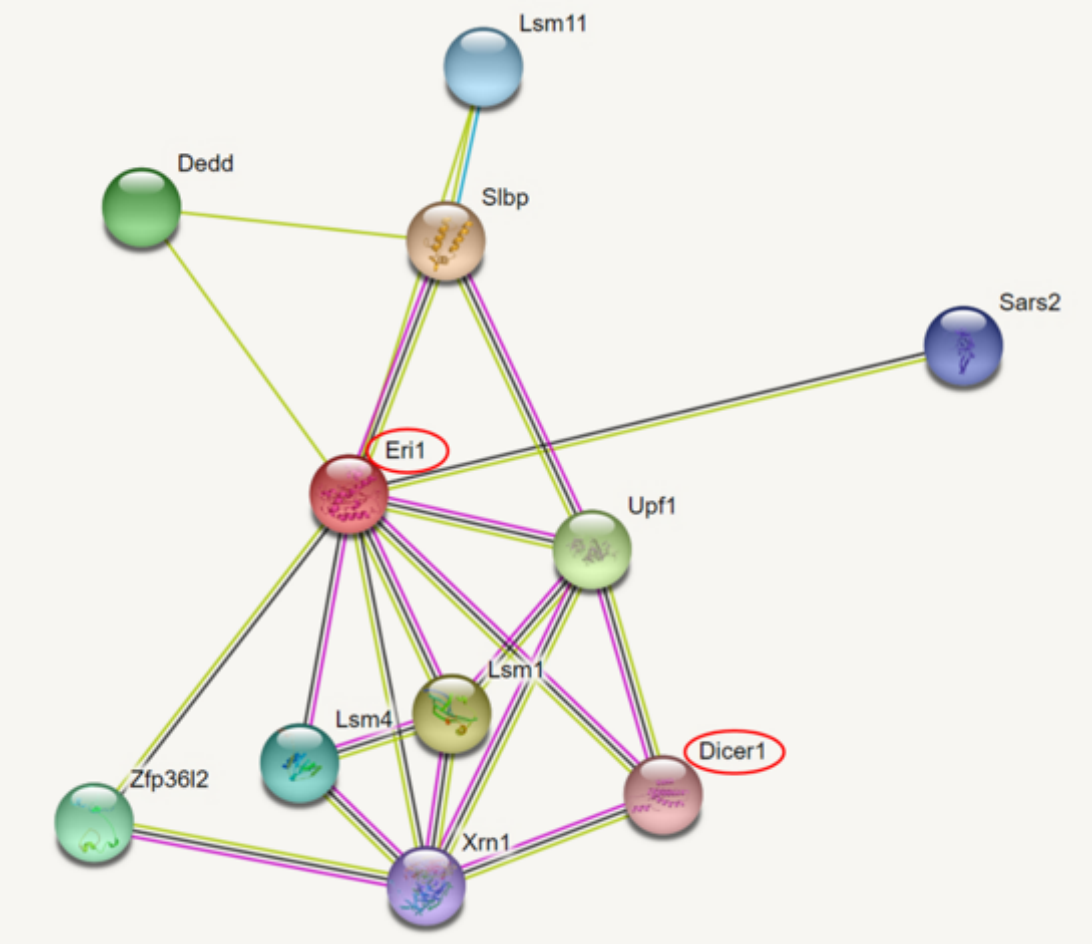

Figure 6.11. Analysis of the predicted protein-protein interactions for the protein Eri1. The protein-protein interactions as returned by the STRING software are depicted. Protein Eri1 and Dicer1 are highlighted as two of the proteins that were identified by Mass Spectrometry analysis of the pulled down eluate. Magenta lines indicate experimentally confirmed interactions, dark lines co-expression and light green text-mining association.

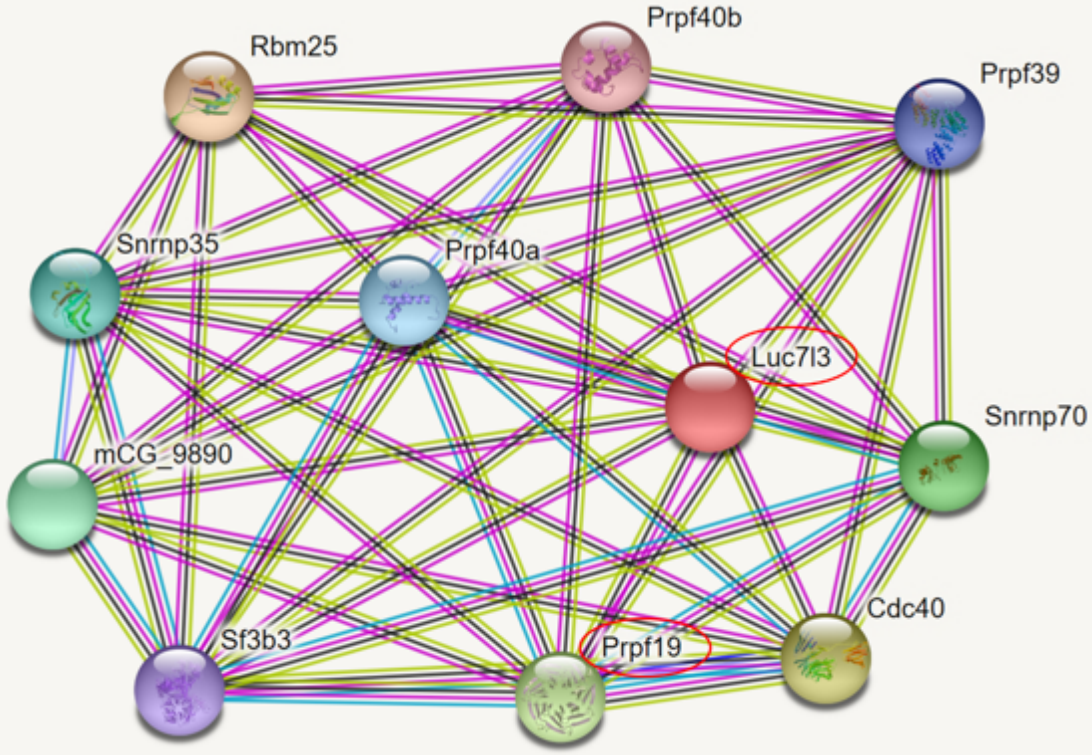

Figure 6.12. Analysis of the predicted protein-protein interactions for the protein Luc7l3. The protein-protein interactions, as returned by the STRING software, show that proteins the identified Luc7l3 and Prpf19 proteins (highlighted in red ovals) are experimentally determined to interact. Magenta lines indicate experimentally confirmed interactions, dark lines co-expression, light green text-mining association and light blue protein homology.

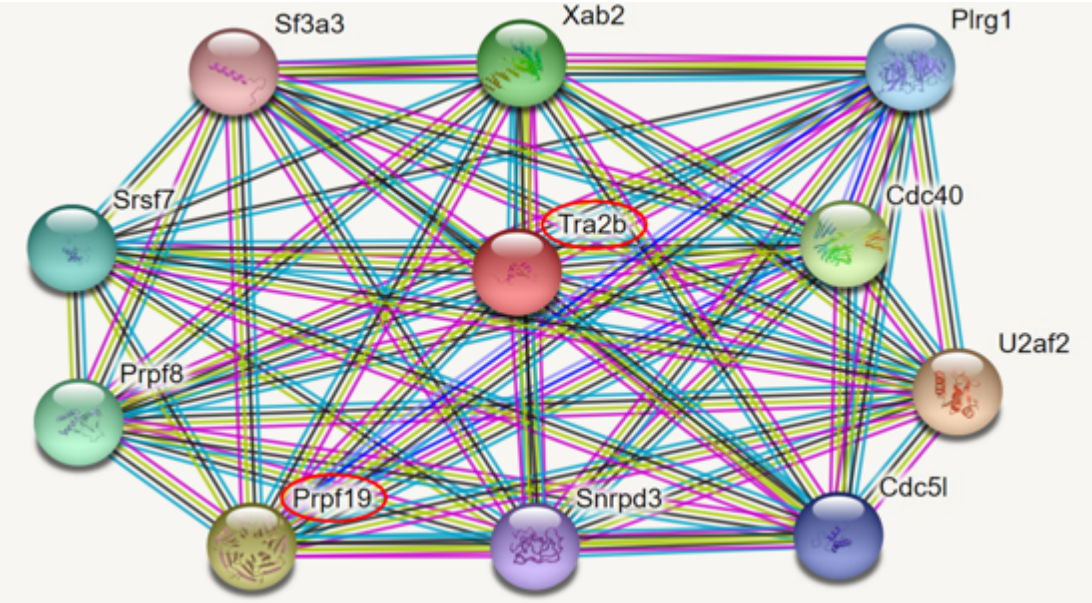

Figure 6.13. Analysis of the predicted protein-protein interactions for the protein Tra2b. The protein-protein interactions, as returned by the STRING software, show the proteins Tra2b and Prpf19 as identified by MS (highlighted in red ovals) are experimentally determined to interact. Magenta lines indicate experimentally confirmed interactions, dark lines co-expression, light green text-mining association, light blue protein homology and blue gene co-occurrence.

In silico analysis of the identified proteins in cluster revealed a less complex but more specific network for the proteins with most of them showing experimentally confirmed interactions. Of note, all of the proteins that participate in the processing of the pre-mRNA (Figure 6.14, red oval) showed interactions with each other and with a part of the generically RNA binding proteins, such as Larp1 and Ddx21 (Figure 6.14).

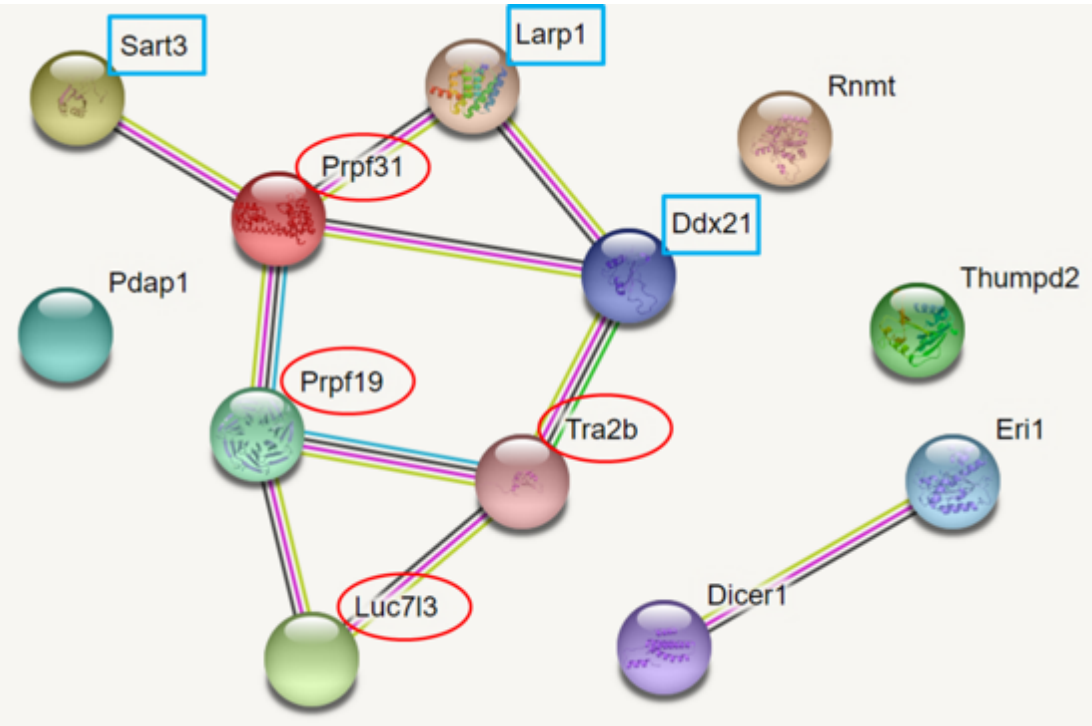

Figure 6.14. Analysis of the predicted protein-protein interactions for the cluster of proteins that bind only the mutant RNA transcript. Interactions of the cluster of proteins that bind only the mutant RNA transcript as returned by STRING. Highlighted in red oval shapes are the proteins that participate in the pre-mRNA splicing and in blue rectangular the ones that are RNA binding, as annotated by UNIPROT.

Further *in silico* analysis with STRING showed that the interactions among the identified proteins are mainly due to binding, with the new analysis revealing a subset of proteins that bind together and create a network of pre-mRNA splicing proteins (Figure 6.15).

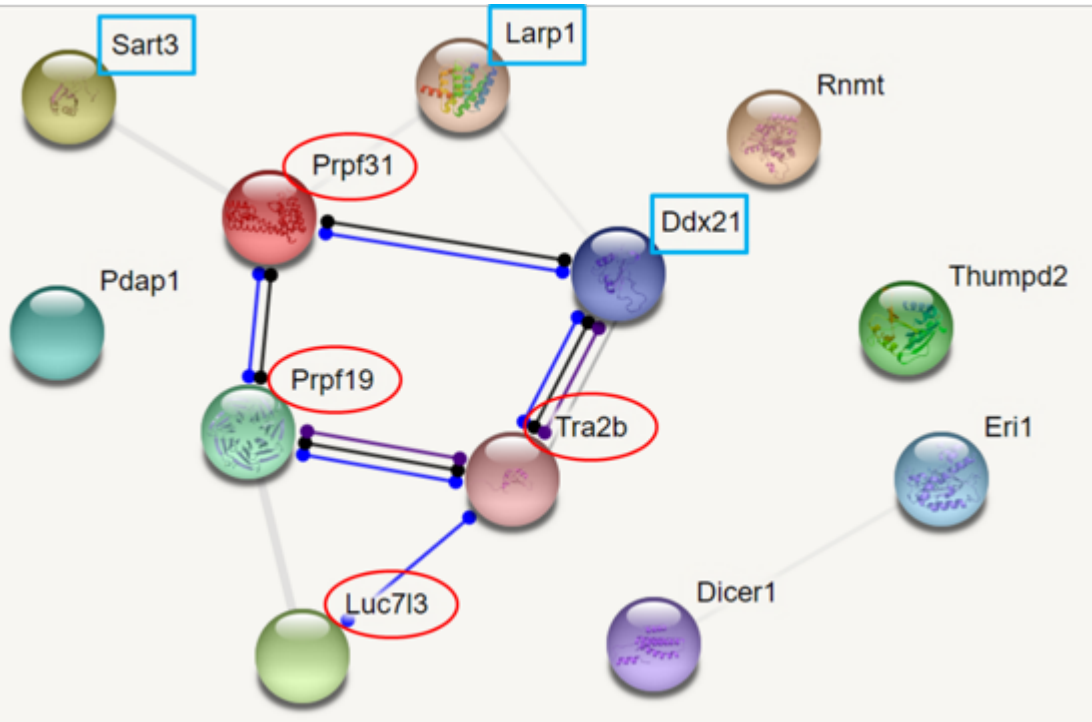

Figure 6.15. Analysis of the molecular action for the predicted protein-protein interactions for the cluster of proteins that bind only the mutant RNA transcript. Assessment of the molecular action of the proteins that were pulled down. Blue lines indicate binding, black reaction, purple catalysis and grey unspecified interaction. No line indicates no action. Highlighted in red oval shapes are the proteins that participate in the pre-mRNA splicing and in blue rectangular the ones that are RNA binding, as annotated by UNIPROT.

The confidence for the predicted protein-protein interactions, as returned by the STRING, showed binding of high confidence for the cluster of the pre-mRNA binding and processing RBPs (Figure 6.16).

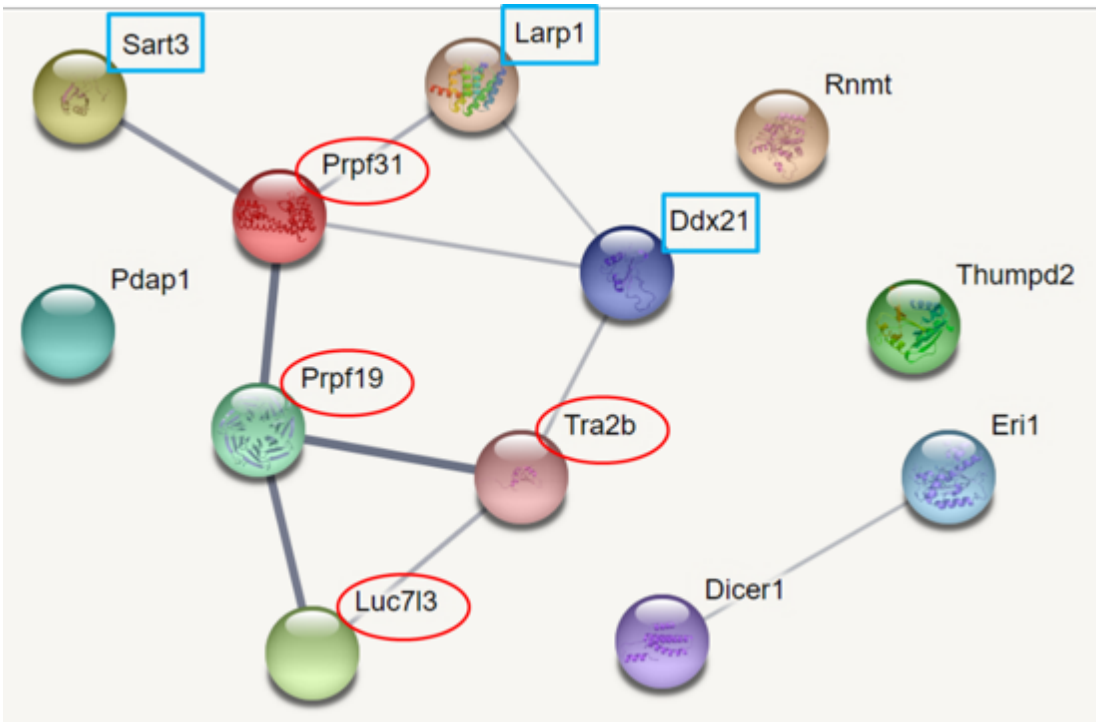

Figure 6.16. Analysis of the confidence for the predicted protein-protein interactions for the cluster of proteins that bind only the mutant RNA transcript. Assessment of the confidence for the functional association of the proteins. The weight of the grey lines is indicative of the confidence level varying from high *(0.9)* to low *(0.15)*, indicating the estimated likelihood that the depicted interaction is specific and meaningful. No grey line indicates no association. Highlighted in red oval shapes are the proteins that participate in the pre-mRNA splicing and in blue rectangular the ones that are RNA binding, as annotated by UNIPROT.

To confirm the protein interactions indicated by STRING and to study the possible pathways that these proteins participate in, Reactome software was used. Except for Eri1 and Dicer1, that interact with each other but do not show to participate in any pathway that is shared by the other proteins, the rest of them display an interaction network. Tra2b, Prpf19 and Luc7l3 interact with each other and the first two with Ddx21 and Prpf31, respectively, proteins that form a different cluster with Larp1 and Sart3. Proteins Tra2b, Prpf19 and Prpf31, interact with each other and partake in an mRNA splicing pathway with a statistical significance of p<0.01.

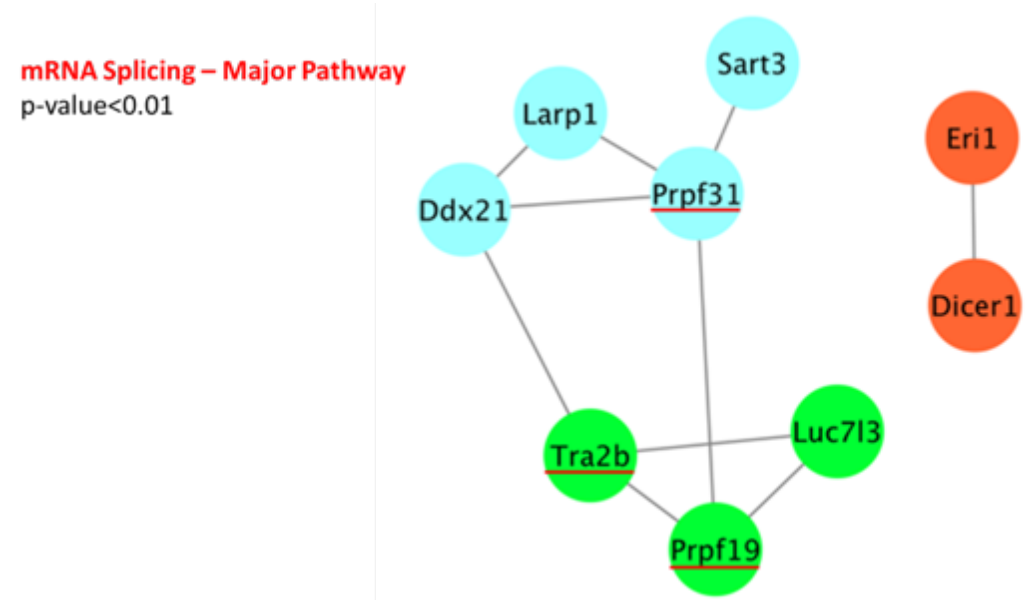

Figure 6.17. Cluster analysis of the identified proteins. Reactome was used to identify interactions between the pulled down proteins and the pathway they participate in. The different proteins, depicted in circles, are coloured according to the interacting groups they participate in. The black lines indicate interaction between proteins while the underlined proteins, according to the Reactome analysis, partake in mRNA splicing pathway with statistical significance of a p-value<0.01.

6.4 Discussion

It is well established that the biogenesis of miRNAs is a multistep process that presents high complexity and is regulated by a number of RBPs[21]. They participate in every step of the maturation of the miRNAs, from recognition and cleavage of the primary transcript, to the export of the pre-miRNA hairpins to the cytoplasm, the further processing to a miRNA duplex and the loading to RISC[263, 266-268]. After these initial steps, the RISC complex binds the corresponding mRNA targets, via imperfect Watson and Crick complementarity between the mature miRNA and the targeted mRNAs and controls their expression[1, 40, 221].

Although they play a central role in the maturation of the miRNAs, only a small fraction (<5%) of these are characterised, contrary to RBPs that participate in the general processing of the miRNAs, such as Drosha and Dicer, that are very well described[263, 269, 270]. Taking into consideration the plethora of the miRNAs, the complicated clusters they form, the interdependent regulation of their transcription and the complexity of the miRNA networks it becomes apparent that more RBPs than just Drosha and Dicer participate in a targeted way in the biogenesis of the miRNAs. Furthermore, studies report specific subsets of RBPs to interact with distinct miRNAs in specific cell types[40, 221, 263]. As an example of the specific role that RBPs play in miRNA biogenesis, TRIM71/LIN41 has been shown to regulate the expression of miR-29a alone, in two different cell lines while the downregulation of the protein affects the levels of the miR-29a targets in a functional approach that provides data regarding how RBPs can both affect directly the maturation of miRNAs and indirectly the silencing of the targeted mRNAs[221].

To gain deeper knowledge in regard to the processing of the miRNAs and how it gets affected by both sequence and tertiary changes in the pri-miRNAs, further identification of the RBPs that regulate the miRNA biogenesis is needed. To this end, in this chapter, the study focused on characterising the RBPs that interact with the WT pri-miR-195a and to elucidate the mechanism that result in the downregulation of both miRNAs of the cluster, mmu-miR-497a and mmu-miR-195a, upon editing of the latter.

6.4.1 Expression levels of RBPs

As a first approach, a panel of RBPs that have been previously described[221] to participate in the maturation process of miRNAs and share RNA binding domains that recognise sequence motifs located in the primary transcript of mmu-miR-195a was assessed upon miRNA overexpression with pLKO.1 (Figure 6.1). After editing the genomic locus of mmu-miR-195a, DNA sequences harbouring deletions of various lengths (1bp, 4bp and 126bp) were PCR amplified and cloned into pLKO.1 vectors. QPCR quantification did not show any significant changes in the expression levels of the RBPs when compared to the levels of the cells at baseline, infected with lentiviral particles with an empty vector. These results indicated that the differences of the levels of mature mmu-miR-497a and mmu-miR-195a upon editing were not due to the downregulation of the expression of certain RBPs but a result of the editing *per se* and the differential processing of the primary transcript.

6.4.2 Proteomic Analysis

MS is an unbiased screening technique for single protein analysis that offers a platform for the thorough examination of multiple proteins from tissue or cell lysates. An additional advantage that it presents is the unbiased detection of proteins since there is no need for antibodies designed to recognise specific epitopes to be employed.

In the present study, MS was employed to identify differential binding of RBPs to the mutant primary transcript of mmu-miR-195a~497 cluster that result in the downregulation of the mmu-miR-497a expression levels, two miRNAs that reside on the same cluster and are transcribed as one primary transcript. Results already presented above in Chapter 5, have shown that no editing occurs within the genomic locus of mmu-miR-497a.

To decipher the changes in the maturation process that led to the differential expression of the miRNAs, RNA Pull-down assays were conducted and the eluted proteins were analysed. As an initial step, the Western Blotting was tested using the conditions following the company's recommendations. In more detail, two RNA

molecules are provided with the kit, a positive control, that corresponds to the 3'-untranslated region androgen receptor RNA which is recognised and bound by HuR, and a negative control of a poly(A) sequence consisting of 25nt that are not recognised by the protein. In the initial experiment, the RNA transcripts biotin labelled together with the positive and negative RNA control and, following the pull-down, a HuR mouse monoclonal antibody was used to detect the protein (Figure 6.2). Results showed that, under the tested conditions, HuR is able to bind all the transcripts, even including the negative control although with significantly lower efficiency. Noteworthy, the mutant transcript in both of the two independent experiments presented, although bound by HuR, was bound with an efficiency almost as low as that of the negative control and notably lower than that of the WT. Interestingly, the 16nt deletion does not contain any AU element, which means that the difference in the binding efficiency that was observed was not due to the excision of any AU sequences but possibly due to a different tertiary structure that does not let the transcript to get accessed by the RBPs. These results contradict the previously presented MS results[221], that showed that Tial1, that binds AU-rich elements, is enriched in the eluate of proteins pulled down with IVT mutant RNA, indicating that the recognition of the AU sequence motifs is not enough for the interaction between the transcripts and the RBPs. In more detail, the differential binding of the WT and mutant transcript by HuR cannot be attributed to sequence differences since the number of AU motifs in the sequence of the two transcripts are the same. Therefore, the differential binding can only be explained either by differences in the tertiary structure of the mutant transcript or the inability of other necessary co-factors to bind the transcript.

Further titration experiments, concluded in that the amount of DNA, corresponding either to the WT or the mutant sequence, does not affect the efficiency of the *in vitro* transcription. As shown in Figure 6.3, regardless of the amount of DNA that was *in vitro* transcribed, blotting with HuR antibody did not demonstrate any differences in the amount of the RBP that was pulled down. Negative RNA control did not show any binding of the protein. Moreover, streptavidin magnetic beads that bound labelled positive RNA controls were incubated for a second time with sample buffer containing SDS, at 95°C, elution conditions that were more extreme than the recommended ones. Western blotting revealed a distinct, although diffuse band of HuR protein, results that showed that with elution under the recommended conditions, not the whole amount of proteins were eluted. The intensity of the band of the positive control, compared to the intensity of the band of the input, demonstrated that the pull-down,

although highly specific, did not enrich for the pulled down proteins. On top of that, the fact that we were able to detect pulling down of HuR with an artificial positive control transcript indicates that binding of RBPs to the bio-transcript does not mean RBP depletion of the sample. Further blotting with beta-actin revealed a distinct band only for the input, showing the specificity of the pull-down. Next, following labelling of the IVT RNA transcripts, different amounts of labelled transcripts were used for the pull-down with the results demonstrating that half of the amount of the recommended labelled RNA to be used had the same results while the use of smaller amount of labelled RNA improved the results. Absence of PEG in the labelling experiment showed detrimental results for the pull-down. PEG provides a hydrophobic environment to the RNA molecules improving the precipitation efficiency which in its absence decreases. Lastly, blotting with antibody against Dicer, showed that regardless of the amount of labelled RNA used, Dicer was pulled down only for the WT transcript (Figure 6.5). Although Dicer, according to the canonical pathway of the maturation of miRNAs binds to the pre-miRNA in the cytoplasm, the lack of cell compartmentalisation exposed the primary transcript to Dicer which resulted in its binding, contrary to the MS results that showed binding only of the mutant transcript by Dicer. Nonetheless, although these results revealed the binding of Dicer, they cannot provide any insight of the nature of interactions. More specifically, the binding could have been detected due to the physiological recognition of the pre-miRNA stem loop, as part of the primary transcript, by Dicer or due to the participation of the protein in a complex that bind the transcript.

The proteomics data outlined in the current chapter, offer a unique description of the RBPs that interact with both the WT and the mutant transcript. In total, 766 proteins were identified of which only 141 were quantifiable according to quality control of the data (Supplementary Table 7). Of them, about 45% are annotated in UNIPROT database as RNA binding proteins (Figure 6.6). The relatively small percentage of the identified RBPs, compared to the total number of proteins that were pulled down, can be indicative either of innate limitations of the pull-down assay or of specific protein-protein interactions between RBPs and other co-factors that led to non RBPs to be pulled down in complexes. More specifically, this assay was performed *in vitro*, and high activity of background binding was expected. Furthermore, it should be considered that the differences between conditions of the presented assay and the physiological conditions of the processing of the miRNAs are notably different. Firstly, during the maturation of the miRNAs, cell compartmentalisation plays a pivotal role

in the process, with primary transcript being exported from the nucleus to the cytoplasm after the initial cleavage by Drosha. In the case of the RNA Pull-down, the lack of compartmentalisation could have potentially led to different, non-physiological and not related interactions between RBPs and co-factors, thus hindering the ability of specific RBPs to freely recognise and bind the pri-miR-497~195, while resulting in more proteins being pulled down. Secondly, the concentration of the primary transcript, which is used for the pull-down, is significantly higher than under physiological condition. The transcription of the pri-miR-497~195 is tightly regulated, by various regulatory factors that expose the primary transcript to the maturation machinery in waves, thus its high, non-physiological concentration could affect its binding by RBPs and subsequently the proteins that are identified by MS, as it was previously described[221, 260].

Following these results, the identified RBPs were further analysed regarding their localisation as annotated by UNIPROT. Of the proteins identified, 50% are localised either in the nucleus or the cytosol while the vast majority of them (40%) are nuclear proteins, as expected (Figure 6.7). Under the physiological pathway of the maturation of miRNAs, the primary transcript is, in a first step, bound by the RBPs localised in the nucleus. With this in mind, it was expected that the primary transcript would be recognised by nuclear proteins even in the lack of cell compartmentalisation.

Further statistical analysis of the data showed that despite the various changes that were noted between the proteins pulled down with the WT and the mutant primary transcript, only 5 of them were statistically significant (Figure 6.9), with the rest of the proteins either showing small differences between the two groups or no statistical significance, results that lead to the conclusion that these proteins bound the two transcripts at the same level . Noteworthy, all of the statistically significant proteins were bound with higher affinity to the mutant transcript, contrary to the expected results. It was thought that the 16nt deletion in the sequence of the mutant transcript would, on the one hand, result in the abolition of sequence motifs able to be recognised by the RBPs and, on the other hand, a non-physiological tertiary structure that would restrain the RBPs from approaching and binding the transcript. Furthermore, although not statistical significance was identified, a trend was observed for the majority of the pull-down proteins to bind the primary transcript with higher affinity when compared to the WT transcript (Figure 6.9, lower right panel). Of the 5

statistically significant proteins identified, 3 showed a smaller than a 2-fold increase. Tial1 is an RBP that has not been previously described in detail, with an AU-rich binding element, Ran is a GTP-ase that is involved in the nucleo-cytoplasmic transportation of proteins and RNA molecules and Apex1 is an endoribonuclease that recognises ssRNA molecules and exerts control on their metabolism. Moreover, proteins Sec63 and Copb2 showed a 2.5 and 4-fold increase, respectively, in their affinity to the mutant transcript.

In fact, it has been proposed that Tial1 binds both to mRNA and ssDNA via its RRM domains (RRM1 and RRM2) located in its C terminus. It participates in the splicing regulation and translational repression of the mRNA, via the alteration of their half-life, and transcription regulation of the DNA[271-274]. Nevertheless, the precise mechanisms that Tial1 employs to bind to and thereby repress the translation of specific target mRNAs has not been specified. Tial-1 has been shown to assist the aggregation of complexes, such as eIF2 and eIF5, in discrete cytoplasmic foci called stress granules that inhibit the translation of the bound mRNAs[275]. It is thought that via this interaction both the mRNA stability and the translation is regulated during stress the composition of mRNA RNPs and their subsequent binding and processing with the translation or degradation machineries[276, 277]. In our experiments, Tial1 was detected to bind a non-coding transcript therefore it is thought to partake in the degradation of the transcript.

Ran is a predominantly nuclear GTPase protein, a member of the Ras superfamily[278]. It is associated with different proteins and depending on the binding of a Guanine (RanGTP or RanGDP) it is located either in the cytoplasm or the nucleus[279]. It regulates the nuclear trafficking and the translocation of mRNA[280].

Apex1 is a multifunctional protein that has been implicated in binding of ssDNA, DNA/RNA hybrids and ssRNA molecules and participates in the response to oxidative stress with its two functions being the DNA repair and regulation of transcriptional factors. Functions as an endodeoxyribonuclease in the DNA repair during oxidative stress. Apex1 is involved in the regulation of transcription by repressing it together with HNRNPL and partakes in the metabolism of ssRNA. It is associated with proteins non-sense mediated decay-1 (NMD1) and Y-box protein 1 (YBX1) that regulate the alternative splicing of pre-mRNA[281, 282].

Furthermore, Sec63 has been implicated in the transport of proteins through the endoplasmatic reticulum (ER) while Copb2 participates in the transportation of proteins from the ER to the Golgi network in association with GTP-binding proteins[283].

Taken together these results indicate that the mutant transcript follows a different processing pathway. Although further *in silico* analysis with STRING online software did not reveal any interaction between the identified proteins (data not shown), according to their annotation they can be organised in two groups. To be specific, Tial1 and Apex1 are RBPs that recognise specific motifs (AU-rich and UACA respectively) in ssRNA molecules and partake in their processing. Their function is indicative, although not conclusive, of how the editing of mmu-miR-497~195a locus, through a 16nt deletion in the mmu-miR-195a hairpin, can affect its processing. These proteins, being identified in higher abundance bound to the mutant transcript, could potentially be due to differential processing that leads to the clearance of the non-physiological transcript. Furthermore, a second cluster, comprised of Ran, Sec63 and Copb2, regulates the identification and transportation of proteins to Golgi network. Although, these results seem not to be relevant to the processing of RNAs and miRNAs, they should be analysed under the light of both the presence of the non-physiological pri-miRNA and the lack of compartmentalisation. The RBPs that bind the mutant transcript could form a complex that potentially attract a group of proteins that do not naturally bind the RBPs organised around the WT pri-miR-497~195 transcript. Thus, these results could be suggestive of a pathway that does not reflect any canonical processing and is not followed under physiological conditions in cells.

Interestingly, a set of proteins that bound only the mutant transcript was identified (Figure 6.10, Supplementary Table 7). Nonetheless, the possibility that the primary transcript forms a new structure, because of the different sequence, cannot be excluded. Of them, a small subset of 12 proteins were annotated to bind RNA molecules. More specifically, two subsets were identified according to UNIPROT annotation. A subset of 8 proteins that are generally RBPs, such as Dicer1 which binds primary transcripts and leads to specific cleavage, was identified and a subset of 4 proteins that is involved in the pre-mRNA splicing. The representative spectra of the identified proteins are shown in Supplementary Figure 1 and Supplementary Figure 2. Although these interactions could be due to new sequences being created,

analysis of the sequence of the mutant primary transcript did not show any known RNA binding motifs to be created.

Further analysis of the associations of these proteins with online software, revealed functional interactions between the proteins and between the two clusters. STRING software, a free online database of known and predicted functional and physical protein-protein interactions[284], was used for a preliminary analysis to highlight the functional relationship of the proteins. STRING uses experimental evidence, database information, text-mining from PubMed abstracts[285], co-expression data[284], neighbourhood, ortholog analysis and phylogenetic contribution genome-based prediction data[286] to reveal interactions indicative of biological pathways. When proteins were analysed individually, interactions showed a group of proteins that have been experimentally shown to interact. More specifically, in the case of Eri1 (Figure 6.11), the proteins it interacts with include Dicer1, a type III ribonuclease that plays a pivotal role in the maturation of miRNAs. Eri1 is an RNA exonuclease that has been shown to participate in the degradation of histone mRNA along with the 3' overhangs of siRNAs. Additionally, Dicer1's function of cleaving miRNAs, as double stranded RNAs that form short hairpin structures, is well described. Taken together, these data suggest that either the two proteins work together conferring similar functions or that Dicer's activity supplements Eri1 with cleaving the RNA molecules that the latter recognises. Furthermore, Luc7-like 3 protein, that is involved in the RNA splicing has been experimentally shown to interact with Prpf19 (Figure 6.12), a core component of complexes participating in pre-mRNA splicing, while Tra2b, a sequence specific RBP that participate in pre-mRNA splicing, interacts with Prpf19 according to experimentally proved data (Figure 6.13). These results are suggestive of a possible interaction between two groups of proteins (Eri1-Dicer1 and Luc7l3-Prpf19-Tra2b) that recognise the mutant transcript and cleave it.

Intriguingly, when the 12 RBPs that bind solely the mutant transcript, were input in the software together, a network of experimental validated protein-protein interactions was highlighted (Figure 6.14). The cluster analysis revealed that 7 of the input proteins form a network of interacting RBPs while the interaction between Eri1 and Dicer1 was confirmed. Additionally, a second clustering became apparent when they were grouped on the basis of their function. Proteins that participate in the pre-mRNA splicing (Figure 6.14 red oval) form a cluster of closer interacting members that show

an association through proteins Tra2b and Prpf31 with the second cluster of Larp1, Ddx21 and Prpf31 (Figure 6.14 red rectangular). Further analysis, with STRING software, demonstrated co-operative binding among the pre-mRNA splicing proteins indicating either an interdependent binding of the RBPs of the clusters to the mutant transcript or increased binding due to these interactions (Figure 6.15), with the confidence for these interactions being high for the core of the cluster among Tra2b, Prpf19 and Prpf31 (Figure 6.16).

Further analysis was performed with Cytoscape, an open-source software platform for the analysis and visualisation of interactions of proteins and protein networks[287]. Cytoscape analysis of the 12 proteins that bound solely to the mutant transcript returned the same results as STRING software with the formation of 2 distinct clusters that interact with each other through binding between Tra2b-Ddx21 and Prpf19-Prpf31 (Figure 6.17). Lastly, pathway analysis with Reactome, an online software for the detection of biological pathways[288], indicated that these 3 proteins participated in a pathway of mRNA splicing with statistical significance (Figure 6.17, Supplementary Table 8).

In light of these results, it becomes apparent that this set of proteins participate in a different than the canonical pathway of the processing of miRNAs. The newly identified interactions cannot be explained exclusively through the formation of new sequence motifs due to the 16nt deletion. Moreover, although according to UNIPROT annotation these pulled down proteins are RNA binding, the possibility of interactions with the mutant transcript due to association with other proteins that bind the mutant transcript because of a newly created tertiary structure, cannot be excluded. Furthermore, these possible binding interactions would explain the non-RBPs that were pulled down solely for the mutant transcript (Figure 6.10). In addition, results from two independent software showed that 3 proteins (Tra2b, Prpf19 and Prpf31) form a core of interactions with the transcript and pathway analysis implicated them with pre-mRNA splicing.

In more detail, Tra2b has been implicated in mammals with the activation of nonsense-mediated decay splicing upon recognition of a GAA repeats although not specific mechanism has been identified[289]. Furthermore, Prpf19 protein has been shown to be a core component of PRP19C/Prp19 assembly, as part of the U4/U5/U6 tri-snRNP spliceosomal complex, and partakes both in its assembly and activity of

the pre-mRNA splicing[290, 291]. Interestingly, complex PRP19C does not contain any known RNA binding proteins. This feature suggests that the complex interacts with the pre-mRNA through other RNA binding factors, a characteristic that comes in accordance with our results. Additionally, Prpf31 is another component of the spliceosome.

Moreover, it seems that the mutant primary transcript gets processed through a different pathway. Indicative results from the *in silico* analysis of the interactions of the MS analysed proteins suggest that the mutant primary transcript takes part in a pathway that leads to its degradation and clearance from the cells. These results also explain the decrease in the levels of the mature miRNAs, mmu-miR-497a and mmu-miR-195a, since clearance of the primary transcript would lead to a decrease of their levels. Nevertheless, although indicative, these results cannot be conclusive. The possibility of these interactions not reflecting the conditions in cells upon editing of the targeted locus cannot be ruled out. In more detail, as explained above, the conditions of the pull-down experiments do not represent physiological conditions, thus, although *in silico* and statistical analysis identified a set of proteins that potentially participate in a different processing pathway the possibility that these interactions came up as significant due to innate limitations of the assay cannot be excluded. In more detail, as already explained, firstly the presence of a mutant transcript, harbouring a 16nt deletion, does not occur in nature and secondly the conditions of the assay do not represent cellular conditions. This could mean that the showed interactions do not represent any specific pathway that is followed by the cells but artefact interactions that is the result of non-physiological binding of the identified proteins to the mutant transcript.

Although MS is a sensitive technique that is employed for both the identification of new proteins and of a set of known proteins it still presents limitations. It is a semi-quantitative technique that is capable of showing only the presence of proteins and not possible interactions between them. In addition, the need for the validation of the results with an independent technique led to the employment of Western Blotting to test for the proteins, as demonstrated by the analysis of MS data. To elucidate the pathway that lead to the downregulation of the mmu-miR-497a upon editing, the study focused, on the proteins that bind exclusively to the mutant transcript. The hypothesis to be tested was that the deletion changed the tertiary structure of the primary transcript in a way that it could not be processed by the maturation machinery either

due to its degradation, through a different pathway, or due to the binding of RBPs that hinder its recognition.

The experiments that were conducted to identify the optimal conditions of blotting did not lead to successful results while more antibodies were tested against proteins Larp1, IGF2BP2, hnRNPE1, DHX9, EIF2AK2, ILF3 Tra2b (Table 2) but did not allow quantification of the respective protein due to multiple nonspecific bands of multiple sizes being detected.

In conclusion, MS analysis of RNA pull-down with WT and mutant transcripts of pri-miR-497~195 revealed, for the first time, a set of proteins that bind the pri-miR-497~195 as well as RBPs that bind only the mutant transcript. Although the results did not lead to any firm conclusions with regards to the interaction between the proteins and the transcript they imply that alternative pathways may lead to the downregulation of the levels of mature mmu-miR-497a and mmu-miR-195a. Furthermore, as analysis of the 3D structure of the edited transcript revealed, the RNA Pull-down results could also indicate ineffective processing of the transcript. As the different elements of the primary transcript are not easily accessible upon editing, due to its non-canonical conformation, the binding of the identified pulled-down proteins could, potentially, signify differential processing that can explain the lower levels of mmu-miR-497. However, the lack of validation of the MS identified proteins with Western Blot indicate that further analysis and validation is needed in order to conclusively determine the RBPs that participate in the alternative processing of the mutant transcript.

Chapter 7 GENERAL DISCUSSION

7.1 Conclusions

The objective of the study was to specifically inhibit hsa-miR-195 in order to study its implication in aneurysm formation. To this end target the genomic locus of hsa-miR-195 stem loop was edited with the precision offered by CRISPR/Cas9. When designing the guides the short length of the gene was taken into consideration and the guides were chosen based on the position of the site they targeted Three different strategies of delivery were studied.

Plasmid delivery to HEK293T cells, was tested as an initial method because of the transient expression of Cas9 minimising the possibility of off-target editing. DNA sequencing of the edited cells showed that the editing occurred specifically in the targeted sites, as expected, resulting mainly in deletions. However, taking into consideration the high percentage of the transfection that was observed and the relatively modest percentage of the gene editing, the plasmid delivery did not appear as favourable for primary cells, cells that are difficult ot transfect.

In order to address the low efficiency observed with plasmid delivery, lentiviral delivery of the CRISPR/Cas9 was chosen and tested in primary human cells (HUVECs). Results from three independent experiments suggested that infection with lentiviral particles resulted in almost complete editing of the gene that can be attributed to both the high proliferation rate of the cells as well as the efficacy of the delivery.

In a third approach, the use of Cas9/RNPs appeared as an advantageous alternative to the previous strategies deployed because of its transient effects. The fact that, the editing efficiency was similar to the one observed after plasmid transfection with the same guide, lead to the conclusion that it was not possible to obtain a higher efficiency for Cas9/RNPs compared to plasmid delivery.

Next, after assessing the levels of miR-195 in human SMCs in prolonged cell culture conditions and because of their low levels we changed to mouse VSMCs. For the mouse VSMCs three guides were designed due to sequence differences. Lentiviral delivery of the system was tested based on the editing efficiency of the guides. Of interest is the fact that the pattern of the edited bands changed according to the guides used. The difference between the efficiency when targeting with different combination of guides and with each guide alone can possibly be explained by the relative position of the targeted sites influencing their accessibility by the Cas9/RNP complexes. Differences in the editing efficiency among the guides for mouse VSMCs and between the two species (human and mouse) SMCs can be explained by the fact that different guides were used.

Although lentiviral delivery was highly effective, the continuous expression of Cas9 together with the guides was deemed to be a non-favourable feature. Stably expressing Cas9 cells were generated by infecting mouse VSMCs with lentiviral particles harbouring only the gene for Cas9. Next, IVT sgRNAs were used to test their ability to form Cas9/RNP complexes showing a successful and almost complete digestion. By using this approach no off-target editing was expected to occur since the accumulation of the Cas9 was not expected to result in any off-target editing.

Next, to address the limitation of the off-target mutagenesis, 7 possible off-target sites as returned by both CRISPR Online Tool and CRISPR Finder were tested. By using the potential off-target sites that were returned by both software we eliminated the chances of false positive sites being false. T7EI assay demonstrated that none of the guides induced any off-target mutagenesis.

Next, to determine the effect of gene editing in a hetero-cluster the study focused on the mmu-miR-143~145 cluster, consisting of two miRNAs that do not share sequence similarities. Two sgRNAs targeting the mmu-miR-145a locus were designed with qPCR quantification showing that the gene editing had a robust effect on miRNA expression. Interestingly, despite the high levels of gene editing induced by the sgRNAm1 guide, the downregulation in mature mmu-miR-145a and mmu-miR-143 expression was significant but lower than when guide sgRNA145m2 was used. These results indicate that targeting the stem loop is a more efficient strategy for inhibiting miRNA expression.

In order to determine whether mature miR-145a expression exerts transcriptional control on the miR-143~145 cluster, mmu-miR-145a was overexpressed in VSMCs using miRNA mimics. High levels of mmu-miR-145a led to increased miR-143 expression as well as pri-miR-143 and miR-145a expression. Although not conclusive, these results are indicative of a disruption of a feed-forward loop due to miRNA editing as well as of the hindering of the processing of the primary transcript.

Next, the study focused on a highly studied miRNA clusters in the mouse genome, the miR-17~92. Gene editing using sg18 was efficient and although the expression of miR-18a diminished significantly there was no impact on miR-17, miR-19a and miR-20a levels, miRNAs of the same cluster. Intriguingly, RNAfold did not show any significant secondary structure alterations upon editing.

Next, the stem loop of miR-25 was targeted in the miR-106b~25 cluster with qPCR quantification showing a significant downregulation of miR-25 expression with the levels of miR-93 and miR-106b not being affected.

These results show how editing with CRISPR/Cas9 can be employed for the downregulation of different miRNAs of the same cluster. Nonetheless, editing of the DNA sequence of clustered miRNAs showed that the maturation process differs among miRNA clusters with varying effect on the levels of the other miRNAs of the cluster. Additionally, these results showed that expression interdependency is not common in all clustered miRNAs. Gene editing of mmu-miR-497~195 and mmu-miR-143~145 led to downregulation of both of the clustered miRNAs. However, targeting of miR-18a and mmu-miR-25 revealed that the expression of other clustered miRNAs are not affected by editing of the cluster sequence.

In conclusion, these data confirmed that the CRISPR/Cas9 editing technology is extremely precise, since indels occurred only in the vicinity of the DSB while no mutations were identified in the regions encoding the cluster. All in all, CRISPR/Cas9 emerged as a robust system for miRNA inhibition that is able of revealing novel regulatory mechanisms for clustered miRNA expression.

Next, CRISPR/Cas9 was assessed as a tool to understand the maturation of clustered miRNAs. This is the first time, to the best of my knowledge, that the maturation process of the mmu-miR-195a is investigated. Following the preliminary results from editing the DNA sequence of the genomic locus of mmu-miR-195a and the unexpected downregulation of mmu-miR-497a, the study sought to elucidate the mechanism of this downregulation. In order to decipher whether the downregulation was either the direct result of the editing or of the impaired processing of the pri-miRNA, guide sg195m2 was used in the new set of experiments. While no editing was detected in the genomic locus of mmu-miR-497a, overexpression of mmu-miR-195a lead to no differences on the expression of the mature miR-497a suggesting that the mmu-miR-497a expression is not controlled by miR-195a.

The tertiary structure of the primary miRNA transcripts can affect the accessibility of the stem loops by Drosha and Dicer affecting miRNA biogenesis. Therefore, computational analysis assessed if the structure of pri-miRNAs could influence the processing of the mutant pri-miRNAs. Software prediction programmes were used and all of them returned identical results with a 18nt deletion resulting in a wider apical loop and the abolition of a bulge in the stem of the hairpin. Although these results cannot safely lead to definitive conclusions about the mechanism, the possibility of impairing the maturation in a dual manner directly through sequence and structural alterations and disruptions cannot be excluded.

Building on these results together with the alterations in the predicted tertiary structure of the edited primary transcript we postulated that these changes, as a result of the editing of the genomic locus with CRISPR/Cas9, led to differential processing. The biogenesis of miRNAs is a multistep and complex process regulated by a number of RBPs that participate in every step of the maturation. Nonetheless, only a small fraction are characterised. Given the plethora of miRNAs and the complicated clusters they form it becomes apparent that various RBPs partake in the miRNA biogenesis.

It has been previously shown that certain RBPs interact with specific miRNAs to regulate their maturation, with the two most prominent examples being Drosha and Dicer. Although previously published studies had reported a panel of RBPs that participate in the maturation of the miRNAs, pri-miR-497~195 had not been studied

in detail. To elucidate these differences, RNA pull-down experiments were conducted comparing the RBPs that recognise and bind the WT and a mutant primary transcript harbouring a 16nt deletion. The latter transcript, produced with CRISPR/Cas9 editing, was missing both the sequence of the 5p arm of the mmu-miR-195a as well as that of a bulge upstream of the DSB. Secondary structure prediction confirmed the effects of the editing on the structure of the miRNA while the tertiary structure was highly different compared to the WT one. These changes were deemed detrimental for the maturation of the primary transcript by affecting the approach by RBPs.

To gain deeper knowledge in the regulation of RBPs on the miRNA maturation this study focused on characterising the RBPs that interact with the WT pri-miR-195a. To this end, MS was employed to identify differential binding of RBPs to the mutant primary transcript of mmu-miR-195a~497.

The MS data presented, offer a unique description of the RBPs that interact with both the WT and the mutant transcript. In total, 45% of the identified proteins are annotated in UNIPROT database as RNA binding proteins with the small number of the RBPs being suggestive either of innate limitations of the assay or of specific protein-protein interactions between RBPs and other co-factors. Furthermore, 50% of the proteins identified are localised either in the nucleus or the cytosol with the vast majority of them being nuclear proteins, as expected. Further analysis showed that only 5 of the identified proteins were statistically significant.

Taken together these results indicate that the mutant transcript follows a different processing pathway. Although further *in silico* analysis did not show any interaction between the identified proteins, they can be organised in two groups. Tial1 and Apex1 are RBPs that recognise specific motifs in ssRNA molecules and help in their processing while Ran, Sec63 and Copb2, regulate the identification and transportation of proteins to Golgi network.

In addition, 12 RBPs that bind solely the mutant transcript were identified and when analysed with STRING, a network of experimental validated protein-protein interactions was highlighted. The analysis revealed that 7 of the input proteins form a network of interacting RBPs while a second clustering became apparent when they

were grouped on the basis of their function. Proteins that partake in pre-mRNA splicing form a group of closer interacting members results that were confirmed when the identified proteins were analysed with Cytoscape.

In light of these results, it becomes apparent that said proteins participate in a different than the canonical pathway of the processing of miRNAs. Moreover, results from the in silico analysis of the interactions of the MS analysed proteins suggest that the mutant primary transcript takes part in a pathway that leads to its degradation and clearance from the cells results that explain the decrease in the levels of both mmu-miR-497a and mmu-miR-195a.

In conclusion, MS analysis of RNA pull-down with WT and mutant transcripts of pri-miR-497~195 revealed a set of proteins that bind the pri-miR-497~195 together with RBPs that bind only the mutant transcript. Although the results are only indicative they suggest that alternative processing pathways may lead to the downregulation of the levels of mature mmu-miR-497a and mmu-miR-195a.

These results provide a helpful insight in the maturation process of the miRNAs in general and in that of pri-miR-497~195 specifically. They demonstrate that sequence changes lead to differential processing because the tertiary changes that they impose. This conclusion was drawn by the fact that firstly the RBPs that recognise the transcript seem to recognise specific structures and not sequence motifs and secondly no known motifs were created from the deletion. Moreover, pathway analysis of the proteins demonstrated that these proteins partake in the splicing step of miRNAs. This could mean that the structure of the mutant transcript hinders the recognition of the transcript from the miRNA processing machinery, resulting in the transcript not being recognising as a pre-miRNA leading to a new pathway getting triggered through which the mutant transcript gets degraded. However, these interactions that were described can be due to the non-physiological conditions of the assay, such as the lack of cell compartmentalisation, high concentration of primary transcript and the *in vitro* conditions of the interactions that do not correspond to the physiological ones.

7.2 Limitations

The current study investigates the use of CRISPR/Cas9 as a gene editing technique for the specific inhibition of miRNAs. It is the first time it has been shown that CRISPR/Cas9 can be used in primary mammalian cells for the inhibition of miRNAs. Although a reliable and robust workflow is provided, with regards to inducing gene editing in mouse VSMCs to dissect the regulation and function of clustered miRNAs, there are limitations that have to be taken into consideration.

An important limitation is the usage of mouse VSMCs and human SMCs cell line instead of human primary SMCs. The study focused on editing miRNA gene in human SMCs and, to that end, human SMCs cell lines were used for the initial experiments, since they were a limitless source of cells. Nonetheless, and despite the fact that the scope of the study was to examine the effects of editing miR-195 with CRISPR/Cas9 in human primary VSMCs, the low expression of the miRNAs of the miR-15 family, after prolonged culture, conditions that were needed in our study, was an important issue. Prolonged culture of VSMCs was needed in order for the cells to reach senescence and a phenotype as close to AAA. Due to this, the focus of the study shifted from human to mouse VSMCs that expressed the studied miRNAs at satisfactory levels. Additionally, due to the differences of the miRNA gene sequences between the two organisms new guides had to be designed and tested, guides that, due to sequence limitations, cannot be useful for human studies.

Moreover, the delivery of Cas9 to mouse VSMCs was an important step for the study, since they express all of the miRNAs that were evaluated. Although the approach that was finally undertaken resulted in engineering the genome of the cells and in the accumulation of Cas9 protein, that did not affect the phenotype or the proliferation rate (data not shown). Moreover, Cas9 was not expected to lead to any editing unless in complex with a sgRNA. In more detail, the binding between the endonuclease and the guide RNA is dependent on an interaction between the tracrRNA and the protein through a specific sequence. During the maturation process of the crRNA:tracrRNA, Cas9 recognises a sequence in the tracrRNA which binds and then uses the latter's complementarity to crRNA to cleave it. The crRNA:tracrRNA duplex stays tethered to Cas9 with the help of tracRNA[292]. Since Cas9 is an exogenous protein of bacterial

origin it was expected that it would not get activated unless bound to a sgRNA introduced to the cells after transfection. Furthermore, the transient presence of the IVT sgRNA in the cells was thought to protect against potential off-target effects due to the high concentration of the Cas9. Indeed, no off-target effects were detected in any of the possible off-target sites, that were *in silico* predicted, for any of the guides tested.

Delivery of the system is one of the major limitations, especially when it comes to *in vivo* models. In order to address these difficulties various groups have developed new, more elegant techniques over the last years that help the uptake of the RNPs by the cells[114, 212]. Regardless, the technique employed in the present study was deemed suitable for the purpose it was used as sufficient editing occurred with no off-target effects in the 7 most likely targets, according to *in silico* analysis, and no other complications. Although the computationally predicted off-target sites that were tested, were confirmed by two software, the chances that the guides used could lead to non-identified editing in other sites still remains. Additionally, the list of the tested potential off-targets are by no means exhaustive. Hence, whole genome sequencing of edited compared to non-edited cells would possibly provide more convincing results.

Nevertheless, following the generation of mouse VSMCs stably expressing Cas9, the effects of editing the genomic loci of 4 different clusters were assessed. The clusters were chosen based on their implication in cardiovascular disease and their organisation in homo-clusters or hetero-clusters.

Editing of one of the miRNAs of the cluster led to unexpected downregulation of the second clustered miRNA in the case of the mmu-miR-497~195 and mmu-miR-143~145 clusters, while editing of one miRNA stem loop did not show any differences in the regulation of clustered miRNAs in the case of mmu-miR-17~92 and mmu-miR-106b~25. No off-target editing was detected in either case. Additionally, computational modelling suggests important changes in the structure of the primary transcript that was hypothesised to hinder its processing by the maturation machinery. The study concludes that the expression of the clustered miRNAs is not necessarily co-dependent as well as that clusters show strict tertiary structural requirements for their expression.

Although the study underscores the power of CRISPR/Cas9 in the knocking down of miRNAs over conventional methods that can target multiple related paralogs, the approach remains rather imprecise both in the investigation of the editing and its outcome. In regards to the former, the T7EI assay was used for the calculation of the editing efficiency as a technique has innate limitations. Firstly, it can underestimate the final efficiency due to fact that it cannot recognise homodimers of edited strands resulting in those strands not being cut and quantified. Secondly, the technique is based on gel separation of the bands and their intensity after the electrophoresis depends on both their size and the electrophoresis settings. In detail, the smaller sized bands during the electrophoresis get diffused easier and furthermore appear less intense due to less staining dye being bound by smaller DNA strands while high voltage of electrophoresis leads to the gel developing high temperatures and higher diffuse rate. Although the way that the technique was designed accounted for these limitations i.e. the PCR primers were designed so that the predicted cut site was upstream of the middle of the amplicon but as close as possible to it, in order for the two resulting bands to differ as little as possible from each other in size, and the used calculating formula adjusted for these discrepancies, the limitations still remain and need to be taken into consideration. However, at the time of the assessment of the editing efficiency of these experiments, the T7EI assay was the gold standard assay. In order to overcome the aforementioned limitations new techniques have been developed e.g. TIDE/ICE analysis[295] or analysis of Amplicon sequencing data with bioinformatic tools[296]. By employing the NHEJ pathway the formation of mutations, that result in the disruption of the miRNA sequence, is random, not only regarding the type (insertions or deletions) but also regarding the length and the exact position. Although an adequate number of colonies were picked and screened to reveal sequence changes upon induction of editing, these were but a small portion of the occurred alterations. A wider range of mutations was expected to have been induced. In the same line, the structure prediction models presented above are only indicative of a very small number of changes. However, these conclusions were based on a single 3D computational prediction, that of pri-miR-497~195, due to limitations of the software. The length of the cluster miR-143~145 is about 1400bp therefore it cannot be analysed using the currently available algorithms. In addition, changes in the secondary structure due to sequence motifs alterations could affect the expression of the clustered miRNAs.

To address these limitations the study focused on mmu-miR-195a, the miRNA of interest, and sought to decipher how the editing affects the processing of pri-miR-497~195. Proteins that bound to the WT and the mutant transcript were evaluated and analysed with MS. Analysis of the results showed a panel of proteins that bind preferentially to the mutant transcript. Further analysis revealed that the identified proteins bind RNA molecules based on their tertiary structure since, according to published data on their function, they do not recognise specific secondary structures or sequence motifs that were altered upon editing. These results indicate that the differential processing of the mutant transcript was due to changes in the tertiary and not the secondary structure or the abolition of any sequence motif.

Nonetheless, it is likely that the proteins identified do not represent interactions that occur in the edited cells. This could be for a number of reasons. Firstly, it is an *in vitro* assay which means that its conditions under which the proteins, approach, interrogate and bind the primary transcript are different. Additionally, the transcripts that were used in the assay were *in vitro* transcribed which means that the transcripts were isolated from possible post-transcriptional processing that could affect its binding by the RBPs and, subsequently, its maturation[221]. In more detail, it has been shown that RNA-folding, especially for larger miRNA clusters, affects the accessibility of the processing machinery is important[293, 294] therefore, isolating the primary transcripts from the cellular environment can result in differential folding and processing. The concentration of the transcripts was a lot higher than the one that occurs *in vivo* and the protein population of the cells get exposed to the transcript simultaneously which, together with the lack of cell compartmentalisation, means that the interactions between the proteins and the RNA transcripts are not necessarily canonical.

Moreover, although MS is a highly sensitive technique that can identify a vast number of proteins, even in low concentration, it is semi-quantitative. It can only provide data with regards to the detection of proteins and their relative, but not absolute, abundance. Given the above, WB was employed to confirm the MS results and further elucidate the abundance of proteins. Nonetheless, the validation of the MS data failed therefore additional validation is required to experimentally test the concept that emerged from the *in silico* analysis.

All in all, besides the limitations this study presents, it provides strong evidence of the suitability of the CRISPR/Cas9 editing to inhibit miRNAs, via permanent alterations of their genes, adds new concepts to the miRNA study and offers well-founded results regarding the processing of primary miRNA transcripts in primary mammalian cells.

7.3 Future Outlook

The current study offers an insightful groundwork on how editing with CRISPR/Cas9 can be employed for the inhibition of miRNAs. The problem of delivering the system in high efficiency was resolved and no more titration is needed in that front. Additionally, off-target editing seemed not to be an issue in the 7 most likely off-target sites. However, in light of new studies that have shown that CRISPR/Cas9 can result in non-predicted, unintended editing in various, random sites[193, 194], further scrutiny is needed. In more detail, whole genome sequencing has emerged as the method of choice for investigating possible off-target editing. Further investigation using whole genome sequencing would clarify the unintended editing and resolve the issue.

The main aim of the study was to overcome the limitations of the traditional methods for inhibiting specific miRNAs. The results outlined above demonstrated that, although editing with CRISPR/Cas9 can lead to inhibiting miRNAs, the effects of editing differ according to the cluster that is targeted with certain clusters showing abolition of the expression of all the miRNAs that are co-transcribed. Clustered miRNAs have attracted intense interest in the biomedical research and the findings presented here on clustered miRNA regulation offer valuable insights. Secondary and tertiary structure prediction models have shown that the deletion of sequences of the hairpin of miRNAs result in different structures of the stem loop. However, given the small number of the edited sequences that were studied, the presented results can only be suggestive of the effects of the editing in the maturation of the miRNAs. Therefore, additional sequences harbouring deletions need to be analysed *in silico* with regards to how sequence alterations change the secondary and tertiary structures of the hairpin and the primary transcript.

Proteins interact with RNA transcripts through recognition of specific binding motifs with these interactions being significantly influenced by the tertiary structure on the

RNA molecules. RNA pull-down assays are useful in studying these interactions by providing the possibility of extracting RBP–RNA complex for MS or western blotting by exploiting high affinity tags like biotin. Moreover, validation of the MS results with Western Blotting, as an independent method, was not possible since the antibodies used did not produce any conclusive results. Therefore, more titration experiments will resolve the issues raised and will provide a better understanding of the interactions of the identified proteins. In addition, given that this the first time that the maturation of the pri-miR-497~195 is being investigated, these results will provide a list of validated proteins that are important for the process. Quantification of the miRNA levels and MS analysis in experiments where these proteins will be knocked-down, will offer a valuable insight in their effects on the process.

Additionally, RNA pull-down assays and MS analysis of the eluted proteins demonstrated differential binding of certain RBPs. However, only one mutant sequence was analysed. New RNA pull-down assays with more mutant transcripts, harbouring deletions of various lengths and positions, excising various structural features of the hairpins need to be conducted to elucidate the contribution of each structural element in the recognition by RBPs. Thus, supplemental experiments are needed to decipher the mechanisms that affect the expression of the miRNAs especially since studies have shown that the secondary structure of the pri-miR-17~92 influences the processing of the transcript by following a highly specific sequence of cleavage of the clustered stem loops.

In general, the experimental approach outlined in the study can be proved to be useful for the clarification of the maturation of mmu-miR-195a, as well as other miRNAs, and the identification of the involved RBPs.

BIBLIOGRAPHY

1. Bartel DP. MicroRNAs: target recognition and regulatory functions. *Cell*. 2009;136:215-33.
2. Kozomara A and Griffiths-Jones S. miRBase: annotating high confidence microRNAs using deep sequencing data. *Nucleic acids research*. 2014;42:D68-73.
3. Lee CT, Risom T and Strauss WM. Evolutionary conservation of microRNA regulatory circuits: an examination of microRNA gene complexity and conserved microRNA-target interactions through metazoan phylogeny. *DNA and cell biology*. 2007;26:209-18.
4. Lee Y, Kim M, Han J, Yeom KH, Lee S, Baek SH and Kim VN. MicroRNA genes are transcribed by RNA polymerase II. *The EMBO journal*. 2004;23:4051-60.
5. Nguyen TA, Jo MH, Choi YG, Park J, Kwon SC, Hohng S, Kim VN and Woo JS. Functional Anatomy of the Human Microprocessor. *Cell*. 2015;161:1374-87.
6. Lee Y, Ahn C, Han J, Choi H, Kim J, Yim J, Lee J, Provost P, Radmark O, Kim S and Kim VN. The nuclear RNase III Drosha initiates microRNA processing. *Nature*. 2003;425:415-9.
7. Auyeung VC, Ulitsky I, McGeary SE and Bartel DP. Beyond secondary structure: primary-sequence determinants license pri-miRNA hairpins for processing. *Cell*. 2013;152:844-58.
8. Fang W and Bartel DP. The Menu of Features that Define Primary MicroRNAs and Enable De Novo Design of MicroRNA Genes. *Molecular cell*. 2015;60:131-45.
9. Zeng Y and Cullen BR. Efficient processing of primary microRNA hairpins by Drosha requires flanking nonstructured RNA sequences. *J Biol Chem*. 2005;280:27595-603.
10. Han J, Lee Y, Yeom KH, Nam JW, Heo I, Rhee JK, Sohn SY, Cho Y, Zhang BT and Kim VN. Molecular basis for the recognition of primary microRNAs by the Drosha-DGCR8 complex. *Cell*. 2006;125:887-901.
11. Roden C, Gaillard J, Kanoria S, Rennie W, Barish S, Cheng J, Pan W, Liu J, Cotsapas C, Ding Y and Lu J. Novel determinants of mammalian primary microRNA processing revealed by systematic evaluation of hairpin-containing transcripts and human genetic variation. *Genome research*. 2017;27:374-384.
12. Yi R, Qin Y, Macara IG and Cullen BR. Exportin-5 mediates the nuclear export of pre-microRNAs and short hairpin RNAs. *Genes Dev*. 2003;17:3011-6.
13. Chendrimada TP, Gregory RI, Kumaraswamy E, Norman J, Cooch N, Nishikura K and Shiekhattar R. TRBP recruits the Dicer complex to Ago2 for microRNA processing and gene silencing. *Nature*. 2005;436:740-4.
14. Zhang H, Kolb FA, Jaskiewicz L, Westhof E and Filipowicz W. Single processing center models for human Dicer and bacterial RNase III. *Cell*. 2004;118:57-68.
15. MacRae IJ, Zhou K and Doudna JA. Structural determinants of RNA recognition and cleavage by Dicer. *Nature structural & molecular biology*. 2007;14:934-40.
16. Vermeulen A, Behlen L, Reynolds A, Wolfson A, Marshall WS, Karpilow J and Khvorova A. The contributions of dsRNA structure to Dicer specificity and efficiency. *RNA (New York, NY)*. 2005;11:674-82.
17. Zhang H, Kolb FA, Brondani V, Billy E and Filipowicz W. Human Dicer preferentially cleaves dsRNAs at their termini without a requirement for ATP. *The EMBO journal*. 2002;21:5875-85.
18. Park JE, Heo I, Tian Y, Simanshu DK, Chang H, Jee D, Patel DJ and Kim VN. Dicer recognizes the 5' end of RNA for efficient and accurate processing. *Nature*. 2011;475:201-5.
19. Tian Y, Simanshu DK, Ma JB, Park JE, Heo I, Kim VN and Patel DJ. A phosphate-binding pocket within the platform-PAZ-connector helix cassette of human Dicer. *Molecular cell*. 2014;53:606-16.

20. Winter J, Jung S, Keller S, Gregory RI and Diederichs S. Many roads to maturity: microRNA biogenesis pathways and their regulation. *Nature cell biology*. 2009;11:228-34.
21. Ha M and Kim VN. Regulation of microRNA biogenesis. *Nature reviews Molecular cell biology*. 2014;15:509-24.
22. Schwarz DS, Hutvagner G, Du T, Xu Z, Aronin N and Zamore PD. Asymmetry in the assembly of the RNAi enzyme complex. *Cell*. 2003;115:199-208.
23. Kloosterman WP and Plasterk RH. The diverse functions of microRNAs in animal development and disease. *Developmental cell*. 2006;11:441-50.
24. Rana TM. Illuminating the silence: understanding the structure and function of small RNAs. *Nature reviews Molecular cell biology*. 2007;8:23-36.
25. Bang C, Batkai S, Dangwal S, Gupta SK, Foinquinos A, Holzmann A, Just A, Remke J, Zimmer K, Zeug A, Ponimaskin E, Schmiedl A, Yin X, Mayr M, Halder R, Fischer A, Engelhardt S, Wei Y, Schober A, Fiedler J and Thum T. Cardiac fibroblast-derived microRNA passenger strand-enriched exosomes mediate cardiomyocyte hypertrophy. *The Journal of clinical investigation*. 2014;124:2136-46.
26. Liu N and Olson EN. MicroRNA regulatory networks in cardiovascular development. *Developmental cell*. 2010;18:510-25.
27. Barwari T, Joshi A and Mayr M. MicroRNAs in Cardiovascular Disease. *Journal of the American College of Cardiology*. 2016;68:2577-2584.
28. Dreyfuss G, Kim VN and Kataoka N. Messenger-RNA-binding proteins and the messages they carry. *Nature reviews Molecular cell biology*. 2002;3:195-205.
29. Clery A, Blatter M and Allain FH. RNA recognition motifs: boring? Not quite. *Current opinion in structural biology*. 2008;18:290-8.
30. Valverde R, Edwards L and Regan L. Structure and function of KH domains. *The FEBS journal*. 2008;275:2712-26.
31. Linder P and Jankowsky E. From unwinding to clamping - the DEAD box RNA helicase family. *Nature reviews Molecular cell biology*. 2011;12:505-16.
32. Gerstberger S, Hafner M and Tuschl T. A census of human RNA-binding proteins. *Nature reviews Genetics*. 2014;15:829-45.
33. Ascano M, Hafner M, Cekan P, Gerstberger S and Tuschl T. Identification of RNA-protein interaction networks using PAR-CLIP. *Wiley interdisciplinary reviews RNA*. 2012;3:159-77.
34. Lunde BM, Moore C and Varani G. RNA-binding proteins: modular design for efficient function. *Nature reviews Molecular cell biology*. 2007;8:479-90.
35. Hamosh A, Scott AF, Amberger JS, Bocchini CA and McKusick VA. Online Mendelian Inheritance in Man (OMIM), a knowledgebase of human genes and genetic disorders. *Nucleic acids research*. 2005;33:D514-7.
36. Dreyfuss G, Choi YD and Adam SA. Characterization of heterogeneous nuclear RNA-protein complexes in vivo with monoclonal antibodies. *Molecular and cellular biology*. 1984;4:1104-14.
37. Pinol-Roma S, Choi YD, Matunis MJ and Dreyfuss G. Immunopurification of heterogeneous nuclear ribonucleoprotein particles reveals an assortment of RNA-binding proteins. *Genes & development*. 1988;2:215-27.
38. Wang Z, Gerstein M and Snyder M. RNA-Seq: a revolutionary tool for transcriptomics. *Nature reviews Genetics*. 2009;10:57-63.
39. Stoltenburg R, Reinemann C and Strehlitz B. SELEX--a (r)evolutionary method to generate high-affinity nucleic acid ligands. *Biomolecular engineering*. 2007;24:381-403.
40. Ray D, Kazan H, Cook KB, Weirauch MT, Najafabadi HS, Li X, Gueroussov S, Albu M, Zheng H, Yang A, Na H, Irimia M, Matzat LH, Dale RK, Smith SA, Yarosh CA, Kelly SM, Nabet B, Mecenas D, Li W, Laishram RS, Qiao M, Lipshitz HD, Piano F, Corbett AH, Carstens RP, Frey BJ, Anderson RA, Lynch KW, Penalva LO, Lei EP, Fraser AG, Blencowe BJ, Morris QD and Hughes TR. A compendium of RNA-binding motifs for decoding gene regulation. *Nature*. 2013;499:172-7.
41. Forstemann K, Tomari Y, Du T, Vagin VV, Denli AM, Bratu DP, Klattenhoff C, Theurkauf WE and Zamore PD. Normal microRNA maturation and germ-line stem cell

maintenance requires Loquacious, a double-stranded RNA-binding domain protein. *PLoS biology*. 2005;3:e236.
42. Jiang F, Ye X, Liu X, Fincher L, McKearin D and Liu Q. Dicer-1 and R3D1-L catalyze microRNA maturation in Drosophila. *Genes & development*. 2005;19:1674-9.
43. Fukuda T, Yamagata K, Fujiyama S, Matsumoto T, Koshida I, Yoshimura K, Mihara M, Naitou M, Endoh H, Nakamura T, Akimoto C, Yamamoto Y, Katagiri T, Foulds C, Takezawa S, Kitagawa H, Takeyama K, O'Malley BW and Kato S. DEAD-box RNA helicase subunits of the Drosha complex are required for processing of rRNA and a subset of microRNAs. *Nature cell biology*. 2007;9:604-11.
44. Davis BN, Hilyard AC, Lagna G and Hata A. SMAD proteins control DROSHA-mediated microRNA maturation. *Nature*. 2008;454:56-61.
45. Davis BN, Hilyard AC, Nguyen PH, Lagna G and Hata A. Smad proteins bind a conserved RNA sequence to promote microRNA maturation by Drosha. *Molecular cell*. 2010;39:373-84.
46. Suzuki HI, Yamagata K, Sugimoto K, Iwamoto T, Kato S and Miyazono K. Modulation of microRNA processing by p53. *Nature*. 2009;460:529-33.
47. Di Carlo V, Grossi E, Laneve P, Morlando M, Dini Modigliani S, Ballarino M, Bozzoni I and Caffarelli E. TDP-43 regulates the microprocessor complex activity during in vitro neuronal differentiation. *Molecular neurobiology*. 2013;48:952-63.
48. Kawahara Y and Mieda-Sato A. TDP-43 promotes microRNA biogenesis as a component of the Drosha and Dicer complexes. *Proceedings of the National Academy of Sciences of the United States of America*. 2012;109:3347-52.
49. Lee Y, Hur I, Park SY, Kim YK, Suh MR and Kim VN. The role of PACT in the RNA silencing pathway. *The EMBO journal*. 2006;25:522-32.
50. Lee HY, Zhou K, Smith AM, Noland CL and Doudna JA. Differential roles of human Dicer-binding proteins TRBP and PACT in small RNA processing. *Nucleic acids research*. 2013;41:6568-76.
51. Lee HY and Doudna JA. TRBP alters human precursor microRNA processing in vitro. *RNA (New York, NY)*. 2012;18:2012-9.
52. Guil S and Caceres JF. The multifunctional RNA-binding protein hnRNP A1 is required for processing of miR-18a. *Nature structural & molecular biology*. 2007;14:591-6.
53. Michlewski G, Guil S, Semple CA and Caceres JF. Posttranscriptional regulation of miRNAs harboring conserved terminal loops. *Molecular cell*. 2008;32:383-93.
54. Forman JJ, Legesse-Miller A and Coller HA. A search for conserved sequences in coding regions reveals that the let-7 microRNA targets Dicer within its coding sequence. *Proceedings of the National Academy of Sciences of the United States of America*. 2008;105:14879-84.
55. Trabucchi M, Briata P, Garcia-Mayoral M, Haase AD, Filipowicz W, Ramos A, Gherzi R and Rosenfeld MG. The RNA-binding protein KSRP promotes the biogenesis of a subset of microRNAs. *Nature*. 2009;459:1010-4.
56. Heo I, Joo C, Cho J, Ha M, Han J and Kim VN. Lin28 mediates the terminal uridylation of let-7 precursor MicroRNA. *Molecular cell*. 2008;32:276-84.
57. Yang W, Chendrimada TP, Wang Q, Higuchi M, Seeburg PH, Shiekhattar R and Nishikura K. Modulation of microRNA processing and expression through RNA editing by ADAR deaminases. *Nature structural & molecular biology*. 2006;13:13-21.
58. Kawahara Y, Zinshteyn B, Chendrimada TP, Shiekhattar R and Nishikura K. RNA editing of the microRNA-151 precursor blocks cleavage by the Dicer-TRBP complex. *EMBO reports*. 2007;8:763-9.
59. Johnston KW, Rutherford RB, Tilson MD, Shah DM, Hollier L and Stanley JC. Suggested standards for reporting on arterial aneurysms. Subcommittee on Reporting Standards for Arterial Aneurysms, Ad Hoc Committee on Reporting Standards, Society for Vascular Surgery and North American Chapter, International Society for Cardiovascular Surgery. *Journal of vascular surgery*. 1991;13:452-8.
60. Golledge J, Muller J, Daugherty A and Norman P. Abdominal aortic aneurysm: pathogenesis and implications for management. *Arteriosclerosis, thrombosis, and vascular biology*. 2006;26:2605-13.

61. Nordon IM, Hinchliffe RJ, Loftus IM and Thompson MM. Pathophysiology and epidemiology of abdominal aortic aneurysms. *Nature reviews Cardiology*. 2011;8:92-102.
62. Anjum A, von Allmen R, Greenhalgh R and Powell JT. Explaining the decrease in mortality from abdominal aortic aneurysm rupture. *The British journal of surgery*. 2012;99:637-45.
63. Roger VL, Go AS, Lloyd-Jones DM, Benjamin EJ, Berry JD, Borden WB, Bravata DM, Dai S, Ford ES, Fox CS, Fullerton HJ, Gillespie C, Hailpern SM, Heit JA, Howard VJ, Kissela BM, Kittner SJ, Lackland DT, Lichtman JH, Lisabeth LD, Makuc DM, Marcus GM, Marelli A, Matchar DB, Moy CS, Mozaffarian D, Mussolino ME, Nichol G, Paynter NP, Soliman EZ, Sorlie PD, Sotoodehnia N, Turan TN, Virani SS, Wong ND, Woo D and Turner MB. Heart disease and stroke statistics--2012 update: a report from the American Heart Association. *Circulation*. 2012;125:e2-e220.
64. Schermerhorn ML, Bensley RP, Giles KA, Hurks R, O'Malley A J, Cotterill P, Chaikof E and Landon BE. Changes in abdominal aortic aneurysm rupture and short-term mortality, 1995-2008: a retrospective observational study. *Annals of surgery*. 2012;256:651-8.
65. Kramer CM, Cerilli LA, Hagspiel K, DiMaria JM, Epstein FH and Kern JA. Magnetic resonance imaging identifies the fibrous cap in atherosclerotic abdominal aortic aneurysm. *Circulation*. 2004;109:1016-21.
66. Wong DR, Willett WC and Rimm EB. Smoking, hypertension, alcohol consumption, and risk of abdominal aortic aneurysm in men. *American journal of epidemiology*. 2007;165:838-45.
67. MacSweeney ST, Ellis M, Worrell PC, Greenhalgh RM and Powell JT. Smoking and growth rate of small abdominal aortic aneurysms. *Lancet (London, England)*. 1994;344:651-2.
68. Reimerink JJ, van der Laan MJ, Koelemay MJ, Balm R and Legemate DA. Systematic review and meta-analysis of population-based mortality from ruptured abdominal aortic aneurysm. *The British journal of surgery*. 2013;100:1405-13.
69. Shimizu K, Mitchell RN and Libby P. Inflammation and cellular immune responses in abdominal aortic aneurysms. *Arteriosclerosis, thrombosis, and vascular biology*. 2006;26:987-94.
70. Gomez D and Owens GK. Smooth muscle cell phenotypic switching in atherosclerosis. *Cardiovascular research*. 2012;95:156-64.
71. Thomas M, Gavrila D, McCormick ML, Miller FJ, Jr., Daugherty A, Cassis LA, Dellsperger KC and Weintraub NL. Deletion of p47phox attenuates angiotensin II-induced abdominal aortic aneurysm formation in apolipoprotein E-deficient mice. *Circulation*. 2006;114:404-413.
72. Sharma AK, Lu G, Jester A, Johnston WF, Zhao Y, Hajzus VA, Saadatzadeh MR, Su G, Bhamidipati CM, Mehta GS, Kron IL, Laubach VE, Murphy MP, Ailawadi G and Upchurch GR, Jr. Experimental abdominal aortic aneurysm formation is mediated by IL-17 and attenuated by mesenchymal stem cell treatment. *Circulation*. 2012;126:S38-45.
73. Harrison SC, Smith AJ, Jones GT, Swerdlow DI, Rampuri R, Bown MJ, Folkersen L, Baas AF, de Borst GJ, Blankensteijn JD, Price JF, van der Graaf Y, McLachlan S, Agu O, Hofman A, Uitterlinden AG, Franco-Cereceda A, Ruigrok YM, van't Hof FN, Powell JT, van Rij AM, Casas JP, Eriksson P, Holmes MV, Asselbergs FW, Hingorani AD and Humphries SE. Interleukin-6 receptor pathways in abdominal aortic aneurysm. *European heart journal*. 2013;34:3707-16.
74. Yoshimura K, Aoki H, Ikeda Y, Fujii K, Akiyama N, Furutani A, Hoshii Y, Tanaka N, Ricci R, Ishihara T, Esato K, Hamano K and Matsuzaki M. Regression of abdominal aortic aneurysm by inhibition of c-Jun N-terminal kinase. *Nature medicine*. 2005;11:1330-8.
75. Manning MW, Cassis LA and Daugherty A. Differential effects of doxycycline, a broad-spectrum matrix metalloproteinase inhibitor, on angiotensin II-induced atherosclerosis and abdominal aortic aneurysms. *Arteriosclerosis, thrombosis, and vascular biology*. 2003;23:483-8.

76. Lacolley P, Regnault V, Nicoletti A, Li Z and Michel JB. The vascular smooth muscle cell in arterial pathology: a cell that can take on multiple roles. *Cardiovascular research*. 2012;95:194-204.
77. Rensen SS, Doevendans PA and van Eys GJ. Regulation and characteristics of vascular smooth muscle cell phenotypic diversity. *Netherlands heart journal : monthly journal of the Netherlands Society of Cardiology and the Netherlands Heart Foundation*. 2007;15:100-8.
78. Boettger T, Beetz N, Kostin S, Schneider J, Kruger M, Hein L and Braun T. Acquisition of the contractile phenotype by murine arterial smooth muscle cells depends on the Mir143/145 gene cluster. *The Journal of clinical investigation*. 2009;119:2634-47.
79. Regalado ES, Guo DC, Villamizar C, Avidan N, Gilchrist D, McGillivray B, Clarke L, Bernier F, Santos-Cortez RL, Leal SM, Bertoli-Avella AM, Shendure J, Rieder MJ, Nickerson DA and Milewicz DM. Exome sequencing identifies SMAD3 mutations as a cause of familial thoracic aortic aneurysm and dissection with intracranial and other arterial aneurysms. *Circulation research*. 2011;109:680-6.
80. Mao N, Gu T, Shi E, Zhang G, Yu L and Wang C. Phenotypic switching of vascular smooth muscle cells in animal model of rat thoracic aortic aneurysm. *Interactive cardiovascular and thoracic surgery*. 2015;21:62-70.
81. Peshkova IO, Schaefer G and Koltsova EK. Atherosclerosis and aortic aneurysm - is inflammation a common denominator? *The FEBS journal*. 2016;283:1636-52.
82. Airhart N, Brownstein BH, Cobb JP, Schierding W, Arif B, Ennis TL, Thompson RW and Curci JA. Smooth muscle cells from abdominal aortic aneurysms are unique and can independently and synergistically degrade insoluble elastin. *Journal of vascular surgery*. 2014;60:1033-41; discussion 1041-2.
83. Yamanouchi D, Morgan S, Kato K, Lengfeld J, Zhang F and Liu B. Effects of caspase inhibitor on angiotensin II-induced abdominal aortic aneurysm in apolipoprotein E-deficient mice. *Arteriosclerosis, thrombosis, and vascular biology*. 2010;30:702-7.
84. Koch AE, Haines GK, Rizzo RJ, Radosevich JA, Pope RM, Robinson PG and Pearce WH. Human abdominal aortic aneurysms. Immunophenotypic analysis suggesting an immune-mediated response. *The American journal of pathology*. 1990;137:1199-213.
85. Pyo R, Lee JK, Shipley JM, Curci JA, Mao D, Ziporin SJ, Ennis TL, Shapiro SD, Senior RM and Thompson RW. Targeted gene disruption of matrix metalloproteinase-9 (gelatinase B) suppresses development of experimental abdominal aortic aneurysms. *The Journal of clinical investigation*. 2000;105:1641-9.
86. Dobrin PB, Baumgartner N, Anidjar S, Chejfec G and Mrkvicka R. Inflammatory aspects of experimental aneurysms. Effect of methylprednisolone and cyclosporine. *Annals of the New York Academy of Sciences*. 1996;800:74-88.
87. Houard X, Touat Z, Ollivier V, L**oue**dec L, Philippe M, Sebbag U, Meilhac O, Rossignol P and Michel JB. Mediators of neutrophil recruitment in human abdominal aortic aneurysms. *Cardiovascular research*. 2009;82:532-41.
88. Pagano MB, Zhou HF, Ennis TL, Wu X, Lambris JD, Atkinson JP, Thompson RW, Hourcade DE and Pham CT. Complement-dependent neutrophil recruitment is critical for the development of elastase-induced abdominal aortic aneurysm. *Circulation*. 2009;119:1805-13.
89. Armstrong PJ, Franklin DP, Carey DJ and Elmore JR. Suppression of experimental aortic aneurysms: comparison of inducible nitric oxide synthase and cyclooxygenase inhibitors. *Annals of vascular surgery*. 2005;19:248-57.
90. Lopez-Candales A, Holmes DR, Liao S, Scott MJ, Wickline SA and Thompson RW. Decreased vascular smooth muscle cell density in medial degeneration of human abdominal aortic aneurysms. *The American journal of pathology*. 1997;150:993-1007.
91. Howard EW, Bullen EC and Banda MJ. Preferential inhibition of 72- and 92-kDa gelatinases by tissue inhibitor of metalloproteinases-2. *The Journal of biological chemistry*. 1991;266:13070-5.
92. Deng GG, Martin-McNulty B, Sukovich DA, Freay A, Halks-Miller M, Thinnes T, Loskutoff DJ, Carmeliet P, Dole WP and Wang YX. Urokinase-type plasminogen activator

plays a critical role in angiotensin II-induced abdominal aortic aneurysm. *Circulation research*. 2003;92:510-7.
93. Takagi H, Manabe H, Kawai N, Goto SN and Umemoto T. Circulating matrix metalloproteinase-9 concentrations and abdominal aortic aneurysm presence: a meta-analysis. *Interactive cardiovascular and thoracic surgery*. 2009;9:437-40.
94. Longo GM, Xiong W, Greiner TC, Zhao Y, Fiotti N and Baxter BT. Matrix metalloproteinases 2 and 9 work in concert to produce aortic aneurysms. *The Journal of clinical investigation*. 2002;110:625-32.
95. Bonauer A, Boon RA and Dimmeler S. Vascular microRNAs. *Current drug targets*. 2010;11:943-9.
96. Small EM and Olson EN. Pervasive roles of microRNAs in cardiovascular biology. *Nature*. 2011;469:336-42.
97. Huntzinger E and Izaurralde E. Gene silencing by microRNAs: contributions of translational repression and mRNA decay. *Nature reviews Genetics*. 2011;12:99-110.
98. Zampetaki A, Attia R, Mayr U, Gomes RS, Phinikaridou A, Yin X, Langley SR, Willeit P, Lu R, Fanshawe B, Fava M, Barallobre-Barreiro J, Molenaar C, So PW, Abbas A, Jahangiri M, Waltham M, Botnar R, Smith A and Mayr M. Role of miR-195 in aortic aneurysmal disease. *Circulation research*. 2014;115:857-66.
99. Maegdefessel L, Azuma J, Toh R, Merk DR, Deng A, Chin JT, Raaz U, Schoelmerich AM, Raiesdana A, Leeper NJ, McConnell MV, Dalman RL, Spin JM and Tsao PS. Inhibition of microRNA-29b reduces murine abdominal aortic aneurysm development. *J Clin Invest*. 2012;122:497-506.
100. Boon RA, Seeger T, Heydt S, Fischer A, Hergenreider E, Horrevoets AJ, Vinciguerra M, Rosenthal N, Sciacca S, Pilato M, van Heijningen P, Essers J, Brandes RP, Zeiher AM and Dimmeler S. MicroRNA-29 in aortic dilation: implications for aneurysm formation. *Circulation research*. 2011;109:1115-9.
101. Ott CE, Grunhagen J, Jager M, Horbelt D, Schwill S, Kallenbach K, Guo G, Manke T, Knaus P, Mundlos S and Robinson PN. MicroRNAs differentially expressed in postnatal aortic development downregulate elastin via 3' UTR and coding-sequence binding sites. *PloS one*. 2011;6:e16250.
102. Zampetaki A and Mayr M. MicroRNAs in vascular and metabolic disease. *Circulation research*. 2012;110:508-22.
103. Albinsson S, Suarez Y, Skoura A, Offermanns S, Miano JM and Sessa WC. MicroRNAs are necessary for vascular smooth muscle growth, differentiation, and function. *Arteriosclerosis, thrombosis, and vascular biology*. 2010;30:1118-26.
104. Nazari-Jahantigh M, Wei Y and Schober A. The role of microRNAs in arterial remodelling. *Thrombosis and haemostasis*. 2012;107:611-8.
105. Abonnenc M, Nabeebaccus AA, Mayr U, Barallobre-Barreiro J, Dong X, Cuello F, Sur S, Drozdov I, Langley SR, Lu R, Stathopoulou K, Didangelos A, Yin X, Zimmermann WH, Shah AM, Zampetaki A and Mayr M. Extracellular matrix secretion by cardiac fibroblasts: role of microRNA-29b and microRNA-30c. *Circulation research*. 2013;113:1138-47.
106. Makowski MR, Wiethoff AJ, Blume U, Cuello F, Warley A, Jansen CH, Nagel E, Razavi R, Onthank DC, Cesati RR, Marber MS, Schaeffter T, Smith A, Robinson SP and Botnar RM. Assessment of atherosclerotic plaque burden with an elastin-specific magnetic resonance contrast agent. *Nature medicine*. 2011;17:383-8.
107. Cai C, Chen QB, Han ZD, Zhang YQ, He HC, Chen JH, Chen YR, Yang SB, Wu YD, Zeng YR, Qin GQ, Liang YX, Dai QS, Jiang FN, Wu SL, Zeng GH, Zhong WD and Wu CL. miR-195 Inhibits Tumor Progression by Targeting RPS6KB1 in Human Prostate Cancer. *Clinical cancer research : an official journal of the American Association for Cancer Research*. 2015;21:4922-34.
108. Daugherty A and Cassis LA. Mechanisms of abdominal aortic aneurysm formation. *Current atherosclerosis reports*. 2002;4:222-7.
109. Porrello ER, Johnson BA, Aurora AB, Simpson E, Nam YJ, Matkovich SJ, Dorn GW, 2nd, van Rooij E and Olson EN. MiR-15 family regulates postnatal mitotic arrest of cardiomyocytes. *Circulation research*. 2011;109:670-9.

110. Liao M, Zou S, Weng J, Hou L, Yang L, Zhao Z, Bao J and Jing Z. A microRNA profile comparison between thoracic aortic dissection and normal thoracic aorta indicates the potential role of microRNAs in contributing to thoracic aortic dissection pathogenesis. *Journal of vascular surgery*. 2011;53:1341-1349.e3.
111. Nelson PT, Wang WX, Mao G, Wilfred BR, Xie K, Jennings MH, Gao Z and Wang X. Specific sequence determinants of miR-15/107 microRNA gene group targets. *Nucleic acids research*. 2011;39:8163-72.
112. Liang B, Che J, Zhao H, Zhang Z and Shi G. MiR-195 promotes abdominal aortic aneurysm media remodeling by targeting Smad3. *Cardiovascular therapeutics*. 2017;35.
113. Zhang C. MicroRNA-145 in vascular smooth muscle cell biology: a new therapeutic target for vascular disease. *Cell cycle (Georgetown, Tex)*. 2009;8:3469-73.
114. Cordes KR, Sheehy NT, White MP, Berry EC, Morton SU, Muth AN, Lee TH, Miano JM, Ivey KN and Srivastava D. miR-145 and miR-143 regulate smooth muscle cell fate and plasticity. *Nature*. 2009;460:705-10.
115. Davis-Dusenbery BN, Chan MC, Reno KE, Weisman AS, Layne MD, Lagna G and Hata A. down-regulation of Kruppel-like factor-4 (KLF4) by microRNA-143/145 is critical for modulation of vascular smooth muscle cell phenotype by transforming growth factor-beta and bone morphogenetic protein 4. *The Journal of biological chemistry*. 2011;286:28097-110.
116. Kin K, Miyagawa S, Fukushima S, Shirakawa Y, Torikai K, Shimamura K, Daimon T, Kawahara Y, Kuratani T and Sawa Y. Tissue- and plasma-specific MicroRNA signatures for atherosclerotic abdominal aortic aneurysm. *Journal of the American Heart Association*. 2012;1:e000745.
117. Jiang Y, Zhang M, He H, Chen J, Zeng H, Li J and Duan R. MicroRNA/mRNA profiling and regulatory network of intracranial aneurysm. *BMC medical genomics*. 2013;6:36.
118. Elia L, Quintavalle M, Zhang J, Contu R, Cossu L, Latronico MV, Peterson KL, Indolfi C, Catalucci D, Chen J, Courtneidge SA and Condorelli G. The knockout of miR-143 and -145 alters smooth muscle cell maintenance and vascular homeostasis in mice: correlates with human disease. *Cell death and differentiation*. 2009;16:1590-8.
119. Iaconetti C, De Rosa S, Polimeni A, Sorrentino S, Gareri C, Carino A, Sabatino J, Colangelo M, Curcio A and Indolfi C. Down-regulation of miR-23b induces phenotypic switching of vascular smooth muscle cells in vitro and in vivo. *Cardiovascular research*. 2015;107:522-33.
120. Ventura A, Young AG, Winslow MM, Lintault L, Meissner A, Erkeland SJ, Newman J, Bronson RT, Crowley D, Stone JR, Jaenisch R, Sharp PA and Jacks T. Targeted deletion reveals essential and overlapping functions of the miR-17 through 92 family of miRNA clusters. *Cell*. 2008;132:875-86.
121. Maegdefessel L, Azuma J, Toh R, Deng A, Merk DR, Raiesdana A, Leeper NJ, Raaz U, Schoelmerich AM, McConnell MV, Dalman RL, Spin JM and Tsao PS. MicroRNA-21 blocks abdominal aortic aneurysm development and nicotine-augmented expansion. *Science translational medicine*. 2012;4:122ra22.
122. Mogilyansky E and Rigoutsos I. The miR-17/92 cluster: a comprehensive update on its genomics, genetics, functions and increasingly important and numerous roles in health and disease. *Cell death and differentiation*. 2013;20:1603-14.
123. Houbaviy HB, Murray MF and Sharp PA. Embryonic stem cell-specific MicroRNAs. *Developmental cell*. 2003;5:351-8.
124. Liu G, Huang Y, Lu X, Lu M, Huang X, Li W and Jiang M. Identification and characteristics of microRNAs with altered expression patterns in a rat model of abdominal aortic aneurysms. *The Tohoku journal of experimental medicine*. 2010;222:187-93.
125. Papageorgiou N, Tousoulis D, Androulakis E, Siasos G, Briasoulis A, Vogiatzi G, Kampoli AM, Tsiamis E, Tentolouris C and Stefanadis C. The role of microRNAs in cardiovascular disease. *Current medicinal chemistry*. 2012;19:2605-10.
126. De Rosa S, Curcio A and Indolfi C. Emerging role of microRNAs in cardiovascular diseases. *Circulation journal : official journal of the Japanese Circulation Society*. 2014;78:567-75.

127. Maegdefessel L. The emerging role of microRNAs in cardiovascular disease. *Journal of internal medicine*. 2014;276:633-44.
128. Liang Z, Li Y, Huang K, Wagar N and Shim H. Regulation of miR-19 to breast cancer chemoresistance through targeting PTEN. *Pharmaceutical research*. 2011;28:3091-100.
129. Kaluza D, Kroll J, Gesierich S, Manavski Y, Boeckel JN, Doebele C, Zelent A, Rossig L, Zeiher AM, Augustin HG, Urbich C and Dimmeler S. Histone deacetylase 9 promotes angiogenesis by targeting the antiangiogenic microRNA-17-92 cluster in endothelial cells. *Arteriosclerosis, thrombosis, and vascular biology*. 2013;33:533-43.
130. Bonauer A, Carmona G, Iwasaki M, Mione M, Koyanagi M, Fischer A, Burchfield J, Fox H, Doebele C, Ohtani K, Chavakis E, Potente M, Tjwa M, Urbich C, Zeiher AM and Dimmeler S. MicroRNA-92a controls angiogenesis and functional recovery of ischemic tissues in mice. *Science (New York, NY)*. 2009;324:1710-3.
131. Fichtlscherer S, De Rosa S, Fox H, Schwietz T, Fischer A, Liebetrau C, Weber M, Hamm CW, Roxe T, Muller-Ardogan M, Bonauer A, Zeiher AM and Dimmeler S. Circulating microRNAs in patients with coronary artery disease. *Circulation research*. 2010;107:677-84.
132. Diehl P, Fricke A, Sander L, Stamm J, Bassler N, Htun N, Ziemann M, Helbing T, El-Osta A, Jowett JB and Peter K. Microparticles: major transport vehicles for distinct microRNAs in circulation. *Cardiovascular research*. 2012;93:633-44.
133. Biros E, Walker PJ, Nataatmadja M, West M and Golledge J. Downregulation of transforming growth factor, beta receptor 2 and Notch signaling pathway in human abdominal aortic aneurysm. *Atherosclerosis*. 2012;221:383-6.
134. Wang Y, Ait-Oufella H, Herbin O, Bonnin P, Ramkhelawon B, Taleb S, Huang J, Offenstadt G, Combadiere C, Renia L, Johnson JL, Tharaux PL, Tedgui A and Mallat Z. TGF-beta activity protects against inflammatory aortic aneurysm progression and complications in angiotensin II-infused mice. *The Journal of clinical investigation*. 2010;120:422-32.
135. Rijbroek A, Moll FL, von Dijk HA, Meijer R and Jansen JW. Inflammation of the abdominal aortic aneurysm wall. *European journal of vascular surgery*. 1994;8:41-6.
136. Kothapalli CR, Taylor PM, Smolenski RT, Yacoub MH and Ramamurthi A. Transforming growth factor beta 1 and hyaluronan oligomers synergistically enhance elastin matrix regeneration by vascular smooth muscle cells. *Tissue engineering Part A*. 2009;15:501-11.
137. Vaday GG, Schor H, Rahat MA, Lahat N and Lider O. Transforming growth factor-beta suppresses tumor necrosis factor alpha-induced matrix metalloproteinase-9 expression in monocytes. *Journal of leukocyte biology*. 2001;69:613-21.
138. Dews M, Fox JL, Hultine S, Sundaram P, Wang W, Liu YY, Furth E, Enders GH, El-Deiry W, Schelter JM, Cleary MA and Thomas-Tikhonenko A. The myc-miR-17~92 axis blunts TGF{beta} signaling and production of multiple TGF{beta}-dependent antiangiogenic factors. *Cancer research*. 2010;70:8233-46.
139. Petrocca F, Vecchione A and Croce CM. Emerging role of miR-106b-25/miR-17-92 clusters in the control of transforming growth factor beta signaling. *Cancer research*. 2008;68:8191-4.
140. Dews M, Homayouni A, Yu D, Murphy D, Sevignani C, Wentzel E, Furth EE, Lee WM, Enders GH, Mendell JT and Thomas-Tikhonenko A. Augmentation of tumor angiogenesis by a Myc-activated microRNA cluster. *Nature genetics*. 2006;38:1060-5.
141. Woods K, Thomson JM and Hammond SM. Direct regulation of an oncogenic micro-RNA cluster by E2F transcription factors. *The Journal of biological chemistry*. 2007;282:2130-4.
142. Pickering MT, Stadler BM and Kowalik TF. miR-17 and miR-20a temper an E2F1-induced G1 checkpoint to regulate cell cycle progression. *Oncogene*. 2009;28:140-5.
143. Chen T, Zhou G, Zhou Q, Tang H, Ibe JC, Cheng H, Gou D, Chen J, Yuan JX and Raj JU. Loss of microRNA-17 approximately 92 in smooth muscle cells attenuates experimental pulmonary hypertension via induction of PDZ and LIM domain 5. *American journal of respiratory and critical care medicine*. 2015;191:678-92.

144. McNamara CA, Sarembock IJ, Bachhuber BG, Stouffer GA, Ragosta M, Barry W, Gimple LW, Powers ER and Owens GK. Thrombin and vascular smooth muscle cell proliferation: implications for atherosclerosis and restenosis. *Seminars in thrombosis and hemostasis*. 1996;22:139-44.
145. Sheikh AQ, Lighthouse JK and Greif DM. Recapitulation of developing artery muscularization in pulmonary hypertension. *Cell reports*. 2014;6:809-17.
146. Thompson RW, Liao S and Curci JA. Vascular smooth muscle cell apoptosis in abdominal aortic aneurysms. *Coronary artery disease*. 1997;8:623-31.
147. Chen Z, Wu J, Yang C, Fan P, Balazs L, Jiao Y, Lu M, Gu W, Li C, Pfeffer LM, Tigyi G and Yue J. DiGeorge syndrome critical region 8 (DGCR8) protein-mediated microRNA biogenesis is essential for vascular smooth muscle cell development in mice. *The Journal of biological chemistry*. 2012;287:19018-28.
148. Luo T, Cui S, Bian C and Yu X. Crosstalk between TGF-beta/Smad3 and BMP/BMPR2 signaling pathways via miR-17-92 cluster in carotid artery restenosis. *Molecular and cellular biochemistry*. 2014;389:169-76.
149. Weinberg RA. The retinoblastoma protein and cell cycle control. *Cell*. 1995;81:323-30.
150. Yang D, Sun C, Zhang J, Lin S, Zhao L, Wang L, Lin R, Lv J and Xin S. Proliferation of vascular smooth muscle cells under inflammation is regulated by NF-kappaB p65/microRNA-17/RB pathway activation. *International journal of molecular medicine*. 2018;41:43-50.
151. Zhang X, Liu S, Hu T, Liu S, He Y and Sun S. Up-regulated microRNA-143 transcribed by nuclear factor kappa B enhances hepatocarcinoma metastasis by repressing fibronectin expression. *Hepatology (Baltimore, Md)*. 2009;50:490-9.
152. van Rooij E. The art of microRNA research. *Circulation research*. 2011;108:219-34.
153. Krutzfeldt J, Rajewsky N, Braich R, Rajeev KG, Tuschl T, Manoharan M and Stoffel M. Silencing of microRNAs in vivo with 'antagomirs'. *Nature*. 2005;438:685-9.
154. Curtin SJ, Michno JM, Campbell BW, Gil-Humanes J, Mathioni SM, Hammond R, Gutierrez-Gonzalez JJ, Donohue RC, Kantar MB, Eamens AL, Meyers BC, Voytas DF and Stupar RM. MicroRNA Maturation and MicroRNA Target Gene Expression Regulation Are Severely Disrupted in Soybean dicer-like1 Double Mutants. *G3 (Bethesda, Md)*. 2015;6:423-33.
155. Chen B, Chen X, Wu X, Wang X, Wang Y, Lin TY, Kurata J, Wu J, Vonderfecht S, Sun G, Huang H, Yee JK, Hu J and Lin RJ. Disruption of microRNA-21 by TALEN leads to diminished cell transformation and increased expression of cell-environment interaction genes. *Cancer letters*. 2015;356:506-516.
156. Senis E, Mockenhaupt S, Rupp D, Bauer T, Paramasivam N, Knapp B, Gronych J, Grosse S, Windisch MP, Schmidt F, Theis FJ, Eils R, Lichter P, Schlesner M, Bartenschlager R and Grimm D. TALEN/CRISPR-mediated engineering of a promoterless anti-viral RNAi hairpin into an endogenous miRNA locus. *Nucleic acids research*. 2017;45:e3.
157. Uhde-Stone C, Sarkar N, Antes T, Otoc N, Kim Y, Jiang YJ and Lu B. A TALEN-based strategy for efficient bi-allelic miRNA ablation in human cells. *RNA (New York, NY)*. 2014;20:948-55.
158. Lataniotis L, Albrecht A, Kok FO, Monfries CAL, Benedetti L, Lawson ND, Hughes SM, Steinhofel K, Mayr M and Zampetaki A. CRISPR/Cas9 editing reveals novel mechanisms of clustered microRNA regulation and function. *Scientific reports*. 2017;7:8585.
159. Miller J, McLachlan AD and Klug A. Repetitive zinc-binding domains in the protein transcription factor IIIA from Xenopus oocytes. *The EMBO journal*. 1985;4:1609-14.
160. Pavletich NP and Pabo CO. Zinc finger-DNA recognition: crystal structure of a Zif268-DNA complex at 2.1 A. *Science (New York, NY)*. 1991;252:809-17.
161. Pabo CO, Peisach E and Grant RA. Design and selection of novel Cys2His2 zinc finger proteins. *Annual review of biochemistry*. 2001;70:313-40.

162. Kim YG, Cha J and Chandrasegaran S. Hybrid restriction enzymes: zinc finger fusions to Fok I cleavage domain. *Proceedings of the National Academy of Sciences of the United States of America*. 1996;93:1156-60.
163. Isalan M and Choo Y. Rapid, high-throughput engineering of sequence-specific zinc finger DNA-binding proteins. *Methods in enzymology*. 2001;340:593-609.
164. Carroll D. Progress and prospects: zinc-finger nucleases as gene therapy agents. *Gene therapy*. 2008;15:1463-8.
165. Ishino Y, Shinagawa H, Makino K, Amemura M and Nakata A. Nucleotide sequence of the iap gene, responsible for alkaline phosphatase isozyme conversion in Escherichia coli, and identification of the gene product. *Journal of bacteriology*. 1987;169:5429-33.
166. Bolotin A, Quinquis B, Sorokin A and Ehrlich SD. Clustered regularly interspaced short palindrome repeats (CRISPRs) have spacers of extrachromosomal origin. *Microbiology (Reading, England)*. 2005;151:2551-61.
167. Mojica FJ, Diez-Villasenor C, Garcia-Martinez J and Soria E. Intervening sequences of regularly spaced prokaryotic repeats derive from foreign genetic elements. *Journal of molecular evolution*. 2005;60:174-82.
168. Pourcel C, Salvignol G and Vergnaud G. CRISPR elements in Yersinia pestis acquire new repeats by preferential uptake of bacteriophage DNA, and provide additional tools for evolutionary studies. *Microbiology (Reading, England)*. 2005;151:653-63.
169. Tang TH, Bachellerie JP, Rozhdestvensky T, Bortolin ML, Huber H, Drungowski M, Elge T, Brosius J and Huttenhofer A. Identification of 86 candidates for small non-messenger RNAs from the archaeon Archaeoglobus fulgidus. *Proceedings of the National Academy of Sciences of the United States of America*. 2002;99:7536-41.
170. Jansen R, Embden JD, Gaastra W and Schouls LM. Identification of genes that are associated with DNA repeats in prokaryotes. *Molecular microbiology*. 2002;43:1565-75.
171. Haft DH, Selengut J, Mongodin EF and Nelson KE. A guild of 45 CRISPR-associated (Cas) protein families and multiple CRISPR/Cas subtypes exist in prokaryotic genomes. *PLoS computational biology*. 2005;1:e60.
172. Mojica FJ, Diez-Villasenor C, Soria E and Juez G. Biological significance of a family of regularly spaced repeats in the genomes of Archaea, Bacteria and mitochondria. *Molecular microbiology*. 2000;36:244-6.
173. Deveau H, Barrangou R, Garneau JE, Labonte J, Fremaux C, Boyaval P, Romero DA, Horvath P and Moineau S. Phage response to CRISPR-encoded resistance in Streptococcus thermophilus. *Journal of bacteriology*. 2008;190:1390-400.
174. Makarova KS, Wolf YI, Alkhnbashi OS, Costa F, Shah SA, Saunders SJ, Barrangou R, Brouns SJ, Charpentier E, Haft DH, Horvath P, Moineau S, Mojica FJ, Terns RM, Terns MP, White MF, Yakunin AF, Garrett RA, van der Oost J, Backofen R and Koonin EV. An updated evolutionary classification of CRISPR-Cas systems. *Nature reviews Microbiology*. 2015;13:722-36.
175. Kim E, Koo T, Park SW, Kim D, Kim K, Cho HY, Song DW, Lee KJ, Jung MH, Kim S, Kim JH, Kim JH and Kim JS. In vivo genome editing with a small Cas9 orthologue derived from Campylobacter jejuni. *Nature communications*. 2017;8:14500.
176. Deltcheva E, Chylinski K, Sharma CM, Gonzales K, Chao Y, Pirzada ZA, Eckert MR, Vogel J and Charpentier E. CRISPR RNA maturation by trans-encoded small RNA and host factor RNase III. *Nature*. 2011;471:602-7.
177. Doudna JA and Charpentier E. Genome editing. The new frontier of genome engineering with CRISPR-Cas9. *Science (New York, NY)*. 2014;346:1258096.
178. Chylinski K, Makarova KS, Charpentier E and Koonin EV. Classification and evolution of type II CRISPR-Cas systems. *Nucleic acids research*. 2014;42:6091-105.
179. Jinek M, Chylinski K, Fonfara I, Hauer M, Doudna JA and Charpentier E. A programmable dual-RNA-guided DNA endonuclease in adaptive bacterial immunity. *Science (New York, NY)*. 2012;337:816-21.
180. Mali P, Yang L, Esvelt KM, Aach J, Guell M, DiCarlo JE, Norville JE and Church GM. RNA-guided human genome engineering via Cas9. *Science (New York, NY)*. 2013;339:823-6.

181. Gaj T, Gersbach CA and Barbas CF, 3rd. ZFN, TALEN, and CRISPR/Cas-based methods for genome engineering. *Trends in biotechnology*. 2013;31:397-405.
182. Mali P, Aach J, Stranges PB, Esvelt KM, Moosburner M, Kosuri S, Yang L and Church GM. CAS9 transcriptional activators for target specificity screening and paired nickases for cooperative genome engineering. *Nature biotechnology*. 2013;31:833-8.
183. Zetsche B, Gootenberg JS, Abudayyeh OO, Slaymaker IM, Makarova KS, Essletzbichler P, Volz SE, Joung J, van der Oost J, Regev A, Koonin EV and Zhang F. Cpf1 is a single RNA-guided endonuclease of a class 2 CRISPR-Cas system. *Cell*. 2015;163:759-71.
184. Cox DBT, Gootenberg JS, Abudayyeh OO, Franklin B, Kellner MJ, Joung J and Zhang F. RNA editing with CRISPR-Cas13. *Science (New York, NY)*. 2017;358:1019-1027.
185. Koblan LW, Doman JL, Wilson C, Levy JM, Tay T, Newby GA, Maianti JP, Raguram A and Liu DR. Improving cytidine and adenine base editors by expression optimization and ancestral reconstruction. *Nature biotechnology*. 2018.
186. Kaminski R, Chen Y, Fischer T, Tedaldi E, Napoli A, Zhang Y, Karn J, Hu W and Khalili K. Elimination of HIV-1 Genomes from Human T-lymphoid Cells by CRISPR/Cas9 Gene Editing. *Scientific reports*. 2016;6:22555.
187. Lee DW, Kochenderfer JN, Stetler-Stevenson M, Cui YK, Delbrook C, Feldman SA, Fry TJ, Orentas R, Sabatino M, Shah NN, Steinberg SM, Stroncek D, Tschernia N, Yuan C, Zhang H, Zhang L, Rosenberg SA, Wayne AS and Mackall CL. T cells expressing CD19 chimeric antigen receptors for acute lymphoblastic leukaemia in children and young adults: a phase 1 dose-escalation trial. *Lancet (London, England)*. 2015;385:517-528.
188. Long C, Amoasii L, Mireault AA, McAnally JR, Li H, Sanchez-Ortiz E, Bhattacharyya S, Shelton JM, Bassel-Duby R and Olson EN. Postnatal genome editing partially restores dystrophin expression in a mouse model of muscular dystrophy. *Science (New York, NY)*. 2016;351:400-3.
189. Tabebordbar M, Zhu K, Cheng JKW, Chew WL, Widrick JJ, Yan WX, Maesner C, Wu EY, Xiao R, Ran FA, Cong L, Zhang F, Vandenberghe LH, Church GM and Wagers AJ. In vivo gene editing in dystrophic mouse muscle and muscle stem cells. *Science (New York, NY)*. 2016;351:407-411.
190. Nelson CE, Hakim CH, Ousterout DG, Thakore PI, Moreb EA, Castellanos Rivera RM, Madhavan S, Pan X, Ran FA, Yan WX, Asokan A, Zhang F, Duan D and Gersbach CA. In vivo genome editing improves muscle function in a mouse model of Duchenne muscular dystrophy. *Science (New York, NY)*. 2016;351:403-7.
191. Schwank G, Koo BK, Sasselli V, Dekkers JF, Heo I, Demircan T, Sasaki N, Boymans S, Cuppen E, van der Ent CK, Nieuwenhuis EE, Beekman JM and Clevers H. Functional repair of CFTR by CRISPR/Cas9 in intestinal stem cell organoids of cystic fibrosis patients. *Cell stem cell*. 2013;13:653-8.
192. Dever DP, Bak RO, Reinisch A, Camarena J, Washington G, Nicolas CE, Pavel-Dinu M, Saxena N, Wilkens AB, Mantri S, Uchida N, Hendel A, Narla A, Majeti R, Weinberg KI and Porteus MH. CRISPR/Cas9 beta-globin gene targeting in human haematopoietic stem cells. *Nature*. 2016;539:384-389.
193. Iyer V, Shen B, Zhang W, Hodgkins A, Keane T, Huang X and Skarnes WC. Off-target mutations are rare in Cas9-modified mice. *Nature methods*. 2015;12:479.
194. Mianne J, Chessum L, Kumar S, Aguilar C, Codner G, Hutchison M, Parker A, Mallon AM, Wells S, Simon MM, Teboul L, Brown SD and Bowl MR. Correction of the auditory phenotype in C57BL/6N mice via CRISPR/Cas9-mediated homology directed repair. *Genome Med*. 2016;8:16.
195. Pattanayak V, Lin S, Guilinger JP, Ma E, Doudna JA and Liu DR. High-throughput profiling of off-target DNA cleavage reveals RNA-programmed Cas9 nuclease specificity. *Nature biotechnology*. 2013;31:839-43.
196. Cong L, Ran FA, Cox D, Lin S, Barretto R, Habib N, Hsu PD, Wu X, Jiang W, Marraffini LA and Zhang F. Multiplex genome engineering using CRISPR/Cas systems. *Science*. 2013;339:819-23.

197. Adikusuma F, Piltz S, Corbett MA, Turvey M, McColl SR, Helbig KJ, Beard MR, Hughes J, Pomerantz RT and Thomas PQ. Large deletions induced by Cas9 cleavage. *Nature*. 2018;560:E8-E9.
198. Fu Y, Sander JD, Reyon D, Cascio VM and Joung JK. Improving CRISPR-Cas nuclease specificity using truncated guide RNAs. *Nature biotechnology*. 2014;32:279-284.
199. Kuscu C, Arslan S, Singh R, Thorpe J and Adli M. Genome-wide analysis reveals characteristics of off-target sites bound by the Cas9 endonuclease. *Nature biotechnology*. 2014;32:677-83.
200. Ran FA, Hsu PD, Lin CY, Gootenberg JS, Konermann S, Trevino AE, Scott DA, Inoue A, Matoba S, Zhang Y and Zhang F. Double nicking by RNA-guided CRISPR Cas9 for enhanced genome editing specificity. *Cell*. 2013;154:1380-9.
201. Guilinger JP, Thompson DB and Liu DR. Fusion of catalytically inactive Cas9 to FokI nuclease improves the specificity of genome modification. *Nature biotechnology*. 2014;32:577-582.
202. Yoshino H, Yonemori M, Miyamoto K, Tatarano S, Kofuji S, Nohata N, Nakagawa M and Enokida H. microRNA-210-3p depletion by CRISPR/Cas9 promoted tumorigenesis through revival of TWIST1 in renal cell carcinoma. *Oncotarget*. 2017;8:20881-20894.
203. Lin S, Staahl BT, Alla RK and Doudna JA. Enhanced homology-directed human genome engineering by controlled timing of CRISPR/Cas9 delivery. *eLife*. 2014;3:e04766.
204. Xu X, Gao D, Wang P, Chen J, Ruan J, Xu J and Xia X. Efficient homology-directed gene editing by CRISPR/Cas9 in human stem and primary cells using tube electroporation. *Scientific reports*. 2018;8:11649.
205. Fogarty NME, McCarthy A, Snijders KE, Powell BE, Kubikova N, Blakeley P, Lea R, Elder K, Wamaitha SE, Kim D, Maciulyte V, Kleinjung J, Kim JS, Wells D, Vallier L, Bertero A, Turner JMA and Niakan KK. Genome editing reveals a role for OCT4 in human embryogenesis. *Nature*. 2017;550:67-73.
206. Lau CH and Suh Y. In vivo genome editing in animals using AAV-CRISPR system: applications to translational research of human disease. *F1000Research*. 2017;6:2153.
207. Ran FA, Cong L, Yan WX, Scott DA, Gootenberg JS, Kriz AJ, Zetsche B, Shalem O, Wu X, Makarova KS, Koonin EV, Sharp PA and Zhang F. In vivo genome editing using Staphylococcus aureus Cas9. *Nature*. 2015;520:186-91.
208. Schumann K, Lin S, Boyer E, Simeonov DR, Subramaniam M, Gate RE, Haliburton GE, Ye CJ, Bluestone JA, Doudna JA and Marson A. Generation of knock-in primary human T cells using Cas9 ribonucleoproteins. *Proceedings of the National Academy of Sciences of the United States of America*. 2015;112:10437-42.
209. Yu X, Liang X, Xie H, Kumar S, Ravinder N, Potter J, de Mollerat du Jeu X and Chesnut JD. Improved delivery of Cas9 protein/gRNA complexes using lipofectamine CRISPRMAX. *Biotechnology letters*. 2016;38:919-29.
210. Zuris JA, Thompson DB, Shu Y, Guilinger JP, Bessen JL, Hu JH, Maeder ML, Joung JK, Chen ZY and Liu DR. Cationic lipid-mediated delivery of proteins enables efficient protein-based genome editing in vitro and in vivo. *Nature biotechnology*. 2015;33:73-80.
211. Yin H, Xue W, Chen S, Bogorad RL, Benedetti E, Grompe M, Koteliansky V, Sharp PA, Jacks T and Anderson DG. Genome editing with Cas9 in adult mice corrects a disease mutation and phenotype. *Nature biotechnology*. 2014;32:551-3.
212. Lee K, Conboy M, Park HM, Jiang F, Kim HJ, Dewitt MA, Mackley VA, Chang K, Rao A, Skinner C, Shobha T, Mehdipour M, Liu H, Huang WC, Lan F, Bray NL, Li S, Corn JE, Kataoka K, Doudna JA, Conboy I and Murthy N. Nanoparticle delivery of Cas9 ribonucleoprotein and donor DNA in vivo induces homology-directed DNA repair. *Nature biomedical engineering*. 2017;1:889-901.
213. Stower H. TALENs for microRNAs. *Nature Reviews Genetics*. 2013;15:2.
214. Chang H, Yi B, Ma R, Zhang X, Zhao H and Xi Y. CRISPR/cas9, a novel genomic tool to knock down microRNA in vitro and in vivo. *Scientific reports*. 2016;6:22312.

215. Jiang Q, Meng X, Meng L, Chang N, Xiong J, Cao H and Liang Z. Small indels induced by CRISPR/Cas9 in the 5' region of microRNA lead to its depletion and Drosha processing retardance. *RNA biology*. 2014;11:1243-9.
216. Zhao Y, Dai Z, Liang Y, Yin M, Ma K, He M, Ouyang H and Teng CB. Sequence-specific inhibition of microRNA via CRISPR/CRISPRi system. *Scientific reports*. 2014;4:3943.
217. Inoue K, Hirose M, Inoue H, Hatanaka Y, Honda A, Hasegawa A, Mochida K and Ogura A. The Rodent-Specific MicroRNA Cluster within the Sfmbt2 Gene Is Imprinted and Essential for Placental Development. *Cell reports*. 2017;19:949-956.
218. Narayanan A, Hill-Teran G, Moro A, Ristori E, Kasper DM, C AR, Lu J and Nicoli S. In vivo mutagenesis of miRNA gene families using a scalable multiplexed CRISPR/Cas9 nuclease system. *Scientific reports*. 2016;6:32386.
219. Zhang YH, Wu LZ, Liang HL, Yang Y, Qiu J, Kan Q, Zhu W, Ma CL and Zhou XY. Pulmonary surfactant synthesis in miRNA-26a-1/miRNA-26a-2 double knockout mice generated using the CRISPR/Cas9 system. *American journal of translational research*. 2017;9:355-365.
220. Golden RJ, Chen B, Li T, Braun J, Manjunath H, Chen X, Wu J, Schmid V, Chang TC, Kopp F, Ramirez-Martinez A, Tagliabracci VS, Chen ZJ, Xie Y and Mendell JT. An Argonaute phosphorylation cycle promotes microRNA-mediated silencing. *Nature*. 2017;542:197-202.
221. Treiber T, Treiber N, Plessmann U, Harlander S, Daiss JL, Eichner N, Lehmann G, Schall K, Urlaub H and Meister G. A Compendium of RNA-Binding Proteins that Regulate MicroRNA Biogenesis. *Molecular cell*. 2017;66:270-284.e13.
222. Zampetaki A, Zeng L, Margariti A, Xiao Q, Li H, Zhang Z, Pepe AE, Wang G, Habi O, deFalco E, Cockerill G, Mason JC, Hu Y and Xu Q. Histone deacetylase 3 is critical in endothelial survival and atherosclerosis development in response to disturbed flow. *Circulation*. 2010;121:132-42.
223. Zampetaki A, Kiechl S, Drozdov I, Willeit P, Mayr U, Prokopi M, Mayr A, Weger S, Oberhollenzer F, Bonora E, Shah A, Willeit J and Mayr M. Plasma microRNA profiling reveals loss of endothelial miR-126 and other microRNAs in type 2 diabetes. *Circulation research*. 2010;107:810-7.
224. Sanjana NE, Shalem O and Zhang F. Improved vectors and genome-wide libraries for CRISPR screening. *Nature methods*. 2014;11:783-784.
225. Shalem O, Sanjana NE, Hartenian E, Shi X, Scott DA, Mikkelson T, Heckl D, Ebert BL, Root DE, Doench JG and Zhang F. Genome-scale CRISPR-Cas9 knockout screening in human cells. *Science (New York, NY)*. 2014;343:84-87.
226. Ounzain S, Micheletti R, Arnan C, Plaisance I, Cecchi D, Schroen B, Reverter F, Alexanian M, Gonzales C, Ng SY, Bussotti G, Pezzuto I, Notredame C, Heymans S, Guigo R, Johnson R and Pedrazzini T. CARMEN, a human super enhancer-associated long noncoding RNA controlling cardiac specification, differentiation and homeostasis. *Journal of molecular and cellular cardiology*. 2015;89:98-112.
227. Dawson WK, Fujiwara K and Kawai G. Prediction of RNA pseudoknots using heuristic modeling with mapping and sequential folding. *PloS one*. 2007;2:e905.
228. Popenda M, Szachniuk M, Antczak M, Purzycka KJ, Lukasiak P, Bartol N, Blazewicz J and Adamiak RW. Automated 3D structure composition for large RNAs. *Nucleic acids research*. 2012;40:e112.
229. Stewart SA, Dykxhoorn DM, Palliser D, Mizuno H, Yu EY, An DS, Sabatini DM, Chen IS, Hahn WC, Sharp PA, Weinberg RA and Novina CD. Lentivirus-delivered stable gene silencing by RNAi in primary cells. *RNA (New York, NY)*. 2003;9:493-501.
230. Wang L, Wu J, Fang W, Liu G-H and Belmonte JCI. Regenerative medicine: targeted genome editing in vivo. *Cell Research*. 2015;25:271.
231. Kim YK, Wee G, Park J, Kim J, Baek D, Kim JS and Kim VN. TALEN-based knockout library for human microRNAs. *Nature structural & molecular biology*. 2013;20:1458-64.
232. Hu R, Wallace J, Dahlem TJ, Grunwald DJ and O'Connell RM. Targeting human microRNA genes using engineered Tal-effector nucleases (TALENs). *PloS one*. 2013;8:e63074.

233. Zhou J, Wang J, Shen B, Chen L, Su Y, Yang J, Zhang W, Tian X and Huang X. Dual sgRNAs facilitate CRISPR/Cas9-mediated mouse genome targeting. *The FEBS journal*. 2014;281:1717-25.
234. Mandal PK, Ferreira LM, Collins R, Meissner TB, Boutwell CL, Friesen M, Vrbanac V, Garrison BS, Stortchevoi A, Bryder D, Musunuru K, Brand H, Tager AM, Allen TM, Talkowski ME, Rossi DJ and Cowan CA. Efficient ablation of genes in human hematopoietic stem and effector cells using CRISPR/Cas9. *Cell stem cell*. 2014;15:643-52.
235. Hsu PD, Scott DA, Weinstein JA, Ran FA, Konermann S, Agarwala V, Li Y, Fine EJ, Wu X, Shalem O, Cradick TJ, Marraffini LA, Bao G and Zhang F. DNA targeting specificity of RNA-guided Cas9 nucleases. *Nature Biotechnology*. 2013;31:827.
236. Wang H, Yang H, Shivalila CS, Dawlaty MM, Cheng AW, Zhang F and Jaenisch R. One-step generation of mice carrying mutations in multiple genes by CRISPR/Cas-mediated genome engineering. *Cell*. 2013;153:910-8.
237. Wang H, Perrault AR, Takeda Y, Qin W, Wang H and Iliakis G. Biochemical evidence for Ku-independent backup pathways of NHEJ. *Nucleic acids research*. 2003;31:5377-88.
238. Abrahimi P, Chang WG, Kluger MS, Qyang Y, Tellides G, Saltzman WM and Pober JS. Efficient gene disruption in cultured primary human endothelial cells by CRISPR/Cas9. *Circulation research*. 2015;117:121-8.
239. Canver MC, Bauer DE, Dass A, Yien YY, Chung J, Masuda T, Maeda T, Paw BH and Orkin SH. Characterization of genomic deletion efficiency mediated by clustered regularly interspaced palindromic repeats (CRISPR)/Cas9 nuclease system in mammalian cells. *The Journal of biological chemistry*. 2014;289:21312-24.
240. Kim S, Kim D, Cho SW, Kim J and Kim JS. Highly efficient RNA-guided genome editing in human cells via delivery of purified Cas9 ribonucleoproteins. *Genome research*. 2014;24:1012-9.
241. Fu Y, Foden JA, Khayter C, Maeder ML, Reyon D, Joung JK and Sander JD. High-frequency off-target mutagenesis induced by CRISPR-Cas nucleases in human cells. *Nat Biotechnol*. 2013;31:822-6.
242. Smith C, Gore A, Yan W, Abalde-Atristain L, Li Z, He C, Wang Y, Brodsky RA, Zhang K, Cheng L and Ye Z. Whole-genome sequencing analysis reveals high specificity of CRISPR/Cas9 and TALEN-based genome editing in human iPSCs. *Cell stem cell*. 2014;15:12-3.
243. CRISPR off-targets: a reassessment. *Nature methods*. 2018;15:229.
244. Gong S, Yu HH, Johnson KA and Taylor DW. DNA Unwinding Is the Primary Determinant of CRISPR-Cas9 Activity. *Cell reports*. 2018;22:359-371.
245. Farh KK, Grimson A, Jan C, Lewis BP, Johnston WK, Lim LP, Burge CB and Bartel DP. The widespread impact of mammalian MicroRNAs on mRNA repression and evolution. *Science (New York, NY)*. 2005;310:1817-21.
246. Cai X, Hagedorn CH and Cullen BR. Human microRNAs are processed from capped, polyadenylated transcripts that can also function as mRNAs. *RNA (New York, NY)*. 2004;10:1957-66.
247. Mathelier A and Carbone A. Large scale chromosomal mapping of human microRNA structural clusters. *Nucleic acids research*. 2013;41:4392-408.
248. Wang J, Haubrock M, Cao KM, Hua X, Zhang CY, Wingender E and Li J. Regulatory coordination of clustered microRNAs based on microRNA-transcription factor regulatory network. *BMC systems biology*. 2011;5:199.
249. Kwon SC, Nguyen TA, Choi YG, Jo MH, Hohng S, Kim VN and Woo JS. Structure of Human DROSHA. *Cell*. 2016;164:81-90.
250. Ambros V. The functions of animal microRNAs. *Nature*. 2004;431:350-5.
251. Anderson KR, Haeussler M, Watanabe C, Janakiraman V, Lund J, Modrusan Z, Stinson J, Bei Q, Buechler A, Yu C, Thamminana SR, Tam L, Sowick M-A, Alcantar T, O'Neil N, Li J, Ta L, Lima L, Roose-Girma M, Rairdan X, Durinck S and Warming S. CRISPR off-target analysis in genetically engineered rats and mice. *Nature methods*. 2018;15:512-514.

252. Chaulk SG, Xu Z, Glover MJ and Fahlman RP. MicroRNA miR-92a-1 biogenesis and mRNA targeting is modulated by a tertiary contact within the miR-17~92 microRNA cluster. *Nucleic acids research*. 2014;42:5234-44.
253. Chakraborty S, Mehtab S, Patwardhan A and Krishnan Y. Pri-miR-17-92a transcript folds into a tertiary structure and autoregulates its processing. *RNA (New York, NY)*. 2012;18:1014-28.
254. Xin M, Small EM, Sutherland LB, Qi X, McAnally J, Plato CF, Richardson JA, Bassel-Duby R and Olson EN. MicroRNAs miR-143 and miR-145 modulate cytoskeletal dynamics and responsiveness of smooth muscle cells to injury. *Genes & development*. 2009;23:2166-78.
255. Tanzer A and Stadler PF. Evolution of microRNAs. *Methods in molecular biology (Clifton, NJ)*. 2006;342:335-50.
256. Chaulk SG, Thede GL, Kent OA, Xu Z, Gesner EM, Veldhoen RA, Khanna SK, Goping IS, MacMillan AM, Mendell JT, Young HS, Fahlman RP and Glover JN. Role of pri-miRNA tertiary structure in miR-17~92 miRNA biogenesis. *RNA biology*. 2011;8:1105-14.
257. Agarwal V, Bell GW, Nam JW and Bartel DP. Predicting effective microRNA target sites in mammalian mRNAs. *eLife*. 2015;4.
258. Choudhury NR and Michlewski G. Terminal loop-mediated control of microRNA biogenesis. *Biochemical Society transactions*. 2012;40:789-93.
259. Connerty P, Bajan S, Remenyi J, Fuller-Pace FV and Hutvagner G. The miRNA biogenesis factors, p72/DDX17 and KHSRP regulate the protein level of Ago2 in human cells. *Biochimica et biophysica acta*. 2016;1859:1299-305.
260. Lin S and Gregory RI. MicroRNA biogenesis pathways in cancer. *Nature reviews Cancer*. 2015;15:321-33.
261. Ballarino M, Pagano F, Girardi E, Morlando M, Cacchiarelli D, Marchioni M, Proudfoot NJ and Bozzoni I. Coupled RNA processing and transcription of intergenic primary microRNAs. *Molecular and cellular biology*. 2009;29:5632-8.
262. Baltz AG, Munschauer M, Schwanhausser B, Vasile A, Murakawa Y, Schueler M, Youngs N, Penfold-Brown D, Drew K, Milek M, Wyler E, Bonneau R, Selbach M, Dieterich C and Landthaler M. The mRNA-bound proteome and its global occupancy profile on protein-coding transcripts. *Molecular cell*. 2012;46:674-90.
263. Nussbacher JK and Yeo GW. Systematic Discovery of RNA Binding Proteins that Regulate MicroRNA Levels. *Molecular cell*. 2018;69:1005-1016.e7.
264. Choudhury NR, Nowak JS, Zuo J, Rappsilber J, Spoel SH and Michlewski G. Trim25 Is an RNA-Specific Activator of Lin28a/TuT4-Mediated Uridylation. *Cell reports*. 2014;9:1265-72.
265. Choudhury NR, de Lima Alves F, de Andres-Aguayo L, Graf T, Caceres JF, Rappsilber J and Michlewski G. Tissue-specific control of brain-enriched miR-7 biogenesis. *Genes & development*. 2013;27:24-38.
266. Han J, Lee Y, Yeom KH, Kim YK, Jin H and Kim VN. The Drosha-DGCR8 complex in primary microRNA processing. *Genes & development*. 2004;18:3016-27.
267. Gregory RI, Yan KP, Amuthan G, Chendrimada T, Doratotaj B, Cooch N and Shiekhattar R. The Microprocessor complex mediates the genesis of microRNAs. *Nature*. 2004;432:235-40.
268. Denli AM, Tops BB, Plasterk RH, Ketting RF and Hannon GJ. Processing of primary microRNAs by the Microprocessor complex. *Nature*. 2004;432:231-5.
269. Hao J, Duan FF and Wang Y. MicroRNAs and RNA binding protein regulators of microRNAs in the control of pluripotency and reprogramming. *Current opinion in genetics & development*. 2017;46:95-103.
270. Loffreda A, Rigamonti A, Barabino SM and Lenzken SC. RNA-Binding Proteins in the Regulation of miRNA Activity: A Focus on Neuronal Functions. *Biomolecules*. 2015;5:2363-87.
271. Anderson P and Kedersha N. Visibly stressed: the role of eIF2, TIA-1, and stress granules in protein translation. *Cell stress & chaperones*. 2002;7:213-21.

272. Bevilacqua A, Ceriani MC, Capaccioli S and Nicolin A. Post-transcriptional regulation of gene expression by degradation of messenger RNAs. *Journal of cellular physiology*. 2003;195:356-72.
273. Antic D and Keene JD. Embryonic lethal abnormal visual RNA-binding proteins involved in growth, differentiation, and posttranscriptional gene expression. *American journal of human genetics*. 1997;61:273-8.
274. Brennan CM and Steitz JA. HuR and mRNA stability. *Cellular and molecular life sciences : CMLS*. 2001;58:266-77.
275. Mazan-Mamczarz K, Lal A, Martindale JL, Kawai T and Gorospe M. Translational repression by RNA-binding protein TIAR. *Molecular and cellular biology*. 2006;26:2716-27.
276. Kedersha N, Stoecklin G, Ayodele M, Yacono P, Lykke-Andersen J, Fritzler MJ, Scheuner D, Kaufman RJ, Golan DE and Anderson P. Stress granules and processing bodies are dynamically linked sites of mRNP remodeling. *The Journal of cell biology*. 2005;169:871-84.
277. Kedersha N and Anderson P. Stress granules: sites of mRNA triage that regulate mRNA stability and translatability. *Biochemical Society transactions*. 2002;30:963-9.
278. Dupree P, Olkkonen VM and Chavrier P. Sequence of a canine cDNA clone encoding a Ran/TC4 GTP-binding protein. *Gene*. 1992;120:325-6.
279. Sazer S. The search for the primary function of the Ran GTPase continues. *Trends in cell biology*. 1996;6:81-5.
280. Sazer S and Dasso M. The ran decathlon: multiple roles of Ran. *Journal of cell science*. 2000;113 (Pt 7):1111-8.
281. Guikema JE, Linehan EK, Tsuchimoto D, Nakabeppu Y, Strauss PR, Stavnezer J and Schrader CE. APE1- and APE2-dependent DNA breaks in immunoglobulin class switch recombination. *The Journal of experimental medicine*. 2007;204:3017-26.
282. Sabouri Z, Okazaki IM, Shinkura R, Begum N, Nagaoka H, Tsuchimoto D, Nakabeppu Y and Honjo T. Apex2 is required for efficient somatic hypermutation but not for class switch recombination of immunoglobulin genes. *International immunology*. 2009;21:947-55.
283. Lang S, Benedix J, Fedeles SV, Schorr S, Schirra C, Schauble N, Jalal C, Greiner M, Hassdenteufel S, Tatzelt J, Kreutzer B, Edelmann L, Krause E, Rettig J, Somlo S, Zimmermann R and Dudek J. Different effects of Sec61alpha, Sec62 and Sec63 depletion on transport of polypeptides into the endoplasmic reticulum of mammalian cells. *Journal of cell science*. 2012;125:1958-69.
284. Szklarczyk D, Franceschini A, Wyder S, Forslund K, Heller D, Huerta-Cepas J, Simonovic M, Roth A, Santos A, Tsafou KP, Kuhn M, Bork P, Jensen LJ and von Mering C. STRING v10: protein-protein interaction networks, integrated over the tree of life. *Nucleic acids research*. 2015;43:D447-52.
285. Amberger JS, Bocchini CA, Schiettecatte F, Scott AF and Hamosh A. OMIM.org: Online Mendelian Inheritance in Man (OMIM(R)), an online catalog of human genes and genetic disorders. *Nucleic acids research*. 2015;43:D789-98.
286. Franceschini A, Lin J, von Mering C and Jensen LJ. SVD-phy: improved prediction of protein functional associations through singular value decomposition of phylogenetic profiles. *Bioinformatics (Oxford, England)*. 2016;32:1085-7.
287. Shannon P, Markiel A, Ozier O, Baliga NS, Wang JT, Ramage D, Amin N, Schwikowski B and Ideker T. Cytoscape: a software environment for integrated models of biomolecular interaction networks. *Genome research*. 2003;13:2498-504.
288. Fabregat A, Jupe S, Matthews L, Sidiropoulos K, Gillespie M, Garapati P, Haw R, Jassal B, Korninger F, May B, Milacic M, Roca CD, Rothfels K, Sevilla C, Shamovsky V, Shorser S, Varusai T, Viteri G, Weiser J, Wu G, Stein L, Hermjakob H and D'Eustachio P. The Reactome Pathway Knowledgebase. *Nucleic acids research*. 2018;46:D649-d655.
289. Li Z, Vuong JK, Zhang M, Stork C and Zheng S. Inhibition of nonsense-mediated RNA decay by ER stress. *RNA (New York, NY)*. 2017;23:378-394.
290. Song EJ, Werner SL, Neubauer J, Stegmeier F, Aspden J, Rio D, Harper JW, Elledge SJ, Kirschner MW and Rape M. The Prp19 complex and the Usp4Sart3

deubiquitinating enzyme control reversible ubiquitination at the spliceosome. *Genes & development*. 2010;24:1434-47.
291. Kuraoka I, Ito S, Wada T, Hayashida M, Lee L, Saijo M, Nakatsu Y, Matsumoto M, Matsunaga T, Handa H, Qin J, Nakatani Y and Tanaka K. Isolation of XAB2 complex involved in pre-mRNA splicing, transcription, and transcription-coupled repair. *The Journal of biological chemistry*. 2008;283:940-50.
292. Heler R, Samai P, Modell JW, Weiner C, Goldberg GW, Bikard D and Marraffini LA. Cas9 specifies functional viral targets during CRISPR-Cas adaptation. *Nature*. 2015;519:199-202.
293. Contrant M, Fender A, Chane-Woon-Ming B, Randrianjafy R, Vivet-Boudou V, Richer D and Pfeffer S. Importance of the RNA secondary structure for the relative accumulation of clustered viral microRNAs. *Nucleic acids research*. 2014;42:7981-96.
294. Du P, Wang L, Sliz P and Gregory RI. A Biogenesis Step Upstream of Microprocessor Controls miR-17 approximately 92 Expression. *Cell*. 2015;162:885-99.
295. Inference of CRISPR Edits from Sanger Trace Data Tim Hsiau, Travis Maures, Kelsey Waite, Joyce Yang, Reed Kelso, Kevin Holden, Rich Stoner, *BioRXiv,* doi: https://doi.org/10.1101/251082.
296. https://github.com/staciawyman/cortado

SUPPLEMENT

Supplementary Table 1. **Details of mouse miRNA clusters.** Data on miRNA clusters were obtained from the MiRBase database.

miRNA	miRNA Clusters	Coordinates	Sequence
mir-15a	miR-15	chr14: 61632027-61632110 [-]	U**AGCAGCA**CAUAAUGGUUUGUG
mir-15b		chr3: 69009772-69009835 [+]	U**AGCAGCA**CAUCAUGGUUUACA
mir-16-2		chr3: 69009902-69009996 [+]	U**AGCAGCA**CGUAAAUAUUGGCG
mir-16-1		chr14: 61631880-61631972 [-]	U**AGCAGCA**CGUAAAUAUUGGCG
mir-195		chr11: 70235042-70235135 [+]	U**AGCAGCA**CAGAAAUAUUGGC
mir-497a		chr11: 70234717-70234800 [+]	C**AGCAGCA**CACUGUGGUUUGUA
mir-497b		chr11: 70234692-70234816 [-]	CACCACAGUGUGGUUUGGACGUGG
mir-143	miR-143-145	chr18: 61649196-61649258 [-]	G**GUGCAGU**GCUGCAUCUCUGG
mir-145		chr18: 61647825-61647894 [-]	G**UCCAGUU**UUCCCAGGAAUCCCU
mir-17	miR-17~92	chr14: 115043671-115043754 [+]	C**AAAGUGC**UUACAGUGCAGGUAG
mir-20a		chr14: 115044157-115044263 [+]	U**AAAGUGC**UUAUAGUGCAGGUAG
mir-106b		chr5: 138165737-138165818 [-]	U**AAAGUGC**UGACAGUGCAGAU
mir-93		chr5: 138165523-138165610 [-]	C**AAAGUGC**UGUUCGUGCAGGUAG
mir-92a1		chr14: 115044427-115044506 [+]	AGGUUGGGAUUUGUCGCAAUGCU
mir-25		chr5: 138165321-138165404 [-]	AGGCGGAGACUUGGGCAAUUGC
mir-19a		chr14: 115044000-115044081 [+]	UAGUUUUGCAUAGUUGCACUAC
mir-19b-1		chr14: 115044305-115044391 [+]	AGUUUUGCAGGUUUGCAUCCAGC
mir-18a		chr14: 115043851-115043946 [+]	U**AAGGUGC**AUCUAGUGCAGAUAG

Supplementary Table 2. IVT primers. Sequences of the primers used for the IVT of the guides along with the coordinates that they target in the mouse genome.

Assay	Primer	Sequence (5' to 3')	Coordinates
IVT	F 195G1	TAATACGACTCACTATAGTTGAGGCAGAACTTACTCCC	chr17:7017580-7017600
IVT	R 195G1	TTCTAGCTCTAAAACGGGAGTAAGTTCTGCCTCAA	
IVT	F 195G2	TAATACGACTCACTATAGGGAAGCGAGTCTGCCAATAT	chr17:7017672-7017692
IVT	R 195G2	TTCTAGCTCTAAAACATATTGGCAGACTCGCTTCC	
IVT	F 195m2	TAATACGACTCACTATAGGTGGAGCAGCACAGCCAATAT	chr11:70236143-70236163
IVT	R 195m2	TTCTAGCTCTAAAACATATTGGCTGTGCTGCTCCAC	
IVT	F 195mA	TAATACGACTCACTATAGATTTCTGTGCTGCTAGAGCC	chr11:70048515-70048535
IVT	R 195mA	TTCTAGCTCTAAAACGGCTCTAGCAGCACAGAAAT	
IVT	F 195m3	TAATACGACTCACTATAGCTCTAGCAGCACAGAAATAT	chr11:70048561-700488581
IVT	R 195m3	TTCTAGCTCTAAAACATATTTCTGTGCTGCTAGAG	
IVT	F 145m1	TAATACGACTCACTATAGAGGGGCGTGGCACGTGCTGA	chr18:61807217-61807237
IVT	R 145m1	TTCTAGCTCTAAAACTCAGCACGTGCCACGCCCCT	
IVT	F 145m2	TAATACGACTCACTATAGGATGCTAAGATGGGGATTCC	chr18:61807220-61807240
IVT	R 145m2	TTCTAGCTCTAAAACGGAATCCCCATCTTAGCATC	
IVT	F 18a	TAATACGACTCACTATAGTTATGCCAGAAGGAGCACTT	chr14:115443138-115443158
IVT	R 18a	TTCTAGCTCTAAAACAAGTGCTCCTTCTGGCATAA	
IVT	F 25	TAATACGACTCACTATAGGCGGAGACTTGGGCAATTGC	chr5:138606184-138606204
IVT	R 25	TTCTAGCTCTAAAACGCAATTGCCCAAGTCTCCGC	

Supplementary Table 3. Table of primers. Primers that were used for genomic PCR, cloning in pLKO.1 vector and qPCR for gene expression with the corresponding coordinates of the amplified genomic loci.

Assay	Primer	Sequence (5' to 3')	Coordinates
GENOMIC PCR	hsa-mir-195 F	GGGCCTTGTGACAAACTTCT	chr17:7017431-7017863
GENOMIC PCR	hsa-mir-195 R	GCTATTCCCGCATAAGCATC	
GENOMIC PCR	mmu-mir-195 F (P1)	CACACACACACCGTCTAGGG	chr11:70234880-70235407
GENOMIC PCR	mmu-mir-195 R (P2)	CTGAGCCTTCCACCTCTGAC	
GENOMIC PCR	mmu-mir-497 F (P3)	CCTGTGTCTTCCAGCATTTCTC	chr11:70234360-70234977
GENOMIC PCR	mmu-mir-497 R (P4)	GTATCAGACAACCTGGGGGTT	
GENOMIC PCR	mmu-mir-143 F (P5)	GTGCTGCGTGCATAAAGAGA	chr18:61649137-61649567
GENOMIC PCR	mmu-mir-143 R (P6)	GCTATCCCATGCCAACACTT	
GENOMIC PCR	mmu-mir-145 F (P7)	CTTTCCAAGCCACTCAAAGC	chr18:61647566-61648054
GENOMIC PCR	mmu-mir-145 R (P8)	GGAGCCGTCTCATAGTCTGG	
GENOMIC PCR	mmu-mir-18 F (P9)	CCTGGTCAATGTGAGGCTTT	chr14:115043309-115044386
GENOMIC PCR	mmu-mir-18 R (P10)	CCACAGTCAGTTTTGCATGG	
GENOMIC PCR	mmu-mir-25 F (P11)	TTCTCCGACTTTCCACTGCT	chr5:138164956-138165932
GENOMIC PCR	mmu-mir-25 R (P12)	GCCACAAACAGTAGCAGCAA	
pLKO.1 cloning	miR-497~195 F	GACCGGTTGCTGGTTCCTGATTGTTC	chr11:70048081-70048911
pLKO.1 cloning	miR-195 R	GATGAATTCAAAAACTGAGCCTTCCACCTCTGAC	
Gene expression	Carmn F	AATAGACTGGGCCTCCACCT	
Gene expression	Carmn R	GTTCCTCTCTGGGGCTCTTC	
Gene expression	Beta-actin F	CACAACTGGGACGACATGGAG	
Gene expression	Beta-actin R	TTCATGAGGTAGTCAGTCTGG	

Supplementary Table 4. Table of restriction sites. The restriction sites, along with the digestion enzymes that are recognised by, for each miRNA and targeting guide used.

miRNA	sgRNA	sgRNA sequence (5'-3')	Restriction site (5'-3')	Restriction enzyme
mmu-miR-195a	sg195m2	TGGAGCAGCACAGCCAATAT	AATATT	SspI
	sg195mA	ATTTCTGTGCTGCTAGAGCC	GCNNNNNNNGC	MwoI
mmu-miR-145	sg145m2	GATGCTAAGATGGGGATTCC	GANTC	HinfI
mmu-miR-18	sg18	TTATGCCAGAAGGAGCAGTT	GDGCHC	Bsp1268I
mmu-miR-25	sg25	GCGGAGACTTGGGCAATTGC	CAATTG	MfeI

Supplementary Table 5. Table of possible off-target sites. The genomic loci that were possibly targeted by the guides used along with the mismatches (depicted in red), the primers used to study them and their coordinates.

Assay	Gene	OFF-TARGET Sequence	Mismatches	Primer Sequence (5' to 3')		Mismatches
GENOMIC PCR	OFFTARGET1 195m2	AGGAGCAGTGCAGCCAATAT	3MMs [1:9:10]	OFT1 195M2 F	GTGCTGGGATTACAGGCATT	chr17:-3133199
				OFT1 195M2 R	TCCTTGGAATGAGAGGGCTA	
GENOMIC PCR	OFFTARGET2 195m2	AGGAGCAACACAGCCACTAT	3MMs [1:8:17]	OFT2 195M2 F	GCCCCAGAGTGTGTGAAAGT	chr8:-10246601
				OFT2 195M2 R	TCAAGCCTCTGAATGCACAC	
GENOMIC PCR	OFFTARGET3 195m2	ATGAGCAGCACAGCGAATAT	3MMs [1:2:15]	OFT3 195M2 F	TCCACATGGACTGCAGTGTT	chr14:-73777792
				OFT3 195M2 R	GCTCCTGTGTTCAGGTGTGA	
GENOMIC PCR	OFFTARGET4 195m2	TGGAGCACAAAAGCCAATAT	3MMs [8:9:11]	OFT4 195M2 F	ATTCTCGGGGAAATTCCATC	chrX:+72165663
				OFT4 195M2 R	TTGCACTGCTGTCACACAAA	
GENOMIC PCR	OFFTARGET5 195m2	TGGAGCATCACAGCCAACAT	2MMs [8:17]	OFT5 195M2 F	TATCCTCTCGCCTTTGCACT	chr2:+24952183
				OFT5 195M2 R	GCAGAGTGCATCGTTGGAA	
GENOMIC PCR	OFFTARGET6 195m2	TGCAGCAGCAAAGCCACTAT	3MMs [3:11:17]	OFT6 195M2 F	CGACTTGCAATGACATGGAG	chr13:+35216456
				OFT6 195M2 R	CACCCACTCGGGACCTACTA	
GENOMIC PCR	OFFTARGET7 195m2	AGGATTAGCTCAGCCAATAT	4 MMs [1:5:6:17]	OFT7 195M2 F	AGTGCTGGGCATAGGACAAC	chr2:-91834510
				OFT7 195M2 R	CTGCTCTTCCAAAGGTCCTG	

GENOMIC PCR	OFFTARGET1 195m3	CTGTAGCAACACAGAAATAT	2 MMs [3:9]	OFT1 195M3 F	TGGGTTTGAAGGTCCTGAAG	chr1:-196773757
				OFT1 195M3 R	ACATCCTTGTTGCCCATGAT	
GENOMIC PCR	OFFTARGET2 195m3	CTCTAGCAGGACAGAAATAA	2 MMs [10:20]	OFT2 195M3 F	TCTGCCTCAGCTTTCCAAGT	chr4:+62834971
				OFT2 195M3 R	TGCTCAAGCTACACCCAGTG	
GENOMIC PCR	OFFTARGET3 195m3	TTAAAGCAGCACAGAAATAT	3 MMs [1:3:4]	OFT3 195M3 F	TCCCCTGGACTTTGACATTC	chr3:-154152635
				OFT3 195M3 R	AATGCCCTTCCCCAATAATC	
GENOMIC PCR	OFFTARGET4 195m3	AGCTAGCAGCTCAGAAATAT	3 MMs [1:2:11]	OFT4 195M3 F	TGGAGAAGGAGGAGGTCTGA	chr15:-76275971
				OFT4 195M3 R	GTGCCTGAACTCTGTGGTGA	
GENOMIC PCR	OFFTARGET5 195m3	GTCTACCAGAACAGAAATAT	3 MMs [1:6:10]	OFT5 195M3 F	CCCATTTGCATGGAAAGATT	chr:12+31442719
				OFT5 195M3 R	TGAAATGGGGAGTGTGTGA	
GENOMIC PCR	OFFTARGET6 195m3	CTCTGTCTGCACAGAAATAT	3 MMs [5:6:8]	OFT6 195M3 F	GGGAGACTATTGTGCATGATTTTATT	chr9:-22593762
				OFT6 195M3 R	GGTATTACTGTTTAGGGCCACTCT	

Supplementary Table 6. RNA binding proteins with their corresponding RNA binding motifs. The panel of the RNA binding proteins with RNA binding motifs that could potentially bind the primary mmu-miR-195a transcript.

RBP	RNA Binding motifs
Hnrnpl	CACAC
Hnrnph2	GGAGG
RBM6	AUCCA
Hnrnpa1	UAGGG AGGG UGGAU
Hnrnpa2b1	
G3bp2	
Tra2a	ACCCA UGUA
Cpsf3	
Nudt21	
Rbfox2	GCAUG
Matr3	AUCUU
Zc3h10	AGCG
Celf1	UGUNNNNNNNUGU

Supplementary Table 7. Statistical analysis of the MS identified proteins after RNA pull-down. The information from the statistical analysis of the MS data regarding the proteins that were identified. The proteins are presented in order, according to their p-values, following FDR correction, while the p-values for the statistically significant proteins are highlighted in bold. The RBPs that bound only the mutant transcript are highlighted in grey.

PROTEIN NAME	ACCESSION NUMBER	UNIPROT ID	MW (kDa)	MAX sequence coverage	UNIQUE PEPTIDES	TOTAL PSMs	CONTROL (Mean±SD)	MUTANT (Mean±SD)	P VALUE	FOLD CHANGE
Coatomer subunit beta' OS=Mus musculus GN=Copb2 PE=1 SV=2	O55029	COPB2_MOUSE	102.4	NA	1	1	2642550±1740339	10015250±2286433	**0.047545608**	3.79
GTP-binding nuclear protein Ran OS=Mus musculus GN=Ran PE=1 SV=3	P62827	RAN_MOUSE	24.4	29.6%	11	6	6014625±1700654	9125875± 1663758	**0.047545608**	1.52
DNA-(apurinic or apyrimidinic site) lyase OS=Mus musculus GN=Apex1 PE=1 SV=2	P28352	APEX1_MOUSE	35.5	28.7%	7	12	2130005±883254	4017175 ±936713	**0.047545608**	1.89
Translocation protein SEC63 homolog OS=Mus musculus GN=Sec63 PE=1 SV=4	Q8VHE0	SEC63_MOUSE	87.8	2.89%	2	2	636675±367811	1676175 ±516067	**0.047545608**	2.63
Nucleolysin TIAR OS=Mus musculus GN=Tial1 PE=1 SV=1	P70318	TIAL1_MOUSE	43.4	5.1%	3	3	4027650±694148	6402450±288123	**0.047545608**	1.59
Interferon-induced, double-stranded RNA-activated protein kinase OS=Mus musculus GN=Eif2ak2 PE=1 SV=2	Q03963	EIF2AK2_MOUSE	58.2	17.5%	7	8	52845750±9776039	20465475±13084972	0.05	0.39
Serine/arginine-rich splicing factor 4 OS=Mus musculus GN=Srsf4 PE=2 SV=1	Q8VE97	SRSF4_MOUSE	55.9	6.75%	5	2	21982750±3762952	40300500±2500749	0.054097937	1.83
Non-POU domain-containing octamer-binding protein OS=Mus musculus GN=Nono PE=1 SV=3	Q99K48	NONO_MOUSE	54.5	16.5%	9	10	4369675±1658070	8461950±1435566.244553	0.054097937	1.94
Vigilin OS=Mus musculus GN=Hdlbp PE=1 SV=1	Q8VDJ3	HDLBP_MOUSE	141.7	7.81%	8	9	25550250±8691150	42709500±7435685	0.110222347	1.67
Muscleblind-like protein 3 OS=Mus musculus GN=Mbnl3 PE=2 SV=1	Q8R003	MBNL3_MOUSE	37.5	5.56%	13	3	2875075±1047635	5155450±559199	0.110222347	1.79
Replication factor C subunit 5 OS=Mus musculus GN=Rfc5 PE=1 SV=1	Q9D0F6	RFC5_MOUSE	38.1	20%	5	9	2089900±1658585	6156800±490180	0.11529996	2.95
DnaJ homolog subfamily C member 10 OS=Mus musculus GN=Dnajc10 PE=1 SV=2	Q9DC23	DNAJC10_MOUSE	90.5	NA	NA	NA	770700±1125101	2960875±540379	0.11529996	3.84
Radixin OS=Mus musculus GN=Rdx PE=1 SV=3	P26043	RDX_MOUSE	68.5	19.4%	14	19	6109550±1617951	10591300±1681539	0.117490648	1.73
Ezrin OS=Mus musculus GN=Ezr PE=1 SV=3	P26040	EZR_MOUSE	69.4	16.6%	13	17	8582375±3232269	14253750±1295569	0.117490648	1.66
Y-box-binding protein 3 OS=Mus musculus GN=Ybx3 PE=1 SV=2	Q9JKB3	YBX3_MOUSE	38.8	44.3%	10	14	10120000±1038572	14558000±836357	0.117490648	1.44
Cluster of Polyadenylate-binding protein 2 OS=Mus musculus GN=Pabpn1 PE=1 SV=3 (Polyadenylate-binding)	Q8CCS6	PABPN1_MOUSE	32.2	11.9%	4	4	7896850±864314	14105500±2055670	0.117490648	1.79
5'-3' exoribonuclease 1 OS=Mus musculus GN=Xrn1 PE=1 SV=1	P97789	XRN1_MOUSE	194.2	9.19%	14	14	3337150±5604165	8627125±3290583	0.117490648	2.59
RNA binding motif protein, X-linked-like-1 OS=Mus musculus GN=Rbmxl1 PE=1 SV=1	Q91VM5	RBMXL1_MOUSE	42.1	9.28%	3	3	1089855±727860	2785825±819121	0.117490648	2.56
Far upstream element-binding protein 1 OS=Mus musculus GN=Fubp1 PE=1 SV=1	Q91WJ8	FUBP1_MOUSE	68.5	24.3%	12	28	25273500±10539068	40113500±4573025	0.117490648	1.59
Ras GTPase-activating protein-binding protein 1 OS=Mus musculus GN=G3bp1 PE=1 SV=1	P97855	G3BP1_MOUSE	51.8	2.37%	1	2	7735275±3728617	16154500±2456521	0.117490648	2.09
U1 small nuclear ribonucleoprotein 70 kDa OS=Mus musculus GN=Snrnp70 PE=1 SV=2	Q62376	SNRNP70_MOUSE	52	6.25%	2	2	1739742.5±1027569	5044400±1015501	0.117490648	2.90
Regulator of nonsense transcripts 1 OS=Mus musculus GN=Upf1 PE=1 SV=2	Q9EPU0	UPF1_MOUSE	123.9	1.96%	2	2	245387.5±991048	2093775±179931	0.117490648	8.53

PROTEIN NAME	ACCESSION NUMBER	UNIPROT ID	MW (kDa)	MAX sequence coverage	UNIQUE PEPTIDES	TOTAL PSMs	CONTROL (Mean±SD)	MUTANT (Mean±SD)	P VALUE	FOLD CHANGE
Heterogeneous nuclear ribonucleoprotein D0 OS=Mus musculus GN=Hnrnpd PE=1 SV=2	Q60668	HNRNPD_MOUSE	38.3	23.1%	7	15	324040000±117986121	409772500±93472172	0.117490648	1.26
Fibronectin OS=Mus musculus GN=Fn1 PE=1 SV=4	P11276	FN1_MOUSE	272.4	4.28%	8	8	1437215±1127426	2909650±638126	0.117490648	2.02
ATP-binding cassette sub-family E member 1 OS=Mus musculus GN=Abce1 PE=1 SV=1	P61222	ABCE1_MOUSE	67.3	3.51%	2	2	2608500±1718519	6178825±540335	0.117490648	2.37
Lupus La protein homolog OS=Mus musculus GN=Ssb PE=1 SV=1	P32067	SSB_MOUSE	47.7	6.99%	3	3	14736750±2837240	26222500±4450531	0.117490648	1.78
Poly [ADP-ribose] polymerase 1 OS=Mus musculus GN=Parp1 PE=1 SV=3	P11103	PARP1_MOUSE	113	10.4%	8	8	799347.5±1217644	2808225±632890	0.117490648	3.51
Zinc finger protein 2 OS=Mus musculus GN=Znf2 PE=2 SV=1	Q8BIQ3	ZNF2_MOUSE	96.6	60%	3	4	3595650±1017060	5628025±1556055	0.117490648	1.57
Cytoplasmic dynein 1 light intermediate chain 2 OS=Mus musculus GN=Dync1li2 PE=1 SV=2	Q6PDL0	DYNC1LI2_MOUSE	54.2	3.46%	1	1	4432860±5244229	11160275±3413432	0.117490648	2.52
Moesin OS=Mus musculus GN=Msn PE=1 SV=3	P26041	MSN_MOUSE	67.7	25.1%	15	27	7128275±2412050	13050725±1003194	0.117490648	1.83
60S ribosomal protein L15 OS=Mus musculus GN=Rpl15 PE=2 SV=4	Q9CZM2	RPL15_MOUSE	24.1	11.3%	2	3	141000000±26672696	221087500±15479498	0.12191124	1.57
DNA topoisomerase 1 OS=Mus musculus GN=Top1 PE=1 SV=2	Q04750	TOP1_MOUSE	90.8	10.6%	7	7	6548050±4261755	15203300±3234194	0.125107744	2.32
Poly(U)-binding-splicing factor PUF60 OS=Mus musculus GN=Puf60 PE=1 SV=2	Q3UEB3	PUF60_MOUSE	60.2	1.42%	1	1	3907900±4136619	7048650±3588780	0.137147767	1.80
Small nuclear ribonucleoprotein Sm D2 OS=Mus musculus GN=Snrpd2 PE=1 SV=1	P62317	SNRPD2_MOUSE	13.5	8.47%	1	1	1683775±430941	2776300±394620	0.137147767	1.65
Pre-mRNA-splicing factor ATP-dependent RNA helicase DHX15 OS=Mus musculus GN=Dhx15 PE=1 SV=2	O35286	DHX15_MOUSE	90.9	9.81%	7	7	7680850±3219170	14339750±2329582	0.144146871	1.87
Extended synaptotagmin-1 OS=Mus musculus GN=Esyt1 PE=1 SV=2	Q3U7R1	ESYT1_MOUSE	121.5	21%	21	88	3627950±5629331	10550250±3222843.2917741	0.144146871	2.91
High mobility group protein B1 OS=Mus musculus GN=Hmgb1 PE=1 SV=2	P63158	HMGB1_MOUSE	24.9	36.3%	9	16	3350420±2648045	5613600±3554826	0.144146871	1.68
Selenocysteine-specific elongation factor OS=Mus musculus GN=Eefsec PE=1 SV=2	Q9JHW4	EEFSEC_MOUSE	63.5	13.9%	8	8	1089645±717847	2676850±765831	0.144146871	2.46
Cell growth-regulating nucleolar protein OS=Mus musculus GN=Lyar PE=1 SV=2	Q08288	LYAR_MOUSE	43.7	11.3%	3	3	3061125±1490567	5927950±1137195	0.144146871	1.94
tRNA (cytosine(34)-C(5))-methyltransferase OS=Mus musculus GN=Nsun2 PE=1 SV=2	Q1HFZ0	NSUN2_MOUSE	85.4	16.8%	11	13	1381100±2515198	5454075±126193	0.144146871	3.95
Cluster of Transcription elongation factor B polypeptide 3 OS=Mus musculus GN=Tceb3 PE=1 SV=3 (Transcription)	Q8CB77	TCEB3_MOUSE	87.1	4%	3	7	1800550±3764890	6123150±1486485	0.150795222	3.40
Sarcoplasmic/endoplasmic reticulum calcium ATPase 2 OS=Mus musculus GN=Atp2a2 PE=1 SV=2	O55143	ATP2A2_MOUSE	114.8	4.41%	4	4	1007357.5±429427	2442225±818034	0.15911985	2.42
Peptidyl-prolyl cis-trans isomerase FKBP3 OS=Mus musculus GN=Fkbp3 PE=1 SV=2	Q62446	FKBP3_MOUSE	25.1	4.91%	1	1	12152500±2585753	14972750±2475455	0.159536494	1.23
X-ray repair cross-complementing protein 6 OS=Mus musculus GN=Xrcc6 PE=1 SV=5	P23475	XRCC6_MOUSE	69.4	14.8%	7	8	2430825±823244	4157100±1448467	0.159536494	1.71
Ribosomal L1 domain-containing protein 1 OS=Mus musculus GN=Rsl1d1 PE=1 SV=1	Q8BVY0	RSL1D1_MOUSE	50.4	6.42%	2	3	775362.5 ±118701	1492500±557038	0.159536494	1.92
Eukaryotic translation initiation factor 2A OS=Mus musculus GN=Eif2a PE=1 SV=2	Q8BJW6	EIF2A_MOUSE	64.4	11.7%	5	6	24183000±8104034	38507000±7719760	0.159536494	1.59
Nuclear RNA export factor 1 OS=Mus musculus GN=Nxf1 PE=1 SV=3	Q99JX7	NXF1_MOUSE	70.3	4.53%	2	2	4263125±923809	7240125±1222174	0.159536494	1.70

PROTEIN NAME	ACCESSION NUMBER	UNIPROT ID	MW (kDa)	MAX sequence coverage	UNIQUE PEPTIDES	TOTAL PSMs	CONTROL (Mean±SD)	MUTANT (Mean±SD)	P VALUE	FOLD CHANGE
Glycylpeptide N-tetradecanoyltransferase 1 OS=Mus musculus GN=Nmt1 PE=1 SV=1	O70310	NMT1_MOUSE	56.9	9.48%	5	5	1120880±993716	1984257.5±550122	0.159536494	1.77
CDKN2A-interacting protein OS=Mus musculus GN=Cdkn2aip PE=1 SV=1	Q8BI72	CDKN2AIP_MOUSE	59.7	7.64%	3	4	484522.5±645656	1166620±325712	0.159536494	2.41
tRNA-splicing endonuclease subunit Sen34 OS=Mus musculus GN=Tsen34 PE=2 SV=2	Q8BMZ5	TSEN34_MOUSE	34.2	12.3%	3	3	7459100±2698764	10597700±3094819	0.16630515	1.42
Polyribonucleotide 5'-hydroxyl-kinase Clp1 OS=Mus musculus GN=Clp1 PE=1 SV=1	Q99LI9	CLP1_MOUSE	47.7	6.35%	3	3	1192075±1234803	3176175±905991	0.166594012	2.66
Glutamate dehydrogenase 1, mitochondrial OS=Mus musculus GN=Glud1 PE=1 SV=1	P26443	GLUD1_MOUSE	61.3	14.5%	6	8	3927550±1206429	6165450±1870370	0.170066424	1.57
Plasminogen activator inhibitor 1 RNA-binding protein OS=Mus musculus GN=Serbp1 PE=1 SV=2	Q9CY58	SERBP1_MOUSE	44.7	1.97%	1	1	1161127.5±1337659	2331390±649525	0.170066424	2.01
Exosome complex exonuclease RRP44 OS=Mus musculus GN=Dis3 PE=1 SV=4	Q9CSH3	DIS3_MOUSE	108.8	3.44%	3	3	2704230±1595188	4132125±2150342	0.174438825	1.53
U2 small nuclear ribonucleoprotein A' OS=Mus musculus GN=Snrpa1 PE=1 SV=2	P57784	SNRPA1_MOUSE	28.3	5.49%	1	1	420462.5±639106	1284472.5±361454	0.177750263	3.05
Nuclease-sensitive element-binding protein 1 OS=Mus musculus GN=Ybx1 PE=1 SV=3	P62960	YBX1_MOUSE	35.7	59%	12	21	24221500±17321887	45234750±4829264	0.177750263	1.87
CAD protein OS=Mus musculus GN=Cad PE=1 SV=1	B2RQC6	CAD_MOUSE	243.1	2.74%	5	5	2048282.5±3095565	4526770±2070035	0.177750263	2.21
Cold shock domain-containing protein E1 OS=Mus musculus GN=Csde1 PE=1 SV=1	Q91W50	CSDE1_MOUSE	88.7	11.4%	8	8	2004912.5±1622819	4226925±934156	0.177750263	2.11
Gem-associated protein 5 OS=Mus musculus GN=Gemin5 PE=1 SV=2	Q8BX17	GEMIN5_MOUSE	166.5	1.26%	2	2	744720±1253023	1988962.5±525790	0.180912864	2.67
Citrate synthase, mitochondrial OS=Mus musculus GN=Cs PE=1 SV=1	Q9CZU6	CS_MOUSE	51.7	8.19%	3	3	3162525±1078201	3774250±697751	0.180912864	1.19
Serine-threonine kinase receptor-associated protein OS=Mus musculus GN=Strap PE=1 SV=2	Q9Z1Z2	STRAP_MOUSE	38.4	14%	4	4	227540±704776	938017.5±153694	0.180912864	4.12
Uncharacterized protein C5orf52 homolog OS=Mus musculus PE=2 SV=1	NA	NA	NA	NA	NA	NA	792542.5±216262	1444850±611948	0.1891091	1.82
Synaptic functional regulator FMR1 OS=Mus musculus GN=Fmr1 PE=1 SV=1	P35922	FMR1_MOUSE	68.9	7.98%	4	4	561637.5±1509814	2765957.5±579941	0.195375249	4.92
Constitutive coactivator of PPAR-gamma-like protein 1 OS=Mus musculus GN=FAM120A PE=1 SV=2	Q6A0A9	FAM120A_MOUSE	121.6	0.809%	1	1	2043875±1474912	4328500±787991	0.208285124	2.12
Asparagine--tRNA ligase, cytoplasmic OS=Mus musculus GN=Nars PE=1 SV=2	Q8BP47	NARS_MOUSE	64.2	10.9%	5	5	1350312.5±1293492	2670775±1276295	0.208285124	1.98
Double-stranded RNA-binding protein Staufen homolog 1 OS=Mus musculus GN=Stau1 PE=1 SV=1	Q9Z108	STAU1_MOUSE	53.9	36%	16	72	9758700±3222532	13264000±4468473	0.208285124	1.36
Bifunctional glutamate/proline--tRNA ligase OS=Mus musculus GN=Eprs PE=1 SV=4	Q8CGC7	EPRS_MOUSE	170	11%	12	12	6020550±3003296	8958675±1339098	0.208285124	1.49
T-complex protein 1 subunit gamma OS=Mus musculus GN=Cct3 PE=1 SV=1	P80318	CCT3_MOUSE	60.6	24%	14	15	12193000±11058685	18662150±15340493	0.213042051	1.53
Cluster of Myosin-9 OS=Mus musculus GN=Myh9 PE=1 SV=4 (MYH9_MOUSE)	Q8VDD5	MYH9_MOUSE	226.3	2.5%	4	4	1923217.5±432517	3445325±1355486	0.213042051	1.79
Prohibitin OS=Mus musculus GN=Phb PE=1 SV=1	P67778	PHB_MOUSE	29.8	15.1%	4	4	1489715±1018543	2010352.5±798384	0.218496364	1.35
40S ribosomal protein S5 OS=Mus musculus GN=Rps5 PE=1 SV=3	P97461	RPS5_MOUSE	22.9	28.9%	7	17	126127500±14194326	151727500±16230954	0.218496364	1.20
E3 ubiquitin/ISG15 ligase TRIM25 OS=Mus musculus GN=Trim25 PE=1 SV=2	Q61510	TRIM25_MOUSE	71.7	1.74%	1	1	711992.5±1476393	2553432.5±929563	0.218496364	3.59

PROTEIN NAME	ACCESSION NUMBER	UNIPROT ID	MW (kDa)	MAX sequence coverage	UNIQUE PEPTIDES	TOTAL PSMs	CONTROL (Mean±SD)	MUTANT (Mean±SD)	P VALUE	FOLD CHANGE
Splicing factor, proline- and glutamine-rich OS=Mus musculus GN=Sfpq PE=1 SV=1	Q8VIJ6	SFPQ_MOUSE	75.4	14%	10	13	15079500±11686019	27615500±2299843	0.218496364	1.83
Phosphatidylinositol 4-phosphate 5-kinase type-1 alpha OS=Mus musculus GN=Pip5k1a PE=1 SV=2	P70182	PIP5K1A_MOUSE	60.4	5.31%	3	3	487387.5±1101000	1585140±182319	0.218496364	3.25
Putative ATP-dependent RNA helicase Pl10 OS=Mus musculus GN=D1Pas1 PE=1 SV=1	NA	D1PAS1_MOUSE	NA	NA	NA	NA	9920450±2617356	15889750±5177824	0.218496364	1.60
SRA stem-loop-interacting RNA-binding protein, mitochondrial OS=Mus musculus GN=Slirp PE=1 SV=2	Q9D8T7	SLIRP_MOUSE	12.6	52.7%	8	47	2135775±1118873	3447575±239464	0.218496364	1.61
Cluster of ATP-dependent RNA helicase DDX3Y OS=Mus musculus GN=Ddx3y PE=1 SV=2 (ATP-dependent)	Q62095	DDX3Y_MOUSE	73.4	NA	NA	NA	39693750±9857831	49679750±10883320	0.218496364	1.25
DAZ-associated protein 1 OS=Mus musculus GN=Dazap1 PE=1 SV=2	Q9JII5	DAZAP1_MOUSE	43.2	8.87%	3	5	790400±2638501	3463225±912937	0.220382266	4.38
Microtubule-associated protein 4 OS=Mus musculus GN=Map4 PE=1 SV=3	P27546	MAP4_MOUSE	117.4	2.49%	2	2	1777225±675728	2707050±631333	0.225760101	1.52
Filamin-C OS=Mus musculus GN=Flnc PE=1 SV=3	Q8VHX6	FLNC_MOUSE	290.9	1.65%	3	3	2592425±1813665	4140725±1857383	0.225760101	1.60
Calumenin OS=Mus musculus GN=Calu PE=1 SV=1	O35887	CALU_MOUSE	37	4.76%	1	1	1960400±870734	3055875±2015758	0.225760101	1.56
Prolyl 4-hydroxylase subunit alpha-1 OS=Mus musculus GN=P4ha1 PE=1 SV=2	Q60715	P4HA1_MOUSE	60.9	11.8%	5	5	2313500±1009508	3829400±1087413	0.228450181	1.66
Cap-specific mRNA (nucleoside-2'-O-)-methyltransferase 1 OS=Mus musculus GN=Cmtr1 PE=1 SV=1	Q9DBC3	CMTR1_MOUSE	95.6	14.6%	12	15	11128225±4946442	16583500±2442642	0.228450181	1.49
Cluster of Sodium/potassium-transporting ATPase subunit alpha-2 OS=Mus musculus GN=Atp1a2 PE=1 SV=1 (Sodium/potassium-transporting)	Q6PIE5	ATP1A2_MOUSE	112.2	NA	NA	NA	2324925±871731	3300125±1004148	0.24274262	1.42
Staphylococcal nuclease domain-containing protein 1 OS=Mus musculus GN=Snd1 PE=1 SV=1	Q78PY7	SND1_MOUSE	102	31.5%	26	36	9929300±2833623	12503875±4476015	0.247309751	1.26
Protein-glutamine gamma-glutamyltransferase E OS=Mus musculus GN=Tgm3 PE=1 SV=2	Q08189	TGM3_MOUSE	77.3	1.88%	1	1	852855±821545	1951500±620857	0.255693254	2.29
Polypyrimidine tract-binding protein 3 OS=Mus musculus GN=Ptbp3 PE=1 SV=1	Q8BHD7	PTBP3_MOUSE	56.7	1.53%	1	1	62865500±96725099	136527000±22042633	0.255693254	2.17
Drebrin OS=Mus musculus GN=Dbn1 PE=1 SV=4	Q9QXS6	DBN1_MOUSE	77.2	15%	8	36	1036400±1790343	1655930 ±1055643	0.265333671	1.60
Protein PRRC2C OS=Mus musculus GN=Prrc2c PE=1 SV=3	Q3TLH4	PRRC2C_MOUSE	310.7	0.492%	1	1	30270500±17375339	41809000±15067524	0.27983228	1.38
U6 snRNA-associated Sm-like protein LSm8 OS=Mus musculus GN=Lsm8 PE=1 SV=3	Q6ZWM4	LSM8_MOUSE	10.4	10.4%	1	1	5365825±3689424	8027550±1327658	0.289287835	1.50
Interferon-activable protein 204 OS=Mus musculus GN=Ifi204 PE=1 SV=1	P0DOV2	IFI204_MOUSE	69.4	8.72%	5	5	2077400±880682	3080325±579356	0.289287835	1.48
ATP-citrate synthase OS=Mus musculus GN=Acly PE=1 SV=1	Q91V92	ACLY_MOUSE	119.7	9.44%	10	10	488112.5±738904	918090±538154	0.300437115	1.88
Nucleolin OS=Mus musculus GN=Ncl PE=1 SV=2	P09405	NCL_MOUSE	76.7	24.9%	20	47	25658750±8902516	29775250±5587866	0.300437115	1.16
Collagen alpha-2(I) chain OS=Mus musculus GN=Col1a2 PE=1 SV=2	Q01149	COL1A2_MOUSE	129.5	30.8%	24	33	36556250±19835242	45516000±8061173	0.333951034	1.25
D-3-phosphoglycerate dehydrogenase OS=Mus musculus GN=Phgdh PE=1 SV=3	Q61753	PHGDH_MOUSE	56.5	9.01%	4	4	2377830±2461929	3971475±2319231	0.334710701	1.67
Matrin-3 OS=Mus musculus GN=Matr3 PE=1 SV=1	Q8K310	MATR3_MOUSE	94.6	41%	32	175	9027775±3324674	10786575±3147813	0.334710701	1.19
Importin subunit beta-1 OS=Mus musculus GN=Kpnb1 PE=1 SV=2	P70168	KPNB1_MOUSE	97.1	2.4%	2	3	1551980±614704	2203850±1378683	0.338417651	1.42

PROTEIN NAME	ACCESSION NUMBER	UNIPROT ID	MW (kDa)	MAX sequence coverage	UNIQUE PEPTIDES	TOTAL PSMs	CONTROL (Mean±SD)	MUTANT (Mean±SD)	P VALUE	FOLD CHANGE
Tropomyosin alpha-3 chain OS=Mus musculus GN=Tpm3 PE=1 SV=3	P21107	TPM3_MOUSE	32.9	3.51%	1	1	3975250±1370569	5148675±1381974	0.338417651	1.30
Golgi apparatus protein 1 OS=Mus musculus GN=Glg1 PE=1 SV=1	Q61543	GLG1_MOUSE	133.6	3.66%	4	4	1230442.5±1258375	2013830±320118	0.338417651	1.64
Signal recognition particle 54 kDa protein OS=Mus musculus GN=Srp54 PE=1 SV=2	P14576	SRP54_MOUSE	55.7	18.8%	8	8	4255675±1341165	5580800±1064537	0.338417651	1.31
Spermatid perinuclear RNA-binding protein OS=Mus musculus GN=Strbp PE=1 SV=1	Q91WM1	STRBP_MOUSE	73.7	3.42%	3	3	9562125±3739427	12641275±2395981	0.338417651	1.32
Switch-associated protein 70 OS=Mus musculus GN=Swap70 PE=1 SV=2	Q6A028	SWAP70_MOUSE	69	6.67%	4	4	1353410±466691	1936375±1121862	0.341995489	1.43
Probable ribonuclease ZC3H12C OS=Mus musculus GN=Zc3h12c PE=1 SV=2	Q5DTV4	ZC12C_MOUSE	99.4	NA	NA	NA	37968250±7452114	45292250±4965523	0.341995489	1.19
Lysine--tRNA ligase OS=Mus musculus GN=Kars PE=1 SV=1	Q99MN1	KARS_MOUSE	67.8	6.05%	3	3	4315350±2490945	5553350±981796	0.341995489	1.29
Cleavage and polyadenylation specificity factor subunit 7 OS=Mus musculus GN=Cpsf7 PE=1 SV=2	Q8BTV2	CPSF7_MOUSE	52	2.76%	1	1	4500825±1866643	6017375±3003352	0.343837571	1.34
Transitional endoplasmic reticulum ATPase OS=Mus musculus GN=Vcp PE=1 SV=4	Q01853	VCP_MOUSE	89.3	30%	20	108	2684565±1629636	396410 ±1416269	0.371324854	1.48
Dolichyl-diphosphooligosaccharide--protein glycosyltransferase subunit 1 OS=Mus musculus GN=Rpn1 PE=1 SV=1	Q91YQ5	RPN1_MOUSE	68.5	5.76%	3	3	1563612.5±1671729	2536325±672515	0.373058517	1.62
Phosphorylated adapter RNA export protein OS=Mus musculus GN=Phax PE=1 SV=1	Q9JJT9	PHAX_MOUSE	43.2	21%	8	39	1633185±675636	2094875±1177060	0.373233685	1.28
Serpin H1 OS=Mus musculus GN=Serpinh1 PE=1 SV=3	P19324	SERPINH1_MOUSE	46.5	10.3%	4	7	9921575±4176038	13887200±6170504	0.379619198	1.40
Procollagen galactosyltransferase 1 OS=Mus musculus GN=Colgalt1 PE=1 SV=2	Q8K297	COLGALT1_MOUSE	71	7.46%	5	5	670372.5±892384	1287550±472404	0.387195146	1.92
ATP synthase subunit alpha, mitochondrial OS=Mus musculus GN=Atp5a1 PE=1 SV=1	Q03265	ATP5A1_MOUSE	59.7	9.04%	4	4	9428500±2881096	12031375±3208360	0.387195146	1.28
RNA-binding protein FUS OS=Mus musculus GN=Fus PE=1 SV=1	P56959	FUS_MOUSE	52.6	12.9%	5	9	25074750±8327819	30479250±6535074	0.38962883	1.22
Filamin-A OS=Mus musculus GN=Flna PE=1 SV=5	Q8BTM8	FLNA_MOUSE	281	8.65%	16	17	20070000±4023686	22572500±4087434	0.38962883	1.12
Cluster of Keratin, type II cytoskeletal 5 OS=Mus musculus GN=Krt5 PE=1 SV=1 (Keratin,)	Q922U2	K2C5_MOUSE	61.7	NA	43	22	959010000±365196601	336165000±251569289	0.38962883	0.35
14-3-3 protein beta/alpha OS=Mus musculus GN=Ywhab PE=1 SV=3	Q9CQV8	YWHAB_MOUSE	28.1	NA	2	2	20082500±4286450	8912875±7487941	0.38962883	0.44
Junction plakoglobin OS=Mus musculus GN=Jup PE=1 SV=3	Q02257	JUP_MOUSE	81.7	6.44%	4	4	15208075±4264665	4652400±6482450	0.38962883	0.31
Interleukin enhancer-binding factor 3 OS=Mus musculus GN=Ilf3 PE=1 SV=2	Q9Z1X4	ILF3_MOUSE	96	15.8%	12	14	58559000±9145458	47967000±16924078	0.38962883	0.82
Desmoplakin OS=Mus musculus GN=Dsp PE=1 SV=1	E9Q557	DSP_MOUSE	332.7	1.25%	4	4	14623900±6965103	5016095±6967817	0.38962883	0.34
AMP deaminase 2 OS=Mus musculus GN=Ampd2 PE=1 SV=1	Q9DBT5	AMPD2_MOUSE	92	NA	46	18	19893025±5571480	13332350±10528321	0.38962883	0.67
Arf-GAP with GTPase, ANK repeat and PH domain-containing protein 3 OS=Mus musculus GN=Agap3 PE=1 SV=1	Q8VHH5	AGAP3_MOUSE	97.9	3.85%	3	3	4143667.5±1183270	1588475±2462522	0.38962883	0.38
Cluster of Ubiquitin-40S ribosomal protein S27a OS=Mus musculus GN=Rps27a PE=1 SV=2 (RS27A_MOUSE)	P62983	RPS27A_MOUSE	17.9	30.1%	4	7	9635200±2025778	5217800±3756753	0.38962883	0.54
Histone H4 OS=Mus musculus GN=Hist1h4a PE=1 SV=2	P62806	HIST1H4A_MOUSE	11.4	29.1%	3	3	39631250±1696502	26342000±14438573	0.38962883	0.66

PROTEIN NAME	ACCESSION NUMBER	UNIPROT ID	MW (kDa)	MAX sequence coverage	UNIQUE PEPTIDES	TOTAL PSMs	CONTROL (Mean±SD)	MUTANT (Mean±SD)	P VALUE	FOLD CHANGE
Brain acid soluble protein 1 OS=Mus musculus GN=Basp1 PE=1 SV=3	Q91XV3	BASP1_MOUSE	22.1	6.19%	1	1	1560100±609232	777797.5±1155073	0.38962883	0.50
Alpha-1-antitrypsin 1-1 OS=Mus musculus GN=Serpina1a PE=1 SV=4	P07758	SERPINA1A_MOUSE	46	NA	3	3	1419560±386392	472207.5±1023676	0.38962883	0.33
TAR DNA-binding protein 43 OS=Mus musculus GN=Tardbp PE=1 SV=1	Q921F2	TARDBP_MOUSE	44.5	17.1%	7	10	8313450±1086648	6669325±1945379	0.38962883	0.80
6-phosphogluconate dehydrogenase, decarboxylating OS=Mus musculus GN=Pgd PE=1 SV=3	Q9DCD0	PGD_MOUSE	53.2	2.28%	1	1	1499482.5±675104	876217.5±1293204	0.38962883	0.58
Fructose-bisphosphate aldolase A OS=Mus musculus GN=Aldoa PE=1 SV=2	P05064	ALDOA_MOUSE	39.3	25%	8	10	8635075±5049243	7398400±5320273	0.38962883	0.86
Serum albumin OS=Mus musculus GN=Alb PE=1 SV=3	P07724	ALB_MOUSE	68.6	15.8%	8	8	34353600±7076873	12462125±39837680	0.38962883	0.36
Ras-related protein Rab-8A OS=Mus musculus GN=Rab8a PE=1 SV=2	P55258	RAB8A_MOUSE	23.6	NA	3	2	7860000±2373586	7041450 ±1348766	0.38962883	0.90
Cluster of Actin, gamma-enteric smooth muscle OS=Mus musculus GN=Actg2 PE=1 SV=1 (Actin,)	P63268	ACTG2_MOUSE	41.8	NA	NA	NA	22829500±9672418	20988250±7118405	0.38962883	0.92
Rho guanine nucleotide exchange factor 15 OS=Mus musculus GN=Arhgef15 PE=1 SV=1		ARHGEF15_MOUSE	NA	NA	NA	NA	0	0	NA	NA
Actin-related protein 2/3 complex subunit 2 OS=Mus musculus GN=Arpc2 PE=1 SV=3		ARPC2 MOUSE	34	7.67%	2	4	0	0	NA	NA
Aspartyl/asparaginyl beta-hydroxylase OS=Mus musculus GN=Asph PE=1 SV=1		ASPH_MOUSE	83	18.2%	11	33	0	0	NA	NA
Ataxin-2-like protein OS=Mus musculus GN=Atxn2l PE=1 SV=1		ATXN2L MOUSE	111	21.9%	18	36	0	0	NA	NA
Mitotic checkpoint serine/threonine-protein kinase BUB1 OS=Mus musculus GN=Bub1 PE=1 SV=1		BUB1_MOUSE	NA	NA	NA	NA	0	0	NA	NA
Cullin-associated NEDD8-dissociated protein 1 OS=Mus musculus GN=Cand1 PE=1 SV=2		CAND1 MOUSE	136	3.33%	4	13	0	0	NA	NA
Centrosomal protein of 170 kDa OS=Mus musculus GN=Cep170 PE=1 SV=2		CEP170_MOUSE	175	7.75%	9	12	0	0	NA	NA
Calponin-3 OS=Mus musculus GN=Cnn3 PE=1 SV=1		CNN3 MOUSE	36	20.6%	5	27	0	0	NA	NA
Src substrate cortactin OS=Mus musculus GN=Cttn PE=1 SV=2		CTTN_MOUSE	61	16.8%	9	30	0	0	NA	NA
EH domain-binding protein 1 OS=Mus musculus GN=Ehbp1 PE=1 SV=3		EHBP1 MOUSE	139	1.06%	1	1	0	0	NA	NA
Elongator complex protein 3 OS=Mus musculus GN=Elp3 PE=1 SV=1		ELP3_MOUSE	62	8.04%	4	6	0	0	NA	NA
Emerin OS=Mus musculus GN=Emd PE=1 SV=1		EMD_MOUSE	29	30.1%	7	18	0	0	NA	NA
Enhancer of rudimentary homolog OS=Mus musculus GN=Erh PE=1 SV=1		ERH_MOUSE	12	42.3%	4	14	0	0	NA	NA
Phenylalanine--tRNA ligase beta subunit OS=Mus musculus GN=Farsb PE=1 SV=2		FARSB_MOUSE	66	13.6%	8	14	0	0	NA	NA
Gelsolin OS=Mus musculus GN=Gsn PE=1 SV=3		GSN_MOUSE	86	11.7%	6	18	0	0	NA	NA
Host cell factor 1 OS=Mus musculus GN=Hcfc1 PE=1 SV=2		HCFC1_MOUSE	210	2.2%	4	15	0	0	NA	NA

PROTEIN NAME	ACCESSION NUMBER	UNIPROT ID	MW (kDa)	MAX sequence coverage	UNIQUE PEPTIDES	TOTAL PSMs	CONTROL (Mean±SD)	MUTANT (Mean±SD)	P VALUE	FOLD CHANGE
Heterochromatin protein 1-binding protein 3 OS=Mus musculus GN=Hp1bp3 PE=1 SV=1		HP1BP3_MOUSE	61	14.4%	7	12	0	0	NA	NA
Peroxisomal multifunctional enzyme type 2 OS=Mus musculus GN=Hsd17b4 PE=1 SV=3		HSD17B4_MOUSE	79	9.12%	6	15	0	0	NA	NA
Lamin-B receptor OS=Mus musculus GN=Lbr PE=1 SV=2		LBR_MOUSE	71	10.5%	7	35	0	0	NA	NA
Lipoma-preferred partner homolog OS=Mus musculus GN=Lpp PE=1 SV=1		LPP_MOUSE	66	23.2%	8	25	0	0	NA	NA
Magnesium transporter protein 1 OS=Mus musculus GN=Magt1 PE=1 SV=1		MAGT1_MOUSE	38	11%	4	12	0	0	NA	NA
Monofunctional C1-tetrahydrofolate synthase, mitochondrial OS=Mus musculus GN=Mthfd1l PE=1 SV=2		MTHFD1L_MOUSE	106	15.4%	12	25	0	0	NA	NA
Phosphoenolpyruvate carboxykinase [GTP], mitochondrial OS=Mus musculus GN=Pck2 PE=1 SV=1		PCK2_MOUSE	71	16.7%	10	22	0	0	NA	NA
Pleckstrin homology-like domain family B member 2 OS=Mus musculus GN=Phldb2 PE=1 SV=2		PHLDB2_MOUSE	141	19.6%	19	33	0	0	NA	NA
Proline synthase co-transcribed bacterial homolog protein OS=Mus musculus GN=Prosc PE=1 SV=1		PROSC_MOUSE	30	23.4%	6	21	0	0	NA	NA
Recombining binding protein suppressor of hairless OS=Mus musculus GN=Rbpj PE=1 SV=1		RBPJ_MOUSE	59	16.3%	7	16	0	0	NA	NA
RuvB-like 1 OS=Mus musculus GN=Ruvbl1 PE=1 SV=1		RUVBL1_MOUSE	50	14.5%	5	13	0	0	NA	NA
Serine/threonine-protein kinase Sgk2 OS=Mus musculus GN=Sgk2 PE=1 SV=1		SGK2_MOUSE	NA	0%	1	5	0	0	NA	NA
Na(+)/H(+) exchange regulatory cofactor NHE-RF1 OS=Mus musculus GN=Slc9a3r1 PE=1 SV=3		SLC9A3R1_MOUSE	39	21.7%	6	22	0	0	NA	NA
Transmembrane emp24 domain-containing protein 2 OS=Mus musculus GN=Tmed2 PE=1 SV=1		TMED2_MOUSE	23	4.48%	1	5	0	0	NA	NA
WD repeat and SOCS box-containing protein 2 OS=Mus musculus GN=Wsb2 PE=2 SV=2		WSB2_MOUSE	50	33.6%	10	33	0	0	NA	NA
Lamina-associated polypeptide 2, isoforms beta/delta/epsilon/gamma OS=Mus musculus GN=Tmpo PE=1 SV=4		TMPO_MOUSE	NA	NA	NA	NA	0	0	NA	NA
Endoribonuclease Dicer OS=Mus musculus GN=Dicer1 PE=1 SV=3		DICER1_MOUSE	217	6.21%	9	14	0	0	NA	NA
28 kDa heat- and acid-stable phosphoprotein OS=Mus musculus GN=Pdap1 PE=1 SV=1		PDAP1_MOUSE	21	31.5%	5	26	0	0	NA	NA
mRNA cap guanine-N7 methyltransferase OS=Mus musculus GN=Rnmt PE=1 SV=1		RNMT_MOUSE	53	9.25%	4	7	0	0	NA	NA
THUMP domain-containing protein 2 OS=Mus musculus GN=Thumpd2 PE=2 SV=3		THUMPD2_MOUSE	58	15.7%	6	17	0	0	NA	NA
Transformer-2 protein homolog beta OS=Mus musculus GN=Tra2b PE=1 SV=1		TRA2B_MOUSE	34	8.68%	2	12	0	0	NA	NA
3'-5' exoribonuclease 1 OS=Mus musculus GN=Eri1 PE=1 SV=2		ERI1_MOUSE	39	20.9%	5	17	0	0	NA	NA
La-related protein 1 OS=Mus musculus GN=Larp1 PE=1 SV=3		LARP1_MOUSE	121	36.5%	24	63	0	0	NA	NA
Pre-mRNA-processing factor 19 OS=Mus musculus GN=Prpf19 PE=1 SV=1		PRPF19_MOUSE	55	8.53%	4	11	0	0	NA	NA
U4/U6 small nuclear ribonucleoprotein Prp31 OS=Mus musculus GN=Prpf31 PE=1 SV=3		PRPF31_MOUSE	55	14.2%	5	10	0	0	NA	NA

PROTEIN NAME	ACCESSION NUMBER	UNIPROT ID	MW (kDa)	MAX sequence coverage	UNIQUE PEPTIDES	TOTAL PSMs	CONTROL (Mean±SD)	MUTANT (Mean±SD)	P VALUE	FOLD CHANGE
Squamous cell carcinoma antigen recognized by T-cells 3 OS=Mus musculus GN=Sart3 PE=1 SV=1		SART3_MOUSE	110	13.9%	11	41	0	0	NA	NA
GTP:AMP phosphotransferase AK3, mitochondrial OS=Mus musculus GN=Ak3 PE=1 SV=3		AK3_MOUSE	25	35.7%	7	22	0	0	NA	NA
Apoptosis inhibitor 5 OS=Mus musculus GN=Api5 PE=1 SV=2		API5_MOUSE	57	10.9%	5	20	0	0	NA	NA
Caseinolytic peptidase B protein homolog OS=Mus musculus GN=Clpb PE=1 SV=1		CLPB_MOUSE	76	11.5%	6	25	0	0	NA	NA
Calponin-2 OS=Mus musculus GN=Cnn2 PE=1 SV=1		CNN2_MOUSE	33	29.2%	8	36	0	0	NA	NA
Cysteine and glycine-rich protein 1 OS=Mus musculus GN=Csrp1 PE=1 SV=3		CSRP1_MOUSE	21	28%	4	22	0	0	NA	NA
Cluster of Cullin-4B OS=Mus musculus GN=Cul4b PE=1 SV=1 (CUL4B_MOUSE)		CUL4B_MOUSE	111	11.4%	12	39	0	0	NA	NA
Endothelial differentiation-related factor 1 OS=Mus musculus GN=Edf1 PE=1 SV=1		EDF1_MOUSE	16	30.4%	4	21	0	0	NA	NA
Band 4.1-like protein 2 OS=Mus musculus GN=Epb41l2 PE=1 SV=2		EPB41L2_MOUSE	110	12.3%	10	25	0	0	NA	NA
Leucine--tRNA ligase, cytoplasmic OS=Mus musculus GN=Lars PE=1 SV=2		LARS_MOUSE	134	15.4%	15	36	0	0	NA	NA
Methionine aminopeptidase 2 OS=Mus musculus GN=Metap2 PE=1 SV=1		METAP2_MOUSE	53	22%	8	29	0	0	NA	NA
[F-actin]-methionine sulfoxide oxidase MICAL3 OS=Mus musculus GN=Mical3 PE=1 SV=2		MICAL3_MOUSE	NA	NA	NA	NA	0	0	NA	NA
Calcium uptake protein 1, mitochondrial OS=Mus musculus GN=Micu1 PE=1 SV=1		MICU1_MOUSE	54	6.92%	3	7	0	0	NA	NA
1-phosphatidylinositol 4,5-bisphosphate phosphodiesterase beta-3 OS=Mus musculus GN=Plcb3 PE=1 SV=2		PLCB3_MOUSE	139	6.89%	9	24	0	0	NA	NA
DNA-directed RNA polymerases I, II, and III subunit RPABC1 OS=Mus musculus GN=Polr2e PE=1 SV=1		POLR2E_MOUSE	25	19%	4	14	0	0	NA	NA
Sphingosine-1-phosphate lyase 1 OS=Mus musculus GN=Sgpl1 PE=1 SV=1		SGPL1_MOUSE	64	15.8%	8	28	0	0	NA	NA
UDP-glucuronosyltransferase 1-7C OS=Mus musculus GN=Ugt1a7c PE=1 SV=1		UGT1A7C_MOUSE	60	14.3%	7	23	0	0	NA	NA
Nucleolar RNA helicase 2 OS=Mus musculus GN=Ddx21 PE=1 SV=3		DDX21_MOUSE	94	35.1%	27	59	0	0	NA	NA
Luc7-like protein 3 OS=Mus musculus GN=Luc7l3 PE=1 SV=1		LUC7L3_MOUSE	51	10.4%	4	22	0	0	NA	NA

Supplementary Table 8. Table of the pathways as returned by Reactome online software sorted according to the p-values of the identified interactions. The top six pathways, with a p-value<0.05 are highlighted in grey background while the ones with meaningful interactions are highlighted in bold.

Pathway identifier	Pathway name	#Entities found	#Entities total	#Interactors found	#Interactors total	Entities ratio	Entities pValue	Entities FDR	#Reactions found	#Reactions total	Reactions ratio	Submitted entities found	Mapped entities
R-HSA-72163	**mRNA Splicing - Major Pathway**	**3**	**180**	**6**	**633**	**0.016249887**	**0.00998423**	**0.608763792**	**8**	**9**	**7.93E-04**	**Tra2b;Prpf31;Prpf19**	**Q9UMS4;Q8WWY3;P62995**
R-HSA-72172	**mRNA Splicing**	**3**	**188**	**6**	**636**	**0.016972104**	**0.010720796**	**0.608763792**	**9**	**14**	**0.001233154**	**Tra2b;Prpf31;Prpf19**	**Q9UMS4;Q8WWY3;P62995**
R-HSA-9017802	Noncanonical activation of NOTCH3	0	8	2	49	7.22E-04	0.015435875	0.608763792	1	2	1.76E-04		
R-HSA-159236	Transport of Mature mRNA derived from an Intron-Containing Transcript	0	76	3	110	0.006861063	0.020624516	0.608763792	1	4	3.52E-04		
R-HSA-72203	**Processing of Capped Intron-Containing Pre-mRNA**	**3**	**243**	**6**	**725**	**0.021937348**	**0.023863478**	**0.608763792**	**11**	**32**	**0.002818638**	**Tra2b;Prpf31;Prpf19**	**Q9UMS4;Q8WWY3;P62995**
R-HSA-426486	**Small interfering RNA (siRNA) biogenesis**	**1**	**9**	**0**	**0**	**8.12E-04**	**0.029827035**	**0.608763792**	**3**	**5**	**4.40E-04**	**Dicer1**	**Q9UPY3**
R-HSA-77588	SLBP Dependent Processing of Replication-Dependent Histone Pre-mRNAs	0	11	1	2	9.93E-04	0.042801649	0.608763792	1	3	2.64E-04		
R-HSA-72202	Transport of Mature Transcript to Cytoplasm	0	85	3	228	0.007673558	0.071750476	0.608763792	1	13	0.001145072		
R-HSA-169131	Inhibition of PKR	0	2	1	22	1.81E-04	0.074497975	0.608763792	1	2	1.76E-04		
R-HSA-203927	MicroRNA (miRNA) biogenesis	1	24	0	1	0.002166652	0.080712522	0.608763792	3	8	7.05E-04	Dicer1	Q9UPY3
R-HSA-9013507	NOTCH3 Activation and Transmission of Signal to the Nucleus	0	25	2	120	0.002256929	0.083786527	0.608763792	1	15	0.001321237		
R-HSA-73980	RNA Polymerase III Transcription Termination	0	23	1	5	0.002076374	0.08995765	0.608763792	1	2	1.76E-04		
R-HSA-75067	Processing of Capped Intronless Pre-mRNA	0	28	1	6	0.00252776	0.10817507	0.608763792	1	10	8.81E-04		
R-HSA-450604	KSRP (KHSRP) binds and destabilizes mRNA	0	17	2	170	0.001534712	0.128531956	0.608763792	1	5	4.40E-04		
R-HSA-167160	RNA Pol II CTD phosphorylation and interaction with CE during HIV infection	1	27	0	19	0.002437483	0.137745438	0.608763792	1	5	4.40E-04	Rnmt	O43148
R-HSA-77075	RNA Pol II CTD phosphorylation and interaction with CE	1	27	0	19	0.002437483	0.137745438	0.608763792	1	5	4.40E-04	Rnmt	O43148
R-HSA-749476	RNA Polymerase III Abortive And Retractive Initiation	0	41	1	5	0.003701363	0.143543004	0.608763792	1	13	0.001145072		
R-HSA-4570464	SUMOylation of RNA binding proteins	0	49	2	168	0.00442358	0.159675152	0.608763792	3	4	3.52E-04		
R-HSA-8851805	MET activates RAS signaling	0	11	1	49	9.93E-04	0.171962005	0.608763792	1	10	8.81E-04		
R-HSA-9012852	Signaling by NOTCH3	0	49	2	183	0.00442358	0.177542788	0.608763792	1	37	0.00325905		
R-HSA-72086	mRNA Capping	1	29	0	34	0.002618037	0.180305812	0.608763792	7	11	9.69E-04	Rnmt	O43148
R-HSA-8953854	Metabolism of RNA	6	673	7	1453	0.060756523	0.180433934	0.608763792	26	187	0.016471417	Eri1;Rnmt;Tra2b;Prpf31; Ddx21;Prpf19	Q9UMS4;O43148;Q8WWY3; Q8IV48;Q9NR30;P62995
R-HSA-6782210	Gap-filling DNA repair synthesis and ligation in TC-NER	1	64	0	0	0.005777738	0.194029204	0.608763792	2	2	1.76E-04	Prpf19	Q9UMS4
R-HSA-5632987	Defective Mismatch Repair Associated With PMS2	0	2	1	67	1.81E-04	0.204845386	0.608763792	1	1	8.81E-05		

Pathway identifier	Pathway name	#Entities found	#Entities total	#Interactors found	#Interactors total	Entities ratio	Entities pValue	Entities FDR	#Reactions found	#Reactions total	Reactions ratio	Submitted entities found	Mapped entities
R-HSA-74158	RNA Polymerase III Transcription	0	41	1	28	0.003701363	0.207527101	0.608763792	1	25	0.002202061		
R-HSA-168276	NS1 Mediated Effects on Host Pathways	0	44	1	31	0.003972195	0.220803139	0.608763792	1	6	5.28E-04		
R-HSA-6782135	Dual incision in TC-NER	1	65	0	22	0.005868015	0.24159224	0.608763792	6	6	5.28E-04	Prpf19	Q9UMS4
R-HSA-5423599	Diseases of Mismatch Repair (MMR)	0	5	1	82	4.51E-04	0.24159224	0.608763792	1	6	5.28E-04		
R-HSA-512988	Interleukin-3, Interleukin-5 and GM-CSF signaling	0	48	2	257	0.004333303	0.246379564	0.608763792	1	38	0.003347133		
R-HSA-5693548	Sensing of DNA Double Strand Breaks	0	6	1	84	5.42E-04	0.251781733	0.608763792	2	8	7.05E-04		
R-HSA-194441	Metabolism of non-coding RNA	0	55	1	45	0.004965243	0.254308046	0.608763792	1	6	5.28E-04		
R-HSA-191859	snRNP Assembly	0	55	1	45	0.004965243	0.254308046	0.608763792	1	6	5.28E-04		
R-HSA-4608870	Asymmetric localization of PCP proteins	0	64	1	25	0.005777738	0.25933559	0.608763792	2	7	6.17E-04		
R-HSA-168253	Host Interactions with Influenza Factors	0	48	1	43	0.004333303	0.261836876	0.608763792	1	8	7.05E-04		
R-HSA-72165	mRNA Splicing - Minor Pathway	0	52	1	41	0.004694412	0.264329873	0.608763792	1	5	4.40E-04		
R-HSA-5358565	Mismatch repair (MMR) directed by MSH2:MSH6 (MutSalpha)	0	14	1	82	0.00126388	0.264329873	0.608763792	1	10	8.81E-04		
R-HSA-5358508	Mismatch Repair	0	15	1	83	0.001354157	0.264329873	0.608763792	1	17	0.001497402		
R-HSA-8931987	RUNX1 regulates estrogen receptor mediated transcription	0	6	1	91	5.42E-04	0.274219518	0.608763792	1	8	7.05E-04		
R-HSA-450341	Activation of the AP-1 family of transcription factors	0	10	1	103	9.03E-04	0.303112357	0.608763792	3	5	4.40E-04		
R-HSA-170984	ARMS-mediated activation	0	7	1	105	6.32E-04	0.310157384	0.608763792	1	5	4.40E-04		
R-HSA-8849468	PTK6 Regulates Proteins Involved in RNA Processing	0	5	1	119	4.51E-04	0.330875841	0.608763792	2	7	6.17E-04		
R-HSA-6781823	Formation of TC-NER Pre-Incision Complex	1	53	0	75	0.004784689	0.342121002	0.608763792	2	7	6.17E-04	Prpf19	Q9UMS4
R-HSA-211000	Gene Silencing by RNA	1	108	0	22	0.009749932	0.346566964	0.608763792	6	36	0.003170968	Dicer1	Q9UPY3
R-HSA-5099900	WNT5A-dependent internalization of FZD4	0	15	1	116	0.001354157	0.353180686	0.608763792	1	5	4.40E-04		
R-HSA-5620924	Intraflagellar transport	0	53	1	101	0.004784689	0.3575533	0.608763792	2	12	0.001056989		
R-HSA-167172	Transcription of the HIV genome	1	74	0	66	0.006680509	0.359728718	0.608763792	1	45	0.00396371	Rnmt	O43148
R-HSA-169893	Prolonged ERK activation events	0	12	1	131	0.001083326	0.372630265	0.608763792	1	11	9.69E-04		
R-HSA-4641258	Degradation of DVL	0	57	1	93	0.005145798	0.385276652	0.608763792	1	7	6.17E-04		
R-HSA-3769402	Deactivation of the beta-catenin transactivating complex	0	42	2	372	0.00379164	0.385943196	0.608763792	1	14	0.001233154		
R-HSA-450513	Tristetraprolin (TTP, ZFP36) binds and destabilizes mRNA	0	17	1	134	0.001534712	0.391505711	0.608763792	1	4	3.52E-04		

Pathway identifier	Pathway name	#Entities found	#Entities total	#Interactors found	#Interactors total	Entities ratio	Entities pValue	Entities FDR	#Reactions found	#Reactions total	Reactions ratio	Submitted entities found	Mapped entities
R-HSA-6781827	Transcription-Coupled Nucleotide Excision Repair (TC-NER)	1	78	0	80	0.007041618	0.39767283	0.608763792	11	16	0.001409319	Prpf19	Q9UMS4
R-HSA-8943724	Regulation of PTEN gene transcription	0	60	1	97	0.005416629	0.405800346	0.608763792	1	15	0.001321237		
R-HSA-450282	MAPK targets/ Nuclear events mediated by MAP kinases	0	31	1	137	0.002798592	0.411825276	0.608763792	3	16	0.001409319		
R-HSA-187687	Signalling to ERKs	0	32	1	133	0.002888869	0.415808555	0.608763792	1	24	0.002113979		
R-HSA-6796648	TP53 Regulates Transcription of DNA Repair Genes	0	65	1	104	0.005868015	0.421733896	0.608763792	1	17	0.001497402		
R-HSA-450385	Butyrate Response Factor 1 (BRF1) binds and destabilizes mRNA	0	17	1	173	0.001534712	0.467061134	0.608763792	2	6	5.28E-04		
R-HSA-1912408	Pre-NOTCH Transcription and Translation	0	62	1	133	0.005597183	0.474268873	0.608763792	1	27	0.002378226		
R-HSA-2028269	Signaling by Hippo	0	20	1	182	0.001805543	0.474268873	0.608763792	1	30	0.002642473		
R-HSA-450531	Regulation of mRNA stability by proteins that bind AU-rich elements	0	88	2	409	0.007944389	0.484997109	0.608763792	4	26	0.002290144		
R-HSA-450294	MAP kinase activation	0	63	1	167	0.005687461	0.508897248	0.608763792	3	32	0.002818638		
R-HSA-6791226	Major pathway of rRNA processing in the nucleolus and cytosol	2	183	0	359	0.016520719	0.51410522	0.608763792	2	7	6.17E-04	Eri1;Ddx21	Q8IV48;Q9NR30
R-HSA-448424	Interleukin-17 signaling	0	71	1	167	0.006409678	0.522113042	0.608763792	3	35	0.003082886		
R-HSA-8868773	rRNA processing in the nucleus and cytosol	2	193	0	361	0.01742349	0.526703315	0.608763792	2	15	0.001321237	Eri1;Ddx21	Q8IV48;Q9NR30
R-HSA-4615885	SUMOylation of DNA replication proteins	0	48	1	186	0.004333303	0.530195051	0.608763792	1	8	7.05E-04		
R-HSA-4641265	Repression of WNT target genes	0	12	1	214	0.001083326	0.534979725	0.608763792	1	7	6.17E-04		
R-HSA-1912422	Pre-NOTCH Expression and Processing	0	78	1	153	0.007041618	0.534979725	0.608763792	1	37	0.00325905		
R-HSA-5250924	B-WICH complex positively regulates rRNA expression	1	60	0	174	0.005416629	0.536563967	0.608763792	3	3	2.64E-04	Ddx21	Q9NR30
R-HSA-452723	Transcriptional regulation of pluripotent stem cells	0	36	1	211	0.003249977	0.56269983	0.608763792	1	35	0.003082886		
R-HSA-977225	Amyloid fiber formation	0	71	1	193	0.006409678	0.575945273	0.608763792	1	28	0.002466308		
R-HSA-72312	rRNA processing	2	203	0	402	0.018326262	0.576860524	0.608763792	2	21	0.001849731	Eri1;Ddx21	Q8IV48;Q9NR30
R-HSA-4086400	PCP/CE pathway	0	92	1	184	0.008305498	0.599899166	0.608763792	3	24	0.002113979		
R-HSA-912446	Meiotic recombination	0	56	1	231	0.00505552	0.599899166	0.608763792	1	9	7.93E-04		
R-HSA-2871796	FCERI mediated MAPK activation	0	118	1	162	0.010652704	0.603986251	0.608763792	2	20	0.001761649		
R-HSA-6807070	PTEN Regulation	0	139	2	485	0.012548524	0.608763792	0.608763792	3	56	0.004932617		
R-HSA-5696398	Nucleotide Excision Repair	1	110	0	199	0.009930487	0.626384249	0.626384249	11	36	0.003170968	Prpf19	Q9UMS4
R-HSA-5250913	Positive epigenetic regulation of rRNA expression	1	75	0	241	0.006770786	0.637733895	0.637733895	3	7	6.17E-04	Ddx21	Q9NR30

Pathway identifier	Pathway name	#Entities found	#Entities total	#Interactors found	#Interactors total	Entities ratio	Entities pValue	Entities FDR	#Reactions found	#Reactions total	Reactions ratio	Submitted entities found	Mapped entities
R-HSA-165159	mTOR signalling	0	40	1	284	0.003611086	0.637733895	0.637733895	1	28	0.002466308		
R-HSA-5689896	Ovarian tumor domain proteases	0	38	1	274	0.003430532	0.641441401	0.641441401	1	14	0.001233154		
R-HSA-2559580	Oxidative Stress Induced Senescence	0	94	1	229	0.008486052	0.641441401	0.641441401	2	39	0.003435215		
R-HSA-6806834	Signaling by MET	0	79	1	250	0.007131895	0.652341973	0.652341973	1	49	0.00431604		
R-HSA-201681	TCF dependent signaling in response to WNT	0	202	3	907	0.018235984	0.692086216	0.692086216	2	71	0.006253854		
R-HSA-3858494	Beta-catenin independent WNT signaling	0	143	1	218	0.012909633	0.695938789	0.695938789	3	51	0.004492205		
R-HSA-416993	Trafficking of GluR2-containing AMPA receptors	0	17	1	336	0.001534712	0.696982995	0.696982995	3	3	2.64E-04		
R-HSA-73894	DNA Repair	1	296	2	880	0.026722037	0.697125809	0.697125809	14	308	0.027129393	Prpf19	Q9UMS4
R-HSA-373752	Netrin-1 signaling	0	50	1	322	0.004513858	0.705210945	0.705210945	1	37	0.00325905		
R-HSA-162599	Late Phase of HIV Life Cycle	1	150	0	240	0.013541573	0.715188147	0.715188147	1	74	0.006518101	Rnmt	O43148
R-HSA-975138	TRAF6 mediated induction of NFkB and MAP kinases upon TLR7/8 or 9 activation	0	91	1	312	0.008215221	0.716167453	0.716167453	3	47	0.004139875		
R-HSA-975871	MyD88 cascade initiated on plasma membrane	0	85	1	335	0.007673558	0.728601707	0.728601707	3	57	0.005020699		
R-HSA-168142	Toll Like Receptor 10 (TLR10) Cascade	0	85	1	335	0.007673558	0.728601707	0.728601707	3	58	0.005108782		
R-HSA-168176	Toll Like Receptor 5 (TLR5) Cascade	0	85	1	336	0.007673558	0.72953574	0.72953574	3	58	0.005108782		
R-HSA-5687128	MAPK6/MAPK4 signaling	0	89	1	315	0.008034666	0.731394352	0.731394352	1	40	0.003523298		
R-HSA-5693606	DNA Double Strand Break Response	0	60	1	354	0.005416629	0.735074061	0.735074061	2	43	0.003787545		
R-HSA-399719	Trafficking of AMPA receptors	0	31	1	362	0.002798592	0.735986233	0.735986233	3	4	3.52E-04		
R-HSA-399721	Glutamate binding, activation of AMPA receptors and synaptic plasticity	0	31	1	362	0.002798592	0.735986233	0.735986233	3	9	7.93E-04		
R-HSA-168254	Influenza Infection	0	169	1	245	0.015256838	0.7387043	0.7387043	1	59	0.005196864		
R-HSA-975155	MyD88 dependent cascade initiated on endosome	0	92	1	344	0.008305498	0.742285719	0.742285719	3	62	0.005461112		
R-HSA-168181	Toll Like Receptor 7/8 (TLR7/8) Cascade	0	92	1	344	0.008305498	0.742285719	0.742285719	3	63	0.005549194		
R-HSA-162587	HIV Life Cycle	1	163	0	260	0.014715176	0.742285719	0.742285719	1	112	0.009865234	Rnmt	O43148
R-HSA-8866910	TFAP2 (AP-2) family regulates transcription of growth factors and their receptors	0	13	1	397	0.001173603	0.74756772	0.74756772	2	18	0.001585484		
R-HSA-168138	Toll Like Receptor 9 (TLR9) Cascade	0	96	1	347	0.008666606	0.748437666	0.748437666	3	66	0.005813441		
R-HSA-8862803	Deregulated CDK5 triggers multiple neurodegenerative pathways in Alzheimer's disease models	0	23	2	777	0.002076374	0.750740025	0.750740025	2	22	0.001937814		
R-HSA-8863678	Neurodegenerative Diseases	0	23	2	777	0.002076374	0.750740025	0.750740025	2	22	0.001937814		

Pathway identifier	Pathway name	#Entities found	#Entities total	#Interactors found	#Interactors total	Entities ratio	Entities pValue	Entities FDR	#Reactions found	#Reactions total	Reactions ratio	Submitted entities found	Mapped entities
R-HSA-8948751	Regulation of PTEN stability and activity	0	69	1	347	0.006229123	0.751029892	0.751029892	2	13	0.001145072		
R-HSA-187037	Signaling by NTRK1 (TRKA)	0	79	1	359	0.007131895	0.753595906	0.753595906	1	55	0.004844534		
R-HSA-166058	MyD88:Mal cascade initiated on plasma membrane	0	95	1	360	0.008576329	0.755292148	0.755292148	3	63	0.005549194		
R-HSA-157118	Signaling by NOTCH	0	205	2	634	0.018506816	0.755798049	0.755798049	2	151	0.013300449		
R-HSA-168928	DDX58/IFIH1-mediated induction of interferon-alpha/beta	0	77	1	357	0.006951341	0.756976932	0.756976932	1	46	0.004051792		
R-HSA-168179	Toll Like Receptor TLR1:TLR2 Cascade	0	98	1	361	0.008847161	0.758650333	0.758650333	3	65	0.005725359		
R-HSA-168188	Toll Like Receptor TLR6:TLR2 Cascade	0	95	1	364	0.008576329	0.758650333	0.758650333	3	65	0.005725359		
R-HSA-181438	Toll Like Receptor 2 (TLR2) Cascade	0	98	1	364	0.008847161	0.761139259	0.761139259	3	67	0.005901524		
R-HSA-168164	Toll Like Receptor 3 (TLR3) Cascade	0	97	1	372	0.008756884	0.762784534	0.762784534	3	60	0.005284947		
R-HSA-9018519	Estrogen-dependent gene expression	0	120	2	742	0.010833258	0.775759024	0.775759024	2	64	0.005637276		
R-HSA-8939211	ESR-mediated signaling	0	126	2	742	0.011374921	0.777502995	0.777502995	2	69	0.006077689		
R-HSA-937061	TRIF(TICAM1)-mediated TLR4 signaling	0	98	1	401	0.008847161	0.786908873	0.786908873	3	57	0.005020699		
R-HSA-166166	MyD88-independent TLR4 cascade	0	98	1	401	0.008847161	0.786908873	0.786908873	3	59	0.005196864		
R-HSA-195253	Degradation of beta-catenin by the destruction complex	0	82	1	388	0.007402726	0.789840766	0.789840766	1	22	0.001937814		
R-HSA-2454202	Fc epsilon receptor (FCERI) signaling	0	217	1	291	0.019590142	0.800487033	0.800487033	2	63	0.005549194		
R-HSA-9006931	Signaling by Nuclear Receptors	0	169	2	746	0.015256838	0.801779989	0.801779989	2	90	0.00792742		
R-HSA-6798695	Neutrophil degranulation	1	480	0	0	0.043333032	0.805946799	0.805946799	1	10	8.81E-04	Pdap1	Q13442
R-HSA-1257604	PIP3 activates AKT signaling	0	269	2	667	0.024284554	0.809009401	0.809009401	3	85	0.007487008		
R-HSA-4090294	SUMOylation of intracellular receptors	0	31	1	474	0.002798592	0.813862661	0.813862661	1	25	0.002202061		
R-HSA-212165	Epigenetic regulation of gene expression	1	117	0	418	0.010562427	0.816430198	0.816430198	3	33	0.002906721	Ddx21	Q9NR30
R-HSA-1500620	Meiosis	0	88	1	447	0.007944389	0.823313097	0.823313097	1	15	0.001321237		
R-HSA-5617833	Cilium Assembly	0	201	1	383	0.018145707	0.828755675	0.828755675	2	50	0.004404122		
R-HSA-9006925	Intracellular signaling by second messengers	0	300	2	704	0.027083145	0.838335654	0.838335654	3	104	0.009160574		
R-HSA-195721	Signaling by WNT	0	297	3	1123	0.026812314	0.840270443	0.840270443	6	156	0.013740861		
R-HSA-1474165	Reproduction	0	114	1	452	0.010291595	0.841376749	0.841376749	1	24	0.002113979		
R-HSA-8848021	Signaling by PTK6	0	57	1	513	0.005145798	0.846807459	0.846807459	2	52	0.004580287		

Pathway identifier	Pathway name	#Entities found	#Entities total	#Interactors found	#Interactors total	Entities ratio	Entities pValue	Entities FDR	#Reactions found	#Reactions total	Reactions ratio	Submitted entities found	Mapped entities
R-HSA-9006927	Signaling by Non-Receptor Tyrosine Kinases	0	57	1	513	0.005145798	0.846807459	0.846807459	2	52	0.004580287		
R-HSA-166016	Toll Like Receptor 4 (TLR4) Cascade	0	129	1	479	0.011645752	0.847871501	0.847871501	3	94	0.00827975		
R-HSA-112314	Neurotransmitter receptors and postsynaptic signal transmission	0	152	1	457	0.013722127	0.870437722	0.870437722	3	56	0.004932617		
R-HSA-2559583	Cellular Senescence	0	164	1	494	0.014805453	0.874890166	0.874890166	2	88	0.007751255		
R-HSA-168898	Toll-Like Receptors Cascades	0	155	1	527	0.013992958	0.881703694	0.881703694	3	180	0.01585484		
R-HSA-166520	Signaling by NTRKs	0	103	1	572	0.009298547	0.888152779	0.888152779	1	117	0.010305646		
R-HSA-5693532	DNA Double-Strand Break Repair	0	148	1	566	0.013361018	0.891246676	0.891246676	2	106	0.009336739		
R-HSA-5683057	MAPK family signaling cascades	0	302	1	440	0.0272637	0.906820061	0.906820061	1	86	0.00757509		
R-HSA-5619507	Activation of HOX genes during differentiation	0	91	1	619	0.008215221	0.908766466	0.908766466	1	43	0.003787545		
R-HSA-5617472	Activation of anterior HOX genes in hindbrain development during early embryogenesis	0	91	1	619	0.008215221	0.908766466	0.908766466	1	43	0.003787545		
R-HSA-373760	L1CAM interactions	0	120	1	617	0.010833258	0.91556792	0.91556792	1	54	0.004756452		
R-HSA-5688426	Deubiquitination	0	282	1	570	0.025458157	0.927456162	0.927456162	1	77	0.006782348		
R-HSA-8864260	Transcriptional regulation by the AP-2 (TFAP2) family of transcription factors	0	37	1	762	0.003340255	0.932886858	0.932886858	2	44	0.003875628		
R-HSA-202733	Cell surface interactions at the vascular wall	0	245	1	584	0.022117902	0.938356704	0.938356704	1	64	0.005637276		
R-HSA-162906	HIV Infection	1	246	0	649	0.022208179	0.946135197	0.946135197	1	155	0.013652779	Rnmt	O43148
R-HSA-1852241	Organelle biogenesis and maintenance	0	297	1	646	0.026812314	0.947084126	0.947084126	2	86	0.00757509		
R-HSA-5663205	Infectious disease	1	460	1	998	0.041527489	0.950522601	0.950522601	2	320	0.028186382	Rnmt	O43148
R-HSA-8878171	Transcriptional regulation by RUNX1	0	208	1	734	0.018777647	0.955557201	0.955557201	1	132	0.011626883		
R-HSA-112315	Transmission across Chemical Synapses	0	223	1	730	0.020131805	0.960638723	0.960638723	3	104	0.009160574		
R-HSA-449147	Signaling by Interleukins	0	457	3	1650	0.041256658	0.963667754	0.963667754	4	491	0.043248481		
R-HSA-3108232	SUMO E3 ligases SUMOylate target proteins	0	172	2	1440	0.01552767	0.969586635	0.969586635	5	130	0.011450718		
R-HSA-2990846	SUMOylation	0	178	2	1475	0.016069333	0.972728873	0.972728873	5	139	0.01224346		
R-HSA-2262752	Cellular responses to stress	0	405	1	822	0.036562246	0.980699978	0.980699978	2	181	0.015942923		
R-HSA-112316	Neuronal System	0	370	1	799	0.033402546	0.981387061	0.981387061	3	157	0.013828944		
R-HSA-9006934	Signaling by Receptor Tyrosine Kinases	0	471	2	1404	0.042520538	0.98309169	0.98309169	2	628	0.055315776		
R-HSA-8953897	Cellular responses to external stimuli	0	482	1	879	0.043513587	0.987111399	0.987111399	2	251	0.022108694		

Pathway identifier	Pathway name	#Entities found	#Entities total	#Interactors found	#Interactors total	Entities ratio	Entities pValue	Entities FDR	#Reactions found	#Reactions total	Reactions ratio	Submitted entities found	Mapped entities
R-HSA-1643685	Disease	1	1148	4	2413	0.103638169	0.991627006	0.991627006	5	930	0.081916674	Rnmt	O43148
R-HSA-168249	Innate Immune System	1	1180	2	1539	0.106527038	0.993340332	0.993340332	5	643	0.056637012	Pdap1	Q13442
R-HSA-1280215	Cytokine Signaling in Immune system	0	771	3	2042	0.069603683	0.994416838	0.994416838	4	624	0.054963446		
R-HSA-3700989	Transcriptional Regulation by TP53	0	367	1	1307	0.033131714	0.995925754	0.995925754	1	258	0.022725271		
R-HSA-422475	Axon guidance	0	556	1	1279	0.050194096	0.997765002	0.997765002	2	296	0.026072404		
R-HSA-1640170	Cell Cycle	0	621	1	1400	0.056062111	0.998218763	0.998218763	1	423	0.037258874		
R-HSA-109582	Hemostasis	0	723	1	1294	0.06527038	0.998880525	0.998880525	1	327	0.02880296		
R-HSA-74160	Gene expression (Transcription)	3	1416	3	3112	0.127832446	0.999127233	0.999127233	15	817	0.071963358	Rnmt;Dicer1;Ddx21	O43148;Q9NR30;Q9UPY3
R-HSA-73857	RNA Polymerase II Transcription	1	1274	3	2921	0.11501309	0.999524899	0.999524899	5	707	0.062274289	Rnmt	O43148
R-HSA-212436	Generic Transcription Pathway	0	1152	3	2813	0.103999278	0.999842063	0.999842063	4	648	0.057077424		
R-HSA-1266738	Developmental Biology	0	1053	2	2298	0.09506184	0.999850138	0.999850138	4	483	0.042543821		
R-HSA-168256	Immune System	1	2226	4	3053	0.200956938	0.999894313	0.999894313	6	1461	0.128688452	Pdap1	Q13442
R-HSA-597592	Post-translational protein modification	0	1415	2	2339	0.127742168	0.999962946	0.999962946	6	509	0.044833965		
R-HSA-162582	Signal Transduction	0	2738	5	4507	0.247178839	0.999999929	0.999999929	20	2086	0.183739981		
R-HSA-392499	Metabolism of proteins	0	2111	2	3383	0.190575065	0.99999994	0.99999994	7	900	0.079274201		

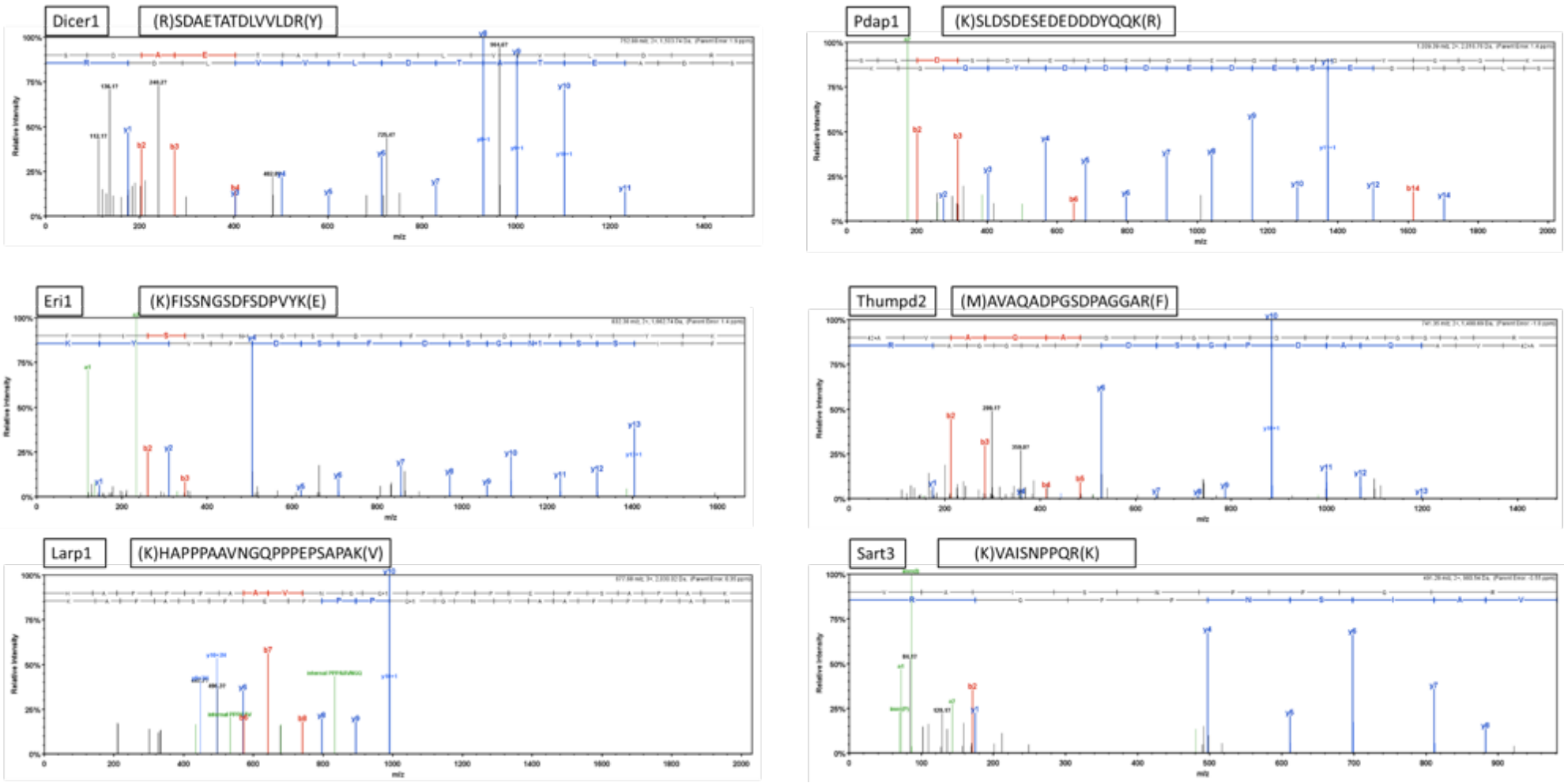

Supplementary Figure 1. Representative MS/MS spectra for the proteins binding only the mutant transcript.

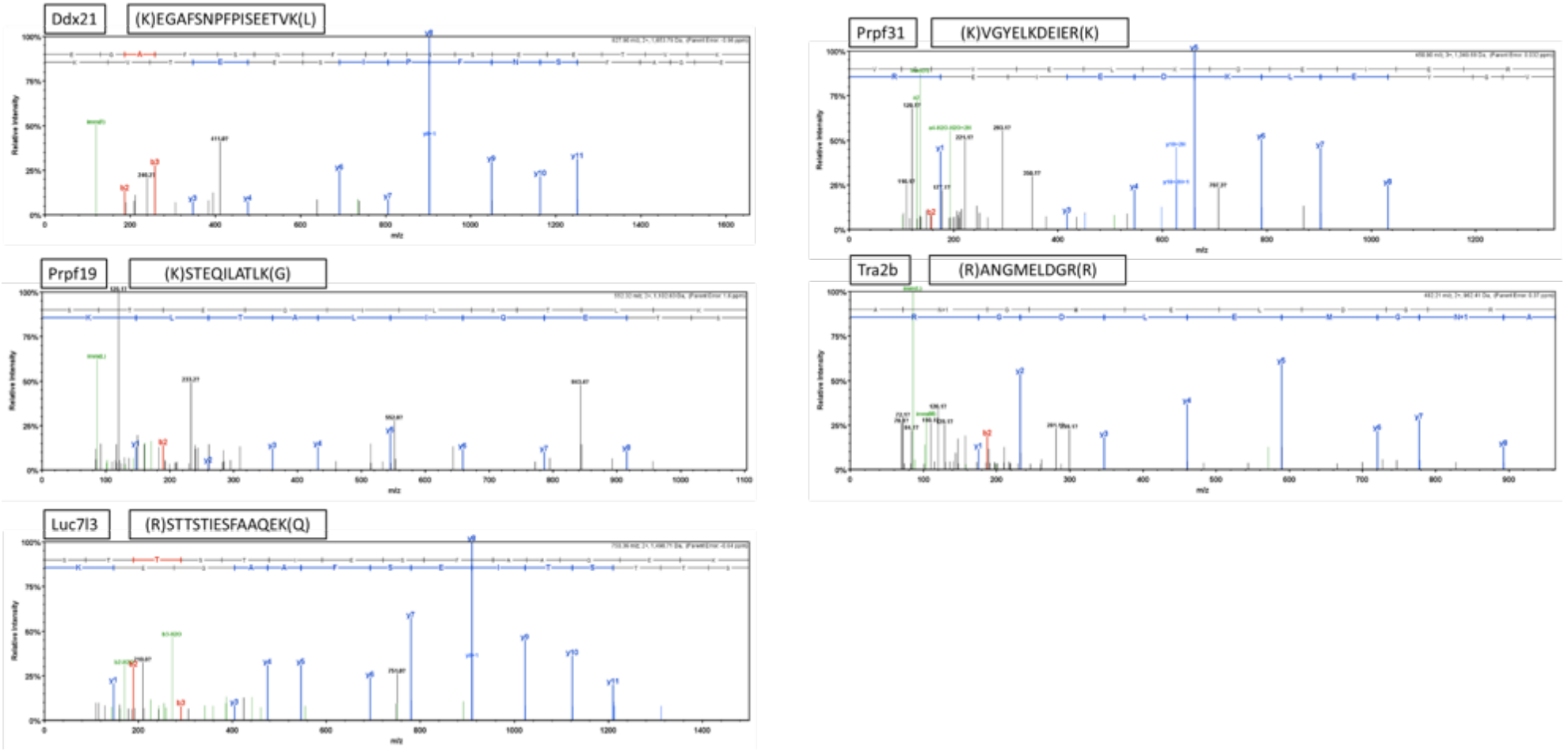

Supplementary Figure 2. Representative MS/MS spectra for the proteins binding only the mutant transcript.

APPENDIX